Pluton Emplacement, Aureole Deformation and Metamorphism, and Regional Deformation Within the Central White-Inyo Range, Eastern California

By

Sven Soren Morgan

Dissertation submitted to the Faculty of the

Virginia Polytechnic Institute and State University

in partial fulfillment of the requirements for the degree of

DOCTOR OF PHILOSOPHY

IN

GEOLOGY

APPROVED:

Dr. Richard D. Law, Chair

Dr. Allen Glazner

Dr. Arthur G. Sylvester

Dr. Robert Tracy

Dr. Krishna Sinha

April 24, 1998

Blacksburg, Virginia

Keywords:
Structural Geology, Pluton Emplacement, Aureole Deformation, White-Inyo Range

Abstract

The central White-Inyo Range in eastern California is a deformed section of Neoproterozoic through Cambrian sedimentary rocks which has been intruded by granitic plutons associated with the Mesozoic Sierra Nevada intrusive suites to the west. My dissertation involves a characterization of the pre-plutonic regional deformation within the central White-Inyo Range and an understanding of the deformation of the wall rocks and magmas associated with pluton emplacement. The four chapters in this dissertation are a compilation of three published articles (two in journals, one in a field guide-book) and one manuscript.

The regional deformation was characterized by measuring the orientation of folds, bedding, and cleavage throughout the range, as well as utilizing these data from other authors and from published geologic maps. Synthesis of the data indicate that all regional structures pre-date the intrusions. The transition from regional structures to aureole structures reveals components of horizontal and vertical translation and rotation of bedding associated with forceful emplacement.

The Jurassic Eureka Valley-Joshua Flat-Beer Creek (EJB) composite pluton and Cretaceous Papoose Flat pluton, as well as the deformed metasedimentary rocks surrounding these plutons, have been examined in detail. Penetrative shortening of the wall rocks was studied in detail along three traverses across the aureole of the EJB pluton and from specific outcrops throughout the aureole. Sedimentary formations have been attenuated to approximately one third of their regional stratigraphic thicknesses. Strain is characterized by flattening and plane strain. Deformation mechanisms vary, but are dominated by intracrystalline slip and climb and by grain boundary sliding. Contact metamorphism is characterized by andalusite followed by sillimanite.

The internal fabric of the EJB pluton has been analyzed through the study of the anisotropy of magnetic susceptibility (AMS). Samples were collected at 210 locations (420 drill cores, approximately 1000 samples) throughout the pluton. Maps of the fabric and magnetic parameters reveal that magnetic fabrics cross-cut some compositional boundaries and parallel others. Comparison between the magnetic fabrics and the aureole structures indicate that the magma and surrounding plastic aureole deformed as a single unit during emplacement.

Detailed porphyroblast-matrix analysis within the concordant metasedimentary aureole rocks surrounding the Papoose Flat pluton indicates that inclusion trails within porphyroblasts can be used as strain markers to restore the aureole rocks to their pre-pluton emplacement position. The kinematics of rotation, the change in thickness and volume, and the amount of translation of the metasedimentary formations within the aureole have been determined using porphyroblast-matrix relationships, in combination with measurement of stratigraphic sections and whole-rock geochemical analyses.

The emplacement of the EJB and Papoose Flat plutons is modeled as occurring in two stages. The first stage is sill-like, producing a thermal aureole which lowers the viscosity of the surrounding sedimentary rocks. The second stage is forceful, causing

upward and outward translation and rotation of the surrounding aureole. Porphyroblast-matrix relationships from the EJB and Papoose Flat pluton, and from the literature on the Ardara pluton, Ireland, and the Cannibal Creek pluton, Australia, support this two stage emplacement model for concordant plutons.

Acknowledgements

I thank my advisor, Dr. Rick Law, for his direction, expert advice concerning structural geology, and overwhelming support through our many years together. His support of my research and of my personal goals has allowed me to come this far. I especially want to thank Rick for giving me the freedom to follow the type of research I thought necessary, even though it always wasn't, and for putting up with an immense amount of stubbornness. I have learned much from Rick and his door has always been open. I hope to continue our collaboration for many years.

I would like to thank committee members Dr. Allen Glazner and Dr. Arthur Sylvester for spending valuable time with me in the White-Inyo Mountains and sharing their ideas and data. Dr. Glazner has also produced needed chemical analyses. I thank Dr. Robert Tracy for the time he spent with me on the microscope and for sharing his expertise on contact metamorphism. I thank Dr. Krishna Sinha for insight into petrogenesis.

Michel Saint Blanquat (CNRS – Toulouse, France) helped me to understand magmatic, tectonic, and magnetic foliations, and is a friend. Bill Seaton helped me with the AMS contouring and images. Dr. Mario Karfakis in Mining Engineering allowed me to use his rock drill.

I am indebted to the many graduate students, past and present, who have spent their time with me, and who have helped to shape my views on geology and life in general. I learned more from you than from any class, and had a lot more fun with you. The camaraderie helped me to grow and provided invaluable support. Rich Whitmarsh, Basil Tikoff, Jim Student, Sam Peavy, Chris Fedo, Mike Pope, Aus Al-Tawil, Michel Markley, are only a few of the fellow classmates who I thank here.

Linda Bland, Karen Hunt, Connie Lowe, Ellen Mathena, Mary McMurray, and Carolyn Williams have always been tremendously friendly and have helped me to finish my degree. I also wish to thank the faculty, and especially the chairperson, Dr. Cahit Coruh, for giving the graduate students a voice and boosting moral, and for providing needed smiles.

My field assistants were tireless and unpaid. Maxine Smith, Ed Cajza, Wes Knight, Adam Henry, Meredith Westington, and John Vines worked hard in the desert heat and I greatly appreciate their efforts.

My partner, spouse, and most valuable friend, Debra Smilo, is always providing love and support and has allowed me to grow way beyond what I dreamed possible. She is the best part of my life.

Financial support was provided by the Geological Society of America, Sigma Xi, The National Science Foundation, The University of California White Mountain Research Station, The Virginia Tech Graduate Student Assembly, and Mr. Bob Morgan.

Table of Contents

Table of Figures

Table of Tables

Chapter 1. An Overview of Paleozoic - Mesozoic Age Structures Developed in the Central White-Inyo Range, Eastern California

SVEN S. MORGAN AND RICHARD D. LAW

Department of Geological Sciences, Virginia Tech., Blacksburg, Virginia 24061

Published in 1998, by International Geology Review, v. 40, p. 245-256

Abstract

The central White-Inyo Range of eastern California is composed of a 7.5 km thick succession of Neoproterozoic to Upper Cambrian age sedimentary rocks which have been deformed into a series of NE and N to NW-trending folds. The map distribution of the sedimentary rocks is primarily controlled by the younger N to NW-trending folds which define the White Mountain-Inyo anticlinorium. Smaller scale folds and associated cleavage, which strongly fans in a divergent pattern about the fold hinge surfaces, are associated with both periods of fold development. Older NE-trending folds and associated cleavage are developed in a NW-trending belt that crosses the range in a structural saddle between the White Mountain and Inyo anticlines. These NE-trending folds are of smaller wavelength than the older N to NW-trending regional scale folds, although both fold generations are developed on the cm-km scale. The intensity of both fold and cleavage development generally increases towards the west. Interference between the NE and the N to NW-trending folds has led to the development of a series of structural basins. We correlate formation of the NE-trending structures to the Antler Orogeny and formation of the younger N to NW-trending structures with translation on the Last Chance thrust which is exposed in the Inyo Range and presumably underlies the entire central White-Inyo Range.

In the eastern and central portions of the range it is clear that both periods of folding pre-date the emplacement of Jurassic and Cretaceous plutons which are correlatives to the intrusive suites exposed in the Sierra Nevada batholith to the west. On the western margin of the range another set of N to NW trending structures, which are coaxial with the earlier N to NW set, is probably associated with the East Sierran thrust belt; this thrust belt is better recorded in the southern Inyo Mountains and developed in the Jurassic period.

Introduction

The central White-Inyo Range is located within the transition zone between the Mesozoic magmatic arc, i.e. Sierra Nevada batholith, to the west and the deformed foreland of the Phanerozoic North American craton to the east. Whereas the magmatic arc is dominated by Mesozoic plutons, the central White-Inyo Range is composed of a Neoproterozoic to Upper Cambrian-age passive-margin shallow shelf sequence which has been intruded by much smaller volumes of Jurassic and Cretaceous plutons which are time correlatives of the much larger intrusive suites to the west. The ages and styles of deformation features preserved within the White-Inyo Range are important for understanding how the passive margin sequence in eastern California responded to the protracted series of Paleozoic and Mesozoic orogenic events, which are better documented to the north, east, and south, and also how these rocks were affected by development of the Mesozoic magmatic arc and associated subduction zone located to the west.

Late Mesozoic deformation has been documented in the northern White Mountains (Hanson et al., 1987), and evidence for protracted deformation throughout the Mesozoic period has been recorded in the southern Inyo Mountains (Dunne et al., 1978; Stevens et al., this volume). However, the orientations and ages of structures exposed within the central portion of the White-Inyo Range, and their relationships to the Mesozoic plutons discussed herein, has only attracted brief reviews (Sylvester and Babcock, 1975; Dunne et al., 1978; Nelson et al., 1991; Paterson et al., 1991). Our purpose in this paper is to describe the dominant Paleozoic through Mesozoic age structures exposed in the central White-Inyo Range, and to present an overview of the relative sequence of deformational and intrusive events. Detailed descriptions of the sedimentary rocks in the central White-Inyo Range can be found elsewhere (Nelson, 1962, 1978; Mount and Signor, 1991); a more regional account of the geologic evolution of eastern California can be found in Stevens et al., (this volume). The central White-Inyo Range has been mapped at the 1:62,500 scale under the auspices of the U.S. Geological Survey (Nelson 1966a & b; McKee and Nelson 1967; Ross, 1967a; Nelson 1971) and many of the structural observations and interpretations reported in this paper are based on these U.S.G.S. maps. A regional-scale map of the central White-Inyo Range and adjacent areas to the south and east has been compiled by Ross (1967b); more detailed compilation maps have subsequently been published by Nelson et al., (1991) and Ernst et al., (1993).

Structural Geology

The dominant structures throughout the range are N to NW-trending folds of all scales (cm to km wavelengths) and an associated N to NW-striking slaty-spaced cleavage which fans about the fold hinge planes in a divergent pattern (terminology after Ramsay, 1967). The range is defined by the N to NW-trending White Mountain-Inyo anticlinorium so that, in general, the western and eastern flanks of the range are coincident with the western and eastern limbs of the anticlinorium (Fig. 1). Older NE-trending folds and cleavage are less commonly observed, and are of smaller scale, than the range-dominating N to NW structures. The areal distribution of the NE structures is domainal and they are best developed in a NW-trending belt that crosses the range. Cleavage formation is believed to be associated with both periods of folding because cleavage consistently strikes sub-parallel to the strike of bedding on the limbs of both the N to NW and NE-trending folds, and dips more steeply than bedding on the limbs of both fold sets (Fig. 2). For both fold sets, cleavage fans in a divergent manner about the hinge surfaces of the folds.

In most of the range, sedimentary structures and fossils are well preserved. Locally, intense penetrative strains within pelitic horizons have resulted in the complete transposition of bedding into the overprinting cleavage. Cleavage is most strongly developed in the pelitic and carbonate units of the Poleta and Harkless formations. In contrast, cleavage is either absent or only weakly developed in the more competent quartzites, sandstones and siltstones which are abundant throughout the Neoproterozoic through Upper Cambrian section. In the pelitic units cleavage is slaty and defined by a preferred alignment of elongate micron-scale white mica, quartz and chlorite grains. In the carbonate units, cleavage is defined by a series of dark colored pressure solution seams which are spaced at the cm-scale.

Excluding the western margin of the range (discussed below) one cleavage is predominantly observed in the rocks. Rarely, two cleavages are preserved, an older NE-trending cleavage and a younger, cross-cutting, NW-trending cleavage (Fig. 3). Both are generally slaty, but the younger fabric is developed in cm-scale zones. In a only a few outcrops are three generations of cleavage visible. The oldest cleavage is preserved as dark, cm spaced seams with a N-trending strike and a variable dip. The significance of this fabric is unknown. Numerous minor faults and joint sets are observed in the sedimentary

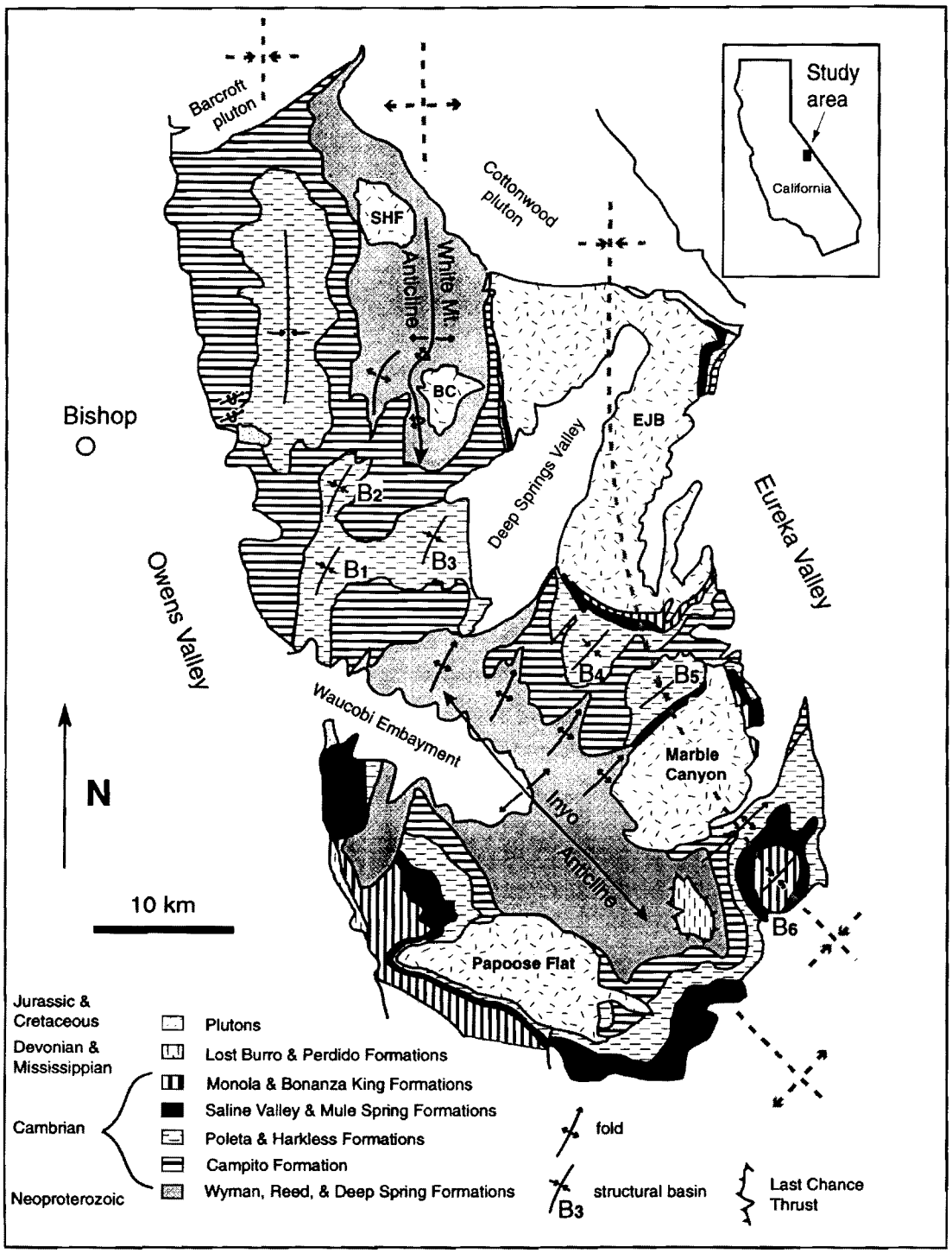

Figure 1. Simplified geologic map of the White-Inyo Range. Adapted from Nelson (1966a & b; 1971), Nelson et al., (1991), and McKee and Nelson (1967).

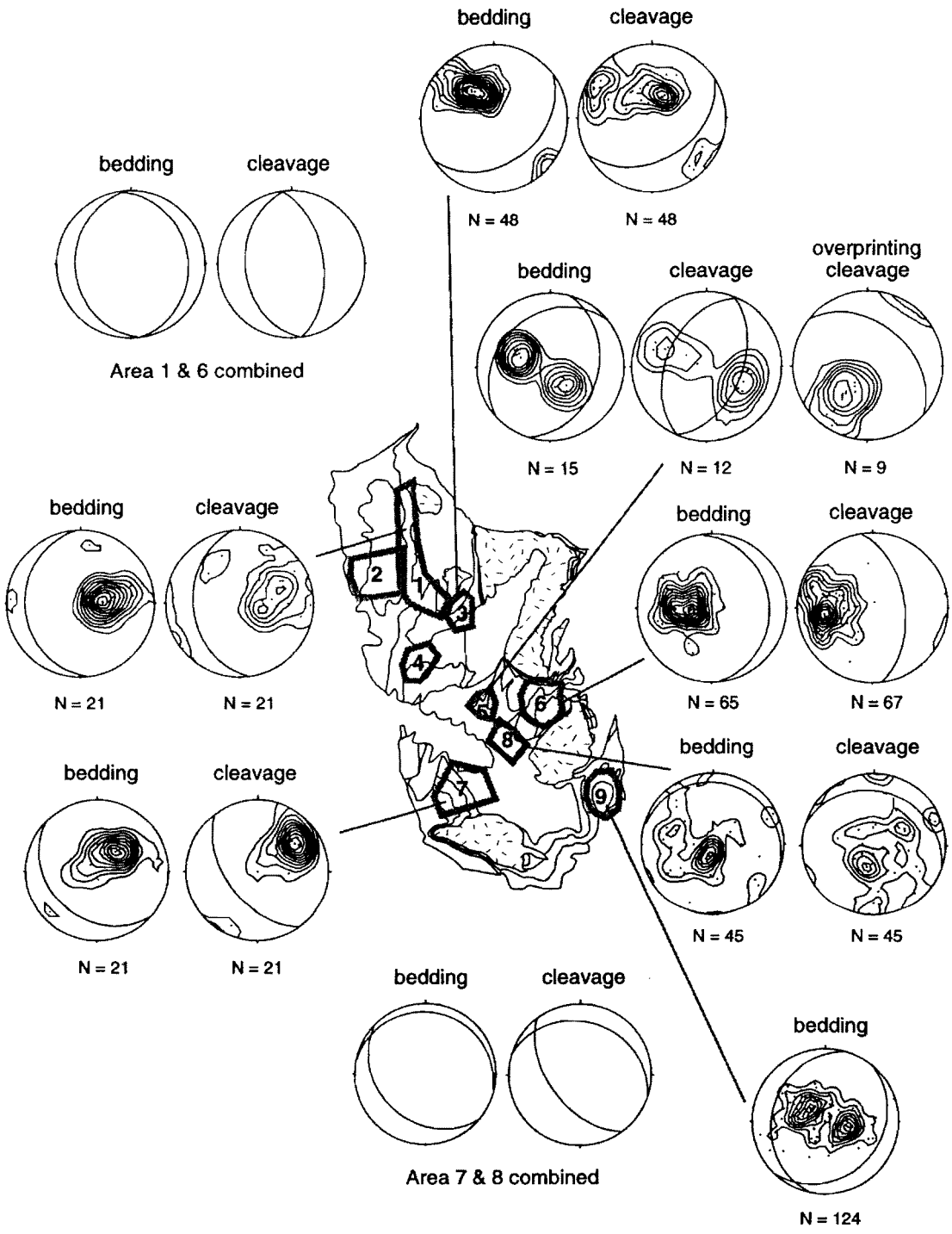

Figure 2. Location map and bedding-cleavage data from areas selected for structural analysis; see Figure 1 for details of regional geology. See text for discussion.

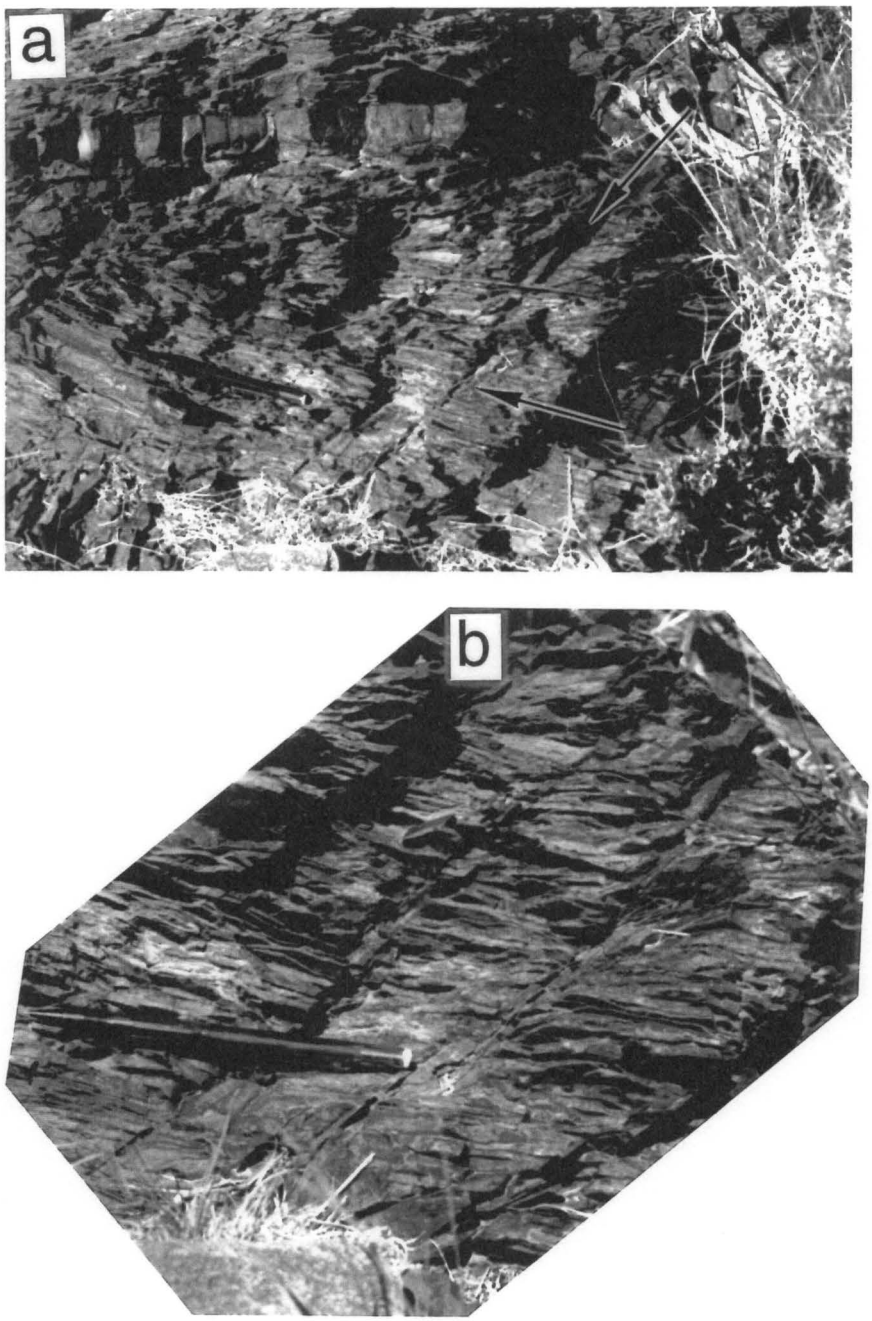

Figure 3. Photographs of crosscutting cleavages. A. Older, NE-striking slaty cleavage is parallel to pencil, and slightly oblique to bedding, which is horizontal. Younger, NW-striking cleavage is slaty in cm-scale zones and crosscuts the NE-striking cleavage. B. Close-up view of relationship seen in A. Pencil is 15 cm long.

rocks of the White-Inyo Range. A detailed analysis of these structures remains to be undertaken.

We correlate folds and cleavage in the central White-Inyo Range to separate events primarily on the basis of orientation (Williams, 1985), but also on scale. NE and N to NW-trending folds are similar in style, both are dominantly upright and horizontal, except in the western part of the range where both sets of folds can be inclined and deformation is more intense.

NE-trending Structures

NE-trending folds are mostly observed in a linear belt that trends NW and crosses the range crest in the saddle between the White Mountain and Inyo anticlines (Fig. 1). Begining on the southeast limb of the Inyo anticline, the NE-trending structures can be traced northwest to the saddle region between the White Mountain and Inyo anticlines (which includes the Poleta folds area, see Fig. 1, basin B3; Nelson, 1980), and then northward along the western limb of the White Mountain anticline. The intensity of the NE-trending structures increases to the west. Along the eastern limb of the Inyo anticline, NE-trending folds have km-scale wavelengths, are upright and open, while in the Poleta folds area located in the saddle region between the White Mountain and Inyo anticlines (Fig. 1, structural basin B3) folds are of smaller wavelength, slightly inclined and tighter, and are associated with low angle, small displacement thrusts. On the western limb of the White Mountain anticline, between the Poleta and Silver canyons (Fig. 2, area 2) NE-trending folds are often recumbent and isoclinal, the folds verging towards the SE (Welch, 1979). The domainal nature of the NE-trending structures is not well understood. Whether folding and cleavage formation associated with the first deformation event was restricted to certain areas, or if they were developed on a regional scale and then largely overprinted by the N to NW oriented structures, is unknown.

We originally assumed that the NE-trending structures post-dated the N to NW-trending structures based on map-scale relations (Morgan and Law, 1994). More recently, both cleavages have been observed by the authors in the same outcrop and the NW-striking cleavage clearly overprints the NE-striking cleavage, documenting the older nature of the NE structures (Fig. 3). This is consistent with the observations of Sylvester and Babcock (1975), in the saddle region, Welch (1979) in the western part of the White Mountains

(Fig. 2, area 2), and Dunne (1986) in the southern Owens Valley region, where NE-trending structures are overprinted by N to NW-trending structures.

The area of overprinting cleavage is located on the eastern limb of the Inyo anticline where map-scale NE-trending folds and associated slaty cleavage are observed (Fig. 1). Poles to bedding from one of these folds (Fig. 2, area 5) document an upright and horizontal fold where cleavage dips approximately 20° more steeply than bedding on both limbs of the fold. Also observed on both limbs of this km-scale fold is a NW-striking and NE-dipping cleavage (Fig. 2, area 5) which cross-cuts the NE-striking slaty cleavage (Fig. 3), and which is apparently related to the development of the larger-scale Inyo anticline. The NW-striking cleavage is slaty in appearance, but only found in 1-2 cm thick zones, spaced 10-15 cm apart, which cross-cuts the more prevalent NE-striking cleavage.

The change in trend from the White Mountain anticline to the Inyo anticline occurs where the belt of older NE-trending folds and cleavage crosses the composite White Mountain-Inyo anticline. This leads us to believe that the change in fold trend from N to NW may have been controlled by the location of pre-existing NE-trending structures during the development of the White Mountain-Inyo anticlinorium.

N to NW-trending structures

The White Mountain anticline trends NS and can be traced southward through a depression in the fold hinge to the NW-trending Inyo anticline. Cleavage and bedding data for both anticlines (Fig. 2) illustrate that cleavage strikes sub-parallel to bedding and also consistently dips 5-20° more steeply than bedding. Poles to bedding and cleavage measured along the western limb of the Inyo anticline (Fig. 2, area 7) define clear point maxima. In contrast, poles to bedding and cleavage measured from the eastern limb of the Inyo anticline (Fig. 2, area 8) are more diffuse; we infer this to be caused by the stronger development of the earlier NE-trending folds in this region. The average strike and dip of bedding and cleavage for both limbs of the Inyo anticline have been combined (Fig. 2, area 7 & 8 combined) to illustrate the shallow plunge of the NW-trending fold and the geometric (and inferred genetic) relationship of cleavage to fold formation.

Orientation data from the White Mountain anticline is limited to the western limb of the fold and the southeastern section of the fold's eastern limb (Fig. 2, area 1 & 3). This is because on the eastern limb of the White Mountain anticline much of the cleavage has been overprinted by strain and metamorphism associated with emplacement of the composite

Eureka Valley-Joshua Flat-Beer Creek (EJB) pluton. Bedding and cleavage from the western limb of the fold (Fig. 2, area 1) strike N and dip W, while bedding and cleavage from the SE portion of the White Mountain anticline strike NE and dip SE (Fig. 2, area 3). We associated the NE-striking orientation of bedding and cleavage in the SE portion of the White Mountain anticline with the earlier NE-trending fold event based on orientation and also on spatial continuity to the NE-trending structures in the B3 structural basin located to the south (Fig. 1).

We recognize a regionally developed N to NW-trending syncline, with a fold hinge located 10 to 15 km to the east of the White Mountain-Inyo anticline (Fig. 1), based on the structures outlined by the U.S.G.S. geologic quadrangle maps of Soldier Pass (McKee and Nelson, 1967), Waucoba Spring (Nelson, 1971), the simplified geologic map of Nelson et al., (1991), and cleavage-bedding data included in this report (Fig. 2). The syncline forms an anticline-syncline fold pair with the White Mountain-Inyo anticline and is believed to have been modified in shape and dimension due to subsequent emplacement of the EJB and Marble Canyon plutons (Fig. 1).

Structural Basins

One of the consequences of two periods of folding in the central White-Inyo Range, especially since the fold axes from the two events are close to being perpendicular to one another, should be the formation of a series of structural domes and basins due to fold interference (Ramsay, 1967). Six structural basins (Fig. 1, B1-6) have been identified, the three most eastern basins (B4-6) being produced by interference between the older NE-trending folds and the regional scale N to NW-trending syncline which forms the eastern fold pair to the White Mountain-Inyo anticline (Fig. 1). The other three structural basins (B1-3) are located in the saddle region between the White Mountain and Inyo anticlines. T. Welch (unpublished data) has also identified cm to m-scale dome and basin structures from the western portion of the southern White Mountains (Fig. 2, area 2).

Map scale structural domes have not been identified in the range. One possibility, on the eastern side of the Inyo anticline, is that they were significantly modified by the intrusion of the Jurassic plutons. In the saddle region, it is possible that the interference patterns produced by orthogonally superimposing large scale anticlines on smaller anticlines is not as pronounced as superimposing large scale anticlines on smaller synclines. In addition, the two generations of fold axes are at a lower angle to each other in

the saddle region than on the eastern limb of the Inyo anticline, and the closer the two sets of fold axes are to each other in orientation, the less well developed the resultant dome and basin structures will be.

The most obvious structural basin produces a bull's-eye map pattern defined by inward-dipping lower and middle Cambrian formations and is located in the southeast corner of the region (Fig. 1, B6). The orientation of bedding at individual outcrops within this basin has been taken from the Waucoba Spring U.S.G.S. Geologic Quadrangle map (Nelson, 1971) and plotted as poles to bedding in Figure 2, area 9. Contouring of these poles reveals a WNW-ESE striking girdle distribution of poles with two point maxima that define the limbs of a SSW plunging fold. However, the distribution of poles within this girdle is drawn out in a NE-SW direction, suggesting the local reorientation of bedding about a NW-SE trending fold axis.

Structural saddle between the White Mountain and Inyo anticlines

A structural saddle (or fold depression) defines the transition between the southward-plunging White Mountain anticline and the NW-plunging section of the Inyo anticline. The exposed stratigraphic units range from Neoproterozoic Wyman Formation located in the cores of both anticlines, to middle Cambrian Harkless Formation in the saddle, passing through almost 6,000 m of section measured along the hinge of the anticline. Development of the saddle may also be the result of fold interference associated with the two periods of folding. As mentioned previously, the belt of NE-trending structures crosses the N to NW-trending White Mountain-Inyo anticline in the saddle region. Imposing a larger wavelength N to NW-trending anticline on an already existing, smaller wavelength NE-trending syncline could produce the observed structural depression in the White Mountain-Inyo anticline.

Structures associated with pluton emplacement

Emplacement of the Jurassic to Cretaceous age plutons in the central White-Inyo Range post-dates the two dominant phases of folding and cleavage development outlined above. This conclusion is based on four lines of evidence.

1). The composite Mid-Jurassic age EJB pluton (dated at 161 - 174 Ma (U/Pb); Gillespie, 1979; Sylvester et al., 1978) and the Marble Canyon pluton (179 Ma (U/Pb);

Sylvester et al., 1978) are the oldest plutons in the study area, and both cross-cut structural basins produced by interference between the two fold sets. The structural basins (labeled B4 and B5 in Fig. 1) located between the two plutons are characterized by moderately dipping (20-60°) beds. Traced away from the basin troughs towards the pluton margins, however, the beds abruptly change their dip direction at a distance of 1-2 km from the pluton margins and rapidly rotate to become subvertical or locally overturned. These rapid changes in the dips of bedding terminate the structural basins and begin at the outer margins of the contact aureoles. The steeply dipping beds within the aureoles strike sub-parallel to the pluton margin. Glazner and Miller (in press) have recently suggested that these rotations may indicate that the granodioritic - dioritic Jurassic plutons began to sink during crystallization as they became more dense than the surrounding country rocks.

2) At a distance of 1-2 km from the Jurassic plutons, bedding rotates from the regional structural grain into concordancy with the pluton margins, and the cleavage (where measurable) is also rotated by a similar amount, hence preserving the angular relationship between bedding and cleavage observed throughout the range. We interpret cleavage to have rotated passively along with bedding as bedding was deformed into concordancy with the plutons. At an approximate distance of 1 km from the pluton margins this cleavage is overprinted by (and transposed into) a new pluton margin-parallel grain shape fabric associated with contact metamorphism and emplacement-related strains (Morgan and Law, 1994). For example, near the southwestern margin of the EJB pluton (Fig. 1), bedding can be traced from its regional NNE-strike towards the pluton margin where bedding rapidly steepens and is rotated into a NW-strike to become concordant to the contact. The SE dip of bedding increases from moderate angles to becoming sub-vertical, and in several areas is overturned. Cleavage can be traced along with bedding, striking sub-parallel to bedding and dipping more steeply. Where the overturned beds are NW-striking and dipping to the SW, cleavage also strikes to the NW but dips less steeply to the SW, suggesting that cleavage had been rotated passively along with bedding and has also been rotated through the vertical.

3) On the SW limb of the Inyo anticline (Fig. 1) bedding and the regionally developed NW striking cleavage have both been rotated into concordancy with the margin of the Cretaceous age Papoose Flat pluton (dated at 83 Ma on U/Pb; Miller, 1996) within the pluton's aureole. Original angular relationships between bedding and cleavage, observed away from the pluton, are preserved as inclusion trails in andalusite porphyroblasts within the pluton's aureole (Morgan et al., in press).

4) The Cretaceous Birch Creek pluton deflects N trending folds and faults in the core of the White Mountain anticline (Nelson and Sylvester, 1971) (Fig. 1). Traced southwards towards the pluton, N trending folds become overturned and more appressed as they wrap around the NW margin of the pluton, indicating that the folds have been deformed by the western expansion of the pluton as it was emplaced (Nelson and Sylvester, 1971).

In addition to the structural evidence above that fold and cleavage development pre-date emplacement of the Jurassic and Cretaceous age plutons, supporting petrologic evidence has recently been described by Ernst (1996) who conducted a detailed geochemical study of the variably metamorphosed sedimentary rocks of the central White-Inyo Range. This study indicates that metamorphic isograds transect the N-NW oriented folds and possibly the NE oriented folds. Ernst (1996, p. 1528) interpreted the observed higher grade metamorphic zonation of the region as being "a composite of local recrystallization episodes attending calc-alkaline pluton emplacement over an approximately 100 m.y. interval, overprinting a pervasive, weak, chloritic metamorphism", indicating that the last re-setting of isograds could be as young as 80 Ma, at least adjacent to the Cretaceous intrusives.

Discussion

Three orientations of folds and cleavage have been recorded in the central White-Inyo Range; NE, N, and NW. We correlate the NE-trending structures with the first deformation event. We associate the N and NW-trending structures to a later event and favor the hypothesis of two dominant periods of deformation resulting in formation of the structures observed in most of the central White-Inyo Range. Based on deformation features observed along the western margin of the White Mountains (Welch, 1979) and in the southern Inyo Mountains (Dunne, 1986; Stevens et al., this volume), it is likely that the increase in intensity of the N to NW-trending structures observed on the western margin of the range is associated with a third period of deformation which post-dates both formation of the NE-trending structures and the earlier N to NW-trending structures.

We associate the N-trending White Mountain anticlinorium and the NW-trending Inyo anticlinorium to the same deformation event for several reasons. 1) They are of the same scale and probably related to the same structure at depth (i.e. the Last Chance thrust system-see justification below). 2) We would expect to see large scale NW-oriented folds (similar in scale to the Inyo anticline) in the White Mountains, and large scale N oriented

folds (similar in scale to the White Mountain anticline), in the Inyo Mountains, if the White Mountain-Inyo anticlinorium was produced by two periods of folding. 3) The change in orientation from N to NW-trending fold hinges occurs where the anticlinorium crosses the NW oriented belt of NE-trending structures, suggesting a genetic link. In this scenario, the regional-scale bend in structures is related to the architecture of the previously deformed sedimentary sequence. We restate, however, that we do not understand why the NE-trending structures are confined to a NW-trending belt.

The transition between the N and the NW-trending structures has been investigated by combining bedding and cleavage data from the northeastern limb of the Inyo anticline, where the regional structural grain curves northwards from a northwest trend (Fig. 1; Fig. 2, area 6), with data from the western limb of the White Mountain anticline (Fig. 2, area 1). The result is a NNW trending upright fold pattern with a sub-horizontal hinge and equally dipping western and eastern fold limbs (Fig. 2, see the data from area 1 & 6 combined); cleavage dips more steeply than bedding on both limbs. This suggests that the range-scale curvature from the NS-trending White Mountain anticline to the NW-SE trending Inyo anticline occurs more to the south in the eastern part of the range, and is consistent with the curvature in our proposed regional scale syncline to the east of the White Mountain-Inyo anticline (Fig. 1). We believe this further supports our interpretion that the curvature from the NS-oriented structures in the White Mountains to NW-oriented structures in the Inyo Mountains is an original feature associated with simultaneous formation of the White Mountain and Inyo anticlinorium.

In contrast, the area of N-striking bedding and cleavage in the eastern Inyo Mountains (Fig. 2, area 6), may be related to an earlier structure which was largely overprinted by NW-oriented structures in the rest of the Inyo Mountains. A.G. Sylvester (pers com., 1997) and students at the University of California at Santa Barbara have measured the orientations of hundreds of folds in the saddle region between the White Mountain and Inyo anticlines (Fig. 2, area 4) and concluded that NE-trending folds are refolded by N to NW-trending folds. Sylvester's data also indicates that there is a third set of structures that trend due north and are of intermediate age between the older NE-trending folds and the younger NW-trending folds (Sylvester and Babcock, 1975). It is possible that the youngest NW-trending folds in area 4 (Fig. 2) are related to the younger NW-oriented structures observed on the west side of the White Mountains (Fig. 2, area 2, Welch, 1979).

Welch (1979) has noted that on the west side of the southern White Mountains, the intensity of the NW-trending deformation increases abruptly towards the west, folds

become tighter and cleavage intensity increases. In addition, early N-NW structures may be overprinted coaxially by later N-NW oriented structures (T.C. Welch, unpublished data). The increase in intensity of structures, and the possibility of successive events being recorded on the western margin of the range, is consistent with a second period of N to NW-oriented deformation recognized in the southern Inyo Mountains and associated with the East Sierran thrust system (Dunne, 1986; Stevens et al., this volume).

Relationship of the NE-trending folds to the Antler orogenic belt

NE-trending folds and cleavage are associated with the Late Devonian to Early Mississippian Antler orogenic belt in: 1) the Silver Peak Range, 60 km to the northeast in Nevada (Oldow, 1984), 2) the Candelaria Hills (Oldow, 1984), 100 km to the north in Nevada, and 3) the Northern Ritter Range pendant (Greene et al., 1997), which is located 120 km to the northwest in the eastern Sierra Nevada Mountains. In all three areas, NE-trending folds are upright, and are associated with emplacement of the Roberts Mountain Allochthon. NE-trending folds and cleavage in the central White-Inyo Range are similar in orientation and style to early folds and cleavage in Nevada, although NE folds in the Northern Ritter Range can be tighter and locally isoclinal (Greene et al., 1997).

We tentatively correlate the early NE-trending folds observed in the central White-Inyo Range with the Antler age NE-trending folds observed to the north and northeast in Nevada and to the northwest in the eastern Sierra Nevada Mountains, as previously proposed by Sylvester and Babcock (1975) and Dunne et al. (1978). However, it should be noted that opinions differ as to what deformational event the NE-trending folds in the central White-Inyo Range are related to (see Stevens et al., this volume). The Antler orogenic belt is defined by fault juxtaposition of allochthonous Lower Paleozoic, dominantly siliceous rocks of deep-water basinal environments with autochthonous Lower Paleozoic carbonate to clastic dominated shallow-shelf rocks, such as those found in the White-Inyo Range. The NE-trending folds in the Northern Ritter Range and in both localities in Nevada are observed in the deep-water sedimentary rocks of the allochthon. If the NE-trending folds in the central White-Inyo Range are related to the Antler orogeny, then they are unusual in being recorded in the shallow shelf sequence. As well, it should also be noted that the central White-Inyo Range was probably much further west in Antler time. Tens of kilometers of eastward displacement on the Last Chance thrust in the late Paleozoic is supported by fault juxtaposition and strain analyses (see below).

The only timing constraint on formation of the NE-trending folds in the central White-Inyo Range are that they developed prior to the NW-trending folds (which are associated to the Permian (?) age Last Chance thrusting, see below). In the Candelaria Hills, Nevada, NE-trending folds are only observed in pre-Permian age rocks, and are possibly pre-Mississippian age (Oldow, 1984).

In the three areas discussed above, as well as in the central White-Inyo Range, NE-trending folds are overprinted by NW-trending folds and cleavage. However, correlation of the NW-trending structures in these areas is problematic because they may be of different ages in each area.

Relationship of N-NW structures to the Last Chance thrust

A structural window through the Last Chance thrust (Stewart et al., 1966; Dunne et al., 1978; Corbett et al., 1988), which places the Neoproterozoic to Upper Cambrian age sequence of the White-Inyo Range on Devonian and Mississipian age strata, is located in the SE part of the range in the Jackass Flat area (Fig. 1). The thrust is constrained to have formed between Early Permian and earliest Triassic times (see Snow, 1992; Stevens et al., this volume, for details) and palinspastic restoration incorporating strain analyses indicate a minimum of 75 km of displacement on the thrust (Corbett et al., 1988). Due to the extensive amount of thrusting necessary to place the ~7750 m thick Neoproterozoic to Upper Cambrian section (Stewart and Suczek, 1977; Nelson, 1980) on top of Devonian and Mississipian strata in the Inyo Mountains, it is assumed that all of the central White-Inyo Range section lies above the thrust surface and is therefore allochthonous (Stewart et al. 1966; Nelson et al., 1991).

Extensive strain and kinematic analyses have been conducted by Corbett (1989) on the hangingwall and footwall rocks. Corbett recorded NNW trending folds and associated cleavage in the footwall rocks, and inferred a N60° E transport direction for the thrust based on the orientation of the NNW trending folds. Corbett et al. (1988) have suggested that the regional-scale N to NW-trending White Mountain and Inyo Mountain anticlines are actually ramp anticlines associated with movement on the underlying Last Chance thrust. This suggestion is supported by the similarity between orientation of structures in the footwall to the thrust and the N to NW-trending structures we have measured throughout the central White-Inyo Range. Following the suggestions of Corbett et al. (1988) and Corbett (1989) we associate formation of the younger N-NW oriented structures exposed in the central

White-Inyo Range with motion on the underlying Last Chance thrust. We further speculate that the NW-trending folds observed in the Candelaria Hills and Silver Peak Range of Nevada may also be related to Last Chance thrusting. However, in the Candelaria Hills, NW-trending folds affect rocks as young as early Triassic and possibly younger (Oldow, 1984): this would indicate that the NW-trending folds in Nevada may be younger than the Last Chance thrusting recognized in eastern California.

Earlier interpretations by Dunne (1986) that the NE-trending folds represent Last Chance structures are not consistent with the data of Corbett et al., (1988) for the northern Inyo Mountains. However, NE-trending folds in the Nelson Range (located 5 km east of the southern Inyo Mountains), are compatible with motion on thrust faults in the southern Inyo Mountains which are correlated with the Last Chance thrust (G. Dunne, pers com, 1997).

We correlate the increase in intensity of N to NW-oriented structures, and possible coaxial overprinting of structures, on the western margin of the White Mountains (Welch, 1979) with the East Sierran thrust system (Dunne et al. 1978; Stevens et al., this volume) which was active intermittently from latest Triassic to Mid-Cretaceous and associated with emplacement of the Mesozoic magmatic arc to the west (Stevens et al., this volume). In the Benton Range, located 15 km to the west of the northern White Mountains, Renne and Turrin (1987) have documented a dominant NW-trending set of folds in the lower Cambrian section that are intruded by undeformed dikes with emplacement ages ranging between 209 and 168 Ma, indicating that NW-trending deformation must be older than 168 Ma (i.e. Mid-Jurassic) in that area.

Conclusions

The sedimentary rocks of the central White-Inyo Range have been subjected to at least two regionally important phases of deformation, each deformation phase being characterized by folds and cleavage which are variably developed throughout the range. A third period of deformation seems to have affected rocks on the western margin of the White Mountains, and may have affected rocks throughout the central White-Inyo Range.

In both the NE and N to NW-trending fold sets, cleavage fans in a divergent pattern about the hinge planes of the folds and maintains a strike sub-parallel to the strike of bedding. The N to NW-trending White Mountain-Inyo anticlinorium defines the large scale

structure of the range, but N to NW-trending folds of all scales are observed. NE-trending folds are older than the N-NW folds, of smaller scale, and are mainly observed in a NW striking belt that crosses the range crest in the saddle between White Mountain and Inyo anticlines.

Six structural basins have been identified as the products of interference between the two fold sets, although no structural domes have been identified. Superimposed folding also offers an explanation for development of the structural saddle (i.e. fold hinge depression) between the White Mountain and Inyo anticlines. The structural basins are abruptly terminated against the Jurassic plutons, and bedding and cleavage are both rotated (maintaining their angular relationship) into concordancy with the Jurassic plutons indicating that the two dominant phases of folding and asociated cleavage formation predate emplacement of the Jurassic plutons.

The NE-trending structures are associated with the deformation observed to the north in the Antler orogenic belt, based on similarity in fold orientation and scale. Formation of the N-NW oriented structures is correlated with movement on the underlying Last Chance thrust. This correlation is based on similarity in orientation of structures in the immediate footwall to the thrust with N to NW-trending structures found throughout the central White-Inyo Range. The change in trend from NW-oriented structures to N-oriented structures is probably an original feature of the regional scale folding that produced the White Mountain-Inyo anticline. This interpretation is consistent with development of the structural saddle between the south-plunging White Mountain anticline and the northwest-plunging section of the Inyo anticline by superimposing the N to NW-trending White Mountain-Inyo anticlinorium on an earlier NE-trending synclinal structure.

The observation that: 1) a structural saddle exists at this location, 2) the NW-trending belt of NE-trending structures crosses the range at the saddle, and 3) the White Mountain-Inyo anticlinorium changes trend at the saddle, leads us to believe that there is a structural control at depth in this area that was certainly active during formation of the N to NW-trending structures, and may previously have influenced the formation and location of the older NE-trending belt of folds.

Based on deformation features observed, both along the western margin of the White Mountains (Welch, 1979) and in the southern Inyo Mountains (Dunne, 1986; Stevens et al., this volume), it is likely that the increase in intensity of the N to NW-trending structures observed on the western margin of the range is associated with a third period of

deformation which post-dates both formation of the NE-trending structures and the N to NW-trending White Mountain-Inyo anticlinorium.

Acknowledgements

The authors gratefully acknowledge discussions with George Dunne, Gary Ernst, Alan Glazner, Clem Nelson, Calvin Stevens and Art Sylvester which have helped to focus their research on the structural evolution of the central White-Inyos. Constructive comments by George Dunne on an earlier draft of the manuscript are gratefully acknowledged. The authors also wish to thank Neil Mancktelow for providing the computer program STEREOPLOT. This project was supported by research grants from the Geological Society of America, Sigma Xi and University of California White Mountain Research Station to S.S. Morgan, and National Science Foundation grants EAR-9018929 and EAR-9506525 to R.D. Law.

References

Corbett K.P., 1989, Structural geology of the Last Chance thrust system, east-central California. Unpubl. PhD dissertation, Univ. California, Los Angeles, 218 p.

Corbett, K.P., Wrucke, C.T., and Nelson, C.A., 1988, Structure and tectonic history of the Last Chance thrust system, *in* Weide, D.L., and Faber, M.L., eds., This extended land, geologic journeys in the southern Basin and Range, Geol. Soc. Amer., Cordilleran Section Guidebook, p. 269-292.

Dunne, G.C., 1986 Mesozoic evolution of southern Inyo, Argus and Slate ranges, in Dunne, G.C., ed., Mesozoic-Cenozoic structural evolution of selected areas, east-central California: Geol. Soc. Amer., Cordilleran Section, Guidebook and volume, fieldtrips 2 and 14, p. 3-22.

Dunne, G.C., Gulliver, R.M., and Sylvester, A.G., 1978, Mesozoic evolution of rocks of the White, Inyo, and Slate Ranges, eastern California, *in* Howell, D.G., and McDougal, K., eds., Mesozoic paleogeography of the western United States: Society of Economic Paleontologists and Mineralogists, Pacific Section, Pacific Coast Paleogeography Symposium 2, p. 189-208.

Ernst, W.G., 1996, Petrochemical study of regional/contact metamorphism in metaclastic strata of the central White-Inyo Range, eastern California: Geol. Soc. Amer. Bull., v. 108, p. 1528 - 1548.

Ernst, W.G., Nelson, C.A., and Hall, C.A., Jr., 1993, Geology and metamorphic mineral assemblages of Precambrian and Cambrian rocks of the central White-Inyo Range, eastern California: California Division of Mines and Geology Map Sheet 46, scale 1:62,500.

Gillespie, J.G., 1979, U-Pb and Pb-Pb ages of primary and detrital zircons from the White Mountains, eastern California [abs.]: Geol. Soc. Amer. Abs. Prog., v. 11, no. 30, p. 79.

Glazner, A.F., and Miller, D.M., in press, Late-stage sinking plutons: Geology, v. 26

Greene, D.C., Schweickert, R.A., and Stevens, C.H., 1997, Roberts Mountains allochthon and the western margin of the Cordilleran miogeocline in the Northern Ritter Range pendant, eastern Sierra Nevada, California: Geol. Soc. Amer. Bull., v. 109, p. 1294-1305.

Hanson, R.B., Saleeby, J.B., and Fates, D.G., 1987 Age and tectonic setting of Mesozoic metavolcanic and metasedimentary rocks, northern White Mountains, California: Geology, v. 15, p. 1074-1078.

Law, R.D., Morgan, S.S., Casey, M., Sylvester, A.G., and Nyman, M., 1992, The Papoose Flat pluton of eastern California: a re-assessment of its emplacement history in the light of new microstructural and crystallographic fabric observations: Trans. Royal Soc. Edinburgh: Earth Sci., v. 83, p. 361-375.

McKee, E.H., and Nelson, C.A., 1967, Geologic map of Soldier Pass Quadrangle: U.S. Geological Survey Geological Quadrangle Map GQ-654, scale1:62,500.

Morgan, S.S. & Law, R.D., 1994, Forceful intrusion of Jurassic plutons in the central White-Inyo Range, eastern California [abs.]: Geol. Soc. Amer.. Abs. Prog., v. 26, No 7, A134.

Morgan, S.S., Law, R.D. & Nyman, M.W., in press, Lacolith-like emplacement model for the Papoose Flat pluton based on porphyroblast-matrix analysis: Geol. Soc. Amer. Bull., v. 110,

Mount, J.F., and Signor, P.W., 1989, Paleoenvironmental context of the metazoan radiation event and its impact on the placement of the Precambrian-Cambrian boundary: examples from the southwestern Great Basin, USA, *in* Christie-Blick, N., and Levy, J., eds., Late Proterozoic and Cambrian tectonics, sedimentation, and record of metazoan radiation in the western United States, Amer. Geophys. Union, Field Trip Guidebook T331, p. 39-46.

McKee, E.H., and Nelson, C.A., 1967, Geologic map of Soldier Pass Quadrangle: U.S. Geological Survey Geological Quadrangle Map GQ-654, scale 1:62,500.

Miller, J., 1996, U/Pb crystallization age of the Papoose Flat pluton, White-Inyo Mountains, California [abs.]: Geol. Soc. Amer.. Abs. Prog., v. 28, no. 5, p. A91.

Nelson, C.A., 1962, Lower Cambrian-Precambrian succession, White-Inyo Mountains, California: Geol. Soc. Amer. Bull., v. 73, p. 139-144.

Nelson, C.A., 1966a, Geologic map of the Waucoba Mountain Quadrangle, Inyo County, California: U.S. Geological Survey Geological Quadrangle Map GQ-528, scale 1:62,500.

Nelson, C.A., 1966b, Geologic map of the Blanco Mountain quadrangle, Inyo County, California: U.S. Geological Survey Geological Quadrangle Map GQ-529, scale 1:62,500.

Nelson, C.A., 1971, Geologic map of the Waucoba Spring quadrangle, Inyo County, California: U.S. Geological Survey Geological Quadrangle Map GQ-921, scale 1:62,500.

Nelson, C.A., 1978, Late Precambrian - early Cambrian stratigraphic and faunal succession of eastern California and the Precambrian-Cambrian boundary: Geol. Mag., v. 115, p. 121-126.

Nelson, C.A., 1980, Guidebook to the geology of a portion of the eastern Sierra Nevada, Owens Valley and White-Inyo Range: Department of Earth and Space Sciences, Univ. California, Los Angeles. ESSSO Guidebook 12, 107 pp.

Nelson, C.A., and Sylvester, A.G., 1971, Wall rock decarbonation and forcible emplacement of Birch Creek pluton, southern White Mountains, California: Geol. Soc. Amer. Bull., v. 82, p. 2891-2904.

Nelson, C.A., Oertel, G., Christie, J.M. and Sylvester, A.G., 1977, Geologic map, structure sections and palinspastic map of the Papoose Flat pluton, Inyo Mountains, California.: Geol. Soc. Amer. Map and Chart Series MC-20.

Nelson, C.A., Hall, C. A., and Ernst, W.G., 1991, Geologic history of the White-Inyo Range, *in* Hall, C.A., ed., Natural History of the White-Inyo Range eastern California: Berkeley and Los Angeles, California, Univ. California Press, p. 42-74.

Oldow, J.S., 1984, Spatial variability in the structure of the Roberts Mountains allochthon, western Nevada: Geol. Soc. Amer. Bull., v. 95, p. 174-185.

Paterson, S.R., Brudos, T., Fowler, K., Carlson, C., Bishop, K and Vernon, R.H., 1991, Papoose Flat pluton: forceful expansion or post-emplacement deformation?: Geology, v. 19, p. 324 - 327.

Ramsay, J.G., 1967, Folding and fracturing of rocks: New York, McGraw-Hill, 568 p.

Renne, P.R., and Turrin, B.D., 1987, Constraints on the timing of deformation in the Benton Range, southeastern California, and implications for Nevadan orogenesis: Geology, v. 15, p. 1031-1034.

Ross, D.C., 1967a, Geologic map of the Waucoba Wash Quadrangle, Inyo County, California: U.S. Geological Survey Geological Quadrangle Map GQ-612, scale 1:62,500.

Ross, D.C., 1967b, Generalized geologic map of the Inyo Mountains region, California: U.S. Geological Survey Miscellaneous Geological Investigations Map I-506, scale 1:125,000.

Snow, J.K., 1992 Large magnitude Permian shortening and continental margin tectonics in the southern Cordillera: Geol. Soc. Amer. Bull., v. 104, p. 80-105.

Stevens, C.H. & Olson, R.C. 1972 Nature and significance of the Inyo thrust fault, eastern California. Geol. Soc. Amer. Bull., v. 83, p. 3761 - 3768.

Stevens, C.H., Stone, P., Dunne, G.C., Greene, D.C., Walker, J.D., and Swanson, B.J., this volume, Paleozoic and Mesozoic evolution of east-central California: in Ernst, W.G., and Nelson, C.A., eds., Integrated Earth and environmental evolution of the southwestern U.S.: International Geology Review.

Stewart, J.H., Ross, D.C., Nelson, C.A., and Burchfiel, B.C., 1966, Last Chance thrust - A major fault in the western part of Inyo County, California: U.S. Geological Survey Professional Paper 550-D, p. D23-D34.

Stewart, J.H., and Suczek, C.A., 1977, Cambrian and latest Precambrian paleogeography and tectonics in western United States, *in* Stewert, J.H., Stevens, C.H., and Fritsche, A.E., eds., Paleozoic paleogeography of the western United States: Society of Economic Paleontologists and Mineralogists, Pacific Section, Pacific Coast Paleogeography Symposium 1, p. 1-18.

Sylvester, A.G., and Babcock, J.W., 1975, Significance of multiphase folding in the White-Inyo Range, eastern California [abs.]: Geol. Soc. Amer.. Abs. Prog., v. 7 p. 1289.

Sylvester, A.G., Miller, C.F., and Nelson, C.A., 1978, Monzonites of the White-Inyo Range, California, and their relation to the calc-alkalic Sierra Nevada batholith: Geol. Soc. Amer. Bull., v. 89., p. 1677-1687.

Welch, T.C., 1979, Superposed Mesozoic deformations in the southern White Mountains, eastern California [abs.]: Geol. Soc. Amer.. Abs. Prog., v. 11, p. 134-135.

Williams, P.F., 1985, Multiply deformed terrains-problems of correlation: J. of Struct. Geol., v. 7, p. 269-280.

Chapter 2. Aureole deformation associated with inflation of the concordant Eureka Valley-Joshua Flat-Beer Creek composite pluton, central White-Inyo Range, eastern California

Field Trip Road Log Included

SVEN S. MORGAN, RICHARD D. LAW

Department of Geological Sciences, Virginia Tech, Blacksburg, VA 24061

MICHEL DE SAINT BLANQUAT

CNRS - Laboratoire de Pétrophysique et Tectonique, Université Paul Sabatier, Toulouse, France

This is an edited version from a GSA guidebook article published under the same title. Aureole deformation associated with inflation of the concordant Eureka Valley-Joshua Flat-Beer Creek composite pluton, central White-Inyo Range, eastern California: 1998, Guidebook to field trip #5, GSA annual meeting, Cordilleran Section, Published by California State University Long Beach, Department of Geological Sciences, p. 5-1 to 5-30.

Introduction

The mechanisms by which plutons are emplaced in the crust have been the subject of an ongoing debate for over 200 years. This long debate is due, in part, to the fact that many plutons are not surrounded by deformed, concordant aureoles and, in part, because there have been relatively few studies on the full strain (shape change, volume change, rotation, and rigid body translation) within deformed aureoles surrounding plutons. Consequently, resolving the pluton-emplacement problem has dominantly been left to the examination of internal-plutonic fabrics (foliation and lineation). But pluton fabrics do not record translation, nor can they record the rotation of the surrounding wall rocks. Therefore, plutons with deformed aureoles need to be studied because wall rocks, especially sedimentary wall rocks, are much better recorders of the full strain and consequently the mechanisms that facilitated emplacement of plutons.

The central White-Inyo Range in eastern California (Fig. 4) has been an excellent field area to study concordant (deformed aureoles) and discordant, or "cookie cutter" plutons (see Nelson and Sylvester, 1971; Sylvester et al, 1978a; Bilodeau and Nelson, 1993; Paterson et al., 1991; Law et al., 1992, 1993; Morgan and Law, 1994; Morgan et al., 1998), because: 1) the range is dominantly composed of a well-mapped sedimentary section where the dominant compressive regional deformation pre-dates emplacement of the plutons, and 2) the plutons are well exposed at various structural levels.

One of the oldest and largest plutons in the central White-Inyo Range is the Jurassic (180-160 Ma) Eureka Valley-Joshua Flat-Beer Creek (EJB) composite pluton, which is surrounded on three sides by an aureole of penetratively deformed metasedimentary rocks belonging to a succession of Lower - Upper Cambrian formations (Fig. 4). The northern margin of the EJB pluton is cross-cut by the younger Cottonwood Pluton (Nelson, 1997). Description and examination of the deformation mechanisms which accommodated the emplacement of the EJB pluton, along with a characterization of the contact metamorphism, are the main foci of this paper and field trip. We also present maps of the magnetic foliation and lineation determined from measurement of the anisotropy of magnetic susceptibility (AMS) of oriented drill-cores taken from within the EJB pluton. Finally, we discuss our model for forceful emplacement of the EJB pluton which combines the internal magnetic fabrics with the deformation and metamorphism in the structural aureole.

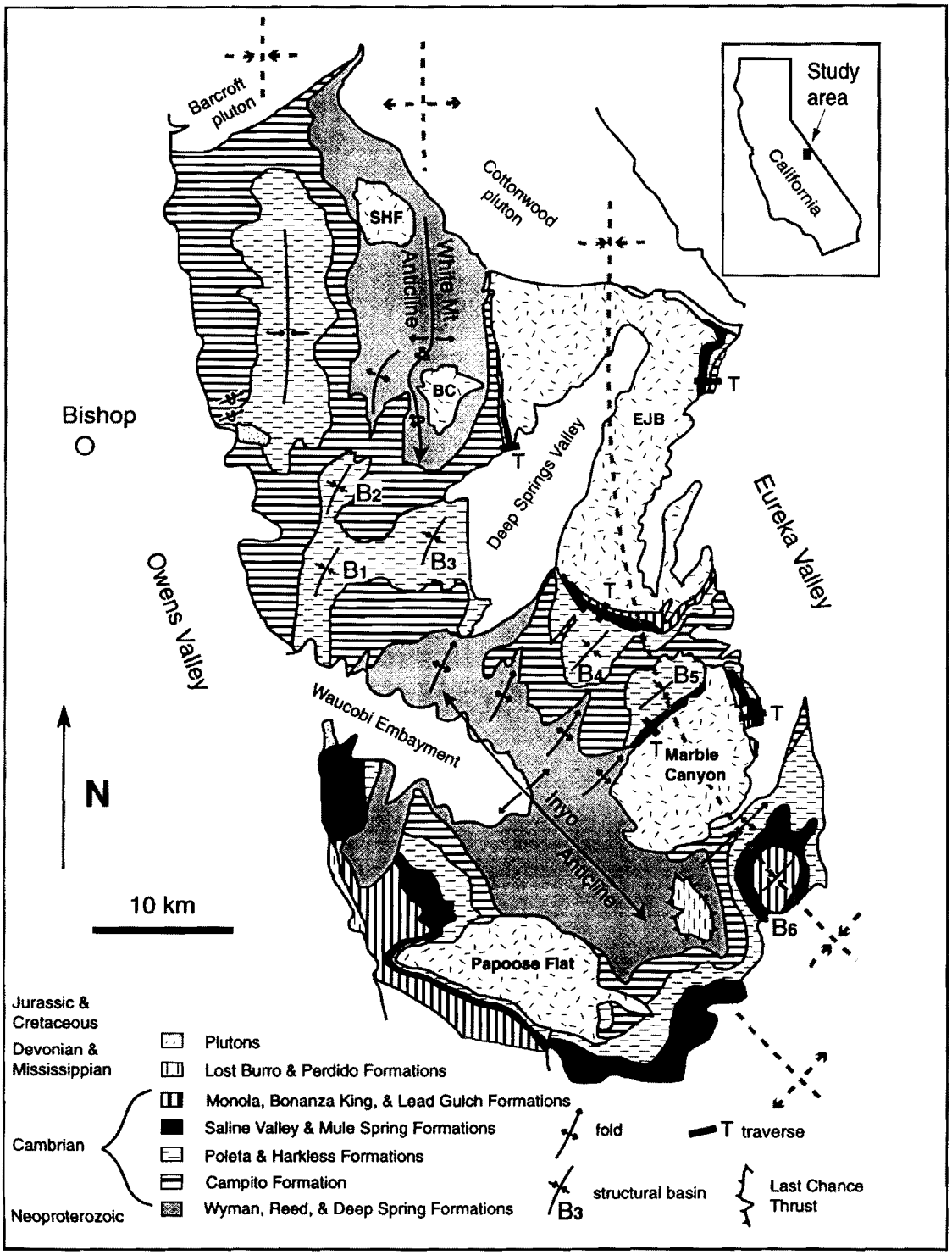

Figure 4. Simplified geologic map of the central White-Inyo Range. BC = Birch Creek pluton, EJB = Eureka Valley-Joshua Flat-Beer Creek composite pluton, SHF = Sage Hen Flat pluton. After Nelson et al., (1991) and Morgan and Law (1998).

The term, "concordant" is used to describe an igneous intrusion which possesses contacts which are parallel to foliation or bedding in the country rocks (Jackson, 1997). The EJB pluton is surrounded by Lower to Upper Cambrian metasedimentary rocks which in the pluton aureole are deflected into sub-parallelism with the pluton margin. Although we use the term "concordant" to describe the EJB pluton, this does not necessarily imply that the EJB pluton margin stays within a specific stratigraphic horizon at the finer scale. For example, 1:62,500 scale mapping by Nelson (1966b, 1971) illustrates that the pluton-wall rock contact, if traced 22 km southwards along the western margin of the EJB pluton, and then eastwards along the southern margin, cuts up stratigraphic section approximately 3 km (regional stratigraphic thicknesses used) from the Lower Cambrian Campito Formation to the Upper Cambrian Lead Gulch Formation. In contrast, the pluton-wall rock contact also remains within two formations (the Bonanza King and Lead Gulch formations) for 16 km along the southern and southeastern margin. The use of the term "concordant" remains a warmly debated subject between the authors of this paper.

The EJB pluton is situated in a structural trough, i.e., the sedimentary formations surrounding the pluton all rotate downward as the contact is approached and young towards the pluton (Fig. 5). Bedding is commonly subvertical and often overturned within 1 km from the pluton-contact. Approximately the same geologic situation exists surrounding the Jurassic (180-160 Ma) Marble Canyon pluton located 5 km to the south. We interpret this structural relationship as an exposure of the lower to middle portions of these plutons and surrounding aureoles, whereas the two Cretaceous plutons in the range are exposed closer to their tops. The Cretaceous Papoose Flat pluton (~83 Ma, Miller 1996) and Birch Creek pluton (Fig. 4) are also surrounded by concordant aureoles, yet the stratigraphy rotates upward towards their contacts. We believe that roughly the same forceful emplacement mechanism operated to create the structural aureoles surrounding all of these plutons, although they are exposed at different structural levels.

The late Jurassic (~141 Ma) Sage Hen Flat pluton is the "cookie cutter" pluton in the central White-Inyo Range, with no deflection of the stratigraphy at its margins, although it is surrounded by a contact metamorphic aureole. We make the distinction between a structural aureole, which is the volume of country rock adjacent to a pluton where the compositional layering begins to become deflected into sub-parallelism with the pluton contact, and the metamorphic aureole, which is the volume of sedimentary rock which has undergone new growth of minerals in association with the thermal pulse of the

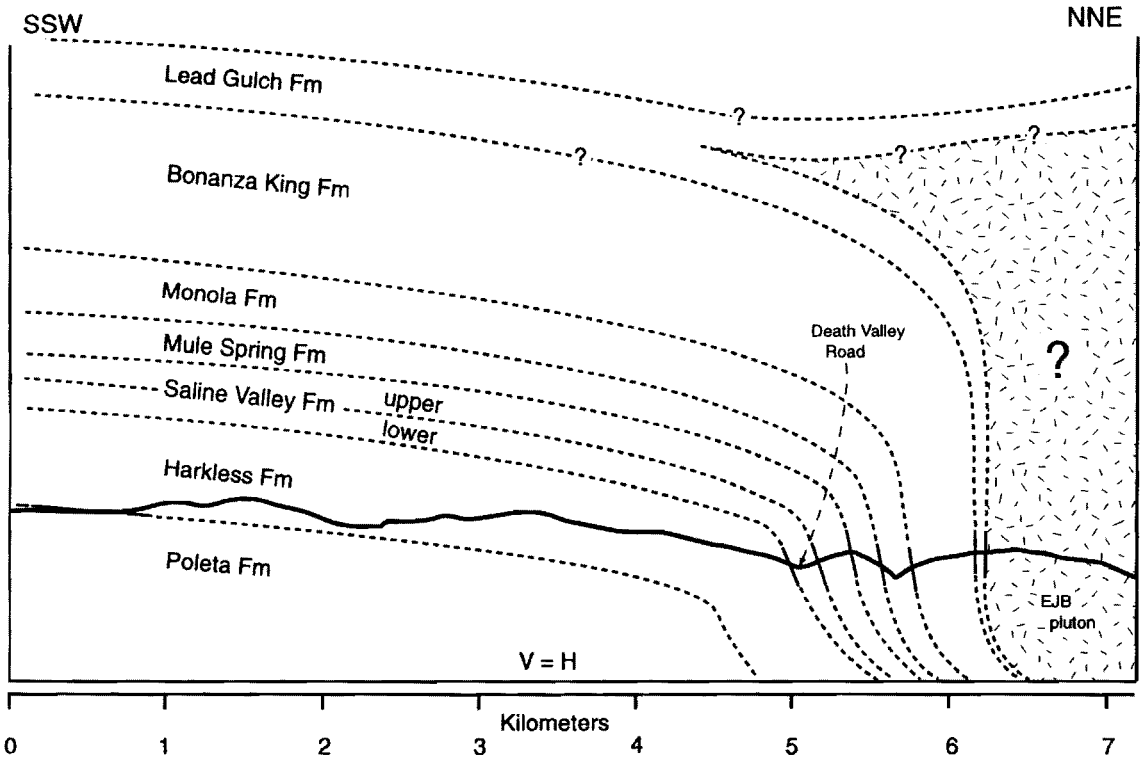

Figure 5. Cross-section across the southern margin of the EJB pluton illustrating the rapid rotation of stratigraphy into concordancy with the pluton and the attenuation of the sedimentary section within the structural aureole. Thickness of the Cambrian formations is projected to increase to a maximum away from the contact based on the measured regional stratigraphic thickness of Nelson (1976), Moore (1976), and Mount and Signor (1989). Note that the Harkless Formation dips down and out of the page between 15 and 65°. Geology based on the 1:62,500 Waucoba Spring geologic quadrangle map of Nelson (1971).

magma. This distinction is useful because the metamorphic aureole extends beyond the structural aureole surrounding the EJB pluton.

Regionally developed structures are sharply deflected at the EJB pluton margin and the concordant Cambrian formations which define the aureole are metamorphosed and intensely attenuated. The deformation and metamorphism within the structural aureole are synchronous, yet distinct periods of deformation versus new mineral growth can be distinguished. We have examined the deformation in the EJB structural aureole through mapping, examining outcrops, and collecting samples throughout the zone of concordancy. We have also studied the rocks in detail along three traverses across the structural aureole (Fig. 4). In all three traverses across the structural aureole, stratigraphic sections are shortened between 60 and 70% compared to their regional thicknesses. This attenuation has been accommodated dominantly by ductile, bulk coaxial deformation, with several deformation mechanisms operating at different scales. Localized simple shear is also an important process, at both the micro- and macro-scale, but it appears to have accommodated more of a larger-scale, bulk, pure shear. Both micro- and macro-scale deformation mechanisms are discussed below.

This intense aureole shortening only accommodates a fraction of the volume necessary to emplace the EJB pluton. The vast majority of the space needed to accommodate emplacement of the pluton is produced by translation and rotation of the structural aureole, and probably by uplift of the roof. We have some control on the kinematics of the translation and rotation of the aureole formations based on mapping the deflection of bedding and pre-existing cleavage in the country rocks, which we use as strain markers.

The central White-Inyo Range has been mapped at the 1:62,500 scale under the auspices of the U.S. Geological Survey (Nelson 1966a & b; McKee and Nelson 1967; Ross, 1967a; Nelson 1971) and we have used these maps extensively in our study. A regional account of the geologic evolution of east-central California can be found in Stevens et al., (1997) and an overview of the regional deformation within the central White-Inyo Range can be found in Morgan and Law (1998).

Rock Descriptions

Plutonic rocks

The EJB pluton was originally mapped as three separate igneous bodies (Fig. 6) (Nelson, 1966a & b; McKee and Nelson, 1967; Nelson 1971, Nelson et al., 1991) which vary widely in composition (Miller, 1978; Sylvester et al., 1978b; Bateman, 1992). Based on cross-cutting field relationships, Sylvester et al. (1978b) suggested the following intrusive sequence from oldest to youngest: 1) Eureka Valley monzodiorite (EVM), 2) Joshua Flat monzonite (JFM) and, 3) Beer Creek quartz monzonite (BCM). Radiometric dating indicates that all three intrusive bodies are of Jurassic age, but individual radiometric ages from the three bodies overlap (Table 1). The Cottonwood pluton, which cross-cuts both the BCM and JFM along the northern margin of the EJB pluton (Nelson, 1997), has two U-Pb (zircon) ages of 168 and 172 Ma (see references in Table 1).

In contrast to the observations of Sylvester et al. (1978b), we conclude that the contacts between the JFM and the BCM are not always clearly defined and that relative ages between the JFM and the BCM are unclear. Contact relationships of the JFM and the BCM with the EVM are the clearest and demonstrate that the EVM is the oldest intrusive; enclaves of EVM are observed within the surrounding igneous bodies. The EVM is also the most mafic of the three intrusives and its composition varies between monzodiorite and monzonite (Sylvester et al., 1978b), although irregular sized bodies of hornblendite and gabbro are also present. The EVM is easily recognizable in the field because of its dark weathering color. The contact relations between the other two intrusives, the JFM and the BCM, are not as clear and at many outcrops it is difficult to distinguish between the two units. The JFM varies in composition between monzonite and quartz monzonite (Sylvester et al., 1978b; Bateman, 1992 p. 170). The BCM is compositionally closer to a true granite, but also varies in its mineralogy (Bateman, 1992 p. 172). The amount of mafic minerals changes abruptly from one outcrop to the next and distinct cm- to meter-scale banding of felsic and slightly more mafic layers is common near mapped contacts. We currently prefer the interpretation that the Joshua Flat and Beer Creek monzonites are gradational between distinct end-member compositions. In summary, our field observations indicate that both magmas had not crystallized fully at the time the contact developed between the JFM and BCM.

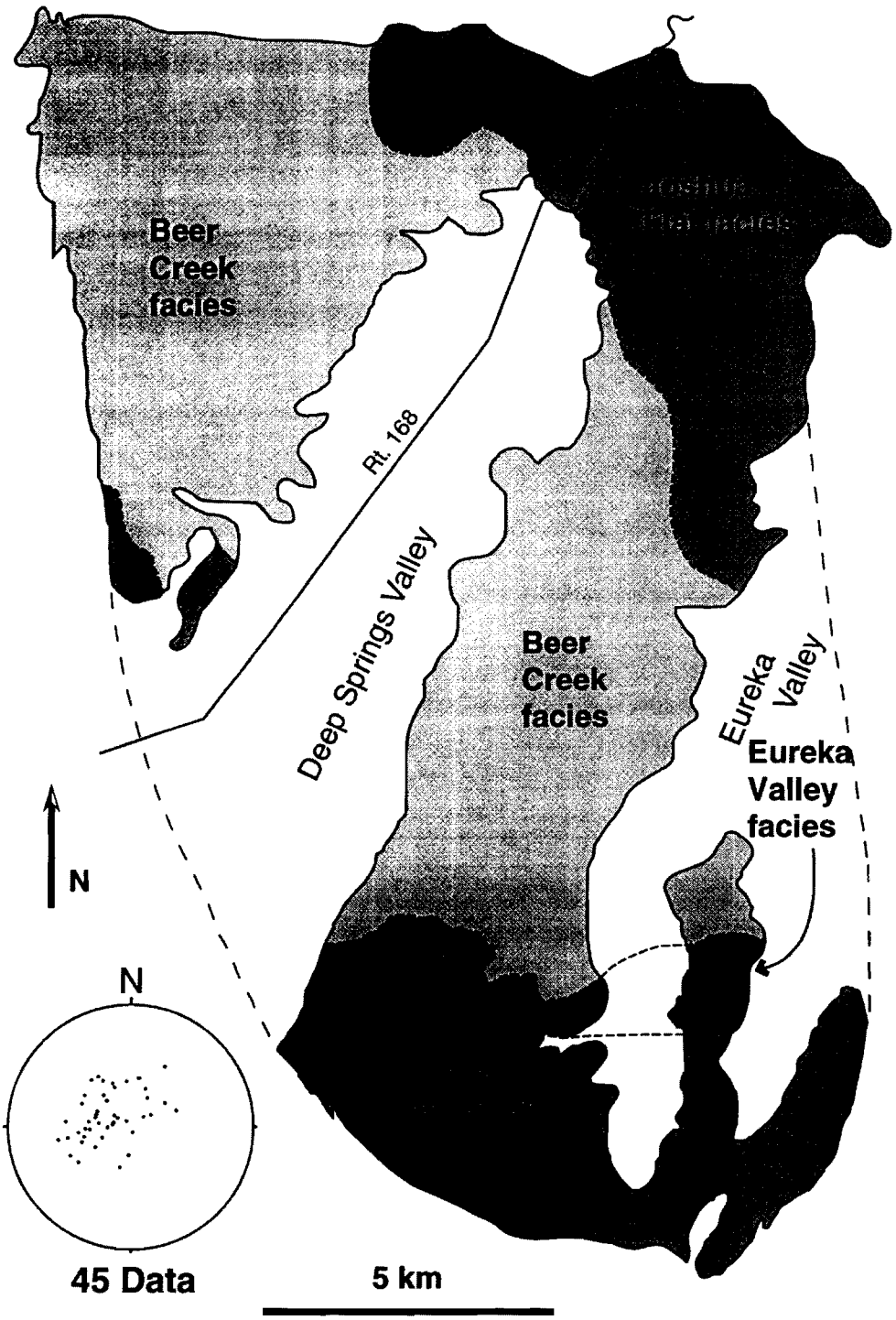

Figure 6. Simplified geologic map of the igneous contacts within the EJB pluton and stereonet of mineral lineations measured within the structural aureole and at the margin of the EJB pluton. Map modified after Nelson et al., (1991).

Pluton	Age	Method	Reference
Cottonwood pluton	168 Ma, 172 Ma	U-Pb, zircon	Stern et al. 1981 *
	162 Ma	K-Ar, biotite	McKee & Nash 1967*
	170 Ma	K-Ar, hornblende	Crowder et al. 1973 *
	149 Ma	K-Ar, biotite	Crowder et al. 1973 *
	175 Ma	K-Ar, hornblende	McKee & Conrad 1996 *
Beer Creek pluton	161 Ma, 180 Ma	U-Pb, zircon	Gillespie 1979
	151 - 170 Ma	K-Ar, biotite	McKee & Nash 1967
	158 Ma	K-Ar, hornblende	McKee & Nash 1967
	170 Ma	K-Ar, biotite	McKee 1968
	174 Ma	K-Ar, biotite	Evernden & Kistler 1970
Joshua Flat pluton	173 Ma, 178 Ma	U-Pb, zircon	Sylvester et al. 1978b
	157 - 175 Ma	K-Ar, biotite	McKee & Nash 1967
	172 - 178 Ma	K-Ar, hornblende	McKee & Nash 1967
Eureka Valley pluton	163 - 171 Ma	K-Ar, biotite	McKee & Nash 1967

* sample locality details discussed in Nelson (1997).

Table 1. Summary of isotopic ages obtained from the Cottonwood pluton and the Eureka Valley-Joshua Flat-Beer Creek composite pluton.

Characteristic outcrops of the BCM are observed on the western side of Deep Springs Valley (Fig. 6), where it is pink to light colored, medium to fine grained and closest to a true granite in composition. Representative outcrops of the JFM are observed along the southern margin of the pluton where it is gray to dark colored, medium grained with euhedral megacrysts of elongate plagioclase and potassium feldspar and smaller, anhedral phenocrysts of augite with hornblende rims. The JFM is also characterized by large light brown crystals of accessory sphene, visible in hand sample.

At many outcrops, especially within 1-2 km from the southern pluton-wall rock contact, a well developed foliation and lineation is defined by 2-3 cm long euhedral tabular plagioclase and K-feldspar phenocrysts and aligned hornblende phenocrysts. The foliation is steeply dipping to subvertical and subparallels the contact. The lineation lies within the foliation and is also subvertical. The phenocrysts waver in their alignment and seem to be floating in a matrix that is not sheared. Quartz is often xenomorphic (the quartz grain outline fits into the spaces between other phases), and biotite and quartz exhibit little deformation: there are no pressure shadows surrounding the feldspar phenocrysts. Based on these observations, we (Morgan and Law, 1994), as well as Stein (1994) and Stein and Paterson (1996), interpret this foliation as developing in the magmatic state.

Sedimentary Rocks

The Neoproterozoic to Middle Cambrian sedimentary section found throughout the central White-Inyo Range is over 7,000 m thick and forms part of the Cordilleran passive margin sequence which developed on the western margin of the rifted North American craton. A stratigraphic column of the White-Inyo sedimentary sequence can be found in Fig. 7. The section is dominated by siltstone, sandstone, limestone, and dolomite deposited in shallow water environments. Detailed descriptions of the sedimentary rocks in the central White-Inyo Range can be found elsewhere (Nelson, 1962, 1978; Mount and Signor, 1989), but in general, the Neoproterozoic to lower Cambrian passive margin sequence thickens to the NW (Stewart, 1966), defining a NE trending paleo-continental margin (Stewart and Poole, 1974, Stevens et al., 1997). The Lower Cambrian portion of this section, originally described by Walcott (1895, 1908) and referred to as the Waucoban Series, is regarded as the type section in North America for rocks of this age, in part due to a relative abundance of fossils including the oldest trilobite faunas in the Americas (Nelson

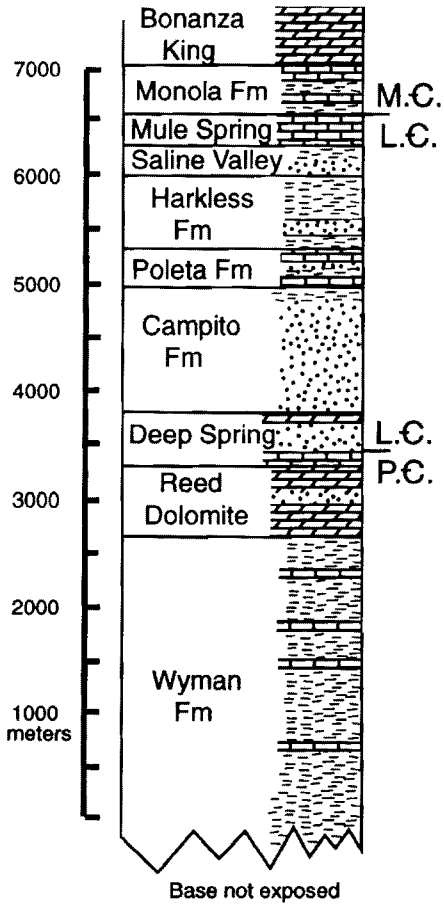

Figure 7. Simplified stratigraphic column of the Neoproterozoic to Cambrian section found in the central White-Inyo Range. After Nelson et al., (1991).

et al., 1991). The boundary between the Proterozoic and the Cambrian is currently believed to be located between the lower and the middle Deep Spring Formation (J. Mount, pers. com., 1997).

Aureole Metamorphism

The metamorphism in the aureole of the EJB pluton was first investigated by Nash (1962) who studied the mineral assemblages at the western margin of Deep Springs Valley (Fig. 4). Nash concentrated his studies on the skarn, but also examined assemblages across the aureole. Away from the skarn, the contact metamorphism associated with intrusion of the EJB pluton is similar to a regional metamorphic/orogenic event in that deformation is associated with the thermal event. A high degree of attenuation of the metasedimentary section accompanied the contact metamorphism and a well defined contact-parallel foliation can be mapped around three sides of the pluton. The foliation is sub-parallel to what we interpret as original compositional layering, and contacts between primary sedimentary units can be mapped throughout the aureole despite the metamorphism and intense deformation (Nelson, 1966a & b; McKee and Nelson, 1967; Nelson 1971, Morgan and Law, 1994).

South of the EJB pluton, the Harkless Formation can be traced in a linear belt which strikes perpendicular to the margin of the pluton for 6 km (Fig. 4). Moving towards the north, the first effects of contact metamorphism are observed at 2.9 km from the pluton where clots of biotite and two other kinds of porphyroblasts, now completely retrograded to white micas, are observed in slate. Approaching the pluton, biotite remains the only preserved porphyroblast until 1.1 km from the contact where the Harkless Formation is metamorphosed into a coarse grained schist and andalusite is first observed. At this point, the Harkless Formation is also rotated horizontally from its pluton margin-perpendicular strike into concordancy with the pluton-contact. At the very southern margin of the pluton, the formations defining the inner-most structural aureole are dominated by marbles and calc-silicate assemblages.

Along the western margin of the EJB pluton, Nash (1962) observed andalusite at a maximum distance of 1.4 km from the pluton contact. We, as well as Nash, first observe sillimanite (coarse grained and fibrolite) at distances of 330 m from the western contact where it co-exists with andalusite right up to the pluton-contact. Within this zone,

andalusite is commonly altered and surrounded by fresh looking biotite. Fibrolite and sillimanite are fresh looking and also associated with the new biotite, and sillimanite does not appear to be a polymorphic replacement of andalusite. The association of biotite with fibrolite in contact aureoles is not unique (Pitcher and Read, 1963; Kerrick, 1987). Fibrolite is more common than sillimanite, and defines shear bands that cross-cut the earlier foliation at low angles. Within a few meters of the contact along the western margin of the pluton, as well as along most of the southern margin, a calc-silicate skarn assemblage is well developed since the pluton-contact is often within calcareous metasedimentary units. Grossular, epidote, wollastonite, diopside, serpentine, fosterite, calcite and dolomite are some of the common minerals (Nash, 1962).

Kyanite was observed at one location along the western margin of the pluton within a sample of quartzite collected at 700 m from the contact. Kyanite was also observed within the aureole at the NE margin of the pluton within three quartzite samples, all located closer (200 m) to the pluton contact than the andalusite + sillimanite assemblage (250 m). Cordierite and muscovite were also observed in several samples within several hundred meters of the contact on both the western and eastern margins.

Within 10 m of the southwestern pluton-contact (southeast Deep Springs Valley) evidence for partial melting exists. Here, the pluton is in contact with pelitic schists. Millimeter-thick layers of igneous-like K-feldspar and quartz are observed. The grains of K-feldspar in these layers are much coarser than in the surrounding schist, they are concentrically zoned, and the quartz is xenomorphic, a textural relationship that Pattison and Harte (1988) used as evidence for partial melting in the aureole of the Ballachulish granite, Scotland. Primary muscovite, along with sillimanite, is observed right up to the contact, indicating that pressures were above the reaction; muscovite + quartz = k-feldspar + sillimanite. The observation that andalusite and sillimanite are the dominant alumino-silicate phases, yet kyanite is also locally observed, suggests that the pressure during metamorphism was close to, but below the alumino-silicate triple point, commonly believed to be close to or slightly above 4 kb (Holdaway, 1971; Pattison, 1992). Given these pressure constraints, and the textural evidence indicating that metamorphic conditions progressed from the andalusite stability field into the sillimanite stability field, temperatures of metamorphism for much of the aureole were probably between 500 to 600°C (depending on the triple point used), and over 650°C in the zone of partial melting. This places the contact metamorphism surrounding the EJB pluton into the Facies Series 2 of Pattison and Tracy (1991).

Regional Deformation

In this section we outline the regional deformational events and discuss why we believe that the EJB pluton intruded into pre-existing regional scale structures. A detailed account of the regional structures and geologic history can be found in Stevens et al., (1997) and Morgan and Law (1998). Compressional deformation of the central White-Inyo Range primarily occurred during two periods of folding, both of which are associated with development of slaty cleavage. Both sets of folds are mostly open and upright and Charles Walcott noted the similarity between the style of folds in the central White-Inyo Range and the Appalachian fold and thrust belt during his field seasons in the 1890's (Walcott, 1895b; Yochelson and Nelson, 1994). Both of these folding events predate emplacement of the Jurassic plutons and are interpreted to be associated with middle and late Paleozoic thrusting (Sylvester and Babcock, 1975; Morgan and Law, 1998).

The dominant and larger-scale fold set trends N to NW, and the central White-Inyo Range is defined by the N to NW-trending White-Inyo anticlinorium which can be traced for over 70 km along its axis. The trend of the mountain range is roughly parallel to the trend of the anticlinorium. The range-dominant fold structure is the White Mountain-Inyo anticline which is well defined in map view (Fig. 4). A less well defined syncline, which forms the eastern fold pair to the White Mountain-Inyo anticline, is also outlined in Figure 4. Development of this regional-scale syncline deformed earlier, smaller-scale NE-trending folds and produced a series of structural basins and anticlinal ridges (Morgan and Law, 1998). The EJB and Marble Canyon plutons were intruded along the axis of this syncline (Fig. 4). We hypothesize that these plutons actually intruded into the fold interference structures, initially intruding into structural basins.

On the very western margin of the southern White Mountains, N to NW-oriented folds are much tighter, locally overturned, and possibly overprinted by folds with a similar orientation (Welch, 1979). This later event only seems to have deformed the sedimentary section on the western margin of the range and is associated with the East Sierran Thrust System and emplacement of the Sierran plutons (Dunne, 1986). This thrust system is better developed in the southern Inyo Mountains and is dominantly Jurassic in age.

There are two reasons why we believe that the two periods of folding and cleavage development which produced the dominant structures throughout the central White-Inyo

Range pre-date emplacement of the EJB and Marble Canyon plutons. First, both plutons cross-cut structural basins produced by the interference of two periods of folding. The most obvious basin is labeled B_6 in Fig. 1 and is circular in map pattern. Basins B_4 and B_5 are circular except where they are in contact with the two plutons, where their shapes are truncated by the plutons. Bedding planes of sedimentary units within the basins have moderate dip angles, except where the stratigraphic units come into close (2 km) contact with the plutons. Secondly, as described in more detail below (see *Rotation and translation of the aureole metasedimentary formations*), the regionally developed slaty cleavage fabric south of the EJB pluton was passively rotated and translated as bedding was deformed into concordancy with the EJB pluton. The angular relationship between bedding and cleavage is preserved, although both are rotated and translated, suggesting that the cleavage was in existence prior to pluton emplacement.

Traverses

The rocks in three traverses across the structural aureole of the EJB pluton and in two traverses across the structural aureole of the Marble Canyon pluton have been studied in detail. Traverses discussed in this paper are located on the western margin (Fig. 8a), on the southern margin (Fig. 8b), and on the northeastern corner (Fig. 8c) of the EJB pluton (Fig. 4). Samples were taken at regular intervals and stratigraphic sections were described and measured in detail through the deformed and metamorphosed Cambrian sequences. Stratigraphic sections were also measured on the eastern and western margins of the Marble Canyon pluton. The measured thicknesses of individual formations within the structural aureoles of both plutons are compared with their undeformed regional thickness' in Table 2.

The sedimentary section surrounding the EJB pluton is slightly overturned in the western and southern traverses and sub-vertical in the northeast traverse. Regardless of position around the EJB aureole, attenuation of the sedimentary formations within the structural aureole is roughly the same amount, between 60 and 70%. The attenuation of the sedimentary formations in the Marble Canyon aureole varies more between the two traverses (83% shortening versus 50%), but there is a greater lithologic contrast between

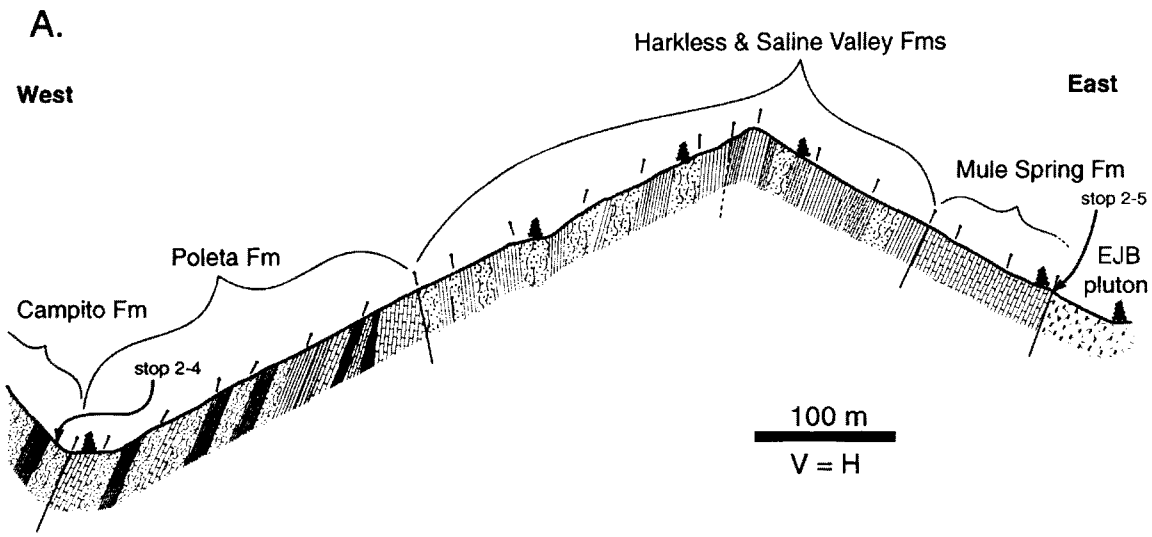

Figure 8a. Cross section of the stratigraphic section measured through the structural aureole along the western traverse, western margin, EJB pluton. Note that the sedimentary section is overturned. For location see Fig. 4. Stop 2-4 and 2-5 correspond to the road log.

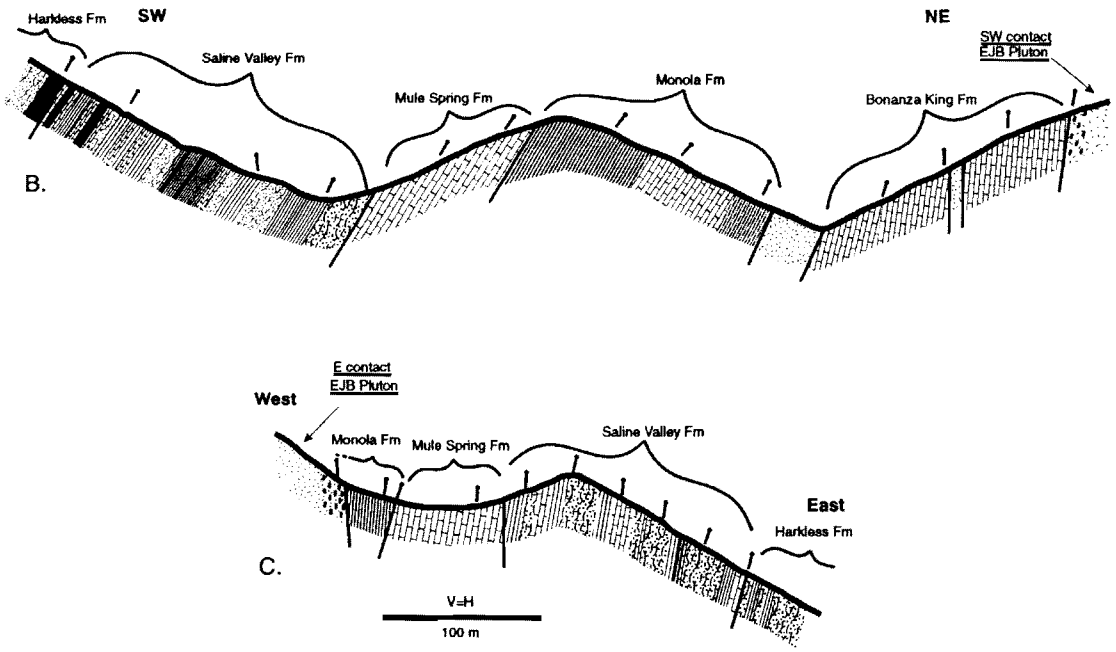

Figure 8b & c. Cross sections of the stratigraphic sections measured through the structural aureole along the southern (b) and eastern (c) traverses. Note that the sedimentary section in the southern traverse is overturned. For locations see Fig. 4.

Cambrian formations	Traverses: EJB pluton aureole western margin	EJB pluton aureole southern margin	EJB pluton aureole eastern margin	Marble Canyon pluton aureole western margin	Marble Canyon pluton aureole eastern margin
aureole thickness		**110m**			**70m**
Monola Fm					
regional thickness	400m - ----	400m - ----	400m - ----	400m - ----	400m - ----
aureole thickness		**37m**	**64m**		**51m**
Mule Spring Fm					
regional thickness	300 - 210m	300 - 210m	300 - 210m	300 - 210m	300 - 210m
aureole thickness	**240m***	**170m**	**158m**	**143m**	
Saline Valley Fm					
regional thickness	*Saline & Harkless combined	275 - 300m	275 - 300m	275 - 300m	275 - 300m
aureole thickness					
Harkless Fm					
regional thickness	925 - 950m*	650 - 650m	650 - 650m	650 - 650m	650 - 650m
aureole thickness	**134m**				
Poleta Fm					
regional thickness	350 - 250m	350 - 250m	350 - 250m	350 - 250m	350 - 250m
combined formations regional thickness	1275-1200m	975-910m	575-510m	275-300m	700m - ---
combined formations aureole thickness	**374m**	**317m**	**222m**	**143m**	**121m**
% shortening	**71 - 69%**	**67 - 65%**	**61 - 56%**	**48 - 52%**	**83% - —**

* The contact between the Harkless Fm and the Saline Valley Fm was not determined

Table 2. Thickness of formations measured along traverses within the structural aureole of the EJB and Marble Canyon plutons compared to their regional thicknesses. The first number representing the regional thickness of the formation is taken from Nelson (1976), the second number is from Mount & Signor (1989). See Fig. 1 for location of traverses.

the two traverses through the Marble Canyon aureole than between the three traverses through the EJB aureole.

These data are an accurate and quantitative measurement of the penetrative strain that occurred within the aureole during emplacement of the EJB and Marble Canyon plutons. Such data are usually lacking within structural aureoles. We know of only one other structural aureole where stratigraphic sections, and therefore accurate finite strains, have been measured, and that aureole surrounds the Papoose Flat pluton (Sylvester et al., 1978a), also located within the Inyo Mountains (Fig. 4). Typically, strain associated with the emplacement of plutons is measured by analyzing the shapes of enclaves within plutons (Holder, 1979; Courrioux, 1987; Ramsay, 1989; John and Blundy, 1993), which entails several assumptions concerning the physical state and relative viscosities of the magma versus the enclave at the time of deformation. Aureole strains have been much more difficult to measure, and the one study we are aware of (excluding the measuring of stratigraphic sections) used the preferred orientation of andalusite porphyroblasts to calculate finite strains (Sanderson and Meneilly, 1981), a technique which involves many assumptions.

Whole rock chemical analyses of the sedimentary formations, within and outside of the EJB aureole, are currently being determined by Allen Glazner at U.N.C Chapel Hill, to investigate the possibility of volume loss associated with the penetrative strain. An understanding of the volume loss will help to complete a full deformational analysis of the rocks within the aureole. A similar study was conducted on the sedimentary rocks within and exterior to the concordant aureole surrounding the Cretaceous age Papoose Flat pluton, located 22 km southwest of the EJB pluton (Fig. 4), and no volume loss was recorded there (Morgan et al., 1998).

We also note that the sedimentary formations surrounding the EJB pluton have maintained their stratigraphic continuity despite the intense attenuation, documenting the ductile nature of the deformation. Individual formations and contacts within the aureole are still, for the most part, mappable (Nelson, 1966a & b; McKee and Nelson, 1967; Nelson, 1971, Morgan and Law, 1994) and were thinned relatively uniformly even though the rocks have been subjected to sillimanite grade contact metamorphism and attenuated to one-third of their original thickness.

Deformation of the Aureole Rocks

Rotation and translation of the aureole metasedimentary formations

The Cambrian sedimentary section surrounding the EJB pluton stratigraphically youngs into the pluton from the east, west, and southern margins. This stratigraphic symmetry defines a structural basin, first described by Nelson et al., (1991). The EJB pluton is situated within this structural basin, and the same structure exists surrounding the Marble Canyon pluton, 5 km to the south.

Even though the structural aureole of the EJB pluton is clearly defined by the contact-parallel strike of Lower to Upper Cambrian formations surrounding the pluton, the width of the structural aureole is narrow given the dimensions of the pluton. As well, the change from the regional structural grain into concordancy occurs over a very short distance (Fig. 5 & 9a). The abrupt change into concordancy is best observed at the southern margin of the pluton where the regional N-S strike of bedding is sharply deflected adjacent to the pluton margin (Fig. 10). At 2 km from the pluton-wall rock contact, bedding begins to rotate and steepen from its N-S strike (and moderate dip) into parallelism with the contact. At 1 km from the pluton, bedding is subparallel to the contact.

This structural aureole lies within the greater metamorphic aureole, and the region where bedding has been rotated and translated enough to become sub-parallel to the pluton-contact roughly coincides with andalusite isograd. The first effects of contact metamorphism are noticeable at 2.9 km from the contact where clots of biotite are observed, yet the strike of bedding does not begin to rotate until 2 km from the contact, and true concordancy is not obtained until a distance of 1 km from the contact where andalusite is first observed.

We have some control on the components of rotation and translation of bedding as it is deformed into concordancy south of the EJB pluton by using the orientation of bedding and cleavage and the orientation of the bedding/cleavage intersection lineation. Based on our regional mapping, we assume that both bedding and cleavage were N-S striking prior to the emplacement of the EJB pluton, so that the cleavage-bedding intersection lineation was subhorizontal and N-trending prior to emplacement of the pluton. In this part of the central White-Inyo Range, bedding strikes to the N and dips E and cleavage has the same strike but dips more steeply to the E (Fig. 10). South of the EJB pluton, bedding can be traced from its regional N-strike towards the pluton margin

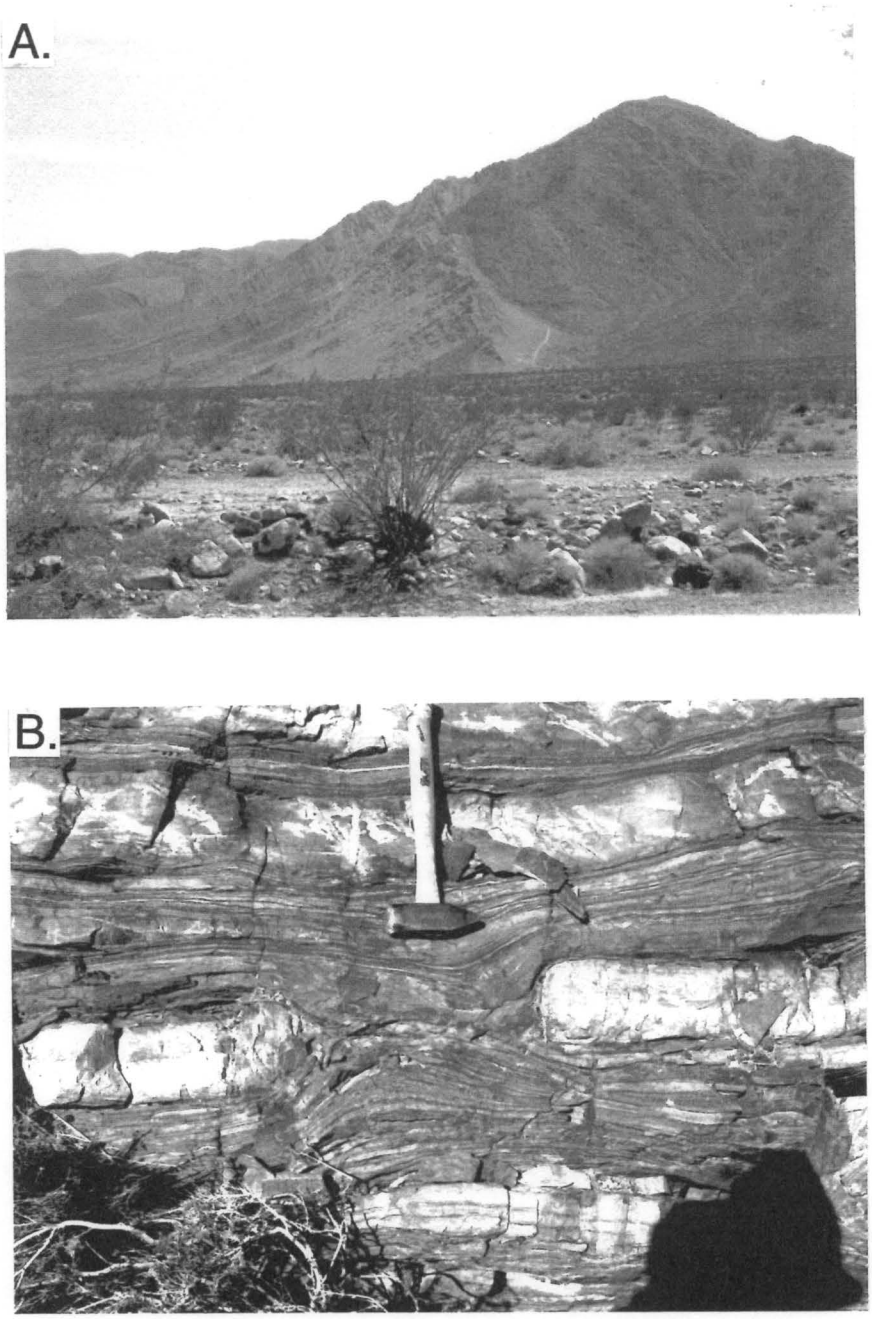

Figure 9. Field photographs. A. View of the sub-vertical SE contact (Stop 3-2). Dark rocks on right are the EJB pluton. Note the sub-horizontal layering (bedding) to the left and how it rapidly rotates into concordancy with the contact. Looking to the SW. B. Boudinage of quartzite bed interlayered with pelitic schist within the lower Cambrian Campito Formation (Stop 2-4). Hammer for scale.

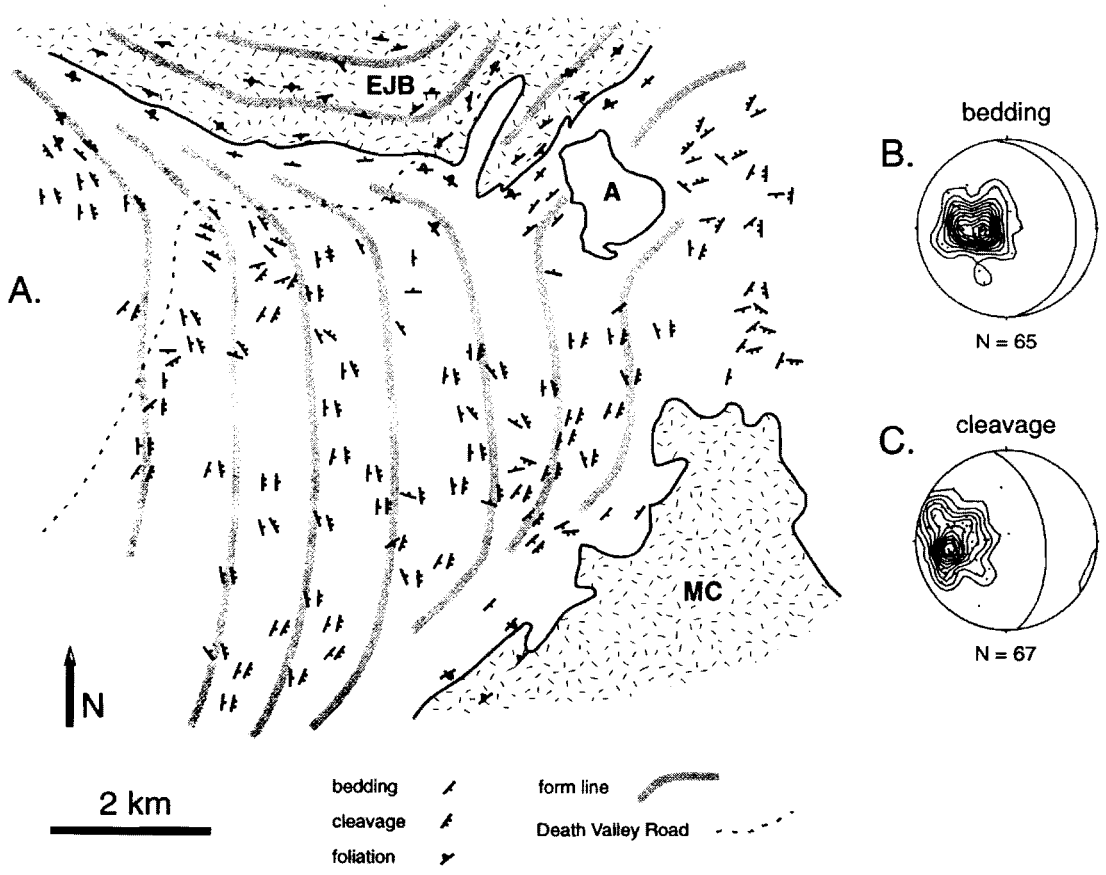

Figure 10. Map (a) and stereonets (b & c) of bedding and cleavage between the EJB and Marble Canyon plutons. Cleavage is overprinted by deformation and contact metamorphism at approximately 1 km from the plutons. Note how bedding and cleavage generally strike N and dip E, except adjacent to the two plutons and also how bedding is overturned and cleavage dips to the SW in the NW corner of map. Shaded form lines are interpreted and represent the general strike of foliation, bedding, and cleavage. A = Anvil pluton.

where bedding rapidly steepens and is rotated into a NW-strike to become concordant to the contact (Fig. 10a). The east dip of bedding increases from moderate angles to becoming sub-vertical, and in several areas is overturned. Cleavage can be traced along with bedding, striking sub-parallel to bedding and dipping more steeply. Where the overturned beds are NW-striking and dipping to the SW, cleavage also strikes to the NW but dips less steeply to the SW, suggesting that cleavage had been rotated through the vertical and also passively rotated along with bedding.

We have also plotted the map distribution of the bedding-cleavage intersection lineation (Fig. 11), in order to help illustrate the kinematics of translation and rotation. Where the beds are deflected by the pluton, the orientation of the intersection lineation rotates counterclockwise (moving to the north) along with bedding indicating that bedding rotated around steeply plunging axes to become concordant with the pluton margin, much the same way a door rotates on hinges. This rotation was also accompanied by a great amount of sub-horizontal translation, because the sedimentary formations are not only rotated in orientation, but they are deflected to the west and out of position from their regional strike.

The dip of bedding steepens considerably as the contact is approached, indicating that downward rotation at the contact also occurred. We can infer the relative timing of the downward rotation versus the horizontal rotation by the orientation of the cleavage-bedding intersection lineation as it is deflected around the southern margin of the pluton. For example, if the downward rotation of bedding had occurred first, prior to the outward rotation/deflection, then as the pluton is approached, the bedding/cleavage intersection lineation should begin to plunge towards the pluton (which is not observed). As well, the outward rotation/deflection would have rotated an already steeply plunging lineation outward, producing steeply plunging NW trending lineations (which is also not observed).

What we do observe is that the intersection lineation rotates outward as the contact is approached, and actually plunges away from the pluton (Fig. 11). We envision the original N-S trending lineation as being rotated outward first, maintaining a subhorizontal orientation, and then bedding was rotated downward, around an axis subparallel to the lineation. We infer that the outward translation of bedding was dominantly a sub-horizontal motion, and that the local overturning of stratigraphy indicates that outward magmatic flow was greatest at deeper structural levels. We also suggest that the present-day SE plunge of the intersection lineations in the western part of the study area (Fig. 11)

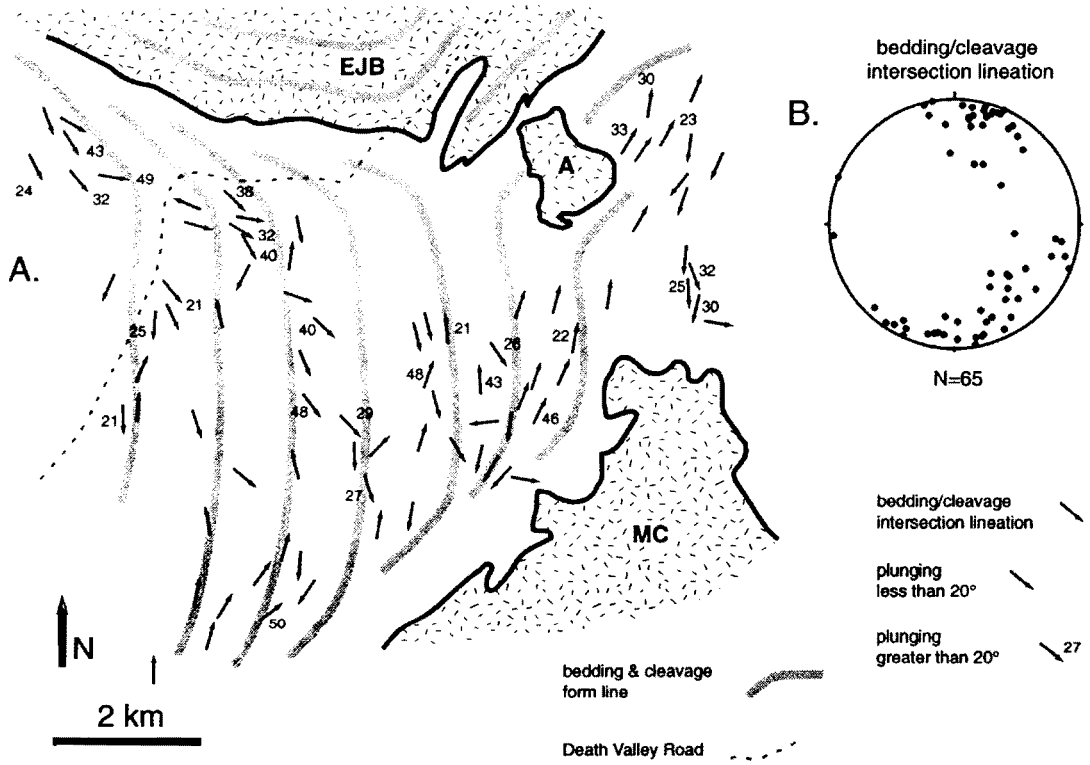

Figure 11. Map (a) and stereonet (b) of the bedding/cleavage intersection lineation in between the EJB and Marble Canyon plutons. The rotation of the intersection lineation approaching the EJB pluton constrains the kinematics of the deformation in the structural aureole. See text for details. Form lines from Fig. 10a. A = Anvil pluton.

could reflect a greater relative down-dropping of aureole rocks to the SE (possibly in response to the pluton expanding more to the SE), or a more complex pre-intrusion basin geometry.

In summary, the kinematics of the aureole rocks can be divided into three components; 1) subhorizontal translation associated with, 2) rotation about a steep to subvertical axis and, 3) rotation about a subhorizontal axis. The subhorizontal translation and rotation around a steep axis occurred first. Later, rotation around a subhorizontal axis (subparallel to the intersection lineation) occurred to place the beds into their steeply dipping orientation parallel to the pluton contact.

Defining the kinematics of the deformation is important because interpretation of motion through examination of two dimensional planes, e.g., cross sections or maps, can be deceiving. For example, cross sections through the aureole of the EJB (Fig. 5; Nelson, 1971) illustrate how bedding is rotated downward to become concordant at the contact, which was interpreted in terms of post-emplacement pluton-sinking by Glazner and Miller (1997), an interpretation we fully supported at the time. However, our new analysis of the cleavage-bedding intersection data forces the interpretation that the concordant aureole is largely a result of outward expansion of the EJB pluton.

We have little control on the kinematics of the transition from regional structures to aureole structures on the western margin of the pluton and even less on the eastern margin, since erosion has removed most of the eastern contact. We do observe, however, that the eastern limb of the White Mountain anticline, which forms the western border of the EJB pluton, is much steeper (sub-vertical) than the gently dipping western limb. In contrast, the eastern and western limbs of the Inyo anticline are gently dipping. We suggest that the steep angle of the eastern limb of the White Mountain anticline adjacent to the EJB pluton is a direct result of westward-directed translation associated with emplacement and lateral expansion of the EJB pluton.

The dip of bedding in the core of the White Mountain anticline, north of the Birch Creek pluton, abruptly increases to subvertical, moving from west to east, at approximately 4 km from the EJB pluton contact (Nelson, 1966b). South of the Birch Creek pluton, bedding is sharply deflected from its regional trend (where bedding curves around the hinge of the plunging White Mountain anticline) into concordancy with the EJB pluton at approximately 1 km from the contact. This deflection of bedding occurs at a similar distance from the pluton as on the southern margin of the EJB pluton.

On the eastern margin of the EJB pluton, erosion and Quaternary fill associated with the recent opening of the Basin and Range extensional province has removed or covered all but a small concordant section of metasediments preserved on the NE corner of the pluton. In this region the structural aureole is a minimum of 1 km wide and our data illustrate the same amount of shortening as observed elsewhere in the structural aureole (Table 2).

Deformation Mechanisms in the Structural Aureole

A wide variety of deformation mechanisms, varying between brittle failure and crystal plasticity, operated to attenuate the metasedimentary rocks within the aureole surrounding the EJB pluton. Brittle deformation occurred only locally within the aureole, and the microstructures and metamorphic textures are consistent with all the penetrative deformation occurring during contact metamorphism. Brittle and ductile structures and microstructures appear to share a common kinematic framework, indicating that all the deformation observed within the aureole took place at elevated temperatures during pluton emplacement.

At the scale of the three traverses across the EJB aureole, the deformation appears homogenous given the approximately equal amounts of shortening, yet, the smaller the scale, the more complex and heterogeneous the deformation mechanisms become. For example, chocolate tablet boudinage is commonly observed (Figs. 9b and 12) and indicates accumulation of flattening strains during aureole rock attenuation. The microfabric of those same rocks indicates crystal plastic deformation locally accommodated simple shear during smaller-scale displacements. The example above illustrates how the strain symmetry also varies between true flattening (k=0), and simple shear (k=1), depending on scale.

Many of the Lower and Middle Cambrian formations contain interbedded sandstone and shale. These aureole quartzite and schist layers, along with the thinly interbedded calc-silicate skarn, attenuated macroscopically by ductile flow into pinch and swell layers and also by brittle fracture into boudinaged layers (Figs. 9b, 12b, & 12c). Shear bands are observed alongside the boudin necks, disrupting the layering/foliation at irregular intervals and often giving the schist a chaotic appearance (Fig. 12a). The shear bands usually only extend for several centimeters, and often give conflicting senses of

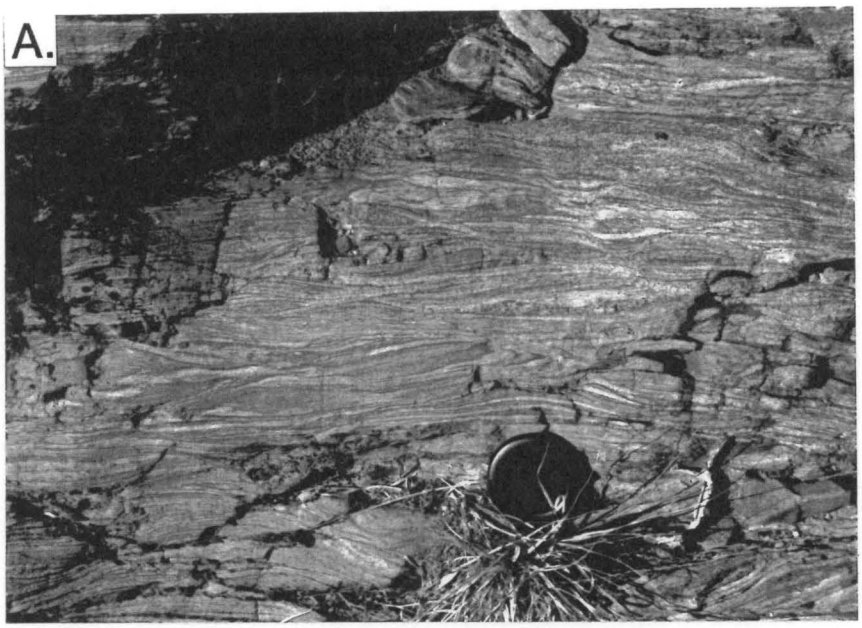

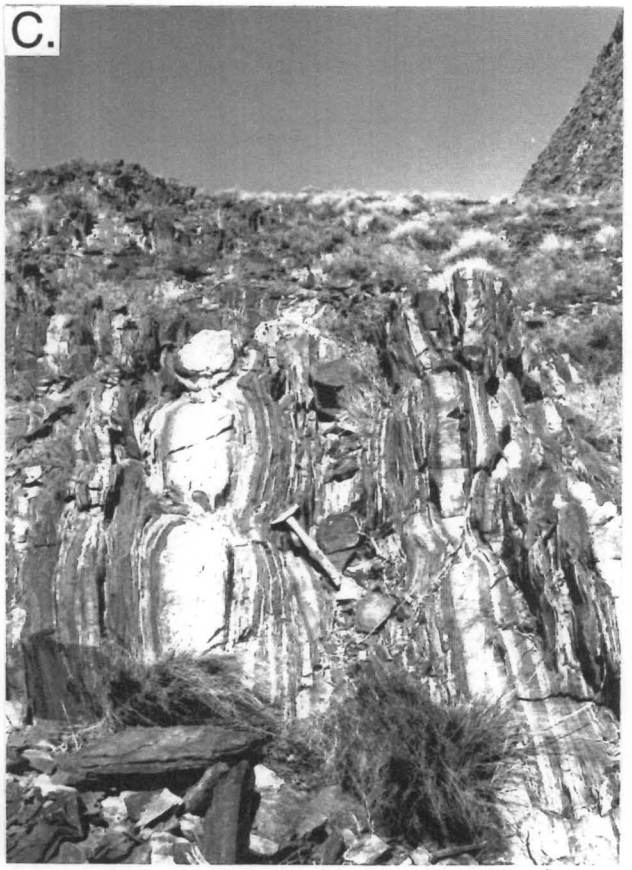

igure 12. Field photographs of deformation within the structural aureole. A. Chaotic foliation developed rough necking of layers and displacement along low angle shear bands. Lense cap for scale. B. Boudinage thick quartzite bed interlayered with pelitic schist within the lower Cambrian Campito Formation (Stop 2- . Note the brittle fractures within the boudins. Hammer for scale. C. Boudinage of thick quartzite terlayered with pelitic schist within the lower Cambrian Campito Formation (Stop 2-4). Hammer for scale.

shear. Mineral lineations are typically not observed at the hand sample to outcrop-scale, although where present, they are steep to subvertical (Fig. 6).

The boudinage varies in morphology between chocolate tablet, accommodating equal extension in two directions, and linear, accommodating extension in one direction. Boudins are typically elongate with the maximum extension direction oriented subvertically. Subvertical mineral lineations measured throughout the aureole (Fig. 6) also support the hypothesis that vertical extension was dominant over horizontal extension, although both occurred. Most of the rounded boudin shapes indicate ductile flow, but many of the quartzite boudins exhibit brittle fracture (Fig. 12b). Most of these fractures are shear fractures, oriented at high angles to the foliation and accommodating modest amounts of displacement. The temperature of the brittle-ductile transition for the deformation of quartz is much lower than the aureole temperatures, indicating that the strain rate must have been too high at times for quartz to deform entirely plastically. Brittle failure is typically seen in thick (10's of cm) quartzite layers surrounded by much lower viscosity schist, suggesting that a high viscosity contrast probably contributed to the brittle failure.

Thickly bedded (> 5 m) marble units exhibit little internal structure in the field, in contrast to the boudinaged and disrupted layering of the schist and quartzite. This apparent contrast is interesting because it is the limestone/marble of the Mule Spring Formation which has been attenuated the most. Therefore, at least macroscopically, the marble has deformed relatively homogeneously.

Microscopically, the quartzite and schist deformed by intracrystalline slip, grain boundary migration recrystallization, grain boundary sliding, pressure solution, and slip along discrete shear bands. There is also evidence for superplastic deformation within the quartzites. Quartz c-axes fabrics have been measured in samples collected along the traverse on the eastern margin of the EJB pluton, and also from selected outcrops throughout the aureole. Quartz fabrics are not presented here, but they are briefly discussed because they provide some control on the temperatures of deformation and on the strain symmetry. Most of the fabrics are weakly defined, but almost all indicate pure shear (k=1) strain and high temperatures of deformation using criteria proposed by Lister and Dornsiepen (1982). Many of the quartzite layers sampled also contain other mineral phases, dominantly muscovite, biotite, feldspar, and andalusite which probably interfered with the deforming quartz grains and allowed grain boundary sliding which would prevent strong fabrics from developing.

We also have strong evidence that slip along grain boundaries occurred within the pelitic schists; this is best illustrated in a sample of biotite schist surrounding a boudinaged monzonite sill. The sill has been deformed into a series of boudins through a combination of necking and brittle faulting. Traced from the faulted and offset margin of the sill, thin section examination reveals no evidence of the fault within the adjacent schist where distributed sliding along abundant biotite grains probably accommodated the offset. As well, larger-scale slip along compositional layering must have occurred to accommodate the boudinage. Examination of the outcrop photograph in Figure 9b reveals that slip must have occurred along the boundary between the quartzite and schist layers in order for the schist layer to flow into the void left behind by the extended quartzite layer. Using this same line of reasoning, slip along compositional layering must have been widespread in order to accommodate the heterogeneity of the strain observed within different layers.

The c-axis fabrics of quartzite layers sampled within meters of the pluton-contact have no preferred crystallographic orientation, although these layers have experienced high strains and were metamorphosed at high temperatures. Layers composed of calcite, wollastonite, grossular, diopside, and tremolite are often interlayered with quartzite which is necked and boudinaged. Quartz grains from the quartzite layers exhibit perfectly equant shapes, straight grain boundaries with 120° terminations, and homogeneous fine grain size, indicating that either superplasticity occurred, or that preferred orientations were completely annealed subsequent to the deformation. We favor the former interpretation, but have no way of proving superplasticity, except for noting that conditions favorable for superplasticity existed, i.e., the quartzite experienced high strains at elevated temperatures and no preferred crystallographic preferred orientation or grain-shape preferred orientation exists.

The absence of internal strain features within quartz grains is a common characteristic throughout most of the aureole samples. Despite the high strains, recovery mechanisms (intracrystalline climb and grain boundary migration recrystallization) kept up with the penetrative deformation, and indicate that high temperatures existed through the end of the deformation. The observed microstructures place the aureole deformation in the quartz recrystallization regime III of Hirth and Tullis (1992). Considering the rapid cooling times for plutons in the mid-to upper crust (10^5- 10^6yrs, Rothstein and Hoisch, 1994), we attribute the lack of lower temperature deformation features to an absence of regional deformation affecting the aureole after pluton emplacement. This is consistent

with our view that the regionally developed structures were in place prior to pluton emplacement.

Within the biotite schists, shear bands that cross cut the primary foliation at a low angle are often observed. Shear bands are defined by elongate folia of fibrolite and or biotite, and most indicate pluton-down sense of shear (c.f., Glazner and Miller, 1997). Based on textural evidence, this localized shearing post-dated the growth of andalusite and occurred late in the metamorphic evolution. Vernon (1987) has noted that in high grade metapelites, fibrolite is commonly observed as fine grained folia defining zones of simple shear because fibrolite deforms easily by grain boundary sliding and is therefore more stable during simple shear than other high temperature metamorphic phases.

In hand sample and under the microscope, the marbles often exhibit a grain shape preferred orientation which defines a lineation and foliation. Multiple twinning is common, but the mechanism for producing mass flow and attenuation within the marbles has yet to be determined. We hypothesize that a combination of intracrystalline slip and recrystallization accommodated the flow of the marbles.

Brittle faulting has cut out a major part of the Lower and Middle Cambrian section in the aureole on the SE margin of the pluton (McKee and Nelson, 1967; Nelson, 1971). The brittle structures (slickenlines, fault gouge) post-date the aureole metamorphism, but are parallel to the ductile structures and seem to accommodate a pluton-down sense of motion (Nelson, 1971). In places along the fault, which parallels the pluton-contact for approximately 7 km (the northern end is obscured by erosion and Quaternary sediments in Eureka Valley), a minimum of 900 m of section has been displaced by high angle faulting. The fault dominantly places marble of the Middle Cambrian Bonanza King Formation against metasiltstone of the Lower Saline Valley Formation, which cuts out the Mule Spring and Monola formations. The Saline Valley Formation is also cut out locally. Movement along this fault must post-date aureole metamorphism, but it is unclear whether the displacement is related to the last stages of emplacement, or pluton-sinking (Glazner and Miller, 1997), or if the fault is related to Basin and Range extension.

Anisotropy of Magnetic Susceptibility

The magnetic fabric of the EJB pluton has been investigated through analysis of the anisotropy of magnetic susceptibility (AMS) from oriented samples. AMS provides a

rapid insight into the bulk internal structure of a pluton, and allows for the definition of planar and especially linear fabrics which are commonly either hard or impossible to recognize in the field. Within the EJB pluton, AMS has also been useful in determining the characteristics of the internal contacts and provided insight into the relative timing of foliation development versus the formation of the internal contacts.

The magnetic fabric is often used to characterize the magmatic fabric of an igneous rock, which is defined by the shape preferred orientation (SPO) of early crystallizing minerals such as the ferromagnesian silicates, dominantly hornblende and biotite, and also feldspar phenocrysts. The assumption is made that the early crystallizing minerals aligned themselves with respect to the flow of the magma, which behaved as a liquid (a large percentage of the magma was still melt) at the time the foliation developed. This assumption is supported by the observations that early crystallizing minerals are relatively undeformed and late crystallizing minerals, such as quartz, are often undeformed and xenomorphic – their shapes are outlined by the shapes of early crystallizing minerals which define the fabric, suggesting that SiO_2 rich melt existed after the fabric developed.

The magnetic fabric is determined through analyzing magnetic susceptibility (K) and is defined by M=KxH, where M is the induced magnetization of the material and H is the inducing magnetic field. K is dimensionless because both M and H are expressed in Amperes per meter. In our analysis, fifteen AMS measurements from each rock sample were combined to produce an ellipsoid of magnetic susceptibility which is defined by the length and orientation of its three principal axes, $k_{max} \geq k_{int} \geq k_{min}$, which are the three eigenvectors of the susceptibility tensor. In ferromagnetic granites, i.e. magnetite-bearing granites such as the EJB pluton, the magnetic fabric results primarily from the shape anisotropy of the grains of magnetite (Khan, 1962; Uyeda et al., 1963; Ellwood and Whitney, 1980; Archanjo et al., 1995; Grégoire et al., 1995 & in press). Paramagnetic granites do not contain magnetite, and therefore their magnetic fabric results from the shape anisotropy of Fe-Mg silicates, dominantly biotite and amphibole (Bouchez, 1997). The anisotropy of magnetic susceptibility in ferromagnetic rocks will result from the mean orientation of all ferromagnesian minerals (Archanjo et al, 1995; Grégoire et al, 1995; Grégoire et al, in press), although the paramagnetic contribution to the AMS signal may be negligible because of the high intrinsic magnetic susceptibility of magnetite (Saint Blanquat and Tikoff, 1997).

Within ferromagnetic granites, the AMS signal may also be a function of the distribution anisotropy of magnetite. Distribution anisotropy occurs when magnetite grains

that are close enough to interact magnetically produce an ellipsoid of susceptiblility that is different from the ellipsoid that would be produced from the individual magnetite grains (Hargraves et al., 1990; Stephenson, 1994; Gregoire et al, 1995). Therefore, in magnetite bearing granites, the contribution of paramagnetic minerals and the affect of the distribution anisotropy limit the susceptibility ellipsoid to a qualitative measure of strain.

Two hundred and ten sites were sampled from the EJB pluton on a 0.5 km grid spacing (Fig. 13) . Most sites were sampled by coring the outcrop with a hand-held gasoline powered drill. Two oriented cores were taken from each site. Hand samples were taken from the rest of the sites and these samples were cored in a machine shop. Each core was cut into at least two (and usually three) sections, and an average of 5 sections were measured from each site. The susceptibility of each section was analyzed using the KLY2 Kappabridge apparatus of Agico (Brno, Czech Republic) at the Laboratoire de Petrophysique et Tectonique, Universite Paul Sabatier, Toulouse, France. Fifteen measurements, each with the section in a different orientation, were taken from each section in order to determine the susceptibility ellipsoid from each section. The data from the sections for each site was then averaged for each site. The data were analyzed, statistically compared, and plotted, using the program EXAMS (Saint Blanquat (de), 1993).

The three axes of the susceptibility ellipsoid, $k_{max} \geq k_{int} \geq k_{min}$ (k_1, k_2, k_3), provide several important parameters disussed below.

$1/3\ (k_1 + k_2 + k_3) = Km$, average bulk susceptibility

$k_1 / k_3 = P$, degree of total anisotropy

$k_1 / k_2 = L$, degree of linear anisotropy

$(2\ (\ln k_2 - \ln k_3)/(\ln k_1 - \ln k_3)) - 1 = T$, shape parameter

In addition, the foliation is obtained by determining the orientation of the plane that contains the k_1 and the k_2 axes, and the lineation is obtained by determining the orientation of the line that contains the k_1 axis. Values for K, P, L, T and the orientation of the foliation and lineation for each sampling location, as well as statistical data, can be found in Appendix 1. Stereograms portraying the orientation of k_1, k_2, and k_3 for each site can be found in Appendix 2.

The map of the magnetic foliation, along with the internal contacts, is found in Figure 14. Interpreted form lines have been drawn to illustrate the uniformity of the foliation orientation and how it curves with respect to the internal contacts and wall-rock

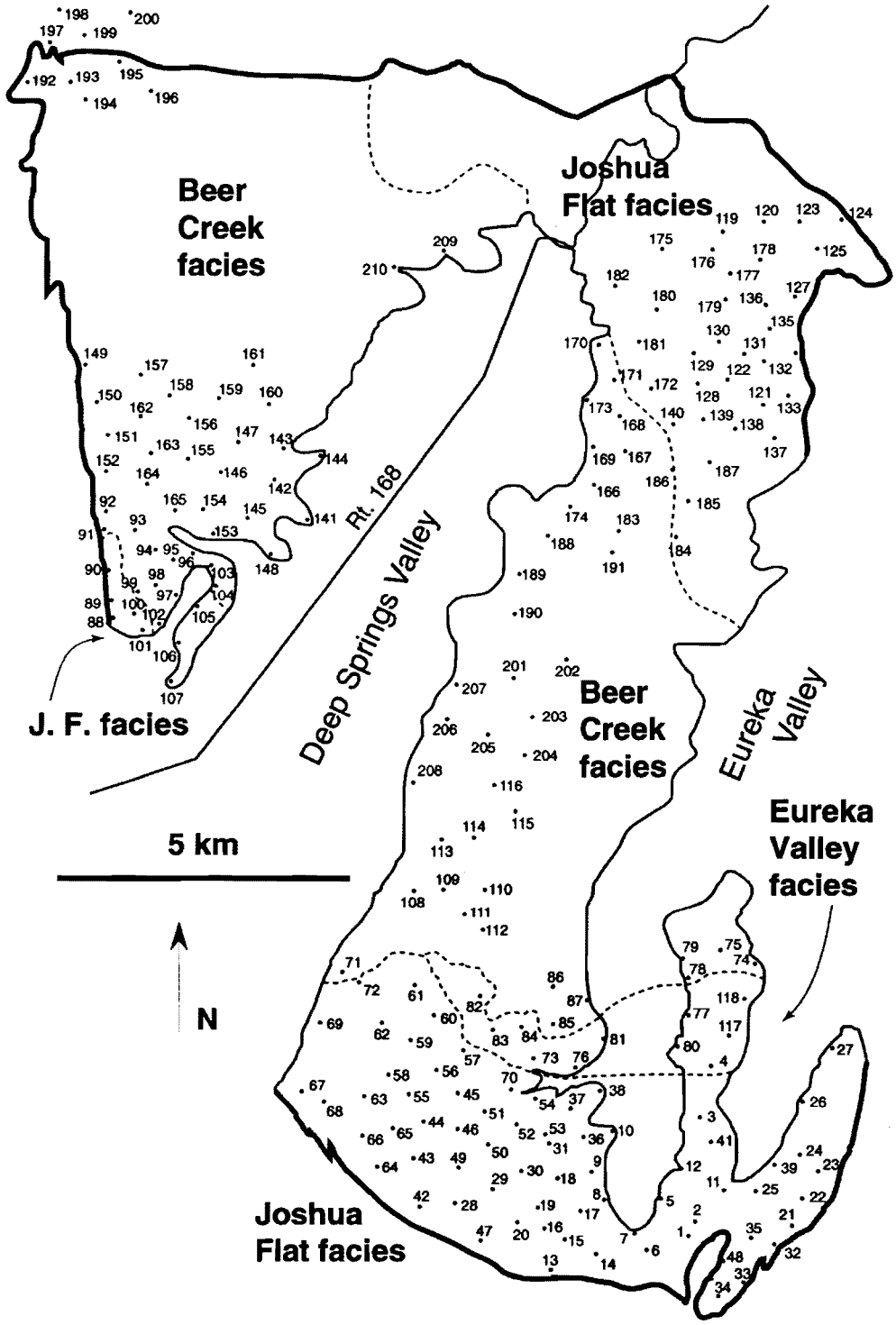

Figure 13. Location map of AMS sample sites.

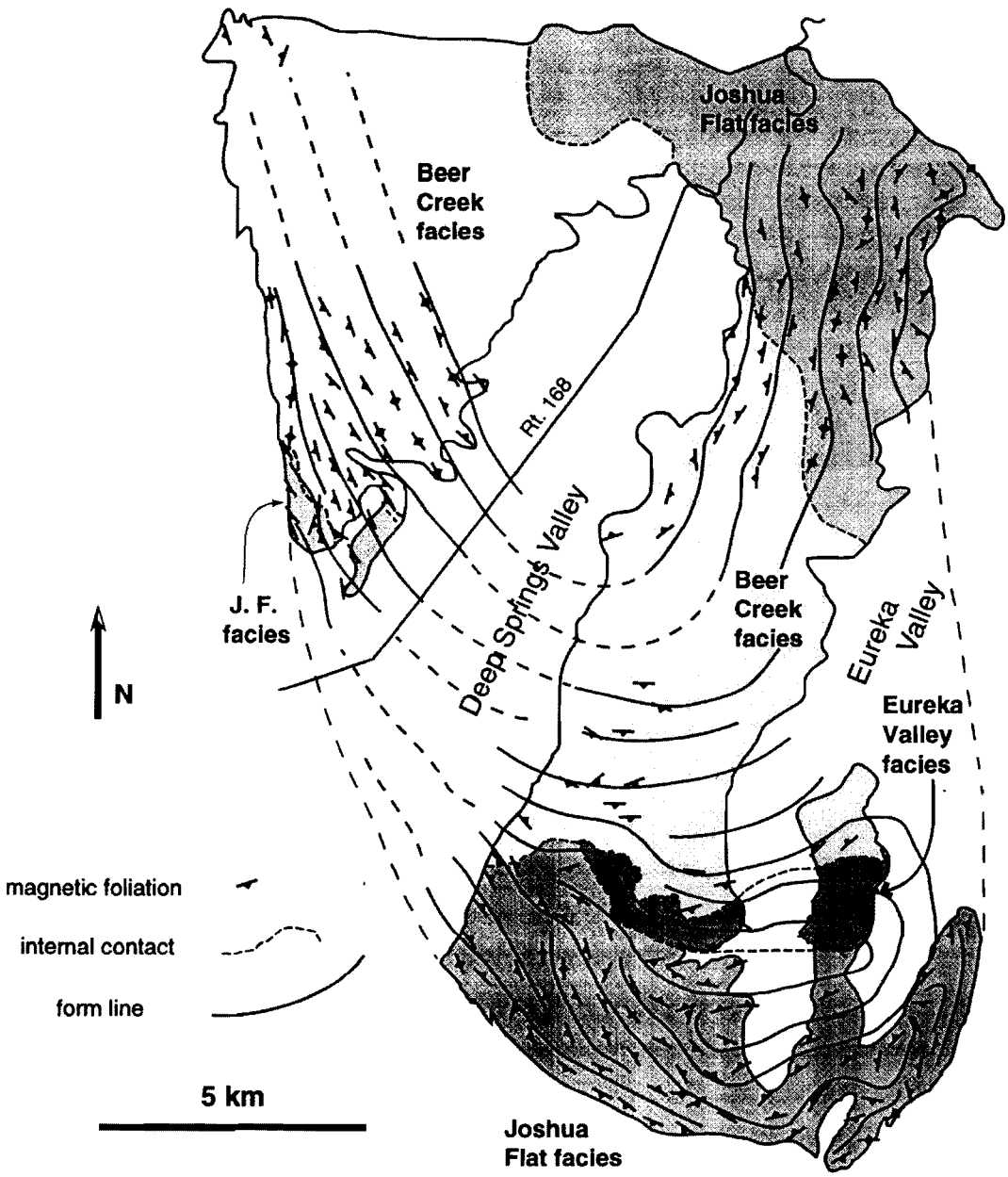

Figure 14. Map of AMS foliations and interpreted form lines. Note the generally concordant nature of the foliation and how the foliation crosses internal contacts.

contact. The internal contacts have been modified after Nelson et al., (1991), and are based on field mapping. Figure 14 also illustrates how the strike of the magnetic foliation crosses the contact between the JFM and the BCM in the northeast, maintaining a subparallel alignment with the wall rock contact. In contrast, the magnetic foliation in the southern portion of the pluton is dominantly subparallel to the internal contacts. The foliation is steeply dipping to subvertical in all three domains (NW, NE, and S). The lineation (Fig. 15) is steeply plunging to the NW in all three domains despite the changing orientation of the foliation. It should also be noted that the magnetic lineations within the pluton are parallel to the solid-state stretching lineations measured within the structural aureole (compare Figs. 6 & 15), indicating a common genetic relationship.

Figure 16 is a frequency histogram of the Kmax (k_1) direction, which shows the within-site angular variability of the Kmax direction and attests to the high quality of the directional data. For example, 52% of all the Kmax orientations are within 10° of the average Kmax orientation for that site, and 82% of all the Kmax orientations are within 20° of the average Kmax orientation for that site. The consistency of the orientation data can be visually checked by examining the stereonets for each site in Appendix 2.

Susceptibility values are generally high, ranging from 86 x 10^{-6} to 95 x 10^{-3}SI, with an average value of 33 x 10^{-3}SI (Appendix 1), and 78% of all values fall between 20 and 50 x 10^{-3}SI (Fig. 17). Figure 18 is a contoured susceptibility map based on the values determined from each site within the pluton. Since the bulk susceptibility (km) is largely a representation of the amount of magnetite in the rock (Bouchez, 1997), it can be used to delineate compostional boundaries. The more mafic EVM exhibits the highest susceptibility values, containing the highest percentage of magnetite and other mafic minerals, and the felsic BCM exhibits the lowest values. Comparison between Figure 14 and Figure 18 indicates that the internal contacts defined in the field are also outlined by strong contrasts in susceptibility, with some minor discrepencies. As stated earlier, the contact between the JFM and BCM can be gradational, which is particularly true in the northeast part of the pluton, and the susceptibility map supports this field-based observation by exhibiting a much wider transitional area between the lowest and higher values of susceptibility. The mapped contact between the JFM and the BCM with the EVM is much more obvious in the field, and also characterized by an abrupt contrast in susceptibility values in the southern portion of the pluton (Fig. 18).

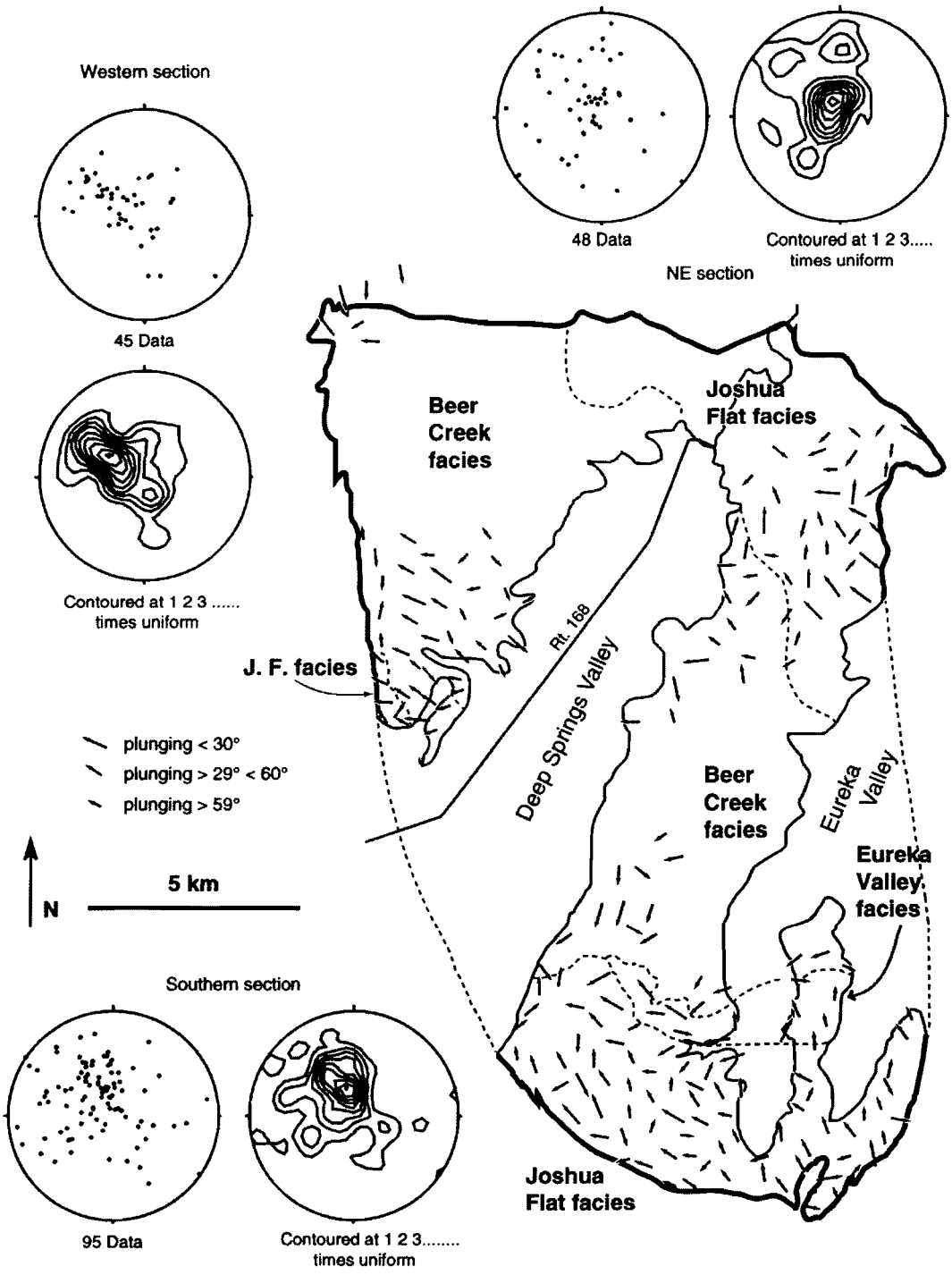

Figure 15. Map of the AMS lineations and stereonets of lineations divided into the western, southern, and northeastern domains. Note the similarity of the orientation of lineations between the three domains despite the curving nature of the foliation (see Fig. 14).

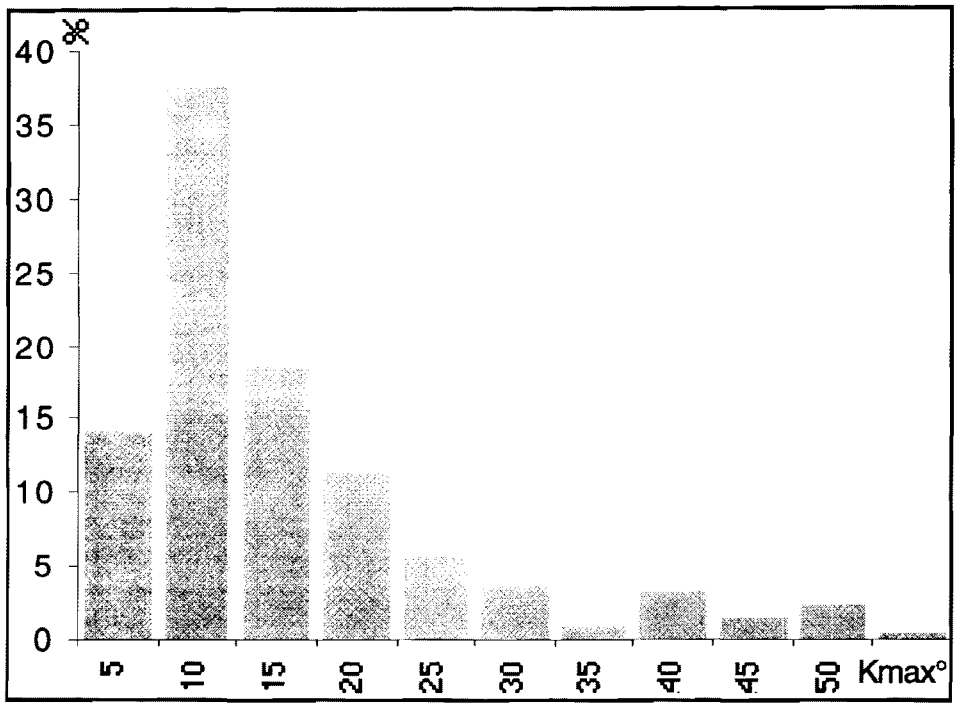

Figure 16. Frequency histogram of within-site angular variability for the kmax directions.

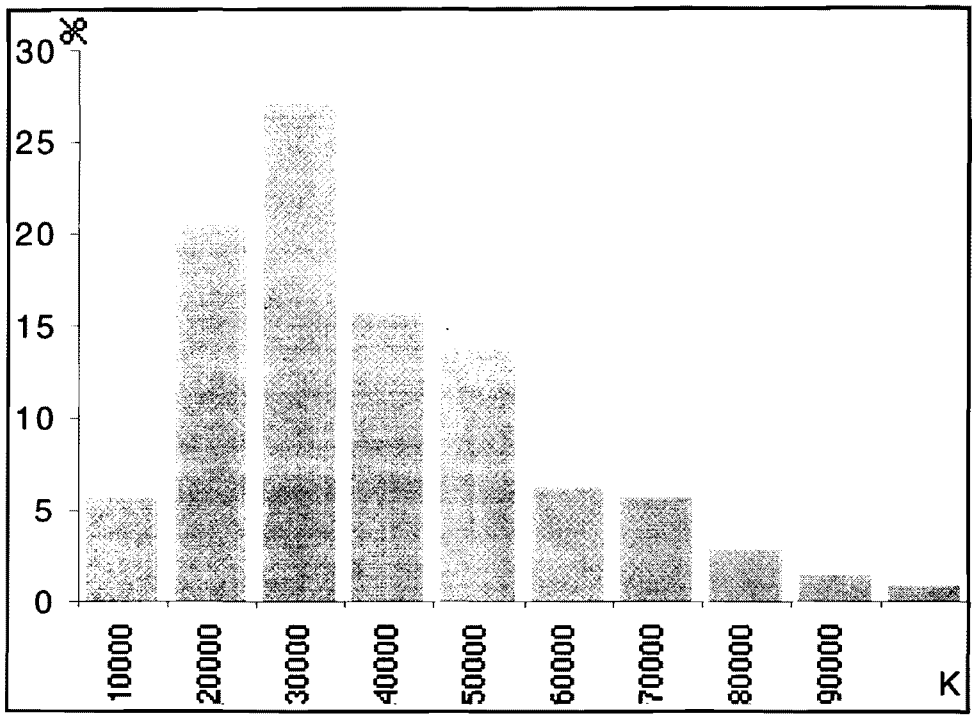

Figure 17. Frequency histogram of magnetic susceptibility. K values are 10^{-3}SI.

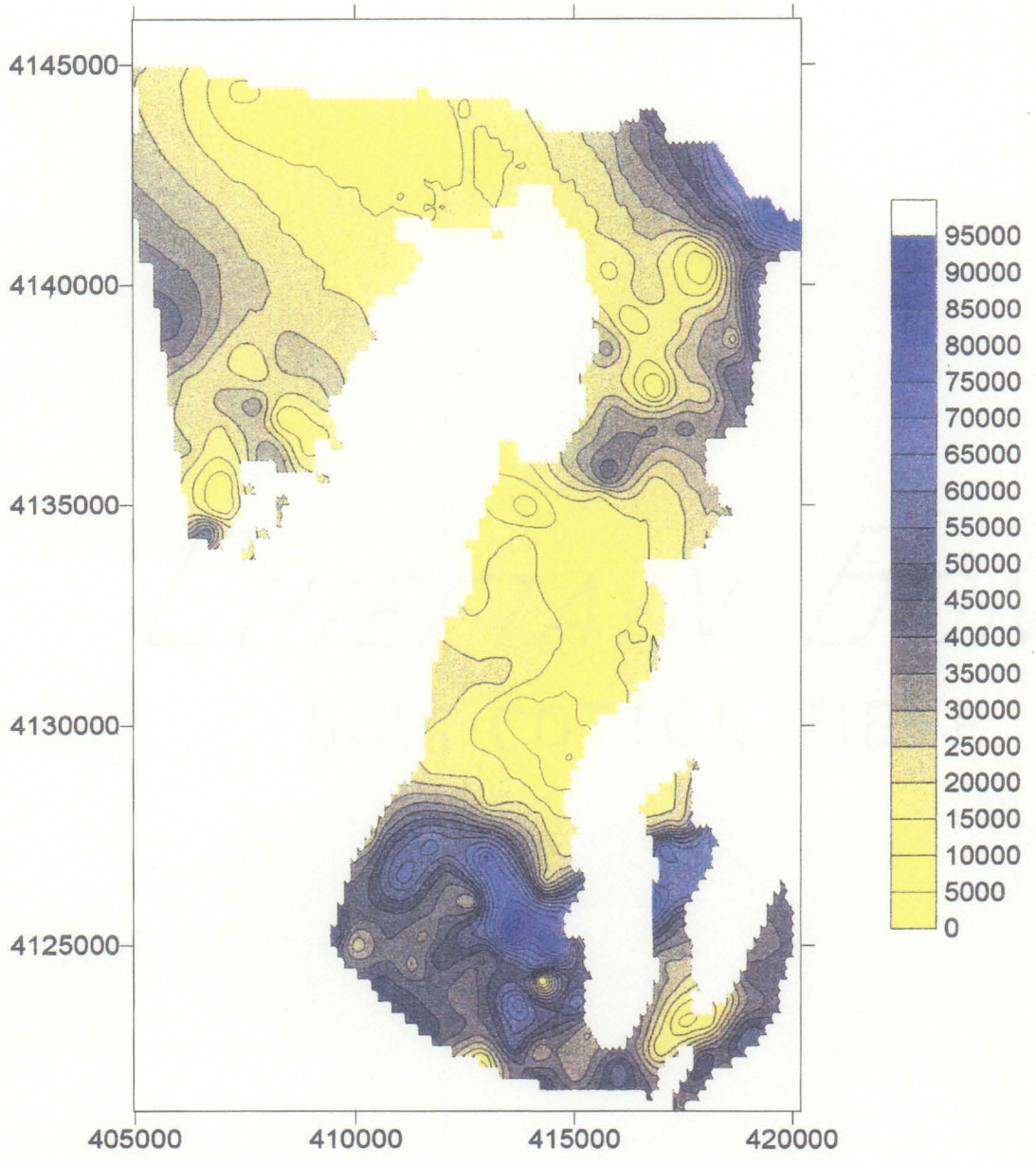

Figure 18. Contoured map of the magnetic susceptibility based on the values determined at each sample location. Susceptibility values are $1x10^{-6}$ SI. Universal Transverse Mercator (UTM) grid points in meters.

The values for the % anisotropy, ($P\% = 100*(k_1+14/ k_3+14) - 1$; $P = k_1/ k_3$), have been contoured in Figure 19. Values range from 69.3% to 1.8% (P = 1.69 to 1.02), with an average value of 18.6% (P = 1.19) (Appendix 1). 80% of the values fall between 10% and 25% (Fig. 20). Anisotropy refers to the degree to which the fabric is developed. The common observation of well developed fabrics (foliation) at the margins of plutons which decrease in intensity towards the interior is only observed at the northeast and western margins of the EJB pluton. Near the southern margin there is a narrow, discontinuous zone of higher anisotropy which is 1 – 2 km from the wall-rock contact and which parallels the wall-rock contact (Fig. 19). The anisotropy at the contact south of this zone is defined by very low values. The interior of the pluton also exhibits very low degrees of anisotropy.

The last parameter discussed is the shape parameter (T), which is representative of the strain symmetry. T values of +1 suggest oblate (flattening) strain and values of –1 suggest prolate (constrictional) strain. Values of 0 suggest plane strain. T values determined from within the EJB pluton have been contoured in Figure 21. There is no observable pattern to the T values, i.e., there is no correlation between zones of strain and internal or external contacts. T ranges from a maximum of 0.84, to a minimum of –0.59, with an average value of 0.26 (Appendix 1). The frequency histogram for the T values illustrates that there is no clustering of values at a specific value, although the vast majority of values are positive or within the flattening field (Fig. 22).

Figure 23 illustrates the positive relationship between P% and K, except for some scatter at very high values of K. A positive correlation between P and K has been attributed to a distribution anisotropy in other magnetite bearing granites, because the wide range in anisotropy at high values of susceptibility cannot entirely be explained by a shape preferred orientation of magnetite alone (Bouchez, 1997; Saint Blanquat and Tikoff, 1997). Distribution anisotropy is most clearly demonstrated where there is an abrupt increase in P with increasing K (Bouchez, 1997), and this is not observed in Figure 23.

Figure 24 illustrates how the shape parameter, T, varies with P%. No correlation between the two variables is noted, although the graph does illustrate the dominance of flattening fabrics at all values of P%.

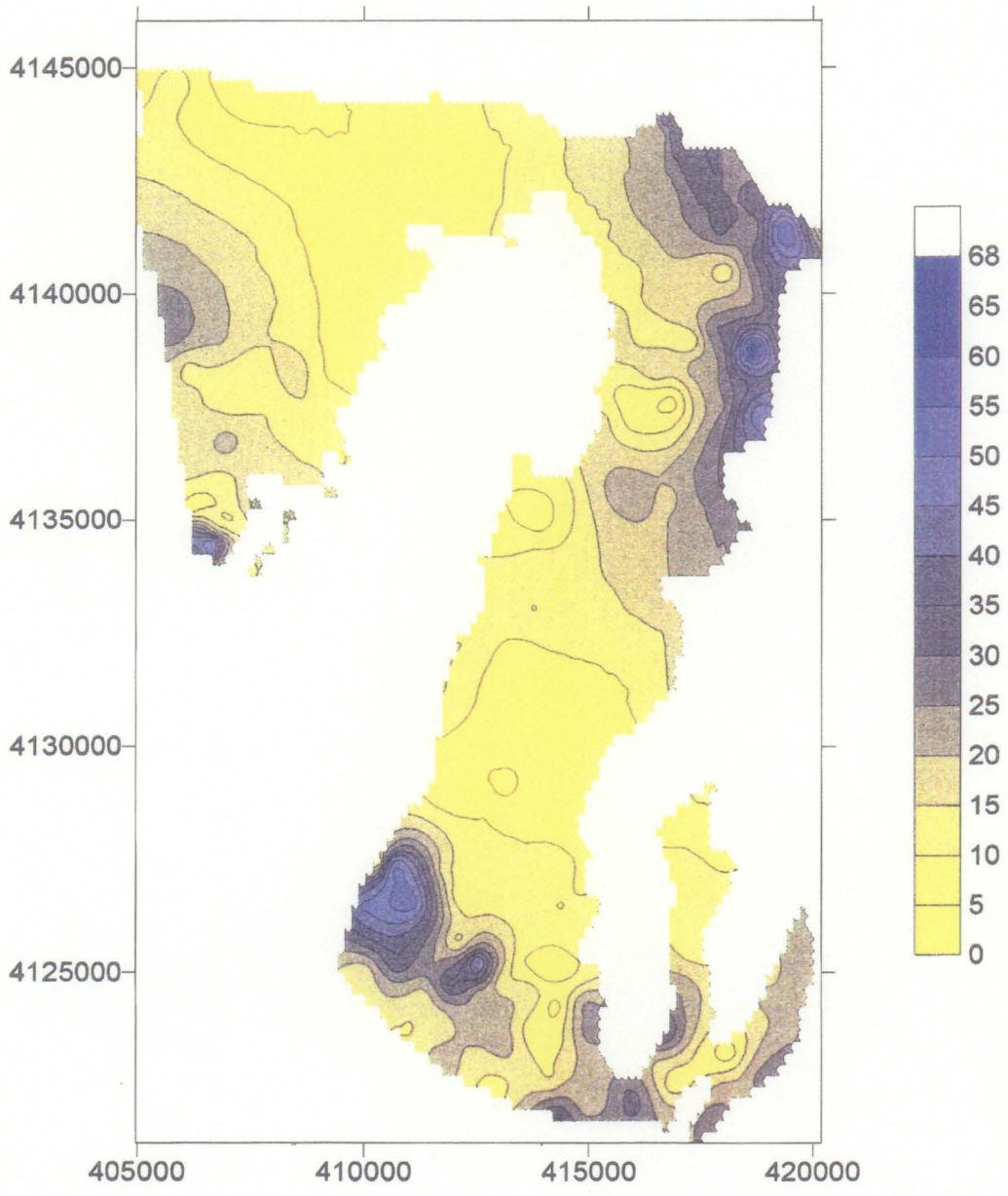

Figure 19. Contoured map of the percent anisotropy. UTM grid points in meters.

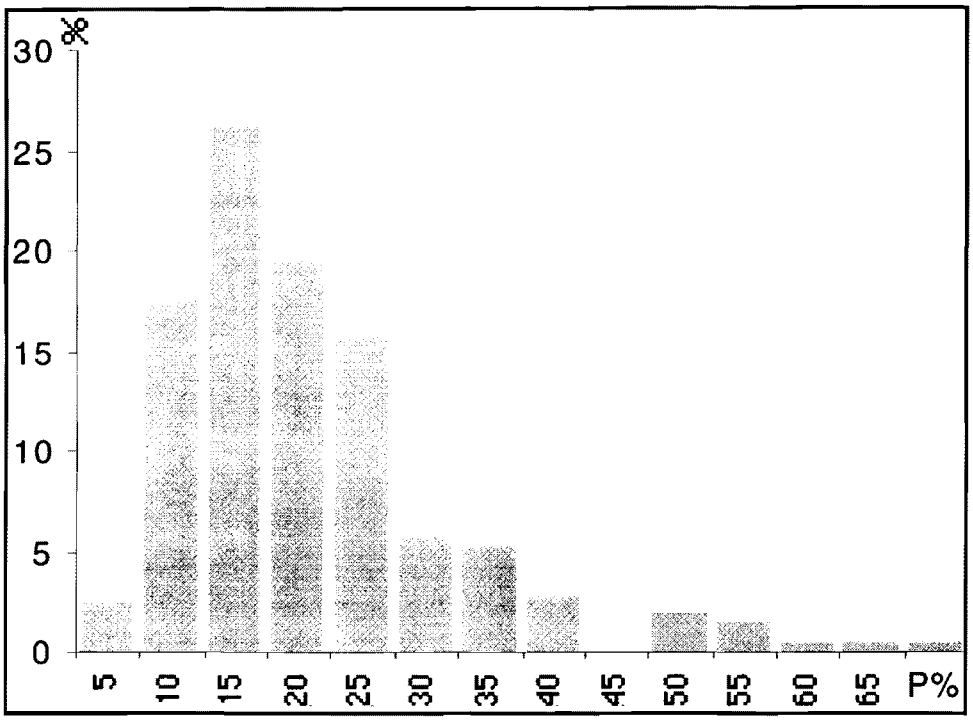

Figure 20. Frequency histogram of magnetic anisotropy.

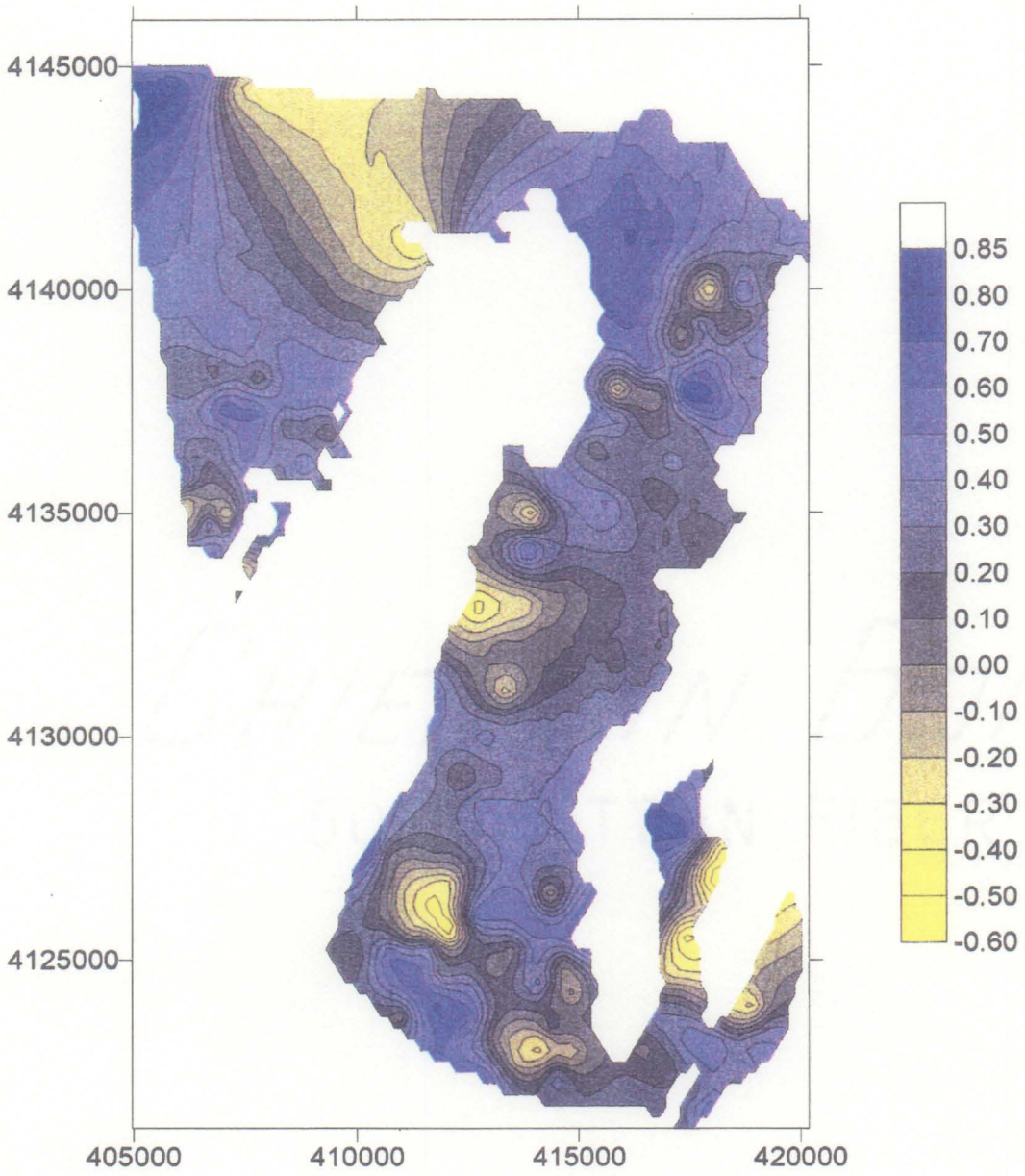

Figure 21. Contoured map fo the shape parameter, T. UTM grid points in meters.

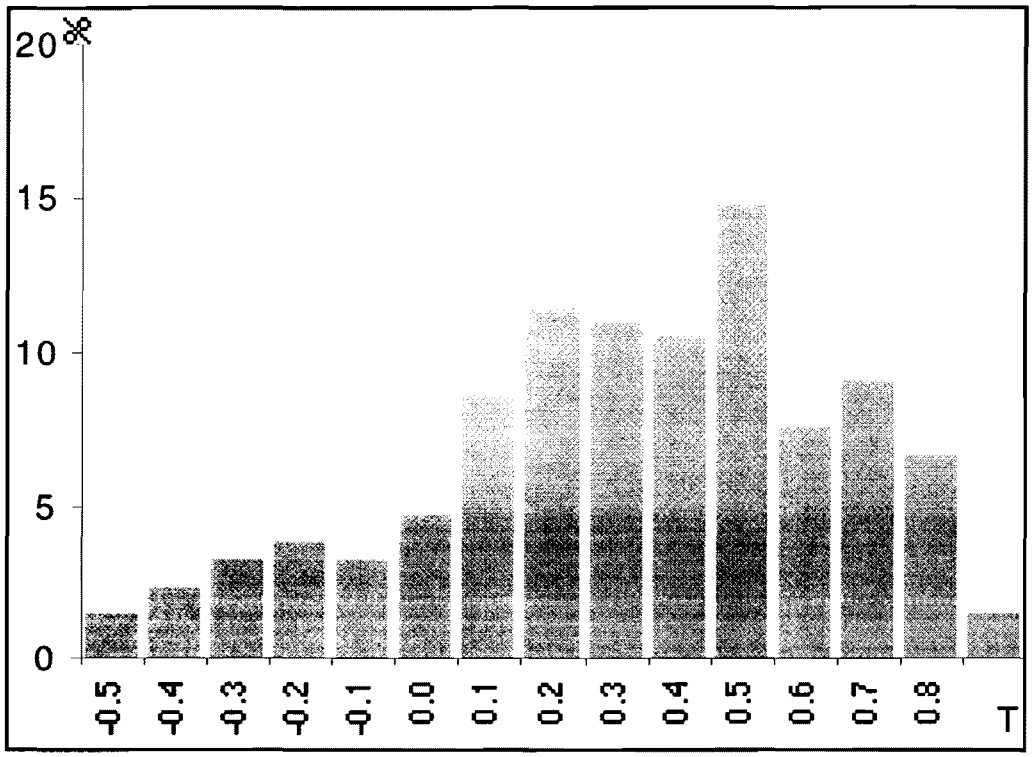

Figure 22. Frequency histogram of the T shape parameter.

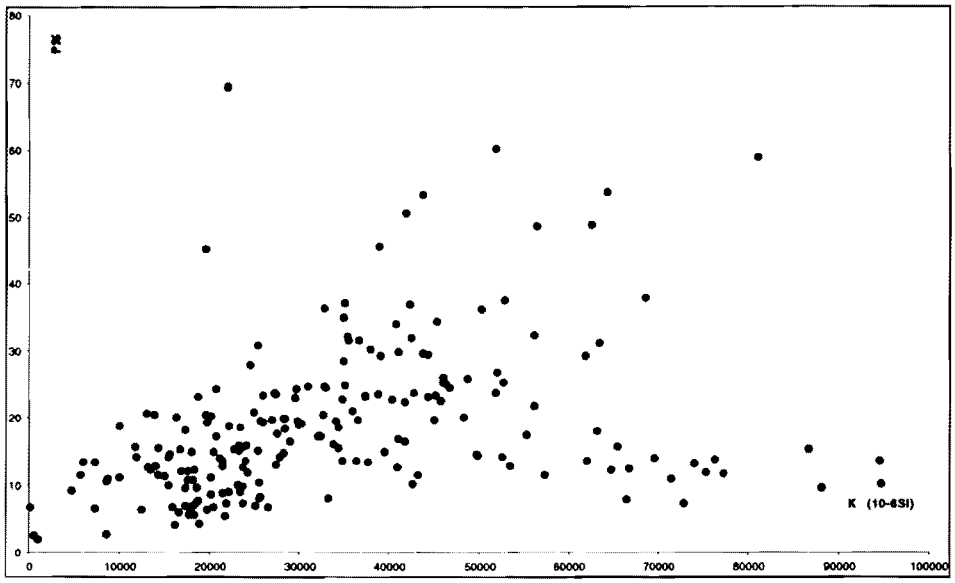

Figure 23. Graph of the relationship between P% and K.

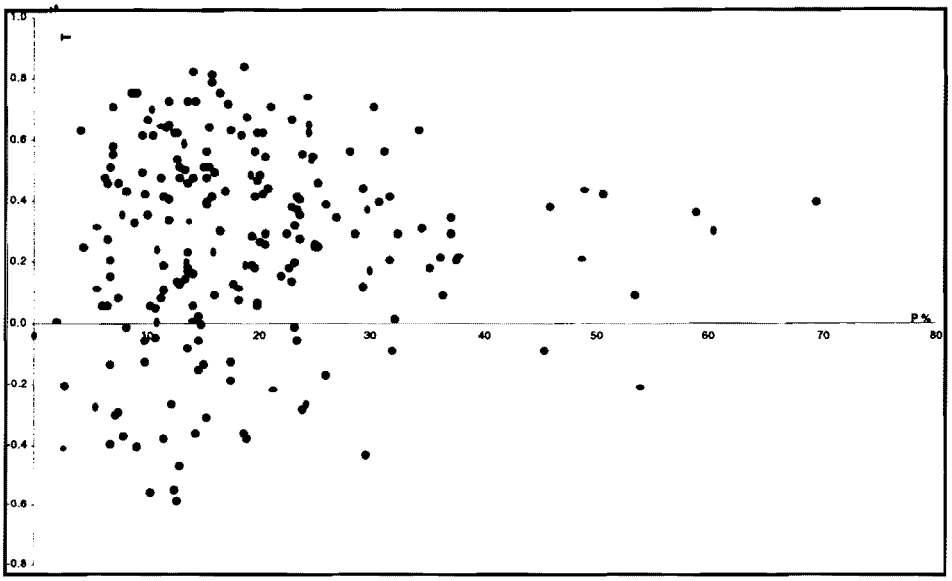

Figure 24. Graph of the relationship between T, shape parameter, and P%.

Discussion

The EJB pluton is a concordant, elliptical pluton (except for the northern margin) which varies spatially between three distinct end-member compositions. Its internal contacts are in places sharp and in other places gradational. The magnetic foliation is sub-parallel to the concordant margin, as seen in many other concordant plutons (Ardara pluton in Ireland, Akaad, 1956; Criffel pluton in Scotland, Courrioux, 1987; Northern Granite in Arran, Scotland, England, 1992; Vrådal pluton in Norway, Sylvester, in press), but it also crosses some internal contacts, indicating that EJB pluton preserves the deformation of an already-assembled or mostly assembled pluton. Microstructural observations (Morgan and Law, 1994; Stein, 1994; Stein and Paterson, 1996), indicate that most of the pluton was in the magmatic state at the time the foliation was preserved.

The EJB pluton is situated in a structural basin defined by metasedimentary wall-rocks which rotate downward to become concordant to the pluton-margin and consistently young towards the pluton. Emplacement of the EJB pluton into this structural basin is related to two possible mechanisms; one involves inflation of a magma chamber which has intruded into a pre-existing structural basin, and the other mechanism involves downward motion of the pluton associated with late stage sinking to produce a structural basin.

The AMS data help resolve the timing of the foliation development relative to the development of the internal contacts, but the AMS data is only a record of the last increments of flow or deformation. In contrast, the microstructures, macrostructures, and metamorphic history of the aureole metasedimentary formations can be interpreted to reflect a greater proportion of the pluton emplacement history. The full strain history, which includes the translation and rotation of the wall rocks, is not completely documented but is best resolved at the southern margin of the EJB pluton. The rotation of the bedding-cleavage intersection lineation into concordancy south of the pluton suggests that bedding was "shouldered" aside, or was translated and rotated outward, to the west, as the EJB pluton expanded southward. Only after the aureole metasedimentary formations were rotated into a sub-parallel strike with the pluton contact were they rotated downward into their present subvertical orientation.

The homogeneous shortening of the aureole metasedimentary formations, from the western, southern, and northeastern margins, suggests that the pluton expanded outward in all directions. The tightening of the White Mountain anticline to the west of the EJB

pluton supports our model of homogeneous outward expansion. This tightening cannot be due solely to the forceful emplacement of the Birch Creek pluton, located to the west of the EJB pluton, because increased dips are observed to the north of the Birch Creek pluton as well.

Within the structural aureole, intense shortening was accommodated by a combination of flattening (chocolate tablet boudinage), pure shear (linear boudinage), and simple shear (shear bands). Mineral lineations within the structural aureole are not commonly observed, which probably attests to the strong flattening component of the deformation. Where mineral lineations are observed, regardless of position around the aureole, they are subvertical, indicating that vertical stretching was also an integral part of the deformation throughout the aureole.

Despite the curving, sub-concordant orientation of the magnetic foliation, the magnetic lineations consistently plunge steeply to the NW throughout the entire pluton. The magnetic lineations are parallel to the stretching mineral lineations observed within the structural aureole, indicating that the pluton's internal foliation and lineation are genetically related to the lineations within the structural aureole, and that the flow/deformation of magma and wall rocks was related. The consistency of the orientation to the magnetic lineations regardless of position or compositional unit also suggests that the whole pluton behaved as a single mass during the last stages of flow.

The changes in susceptibility (K) values (Fig. 18) within the pluton document the change in %magnetite across the internal contacts which were originally mapped in the field (Nelson et al., 1991; McKee, E.H., and Nelson, C.A., 1967; Nelson, C.A., 1966a; Nelson, C.A., 1966b; Nelson, C.A., 1971). As discussed previously, the observed nature of the internal contacts is supported by the susceptibility data, i.e., the gradational contact in the north and the sharp contact in the south are expressed by similar changes in susceptibility values.

The map of the magnetic foliation (Fig. 14) indicates that the internal contact between the JFM and the BCM in the northeast part of the EJB pluton did not act as a rheological boundary to flow, or deformation, of the magma. The foliation crosses the internal contacts in the northeast without deflection, suggesting that the JFM and the BCM were in the same or similar rheological state. Microstructural evidence indicates that the foliation in both of these units developed in the magmatic state (Morgan and Law, 1994; Stein, 1994; Stein and Paterson, 1996), suggesting that the foliation developed after the contact formed, but before complete crystallization.

Based on the magnetic foliation, the only rheological boundaries to flow were 1) the contact with the metasedimentary wall rocks, and 2) the contact of the BCM and JFM with the EVM in the southern portion of the pluton. The EVM had crystallized enough for angular pieces to be incorporated into the other two units, indicating that it should behave as a boundary to flow. Tracing the magnetic foliation from the NW to the S (Fig. 14), the form lines, although somewhat interpretive, are closer to being parallel to the contact between the EVM and the BCM than to being parallel to the external contact with the wall rocks, suggesting that the EVM/BCM contact was a rheological boundary and supporting the field evidence which demonstrates that the EVM was closer to complete crystallization, or fully crystallized, at the time the BCM intruded.

Although the foliation is parallel to the EVM/BC contact in the southern portion of the pluton, the values for anisotropy along this contact (Fig. 19) indicate that the foliation is very weakly defined, i.e., values do not vary much between Kmax and Kmin. The highest values for anisotropy, besides the northeast wall-rock contact, lie in a discontinuous but linear belt located just south of the EVM/JF contact, and the T values in this belt plot well in the prolate (negative T values) field. The reason for this zone of high, prolate "strain" within the interior of the pluton is not known, although it does roughly correspond with contact between the EVM and the JF (compare Fig. 14 and Fig. 19), and therefore is probably related to differences in their rheological state during late stages of flow.

We propose two pluton emplacement models to explain the geological features within and immediately surrounding the EJB pluton discussed in this paper. The first model is termed the *outward inflation* model, and assumes that the basic structure of the region, i.e., the dome and basin structure defined by the sedimentary strata in this portion of the central White-Inyo Range and the basin in which the pluton intruded, was pre-existing when the magma intruded, as discussed in the section under *Regional Deformation* above. The second model, originally proposed by Glazner and Miller (1997), is termed the *sinking* model. In this model, the magma initially intrudes as a sheet-like body, roughly concordant but cutting up section to the south, which sinks during crystallization induced density increases of the more mafic units. The two models are discussed below.

In the outward inflation model, the structural basin that the EJB pluton originally intruded is part of a large syncline that forms a fold-pair with the White Mountain anticline to the west. Structural basin B_4, B_5, and B_6, (Fig. 4), south of the pluton, were also

formed by the interference between this large syncline and smaller scale NE trending folds (Morgan and Law, 1998). Half of basin B4 has been incorporated into the EJB aureole as the pluton expanded southward.

The outward inflation model requires that the original position of the magma was structurally below (perhaps several km) and to the north of, the present level of erosion at the southern margin of the pluton, where the metasedimentary formations have been rotated and translated outward and downward. The initial geometry of the magma body is unknown, but we envision a curved, sheet-like shape that cuts up-section to the south, congruous with the current geometry of the EJB/wall-rock contact.

As the curved sheet inflated into a pluton through injection of several pulses of magma of different compositions, the magma sheet migrated, either in steps or gradually, up through the sedimentary section to the south and followed the upward concave structure of the basin. During final assembly and inflation, outward and upward directed magma flow deformed the basin by pushing the walls outward and the roof upward. The last increments of outward motion steepened the wall rocks by downward rotation of the sedimentary units at the contact, producing the subvertical inward younging structural aureole. The overturned stratigraphy along much of the contact suggests that the outward flow was greatest at the base of the pluton. The sedimentary section above the expanding pluton would have been forced upwards, probably accomodated by faulting and folding.

In the sinking model, the younging of strata towards and abrupt folding of strata downward at the pluton-contact is a result of late stage sinking of the EJB pluton producing it's own structural basin. The sinking occurs because of an increase in density (~5 to 10%) of the pluton to values greater than the surrounding sedimentary rocks as crystallization goes to completion (Glazner and Miller, 1997). The viscosity of the underlying sedimentary rocks is decreased as they are thermally softened from the overlying pluton allowing for the denser pluton to sink several km into the crust.

In support of the sinking model, late pluton-down shear sense indicators are observed in several locations within the structural aureole. Shear sense indicators are not common, and as stated previously, most of the strain symmetry appears to be coaxial, yet within the structural aureole, fibrolite is most commonly observed defining shear bands with a pluton down sense of shear. Other shear sense indicators, such as asymmetric, high temperature, quartz c-axis fabrics, exhibit pluton-up sense of shear. Texturally, the shear bands defined by late fibrolite indicate that the pluton-down sense of shear occurred late in the metamorphic history, but still close to peak thermal conditions. However, the

kinematics of the wall rocks, the dominance of flattening strains, and the overturned stratigraphy within the structural aureole suggests that sinking alone cannot account for the pluton-wall rock geometry. Sinking, if it occurred, must have been accompanied by some outward expansion of the pluton.

In conclusion, regardless of emplacement model, all the data suggest that the flow of magma within the pluton resulted in the high solid-state strains in the structural aureole, and that all observed regional deformation (except for recent Basin and Range extensional structures) predates the emplacement of the EJB pluton. Our analysis of the metasedimentary rocks and sedimentary rocks surrounding the EJB pluton indicates that although the structural aureole is narrow relative to the volume of igneous rock, forceful expansion is a viable model to explain pluton emplacement if rotation and translation of the structural aureole is taken into account.

Road Log

Day One - Saturday April 4, 1998. Los Angeles to Big Pine, California and high elevation overlook of the central White-Inyo Range.

The first day is mostly occupied by the long drive from Los Angeles to the Owens Valley. After arriving in Big Pine, we will drive up into the southern White Mountains and view the structure and Neoproterozoic through Middle Cambrian stratigraphy. A very simplified geologic map of the region, including the field trip stops, is provided in Figure 25. On top of the range we will have an excellent view of the southern contact of the EJB pluton and how the stratigraphy is deflected at the contact. We will also have an excellent view of the eastern Sierra Nevada Mountains/batholith and Owens Valley. The road log begins at the northern end of Big Pine at the intersection between Rt. 395 and State Highway 168 (Westgard Pass - Bristlecone Rd).

The stratigraphic units we will be driving through have been mapped in detail by Clem Nelson who published the four 1:62,500 scale quadrangles that comprise the central White-Inyo Range (Nelson 1966a & b; McKee and Nelson 1967; Nelson 1971) and who also has also published several field guides from UCLA and from the White Mountain Research Station (Nelson et al., 1991) on the geology of the range. We rely heavily on the Nelson et al., (1991) field guide article and the Nelson (1980) UCLA field guide for the regional geology.

inc.	total (miles)	
0.0	0.0	On Rt. 395 at the northern end of Big Pine, turn east onto Westgard Pass-Bristlecone Road (State Highway 168).
1.4	1.4	Cross Owens River.
0.7	2.1	Death Valley - Waucoba Road (on right - we will take this road on Monday when we examine the southern and southeastern margins of the EJB pluton in Eureka Valley - Death Valley National Park).

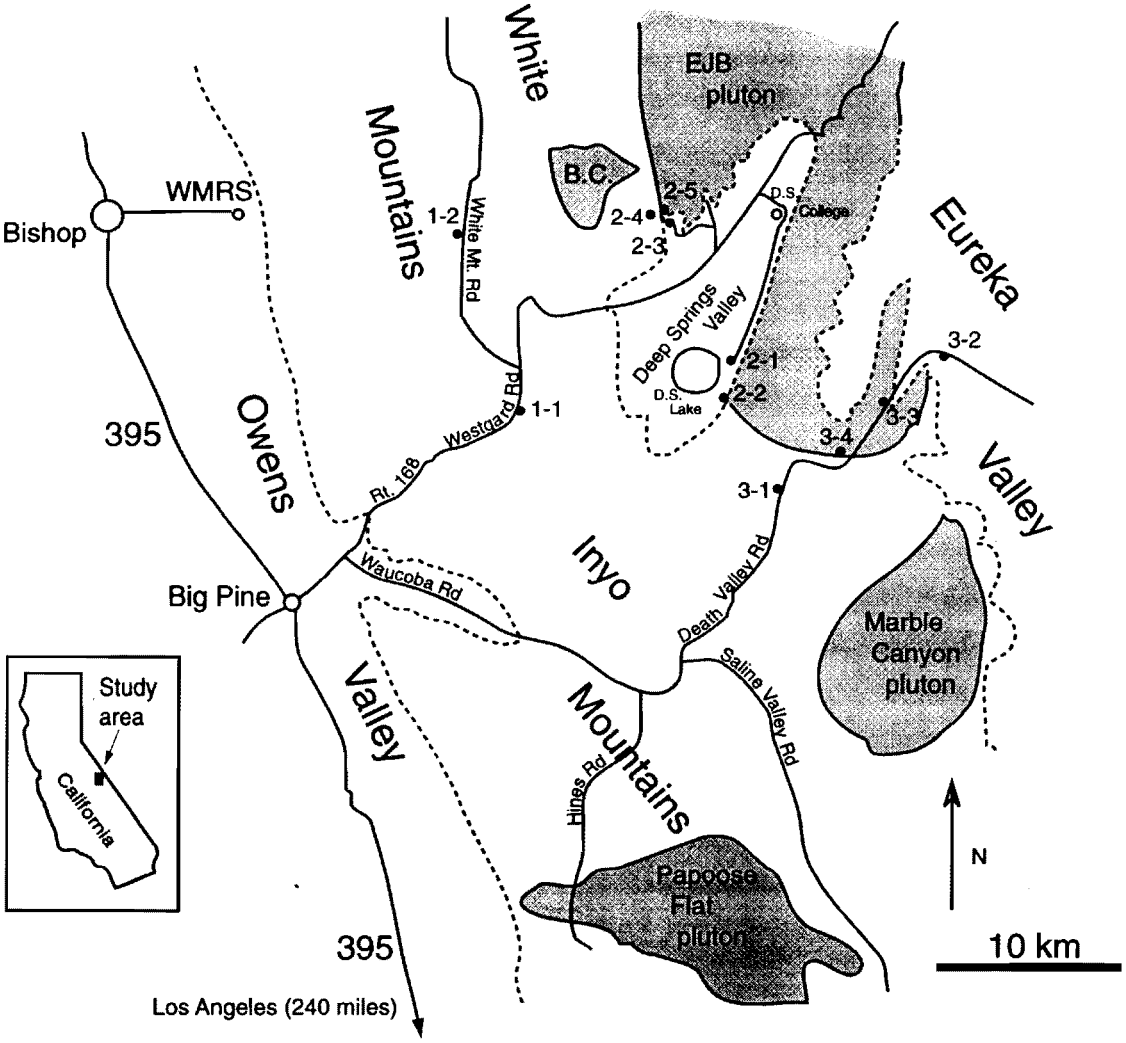

Figure 25. Field trip route map showing locations of stops for Day One (Stops 1-1 and 1-2), Day Two (Stops 2-1 to 2-5) and Day Three (Stops 3-1 to 3-4). Westgard Road (days one and two), White Mountain Road (day one) and Waucoba and Death Valley Roads (day three, as far as Stop 3-2) are paved. Although, all the stops on Day Two involve travel on relatively smooth dirt roads off of Westgard Road. Other routes discussed include: Hines Rd - an unmaintained rough jeep trail requiring a 4WD vehicle, and Saline Valley Road - a maintained gravel road. WMRS = University of California, White Mountain Research Station.

From here, we will be driving up the stream valley that leads to Westgard Pass and which divides the southern White Mountains from the northern Inyo Mountains. Most of the EJB pluton is in the Inyo

Mountains except for the northwest corner (north of Deep Springs Valley). Deep Springs Valley divides the White Mountains from the Inyo Mountains on the eastern part of the range.

The section we will be driving through consists of three formations; the Lower Cambrian Campito, Poleta, and Harkless Formations. These units have been deformed by two major periods of compressional deformation, probably in the Paleozoic. The road passes through the structural saddle between the south plunging White Mountain anticline and the north plunging Inyo anticline. The two anticlines have been interpreted to be related to the same folding event which is the second major period of folding in the central White-Inyo Range (Morgan and Law, 1998). Smaller scale folds, related to these large-scale, N to NW-trending folds, are seen on both sides of the road defined by limestones in the Poleta Formation as we enter the stream valley from Owens Valley. Numerous high angle faults disrupt the stratigraphy throughout the White-Inyo Range and can be seen from the road.

Smaller-scale, NE-trending folds are also observed in this part of the White-Inyo Range (Sylvester and Babcock, 1975). These folds are older, and the superposition of the NE and the N to NW-trending folds has created a series of structural basins which we will be driving through, and which the EJB pluton has intruded into farther to the east.

2.4 4.5 The shallowly dipping outcrops on the east and south sides of the road are gravels and Plio-Pleistocene Waucobi lake bed deposits of the Waucobi embayment.

1.1 5.6 5,000 ft. elevation sign

1.0 6.6 The bedrock exposed on the right side of the valley are quartzites and blue-gray limestones of the Poleta Formation. On top of the hill are the dark shales and siltstones of the overlying Harkless Formation (Nelson et al., 1991).

1.1 7.7 Toll House Spring. This spring marks the former location of a toll-house which demanded one dollar from ranchers who would use this road between Owens Valley and Fish Lake Valley (Nelson et al., 1991).

6,000 ft. elevation sign.

Bedrock here, as well as all exposures of the Campito Formation further up Westgard Road, are of the Andrews Mountain Member of the Campito Formation. The Andrews Mountain Member contains the earliest of the Cambrian trilobites (Nelson et al., 1991)

1.9 9.6 Narrow part of road. Bedrock here is Campito sandstone (Nelson, 1991).

0.4 10.0 Meter-scale fold on the left of road is in the Campito sandstones. This is a NE-trending fold.

0.4 10.4 7,000 ft. elevation sign. Entering another narrow part of the road. Archeocyathan-bearing limestone of the basal part of the Poleta Formation is exposed here (Nelson et al., 1991).

0.5 10.9 Last narrow road-way on this side of the pass. The basal Poleta limestone is exposed here (Nelson, 1991). Note the intense fracturing as the vehicles slow through the curves.

0.8 11.7 **STOP 1-1.** Park on the right side of road to view the Birch Creek pluton. In the middle distance at 12:00, the roughly flat but rugged area of light colored rocks is the Cretaceous Birch Creek Pluton which has also been interpreted to be forcefully emplaced (Nelson and Sylvester, 1971; Barton et al., 1991, p. 730-731; St Blanquat et al., 1998).

0.7 12.4 White Mountain Road. Turn Left. Pass through the Forest Service kiosk just ahead.

4.0 16.4 8,000 ft. elevation sign.

3.5 19.9 **STOP 1-2**. Sierra View. To the west is an excellent view of the high peaks of the Sierra Nevada, as well as Owens Valley and the Bishop Tuff. Mt. Whitney can be seen from the viewing area at the end of the short walk. To the southeast, the southern contact of the EJB pluton with the deflected Lower Cambrian section is visible above and south of Deep Springs Lake. The section, from here, seems to be dipping slightly to the north. Starting in the south (to the far right), at the base is the dark colored Precambrian Wyman Formation. The following formations can be seen above the Wyman moving to the north; Reed Dolomite and Deep Spring formations (striped, lighter colored layers), Campito Formation (black), Poleta Formation (gray-brown-white stripes), Harkless Formation (brown). The saddle just to the north-center of the lake is the contact between the Lower and Middle Cambrian section and the southern margin of the EJB pluton, and is our first stop tomorrow morning. The distinctive white layer above Deep Spring Lake is the upper Poleta limestone. Note how this layer and the layers above it curve downwards toward the lake as the contact is approached. This curvature illustrates the deflection from the regional structural trend into concordancy with the pluton at relatively short distances from the pluton.

The stratigraphic section we are viewing is located structurally in the western limb (facing us) of a northeast plunging anticline. Northeast folds are the older fold generation. This northeast fold is situated on the eastern limb of the larger-scale, northwest trending, Inyo anticline, which is the younger fold set, and is why the section is dipping to the northeast.

Return to vehicles and drive back south on White Mountain Road

7.5 27.4 Westgard Pass Road. Turn right, head back to Big Pine.

12.3 39.7 Route 395. Turn right (north) head to Bishop. The stratigraphic section seen to the east in the White Mountains while driving north consists of mainly the Reed Formation (massive light brown) at the base, followed by the Deep Spring Formation (striped buff beds), and the Campito Formation (black) (Nelson et al., 1991).

14.0 53.7 Line Street, Bishop. Turn right onto East Line Street.

3.6 57.3 White Mountain Research Station.

End of first day.

Day Two

Road log begins at intersection of Westgard Pass and White Mountain Road, via Big Pine, retracing most of yesterday's trip. Day Two is concerned with examination of the deformation within the structural aureole at the southwestern and western margins of the EJB pluton. We will also examine the pluton-contact at both localities. The morning stop at the southwestern margin includes a 5 km (round-trip) hike up a steep canyon with some moderate rock scrambling. The afternoon stop at the western margin entails an easy 2 km hike.

0.0 0.0 Continue north on Westgard Pass Road from the intersection with White Mountain Road. The low relief area here is called Cedar Flats.

0.9 0.9 Westgard Pass, elevation 7,271 ft. From here until Deep Springs Valley, we will be descending through Payson Canyon which is composed of dark weathering Campito sandstones which are strongly jointed. Slaty cleavage is visible in the interbedded shales.

1.2 2.1 Elevation 7,000 ft.

1.3 3.4 Straight ahead, before the road curves sharply to the left, is a mafic dike which, at this position in the road, is perpendicular to the road and resembles a "wall". The dike is undeformed and strikes northeast.

3.3 6.7 To the south are the Poleta folds. Famous to field camp students throughout California and originally mapped and used for teaching purposes by Clem Nelson and students at UCLA. Several folds within the middle and upper Poleta and lower Harkless Formations are visible, as well as some high angle faults.

We are entering Deep Springs Valley. This valley formed less than 0.76 Ma, or after the Bishop Tuff was deposited from the massive eruption of the Long Valley Caldera in

Owens Valley. Tehpra cobbles, correlated to the Bishop Tuff, along with cobbles from the White Mountains to the north, are stranded in paleo-valleys in the mountains just east of Deep Springs Valley (Reheis, 1993). Prior to faulting and opening of Deep Springs Valley, streams continued from the White Mountains into Eureka Valley to the southeast.

1.8 8.5 At the "cattle" road sign, look to 9:00 for a view of the contact between the western margin of the EJB pluton and the Middle Cambrian section. The contact here is between a thin portion of the Joshua Flat Monzonite and the Monola and Mule Spring Formation marbles. Most of the igneous rocks north of the road are Beer Creek Monzonite. This is the location of our afternoon stop and also a measured section (western traverse, Fig. 8a).

0.9 9.4 To the east, especially in the morning light, shadows highlight the exposed fault scarp within alluvial fans along the eastern margin of Deep Springs Valley.

4.1 13.5 Entrance to Deep Springs College, turn right. Pass through campus bearing to the right. Head south along base of cliff along dirt road.

7.4 20.9 Gate.

0.7 21.6 Pass through gate on left.

0.1 21.7 **STOP 2-1.** Park and lock cars. From here we will hike and scramble up the canyon that crosses the southern contact of the EJB with the Cambrian section and will not return until lunch. The canyon that we will hike up is a little over one km south of the parked cars and has the largest alluvial fan emitting from it.

Walk through the cattle yard heading southeast and follow the trail that passes through a marshy area and around the eastern margin of a small pond east of Deep Springs Lake. As the trail begins to climb over the scree, note the boulder defined gulleys originating up-slope that have been left behind by rock falls. These boulders are Joshua Flat monzonite.

A little over one km from the cars, begin hiking up the alluvial fan and into the canyon.

STOP 2-2. Stop at the mouth of the canyon and examine the abundant leucocratic sills intruded into the schist of the Harkless Formation on the north side of the canyon. Here the contact is one-two hundred meters to the north. Some of the sills have been boudinaged and a few have been sheared. Shear sense indicators are not well developed. The few we have seen, mostly indicate a pluton-down sense of shear.

From here we will hike up the canyon towards the EJB pluton-wall rock contact. The objectives are to examine and discuss the syn-intrusive nature of the deformation and the deformation mechanisms that accommodated 65% shortening of the Cambrian formations. We will pass through quartzite and schist of the Harkless Formation and into the marble and calc-silicate and schist of the Saline Valley Formation, all deformed at high temperature. There are no formal stops, only many interesting outcrops. Look for sills, boudinage, necking, low-angle shear bands, chaotic foliation, folding, lineations and shear sense indicators. Lineations are obvious at some outcrops, but mostly absent. Shear sense indicators are also not prevalent and are not consistently oriented from outcrop to outcrop, although, there seems to be more 'pluton-down' than 'pluton-up' indicators.

We have measured a stratigraphic section (see Fig. 8b and Table 2) through the structural aureole 2 km east from here at the top of the pass. At the pass, the EJB pluton intrudes into the middle Cambrian Bonanza King Formation. Moving away from the contact (and into older formations), we measured the thickness of the Monola, Mule Spring, and Saline Valley formations. These units have a combined structural aureole thickness of 317 m, which is 36% of it's regional thickness of ~940 m.

At the beginning of the deformed marbles within the Saline Valley Formation, note the impressive boudinage and chaotic folding. On the south side of the narrow gorge, note the boudinage of a calc-silicate layer that is originally 2-3 m thick.

At the contact with the monzonite of the EJB pluton and the schists of the Saline Valley Formation, note the discrete, mm-scale seams of K-feldspars and quartz grains which parallel the foliation. These are either leucocratic sills or zones of partial melting. Microscopically the K-feldspars are coarser grained than in the matrix, some are concentrically zoned, and some quartz grains are xenomorphic, suggesting crystallization from melt (Pattison and Harte, 1988).

Within the first few meters of the pluton, note the foliation of the monzonite and the many green-colored mafic enclaves which are probably products of exchange reactions with rafts of the marble wall rock. The foliation here seems to vary in appearance between solid state and magmatic. Within the first 20 m from the contact, note the folded, magma-mixed appearance of folds within rafts of schistose wall rock.

30 m from the contact, the canyon becomes very narrow and steep walled. Within 50 m from here, the canyon passes back into wall rocks again, indicating that the contact fingers in between the Cambrian section and the main mass of the EJB pluton. Turn around and head back down the canyon and back to the cars and lunch.

0.1 21.7 Turn the cars around and head back to Deep Springs College and Westgard Pass Road.

8.2 29.9 Westgard Pass Road (Route 168). Turn left (south).

3.0 32.9 Turn right onto dirt road. Vehicles will be on dirt roads until we return to Westgard Pass Road.

0.5 33.4 Turn left onto dirt road.

1.4 34.8 Gulley and intersection. Beware of low clearance. Turn right as the road wraps around the outcrop of Beer Creek Monzonite to the right.

0.2 35.0 Bear left at "v" intersection.

0.4 35.4 Bear left at intersection heading towards the wider canyon and Birch Creek.

0.4 35.8 Turn right (if you go straight ahead, the road is washed out a few meters further) and head towards saddle and contact.

0.1 35.9 **STOP 2-3.** Park vehicles. Here we will hike to two outcrops, the first one is 700 m from the contact, and then, time permitting, we will examine the contact

between the EJB and marble and calc-silicate of the Monola Formation (closer to the vehicles). In between the two outcrops is the location of the western traverse and a measured section (see Fig. 8a & Table 2) through the structural aureole. Along this traverse, the Saline Valley, Harkless, and Poleta formations have a combined structural aureole thickness of 374 m, which is 30% of their regional stratigraphic thickness of ~1237 m.

Walk up the main canyon to the northwest, parallel to Birch Creek, keeping close to the hills on the right (north). Walk approximately 700 m to the first minor stream valley on the right (north), off of the Birch Creek Canyon. Follow this streambed to outcrops on the left side of the stream in the Campito Formation where excellent outcrops of boudinage in quartzites of the Campito Formation have developed within the structural aureole.

0.7 36.6 **STOP 2-4.** Boudinaged Campito Formation. This outcrop is 700 m from the EJB pluton contact. The objective of this stop is similar to the morning stop, i.e., examination and discussion of the syn-intrusive nature of the deformation and the deformation mechanisms, with a focus on the boudinage.

In the few places where the third dimension can be observed, it is clear that this is chocolate tablet boudinage, i.e., the boudins have extended in all directions within the foliation plane and represent flattening strains. The boudins are principally developed in quartzite layers surrounded by pelitic schist. Note that some of the boudins have deformed internally by fracture. These are shear fractures with minor displacement consistent with the extension of the boudins. Some of the necks in between boudins exhibit features indicative of partial melting, or precipitation of fluids during deformation.

Andalusite is the stable Al_2SiO_5 phase in the pelitic schists here, 700 m from the contact, and is commonly observed right up to the pluton-contact. Sillimanite is observed closer to the pluton, at distances less than 300 m from the pluton-contact and texturally is later than andalusite. Kyanite is also observed at this outcrop but only within some of the quartzite boudins. Within the eastern aureole of the EJB pluton, kyanite is also only observed within quartzite, but is found closer to the pluton-contact than sillimanite. Presently we do not understand why kyanite is observed at varying distances from the pluton relative to

sillimanite and why kyanite only exists with quartz. Large porphyroblasts of corundum also exist at this outcrop within quartz-rich schist and are also puzzling.

Microstructurally, many of the samples collected in between Stop 2-4 and the pluton-contact contain shear bands defined by fibrolite fibers. These shear bands cross-cut the earlier foliation and also post-date the growth of andalusite, which has broken down into white mica.

Hike back towards the vehicles (~700 m) but follow along contour to the left and head to the EJB pluton contact. The contact is directly uphill from the parked vehicles.

STOP 2-5. EJB pluton-metasedimentary aureole contact. Objectives are to examine the foliation in the pluton for shear sense indicators and to discuss the physical state of the magma at the time of foliation development. The skarn is particularly well developed here.

Head back to the vehicles and follow the same dirt roads to Westgard Pass Road (right turn), Big Pine and Rt. 395 (right turn), and Bishop (right turn on East Line St.), which will take us back to the White Mt. Research Station.

End of Second day.

Day three

Day three will consist of a half-day in the field and then the long drive back to Los Angeles. In the morning we will drive to Eureka Valley where we will view, from a distance, the rapid change in orientation of the sedimentary rocks as they curve from roughly horizontal dips to subvertical dips at the southeastern EJB pluton-contact. Then we will drive through the pluton, stopping briefly to examine the foliation within the interior. The last and longest stop will include a hike to examine the boudinage within the calc-silicate layering at the southern contact of the EJB pluton.

Begin at the northern end of Big Pine at the intersection of Route 395 and Westgard Pass Road (Rt. 168).

0.0 0.0 Drive east on Westgard Pass Road (Rt. 168).

2.2 2.2 Turn right onto Waucoba Road.

2.9 5.1 On the left are the Plio-Pleistocene Waucobi Lake beds which dip towards Owens Valley (Nelson et al., 1991). Volcanic tuff within the succession has been dated at 2.3 Ma (Bachman, 1978).

Bedrock exposures driving up to the top of the range are of the Cambrian and Neoproterozoic section. At the top of the pass, we will be driving through the core of the Inyo anticline and the bedrock exposures will be in the Wyman Formation. The base of the Wyman is not exposed.

5.3 10.4 Devils Gate. These highly folded and faulted quartzites and dolomites are within the Reed Dolomite. Folds here trend NNE and may be related to the first period of deformation in the central White-Inyo Range.

3.2 13.6 Hines Road on right. This winding jeep trail leads up into the Inyo Range and to the Papoose Flat pluton which is also believed to have been forcibly emplaced (Sylvester et al., 1978a; Law et al. 1992, 1993; Nyman et al., 1995; Morgan et al., 1998). Four-wheel drive vehicles recommended.

Outcrops on the left of road are Neoproterozoic Wyman Formation.

1.9 15.5 Saline Valley Road on right. This road leads to the eastern end of Papoose Flat pluton and down into Saline Valley. This intersection also marks the top of the range and the core of the Inyo anticline. From here on we will be descending into Eureka Valley and back up through the stratigraphic section.

7.2 22.7 **STOP 3-1.** Stop along the road. We are now within the metamorphic aureole of the EJB pluton. The structural aureole is still over 1 km away. The Harkless Formation quartzites form the ridge parallel to the road on the right. Note the shallow dip of the stratigraphy here. The cross section in Fig. 5 of the field guide article is drawn

along this ridge. Straight ahead is the EJB pluton with the structural aureole in the foreground.

Examination of the map pattern of the cleavage and bedding relationships in this vicinity (see Figs. 10 & 11) helps us to understand the kinematics of the deformation in the structural aureole.

1.2 23.9 Road curves sharply to the right, just after entering the structural aureole. The road winds along within the structural aureole for a little over 2 miles. Note the dip of the stratigraphy here, now that we are within the structural aureole. The road passes through the Harkless, Saline Valley, Mule Spring, Monola, and Bonanza King formations before entering the pluton.

1.7 25.6 Road crosses stream valley that leads to Stop 3-4 on return trip.

0.6 26.2 Contact with EJB pluton. Contact not exposed along road.

Start descending into Eureka Valley. Marbles to the right of road are a large section of Bonanza King Formation which juts into the main body of the EJB pluton.

4.5 30.7 Road curves to the right and turns into a gravel road. Entering Eureka Valley and a little further ahead Death Valley National Park. The Eureka Sand Dunes are to the southeast and are the largest dunes in California.

1.2 31.9 **STOP 3-2.** Stop along road. The prominent ridge to the south contains the southeastern EJB pluton-contact which is subvertical. To the left is the Lower Cambrian section. Note how rapidly the section rotates from subhorizontal dips to subvertical dips adjacent to the pluton-contact. This view also illustrates the smoothly curving nature of the folded stratigraphy as it rotates from regional dips to dips associated with pluton emplacement.

Turn cars around and begin climbing back out of Eureka Valley.

4.4 36.3 **STOP 3-3.** Stop along road. Here we will examine the interior of the Joshua Flat Monzonite to the right (west) of road, focusing on the physical nature of the magma during foliation and lineation development. K-feldspar and plagioclase megacrysts and hornblende phenocrysts define both a well developed foliation and locally, a lineation.

1.2 37.5 Cross the contact and continue into the structural aureole.

0.6 38.1 **STOP 3-4.** Stop where the road crosses the stream valley. Park the vehicles at the turnoff on the right. From here we will hike (less than 1 mile round-trip) down the stream valley to the EJB pluton-contact where excellent exposures of chocolate tablet boudinage have developed in calc-silicate layers and within leucocratic sills.

End of field trip. Return to vehicles and continue driving south on Waucoba/Death Valley Road to Westgard Pass Road and Big Pine. South on Rt. 395 to Los Angeles.

Acknowledgements

Field and laboratory work was funded through grants from the Geological Society of America, Sigma Xi and University of California White Mountain Research Station to S.S. Morgan, and National Science Foundation grants EAR-9018929 and EAR-9506525 to R.D. Law. The authors particularly wish to thank Maxine Smith, Edward Czaja, Wesley Knight, Adam Henry, Meredith Westington, and John Vines for their help in collecting field data and samples, and Clem Nelson for support and encouragement of our work in the White-Inyo Range. A critical review of this manuscript by Rick Behl is gratefully acknowledged. Our friends at WMRS have provided abundant support, along with home-made beer and cookies, and have greatly added to our experience in the central White-Inyo Range.

References

Akaad, M.K., 1956, The northern aureole of the Ardara pluton of County Donegal: Geological Magazine, v. 93, p. 377-392.

Archanjo, C.J., Launeau, P., and Bouchez, J.L. (1995) Magnetic fabric versus magnetite and biotite shape fabrics of the magnetite-bearing granite pluton of Gameleiras (Northeast Brasil), Phys. Earth Plan. Inter. 89, 63-75.

Bachman, S.B., 1978, Pliocene, Pleistocene break-up of the Sierra Nevada - White-Inyo mountain block and formation of Owens Valley: Geology, v. 6, p. 461-463.

Barton, M.D., Staude, J.M., Snow, E.A., and Johnson, D.A., 1991, Aureole Systematics, *in* Kerrick, D.M., ed., Contact metamorphism: Mineralogical Society America, Reviews in Mineralogy, v. 25, p. 723-820.

Bateman, P.C., 1992, Plutonism in the Central Part of the Sierra Nevada Batholith, California: U.S. Geological Survey Professional Paper 1483, 186p.

Bilodeau, B.J., and Nelson, C.A., 1993, Geology of the Sage Hen Flat pluton, White Mountains, California; Geological Society of America, Map and Chart Series MCH077, scale 1:24,000.

Bouchez, J.L., 1997, Granite is never isotropic: An introduction to AMS studies of granitic rocks, in: Granite: From segregation of melt to emplacement fabrics, Bouchez, J.L., et al., eds., Kluwer Academic Publishers, Netherlands, p. 95-112.

Courrioux, G., 1987, Oblique diapirism: the Criffel granodiorite/granite zoned pluton (southwest Scotland): Journal of Structural Geology, v. 9, p. 313-330.

Crowder, D.F., McKee, E.H., Ross, D.C., and Krauskopf, K.B., 1973, Granitic rocks of the White Mountains area, California-Nevada: age and regional significance: Geological Society of America Bulletin, v. 84, p. 285-296.

Dunne, G.C., 1986, Mesozoic evolution of southern Inyo, Argus and Slate ranges, in Dunne, G.C., ed., Mesozoic-Cenozoic structural evolution of selected areas, east-central California: Geological Society of America Bulletin, Cordilleran Section, Guidebook and volume, fieldtrips 2 and 14, p. 3-22.

Ellwood, B.B. and Whitney, J.A. (1980) Magnetic fabric of the Elberton granite, Northeast Georgia, J. Geophys. Res. 85, 1481-1486.

England, R.W., 1992, The genesis, ascent, and emplacement of the Northern Arran Granite, Scotland: Implications for granitic diapirism: Geological Society of America Bulletin, v. 104, p. 606-614.

Evernden, J.F., and Kistler, R.W., 1970, Chronology of emplacement of Mesozoic batholithic complexes in California and western Nevada: U.S. Geological Survey Professional Paper 623, 42 p.

Gillespie, J.G., 1979, U-Pb and Pb-Pb ages of primary and detrital zircons from the White Mountains, eastern California: Geological Society of America Abstracts with Programs, v. 11, no. 30, p. 79.

Glazner, A.F., and Miller, D.M., 1997 , Late-stage sinking of plutons: Geology, v. 25, p. 1099-1102.

Grégoire, V., de Saint-Blanquat, M., Nédélec, A., and Bouchez, J.L. (1995) Shape anisotropy versus magnetic interactions of magnetite grains: experiments and application to AMS in granitic rocks, Geophys. Res. Letters 22, 2765-2768.

Grégoire, V., Darrozes, J., Gaillot, P., Nédélec, A., and Launeau, P., in press, Magnetite grain shape fabric and distribution anisotropy versus magnetic fabric : a 3D-case study. Journal of Structural Geology.

Hargraves, R.B., Johnson, D., and Chan, C.W., 1991, Distribution anisotropy: the cause of AMS in igneous rocks? Geophysics Research Letters, v. 18, p. 2193-2196.

Hirth, G., and Tullis, J., 1992, Dislocation creep regimes in quartz aggregates: Journal of Structural Geology v. 14, p. 145-159.

Holdaway, M.J., 1971, Stability of andalusite and the aluminum silicate phase diagram: American Journal of Science, v. 271, p. 97-131.

Holder, M.T., 1979, An emplacement mechanism for post-tectonic granite and its implications for their geochemical features, In: Origin of Granite Batholiths: Geochemical Evidence, Atherton, M.P., and Tarney, J., eds., Shiva, Kent, p. 116-128.

Jackson, J.A., ed., 1997, Glossary of Geology, Fourth Edition: Alexandria, Virginia, American Geological Institute, 769p.

John, B.E., and Blundy, J.D., 1993, Emplacement-related deformation of granitoid magmas, southern Adamello Massif, Italy: Geological Society of America Bulletin, v. 105, p. 1517-1541.

Khan, M.A. (1962) The anisotropy of magnetic susceptibility of some igneous and metamorphic rocks, J. Geophys. Res. 67, B7, 2873-2885.

Kerrick, D.M., 1987, Fibrolite in contact aureoles of Donegal, Ireland: American Mineralogist, v. 72, p. 240-254.

Launeau, P. and Cruden, A.R., in press, Magmatic fabric acquisition mechanisms in a syenite : Results of a combined AMS and image analysis study. Journal of Geophysical Research.

Law, R.D., Morgan, S.S., Casey, M., Sylvester, A.G., and Nyman, M., 1992, The Papoose Flat pluton of eastern California: a re-assessment of its emplacement history in the light of new microstructural and crystallographic fabric observations: Transactions Royal Society Edinburgh: Earth Sciences., v. 83, p. 361-375.

Law, R.D., Sylvester, A.G., Nelson, C.A., Morgan, S.S., and Nyman, M.W., 1993, Deformation associated with emplacement of the Papoose Flat pluton, Inyo Mountains, eastern California: Geologic Overview and Field Guide, in Lahren, M.M., Trexler, J.H., Jr. and Spinosa, C., eds., Crustal evolution of the Great Basin and Sierra Nevada: Cordilleran/Rocky Mountain Section, Geological Society of America Guidebook, Department of Geological Sciences, University of Nevada, Reno, p. 231-261.

Lister, G.S., and Dornsiepen, U.F., 1982, Fabric transitions in the Saxony Granulite Terrain. Journal of Structural Geology, v. 4, p. 81-92.

McKee, E.H., 1968, Geology of the Magruder Mountain area, Nevada-California: U.S. Geological Survey Bulletin 1250-1H, 40p.

McKee, E.H., and Conrad, J.E., 1996, A tale of 10 plutons - revisited: Age of granitic rocks in the White Mountains, California and Nevada: Geological Society of America Bulletin, v. 108, 1515-1527.

McKee, E.H., and Nash, D.B., 1967, Potassium-argon ages of granitic rocks in the Inyo batholith, east-central California: Geological Society of America Bulletin, v. 78, p. 669-680.

McKee, E.H., and Nelson, C.A., 1967, Geologic map of Soldier Pass Quadrangle: U.S. Geological Survey Geological Quadrangle Map GQ-654, scale1:62,500.

Miller, C.F., 1977, Alkali-rich monzonites, California, origin of near silica-saturated alkaline rocks and their significance in a calc-alkaline batholithic belt [PhD thesis]: Los Angeles, University of California, 289 p.

Miller, C.F., 1978, Monzonitic plutons, California, and a model for generation of alkali-rich, near silica-saturated magmas: Contributions to Mineralogy and Petrology, v. 67, p. 349-355.

Miller, J., 1996, U/Pb crystallization age of the Papoose Flat pluton, White-Inyo Mountains, California: Geological Society of America Abstracts with Programs, v. 28, no. 5, p. A91.

Moore, J.N, 1976, Depositional environments of Lower Paleozoic rocks in the White-Inyo Range, Inyo Country, California; a field trip road log, *in* Moore, J.N. and Fritsche, A.E., eds., Depositional environments of Lower Paleozoic rocks in the White-Inyo Mountains, Inyo County, California: Los Angeles, California, Society of Economic Paleontologists and Mineralogists, Pacific Section, p. 1-11.

Morgan, S.S. & Law, R.D., 1994, Forceful intrusion of Jurassic plutons in the central White-Inyo Range, eastern California: Geological Society of America Abstracts with Programs, v. 26, No 7, A134.

Morgan, S.S. & Law, R.D., 1998, An Overview of Paleozoic - Mesozoic Age Structures Developed in the Central White-Inyo Range, Eastern California. International Geology Review, v 40, p. 245-256.

Morgan, S.S., Law, R.D. & Nyman, M.W., 1998, Laccolith-like emplacement model for the Papoose Flat pluton based on porphyroblast-matrix analysis: Geological Society of America Bulletin, v. 110, p. 96-110.

Mount, J.F., and Signor, P.W., 1989, Paleoenvironmental context of the metazoan radiation event and its impact on the placement of the Precambrian-Cambrian boundary: examples from the southwestern Great Basin, USA, *in* Christie-Blick, N., and Levy, J., eds., Late Proterozoic and Cambrian tectonics, sedimentation, and record of metazoan radiation in the western United States, Amer. Geophys. Union, Field Trip Guidebook T331, p. 39-46.

Nash, D.B., 1962, Contact metamorphism at Birch Creek, Blanco Mountain Quadrangle, Inyo County, California [PhD thesis]: Berkeley, University of California.

Nelson, C.A., 1962, Lower Cambrian-Precambrian succession, White-Inyo Mountains, California: Geological Society of America Bulletin, v. 73, p. 139-144.

Nelson, C.A., 1966a, Geologic map of the Waucoba Mountain Quadrangle, Inyo County, California: U.S. Geological Survey Geological Quadrangle Map GQ-528, scale 1:62,500.

Nelson, C.A., 1966b, Geologic map of the Blanco Mountain quadrangle, Inyo County, California: U.S. Geological Survey Geological Quadrangle Map GQ-529, scale 1:62,500.

Nelson, C.A., 1971, Geologic map of the Waucoba Spring quadrangle, Inyo County, California: U.S. Geological Survey Geological Quadrangle Map GQ-921, scale 1:62,500.

Nelson, C.A., 1978, Late Precambrian - early Cambrian stratigraphic and faunal succession of eastern California and the Precambrian-Cambrian boundary: Geological Magazine, v. 115, p. 121-126.

Nelson, C.A., 1980, Guidebook to the geology of a portion of the eastern Sierra Nevada, Owens Valley and White-Inyo Range: Department of Earth and Space Sciences, Univ. California, Los Angeles. ESSSO Guidebook 12, 107 pp.

Nelson, C.A., 1997, The Beer Creek-Cottonwood igneous contact, Southern White Mountains, California: International Geology Review, v. 39, p. 855-859.

Nelson, C.A., and Sylvester, A.G., 1971, Wall rock decarbonation and forcible emplacement of Birch Creek pluton, southern White Mountains, California: Geological Society of America Bulletin, v. 82, p. 2891-2904.

Nelson, C.A., Oertel, G., Christie, J.M. and Sylvester, A.G., 1977, Geologic map, structure sections and palinspastic map of the Papoose Flat pluton, Inyo Mountains, California.: Geological Society of America Map and Chart Series MC-20, scale 1:32,300.

Nelson, C.A., Hall, C. A., and Ernst, W.G., 1991, Geologic history of the White-Inyo Range, *in* Hall, C.A., ed., Natural History of the White-Inyo Range eastern California: Berkeley and Los Angeles, California, Univ. California Press, p. 42-74.

Nyman, M.W., Law, R.D., and Morgan, S.S., 1995, Conditions of contact metamorphism, Papoose Flat Pluton, eastern California, USA: implications for cooling and strain histories: Journal of Metamorphic Geology, v.13, 627-643.

Paterson, S.R., Brudos, T., Fowler, K., Carlson, C., Bishop, K and Vernon, R.H., 1991, Papoose Flat pluton: forceful expansion or post-emplacement deformation?: Geology, v. 19, p. 324 - 327.

Paterson, S.R., and Fowler, K., 1993, Re-examining pluton emplacment processes: Journal of Structural Geology, v. 15, p. 191-206.

Pattison, D.R.M., 1992, Stability of andalusite and sillimanite and the Al_2SiO_5 triple point: Constraints from the Ballachulish aureole, Scotland: Journal of Geology, v. 100, p. 423-446.

Pattison, D.R.M., and Harte, B., 1988, Evolution of structurally contrasting anatectic migmatites in the 3-kbar Ballachulish aureole, Scotland: Journal of Metamorphic Geology, 6, 475-494.

Pattison, D.R.M., and Tracy, R.J., 1991, Phase equilibria and thermobarometry of metapelites, *in* Kerrick, D.M., ed., Contact metamorphism: Mineralogical Society America, Reviews in Mineralogy, v. 25, p. 105-206.

Pitcher, W.S., and Read, H.H., 1963, Contact metamorphism in relation to manner of emplacement of the granites of Donegal, Ireland: Journal of Geology, v. 71, p. 261-296.

Ramsay, J.G., 1989, Emplacement kinematics of a granite diapir: the Chindamora batholith, Zimbabwe: Journal of Structural Geology, v. 11, p. 191-209.

Reheis, M., C., 1993, Neogene tectonism from the southwestern Nevada volcanic field to the White Mountains, California: Part II. Late Cenozoic history of the southern Fish Lake Valley Fault zone, Nevada and California: in Lahren, M. M., Trexler, J.H., Jr., and Spinosa, C., eds., Crustal evolution of the Great Basin and Sierra Nevada: Cordilleran/Rocky Mountain Section, Geological Society of America Guidebook, Department of Geological Sciences, University of Nevada, Reno, p. 370-382.

Ross, D.C., 1967a, Geologic map of the Waucoba Wash Quadrangle, Inyo County, California: U.S. Geological Survey Geological Quadrangle Map GQ-612, scale 1:62,500.

Rothstein, D.A., and Hoisch, T.D., 1994, Multiple intrusions and low-pressure metamorphism in the central Old Woman Mountains, south-eastern California: constraints from thermal modelling: Journal of Metamorphic Geology, v. 12, p. 723-734.

Saint Blanquat, M., 1993, EXAMS; an Excel macro for automatic computing of AMS data. Unpublished program, University of Toulouse.

Saint Blanquat, M., and Tikoff, B., 1997, Development of magmatic to solid-state fabrics during syntectonic emplacement of the MonoCreek granite, Sierra Nevada batholith: in: Granite: From segregation of melt to emplacement fabrics, Bouchez, J.L., et al., eds., Kluwer Academic Publishers, Netherlands, p. 231-252.

Saint Blanquat, M., Law, R.D., Barton, M. and Morgan, S.S., 1998, Internal structure of the Birch Creek pluton, White Mountains, California; new A.M.S. and microstructural data and relationships to intrusive suites: Geological Society of America Abstracts with Programs, v. 30, p.

Sanderson, D.J., and Meneilly, A.W., 1981, Analysis of three-dimensional strain modified uniform distributions: andalusite fabrics from a granite aureole: Journal of Structural Geology, v. 3, p. 109-116.

Stacey, F.D. (1960) Magnetic anisotropy of igneous rocks, J. Geoph. Res. 65, 2429-2442.

Stein, E., 1994, Structures in the aureole of the Joshua Flat pluton: Implications for country rock flow patterns during emplacement: Geological Society of America Abstracts with Programs, Cordilleran Section, v. 26, p. 95.

Stein, E., and Paterson, S.R., 1996, Country rock displacement during emplacement of the Joshua Flat pluton, White-Inyo Mountains, California: in Oncken, O., and Janssen, C., eds., Basement Tectonics, v. 11, p. 35-49, Boston, Kluwer Academic Publishers.

Stephenson, A., 1994, Distribution anisotropy: two simple models for magnetic lineation and foliation, Physics of the Earth and Planetary Interiors, v. 82, 49-53.

Stern, T.W., Bateman, P.C., Morgan, B.A., Newell, M.F., and Peck, D.L., 1981, Isotopic U-Pb ages of zircon from the granitoids of the central Sierra Nevada, California: U.S. Geological Survey Professional Paper H85, 17p.

Stevens, C.H., Stone, P., Dunne, G.C., Greene, D.C., Walker, J.D., and Swanson, B.J., 1997, Paleozoic and Mesozoic evolution of east-central California: International Geology Review, v. 39, p. 788-829.

Stewart, J.H., 1966, Correlation of Lower Cambrian and some Precambrian strata in the southern Great Basin, California and Nevada. U.S. Geological Survey Professional Paper 550-C, p. C66-C72.

Stewart, J.H., and Poole, F.G., 1974, Lower Paleozoic and uppermost Precambrian Cordilleran miogeocline, Great Basin, Western United States, in Dickinson, W.R., ed., Tectonics and Sedimentation: Society of Economic Paleontologists and Mineralogists Special Publication 22, p. 28-57.

Sylvester, A.G., 1964, The Precambrian rocks of the Telemark area in south central Norway. III. Geology of the Vrådal granite: Norsk Geologisk Tidsskrift, v. 44, p. 445-482.

Sylvester, A.G., in press, Magma mixing, structure, and re-evaluation of the emplacement mechanism of Vrådal pluton, central Telemark, southern Norway: Norsk Geologisk Tidsskrift.

Sylvester, A.G., and Babcock, J.W., 1975, Significance of multiphase folding in the White-Inyo Range, eastern California: Geological Society of America Abstracts with Programs, v. 7 p. 1289.

Sylvester, A.G., Oertel, G., Nelson, C.A., and Christie, J.M., 1978a, Papoose Flat pluton: A granitic blister in the Inyo Mountains, California: Geological Society of America Bulletin, v. 89, p. 1205-1219.

Sylvester, A.G., Miller, C.F., and Nelson, C.A., 1978b, Monzonites of the White-Inyo Range, California, and their relation to the calc-alkalic Sierra Nevada batholith: Geological Society of America Bulletin, v. 89., p. 1677-1687.

Uyeda, S., Fuller, M.D., Belshe, J.C., and Girdler, R.W. (1963) Anisotropy of magnetic susceptibility of rocks and minerals, J. Geophys. Res. 68, 279-291.

Vernon, R.H., 1987, Growth and concentration of fibrous sillimanite related to heterogeneous deformation in k-feldspar-sillimanite meta-pelites: Journal of Metamorphic Geology, v. 5, p. 51-68.

Walcott, C.D., 1895a, Lower Cambrian rocks in eastern California. American Journal of Science, 49, 141-144.

Walcott, C.D., 1895b, The Appalachian type folding in the White Mountain Range of Inyo county, California: American Journal of Science, v. 49, p. 169-174.

Walcott, C.D., 1908, Cambrian sections of the Cordilleran area: Smithsonian Miscellaneous Collections 53, 167-230.

Welch, T.C., 1979, Superposed Mesozoic deformations in the southern White Mountains, eastern California: Geological Society of America Abstracts with Programs, v. 11, p. 134-135.

Yochelson, E.L., and Nelson, C.A., 1994, Walcott and the Early Cambrian of eastern California: Geology of the White-Inyo Area, 1894-1897, in Hall, C.A., and Widawski, B., eds., The Crooked Creek Guidebook: p. 15-38. University of California, White Mountain Research Station.

Appendix A AMS Data

KEY

Site	Location identification number
Km	Average susceptibility of K1, K2, and K3, in 10^{-6} SI
K1m	Average susceptibility of K1 at this location in 10^{-6} SI
K2m	Average susceptibility of K2 at this location in 10^{-6} SI
K3m	Average susceptibility of K3 at this location in 10^{-6} SI
P%	Percent anisotropy = 100*(K1+14) / (K3+14)-1
L%	Percent anisotropy = 100*(K1+14) / (K2+14)-1
Pflinn	Flinn parameter = L% / (P%-L%)
T	T shape parameter = 2*(lnK2 – lnK3) / (lnK1-lnK3)-1
Lineation	Trend and plunge of the lineation
K2D	Declination of K2
K2I	Inclination of K2
K3D	Declination of K3
K3I	Inclination of K3
Foliation	Azimuth, dip direction, and dip angle of the foliation
Nb	number of samples at this location (taken from the two cores)
A(K1)	half angle of confidence for K1, in degrees (within 95% probability)
A(K3)	half angle of confidence for K3, in degrees (within 95% probability)
St Er	Standard Error of Km

site	Km	K1m	K2m	K3m	P%	L%	Pfinn	T	linea	tion	K2D	K2I	K3D	K3I	folia	t	ion	nb	a(K1)	a(K3)	St Er
EB001	23895.1	25338.3	24035.8	22311.2	13.6	5.4	0.67	0.17	331	36	233	14	125	52	35	W	38	4	3	2	0.82
EB002	14279.4	15031.9	14320.7	13485.6	11.5	5.0	0.76	0.11	333	43	235	7	137	47	47	N	43	4	3	3	0.53
EB003	29627.6	33192.3	28949.5	26740.9	24.1	14.6	1.55	-0.27	298	48	48	17	153	38	63	N	52	4	1	7	1.49
EB004	42605.5	45069.4	41815.9	40931.3	10.1	7.8	3.34	-0.56	356	39	112	33	230	39	140	E	51	4	2	6	1.39
EB005	36491.6	39755.2	36512.6	33206.9	19.7	8.9	0.82	0.05	355	42	251	15	146	45	56	N	45	4	2	2	1.73
EB006	56191.4	63355.0	57328.6	47890.6	32.3	10.5	0.48	0.29	352	42	260	2	168	48	78	N	42	4	2	1	3.39
EB007	41071.3	46186.6	41433.9	35593.5	29.7	11.5	0.63	0.17	254	53	32	29	134	21	44	W	69	4	2	2	2.82
EB008	28412.4	30955.5	28440.4	25841.4	19.8	8.8	0.81	0.06	336	63	243	3	148	25	58	N	65	5	3	3	2.74
EB009	61979.7	69685.9	62266.6	53986.5	29.1	11.9	0.69	0.12	288	74	114	15	23	1	113	S	89	5	1	1	2.01
EB010	41864.4	45684.3	42543.0	37365.6	22.3	7.4	0.50	0.29	357	49	267	0	177	41	87	N	49	6	2	1	1.87
EB011	7280.2	7660.1	7423.2	6757.5	13.3	3.2	0.31	0.50	340	44	239	10	142	43	52	N	47	7	5	2	1.52
EB012	35128.7	40042.1	36117.5	29226.4	37.0	10.9	0.42	0.34	305	64	63	13	159	22	69	N	68	4	4	2	3.54
EB013	52887.7	60823.5	53549.0	44290.4	37.3	13.6	0.57	0.20	126	58	302	32	31	3	121	S	87	4	3	2	4.40
EB014	29835.6	32358.6	30062.8	27085.2	19.5	7.6	0.65	0.17	323	60	115	26	210	12	120	N	78	4	3	3	2.77
EB015	37309.4	40666.8	38256.4	33005.2	23.2	6.3	0.37	0.41	223	66	263	6	332	5	62	S	85	4	4	2	3.19
EB016	28221.6	30201.4	28105.4	26358.1	14.6	7.5	1.05	-0.06	276	66	97	24	7	0	97	S	90	4	2	3	1.21
EB017	35886.0	39635.8	35277.7	32744.5	21.0	12.3	1.42	-0.22	337	62	115	24	213	19	123	N	71	4	2	3	1.93
EB018	52587.3	55896.2	52869.3	48996.3	14.1	5.7	0.69	0.15	298	41	165	40	47	37	137	W	53	4	3	2	2.29
EB019	49973.9	53785.7	49084.0	47052.1	14.3	9.6	2.02	-0.37	97	80	331	6	240	8	150	E	82	5	2	4	2.03
EB020	55314.7	60081.5	54635.2	51227.3	17.3	10.0	1.36	-0.19	303	51	110	39	204	5	114	N	85	4	2	4	2.95
EB021	52002.1	57472.9	53194.0	45339.2	26.8	8.0	0.43	0.35	348	21	172	72	256	12	166	E	78	4	3	2	3.03
EB022	52751.3	57750.4	54345.7	46157.9	25.1	6.3	0.33	0.46	350	75	191	15	100	6	10	W	84	4	3	1	2.38
EB023	38850.4	42611.0	39442.5	34497.7	23.5	8.0	0.52	0.27	100	40	192	2	285	51	15	E	39	4	3	1	1.81
EB024	34313.0	37642.1	33529.3	31767.6	18.5	12.3	1.97	-0.36	342	84	158	8	68	4	158	W	86	4	2	4	2.30
EB025	12418.6	12741.4	12531.7	11982.7	6.3	1.7	0.36	0.46	322	56	201	19	99	27	9	W	63	2	6	2	1.20
EB026	32056.4	34758.7	31762.6	29648.0	17.2	9.4	1.21	-0.13	12	63	228	22	132	14	42	W	76	4	1	2	1.09
EB027	42806.0	47885.1	41796.3	38736.4	23.6	14.6	1.61	-0.28	324	48	193	31	86	25	176	W	65	2	1	3	2.07
EB028	41125.7	43863.8	41958.8	37554.7	16.8	4.5	0.37	0.43	162	52	279	20	20	32	110	S	58	4	5	2	2.14
EB029	44421.3	49114.2	44218.7	39931.0	23.0	11.1	0.93	-0.01	21	69	142	11	235	17	145	E	73	4	2	2	1.83
EB030	71522.5	75226.0	71464.1	67877.2	10.8	5.3	0.95	0.00	301	8	67	76	209	11	119	N	79	4	2	2	2.02
EB031	86.0	89.1	86.3	82.6	6.7	2.8	0.72	0.15	329	52	207	23	105	30	15	W	60	5	16	4	1.24
EB032	32738.7	35532.0	33160.6	29523.6	20.3	7.1	0.54	0.25	39	83	230	8	139	1	49	N	89	5	4	3	3.06
EB033	37994.6	41751.6	40162.5	32069.6	30.2	4.0	0.15	0.71	340	80	272	8	178	0	88	N	90	6	8	1	2.82
EB034	35109.7	38707.7	35621.5	30999.9	24.9	8.7	0.53	0.25	102	67	235	16	329	16	59	S	74	3	3	2	2.49
EB035	51933.9	56690.8	53221.5	45889.4	23.5	6.5	0.38	0.40	254	77	98	15	9	4	99	S	86	4	5	2	3.39
EB036	46095.1	51825.7	45280.3	41179.3	25.8	14.5	1.27	-0.17	331	41	67	8	166	49	76	N	41	4	2	3	3.31
EB037	88162.8	92318.5	87941.8	84227.8	9.6	5.0	1.08	-0.06	23	49	286	6	191	39	101	N	51	5	2	2	0.93
EB038	18600.2	19266.4	18933.6	17600.6	9.5	1.8	0.23	0.61	252	10	12	70	160	16	70	N	74	4	8	2	1.32
EB039	17948.7	19272.5	17804.6	16768.8	14.9	8.2	1.23	-0.14	359	74	229	12	136	13	46	N	77	5	2	3	1.95
EB040	45211.1	50106.5	44869.7	40657.0	23.2	11.7	1.01	-0.06	152	43	254	15	358	46	88	S	44	4	3	4	3.16
EB041	29569.9	32512.2	29738.1	26459.4	22.9	9.3	0.69	0.13	24	85	258	3	167	5	77	N	85	4	4	3	2.53
EB042	46822.4	50820.6	48768.9	40877.7	24.3	4.2	0.21	0.62	279	30	156	32	34	49	124	S	41	5	6	2	2.79
EB043	41810.5	44156.1	43329.2	37946.2	16.4	1.9	0.13	0.75	338	20	181	68	70	8	160	W	82	5	13	1	1.89
EB044	50398.9	57676.6	51101.2	42418.9	36.0	12.9	0.56	0.21	325	53	160	36	65	7	155	W	83	4	2	2	3.38
EB045	56508.8	67063.1	57307.6	45155.6	48.5	17.0	0.54	0.21	337	67	205	15	113	16	23	W	74	4	1	1	2.56
EB046	40421.9	44041.5	41320.9	35903.2	22.7	6.6	0.41	0.38	347	67	147	23	240	9	150	E	81	4	2	1	1.58
EB047	9964.9	10375.5	10181.8	9337.5	11.1	1.9	0.21	0.64	290	33	164	43	37	33	127	S	57	4	4	1	1.25
EB048	46431.2	51214.2	47106.0	40973.1	25.0	8.7	0.54	0.25	80	9	180	42	340	46	70	S	44	4	1	1	1.50
EB049	34869.7	37615.0	36349.2	30644.7	22.7	3.5	0.18	0.67	354	76	149	13	249	2	159	E	88	4	4	1	1.90
EB050	45772.4	50190.6	46170.9	40955.6	22.5	8.7	0.63	0.18	330	73	140	17	231	3	141	E	87	5	2	2	1.90
EB051	39547.4	42316.1	39468.8	36857.2	14.8	7.2	0.95	-0.01	274	73	152	9	59	14	149	W	76	5	2	3	1.52
EB052	48302.2	52333.3	48949.5	43623.6	20.0	6.9	0.53	0.27	4	68	111	19	209	24	119	N	66	8	2	2	1.91
EB053	53472.9	56159.3	54429.3	49830.0	12.7	3.2	0.33	0.48	297	64	81	11	162	35	72	N	55	8	7	1	1.55
EB054	72924.3	75076.7	73669.4	70026.6	7.2	1.9	0.36	0.46	219	81	125	1	35	9	125	S	81	4	4	2	1.38
EB055	32847.6	35785.5	34049.6	28707.4	24.6	5.1	0.26	0.55	359	46	184	44	92	3	2	W	87	6	4	1	2.55
EB056	40896.5	43845.3	39906.7	38937.6	12.6	9.9	3.61	-0.59	282	37	179	14	73	48	163	W	42	6	2	9	1.64
EB057	28368.1	30246.7	29271.6	25585.9	18.2	3.3	0.22	0.61	63	82	163	1	251	7	161	E	83	6	5	1	1.91
EB058	42513.1	48699.1	41896.9	36943.5	31.8	16.2	1.04	-0.09	184	55	5	41	265	2	175	E	88	5	2	2	2.32
EB059	44354.8	51084.8	42467.7	39511.7	29.3	20.3	2.25	-0.44	318	50	113	37	214	13	124	N	77	5	1	4	2.67
EB060	43180.0	45835.9	42553.0	41151.2	11.4	7.7	2.10	-0.38	301	17	119	73	211	1	121	N	89	5	1	3	0.99
EB061	63259.4	68404.2	63364.3	58009.6	17.9	8.0	0.80	0.07	242	23	116	55	344	25	74	S	65	6	2	2	2.47
EB062	64347.3	79711.9	61456.6	51873.5	53.7	29.7	1.24	-0.21	282	53	166	18	63	32	153	W	58	5	1	2	4.91
EB063	40771.8	45404.7	43028.8	33881.9	34.0	5.5	0.19	0.63	332	46	167	43	70	7	160	W	83	6	6	2	3.35
EB064	49835.0	53228.1	49801.3	46475.5	14.5	6.9	0.90	0.02	319	20	213	4	70	13	160	W	77	6	3	4	2.02
EB065	32365.2	34287.2	33529.3	29279.1	17.1	2.3	0.15	0.72	152	27	343	63	244	4	154	E	86	6	4	1	1.21
EB066	45037.7	48447.2	46184.3	40481.7	19.7	4.9	0.33	0.47	240	50	359	22	104	31	14	W	59	3	2	1	1.30
EB067	56207.3	61515.8	56592.2	50513.8	21.8	8.7	0.67	0.15	351	68	160	21	251	4	161	E	86	5	1	1	1.74
EB068	24112.7	25848.5	24176.2	22313.4	15.8	6.9	0.78	0.09	341	58	127	27	224	14	134	N	76	4	2	2	1.89
EB069	38920.7	45317.8	40318.7	31125.8	45.6	12.4	0.37	0.38	49	41	141	2	233	48	143	E	42	5	2	1	2.30

site	Km	K1m	K2m	K3m	P%	L%	Pflinn	T	linea	tion	K2D	K2I	K3D	K3I	folia	t	lon	nb	a(K1)	a(K3)	St Er
EB070	94706.3	99195.9	94786.8	90136.1	10.0	4.7	0.86	0.05	239	53	95	32	353	17	83	S	73	4	4	3	1.86
EB071	22059.7	22768.5	22529.3	20881.3	9.0	1.1	0.13	0.76	143	58	308	31	42	7	132	S	83	6	11	2	1.54
EB072	43747.6	53019.3	43633.3	34590.3	53.3	21.5	0.68	0.09	8	56	150	27	249	17	159	E	73	4	1	1	3.30
EB073	77338.8	80678.0	79093.6	72245.1	11.7	2.0	0.21	0.64	104	57	301	32	207	8	117	N	82	5	4	1	1.43
EB074	66416.2	69240.8	65763.2	64244.8	7.8	5.3	2.12	-0.38	114	68	344	15	250	16	160	E	74	5	2	4	1.38
EB075	23449.2	24190.7	23942.2	22214.6	8.9	1.0	0.13	0.76	252	47	33	36	139	19	49	N	71	5	12	1	1.50
EB076	75336.0	78615.7	77099.4	70293.0	11.8	2.0	0.20	0.65	263	9	105	78	5	3	95	S	87	4	5	1	1.79
EB077	57361.2	60056.7	58155.5	53871.4	11.5	3.3	0.40	0.41	338	47	81	12	185	43	95	N	47	5	4	2	1.97
EB078	69589.0	73411.0	70944.8	64411.1	14.0	3.5	0.33	0.48	96	30	296	58	191	9	101	N	81	4	3	1	1.91
EB079	25504.8	26454.3	26073.2	23986.7	10.3	1.5	0.17	0.70	231	20	12	65	136	14	46	N	76	4	7	1	1.48
EB080	86777.3	92126.8	88233.0	79971.9	15.2	4.4	0.41	0.39	26	22	289	17	165	61	75	N	29	4	3	1	1.95
EB081	65484.9	68899.5	67953.4	59601.7	15.6	1.4	0.10	0.81	355	50	103	15	204	36	114	N	54	4	13	1	2.29
EB082	76354.7	80711.7	77329.5	71023.0	13.6	4.4	0.47	0.33	321	16	204	58	59	26	149	W	64	4	2	1	1.32
EB083	74063.2	77730.0	75761.8	68697.8	13.1	2.6	0.25	0.58	286	33	163	40	39	32	129	S	58	4	4	1	1.86
EB084	66727.6	69935.3	68047.9	62199.6	12.4	2.8	0.29	0.53	304	0	214	78	34	12	124	S	78	4	5	2	2.40
EB085	23590.0	24735.0	23479.2	22555.7	9.7	5.3	1.24	-0.13	228	46	91	35	344	23	74	S	67	4	2	3	0.74
EB086	24215.0	25414.5	24491.9	22738.7	11.8	3.8	0.47	0.34	211	76	97	5	6	12	96	S	78	4	4	2	0.82
EB087	21409.7	22221.4	21593.3	20414.3	8.8	2.9	0.49	0.32	251	32	93	56	348	10	78	S	80	4	6	3	0.85
EB088	39039.6	43299.9	40307.4	33511.4	29.2	7.4	0.34	0.44	326	29	187	54	68	19	158	W	71	4	6	2	3.66
EB089	19577.6	23451.2	19124.8	16156.7	45.1	22.6	1.00	-0.09	273	33	168	22	51	48	141	W	42	4	1	2	2.93
EB090	18350.9	19061.7	18217.4	17773.4	7.2	4.6	1.77	-0.29	295	54	161	28	57	24	147	W	66	6	2	4	0.94
EB091	23719.7	24967.1	24583.2	21608.7	15.5	1.6	0.11	0.79	311	39	178	40	63	26	153	W	64	4	12	2	2.84
EB092	26028.2	28198.0	26245.0	23641.6	19.3	7.4	0.63	0.19	354	81	186	6	97	1	7	W	89	4	2	2	2.57
EB093	13086.4	13837.2	13139.9	12282.2	12.6	5.3	0.72	0.13	294	59	176	15	75	26	165	W	64	5	2	2	1.18
EB094	6031.2	6392.3	6058.8	5642.5	13.3	5.5	0.71	0.14	292	51	161	28	56	24	145	W	66	4	2	2	1.91
EB095	19571.1	21220.7	19668.4	17624.3	20.4	6.8	0.50	0.29	311	69	158	18	65	9	155	W	81	4	2	1	1.40
EB096	27280.6	29633.1	28253.7	23954.9	23.7	4.9	0.26	0.55	165	39	289	36	45	31	135	W	59	4	2	1	1.84
EB097	21357.2	22373.8	21984.1	19713.5	13.5	1.8	0.15	0.72	304	35	193	30	74	38	164	W	52	4	9	1	2.00
EB098	4656.4	4889.8	4598.4	4480.9	9.1	6.3	2.27	-0.41	303	60	170	23	70	18	160	W	72	4	2	5	1.21
EB099	11739.7	12479.3	11954.0	10785.9	15.7	4.4	0.39	0.41	305	55	191	16	92	30	2	W	60	4	2	1	1.38
EB100	51919.3	63039.2	53384.3	39334.3	60.2	18.1	0.43	0.30	36	45	186	39	288	15	18	E	75	4	1	1	2.68
EB101	23671.3	24781.3	24226.3	22006.3	12.6	2.3	0.22	0.62	297	62	157	22	60	16	150	W	74	3	5	1	1.88
EB102	19695.2	21278.1	19969.9	17837.7	19.3	6.5	0.51	0.28	275	25	170	25	34	50	124	S	40	5	3	2	2.11
EB103	24600.2	27039.9	25622.9	21137.8	27.9	5.5	0.25	0.56	282	63	146	20	49	17	139	W	73	4	3	1	2.73
EB104	29971.6	31951.2	31064.8	26898.8	18.8	2.9	0.18	0.67	253	62	155	5	61	25	151	W	65	4	9	1	3.10
EB105	20112.1	21706.7	20580.2	18049.6	20.2	5.5	0.37	0.42	253	75	160	3	68	14	158	W	76	5	4	2	2.53
EB106	18191.1	19345.5	17983.0	17244.9	12.2	7.6	1.65	-0.27	249	69	149	4	57	20	147	W	70	4	2	4	1.96
EB107	35574.3	40164.6	36012.1	30546.1	31.5	11.5	0.58	0.20	7	60	168	28	262	9	172	E	81	4	3	2	2.93
EB108	18330.4	18775.0	18428.7	17787.6	5.5	1.9	0.51	0.31	196	13	287	3	28	75	118	S	15	4	6	3	1.09
EB109	16484.9	16954.5	16496.6	16003.4	5.9	2.8	0.88	0.05	197	10	105	15	320	72	50	S	18	4	3	3	0.88
EB110	18869.1	19226.4	18930.8	18450.1	4.2	1.6	0.59	0.25	197	40	88	20	338	42	68	S	48	4	7	4	1.15
EB111	23673.9	24612.9	23964.0	22444.8	9.7	2.7	0.39	0.42	124	34	241	34	1	37	91	S	53	4	5	2	2.03
EB112	17300.9	17959.1	17549.1	16394.3	9.5	2.3	0.32	0.49	241	48	105	33	359	23	89	S	67	4	7	2	1.55
EB113	18701.2	19312.6	18856.2	17934.9	7.7	2.4	0.46	0.35	183	64	299	12	34	22	124	S	68	4	4	2	1.09
EB114	12382.1	12700.8	12497.0	11948.4	6.3	1.6	0.35	0.47	128	39	248	31	3	35	93	S	55	4	4	1	0.45
EB115	7319.5	7528.4	7358.9	7071.2	6.5	2.3	0.55	0.27	258	51	125	29	21	24	111	S	66	4	5	3	0.88
EB116	21631.5	22251.6	21521.0	21122.0	5.3	3.4	1.74	-0.28	237	81	93	8	2	6	92	S	84	4	2	4	0.89
EB117	62047.2	66137.4	61735.6	58268.3	13.5	7.1	1.12	-0.09	347	70	118	13	211	15	121	N	75	4	2	2	1.84
EB118	64721.8	69208.9	63285.5	61671.2	12.2	9.4	3.27	-0.55	3	65	100	3	191	24	101	N	66	4	1	5	1.84
EB119	36723.7	41064.9	37875.6	31230.5	31.5	8.4	0.37	0.41	229	71	356	12	89	14	179	W	76	4	4	2	3.18
EB120	48803.9	53685.5	50051.8	42674.2	25.8	7.3	0.39	0.39	309	74	215	1	124	19	34	W	71	4	3	1	2.67
EB121	45339.7	51362.0	46396.9	38260.3	34.2	10.7	0.45	0.31	40	68	193	6	269	9	179	E	81	4	2	1	3.56
EB122	30941.9	33717.7	32024.4	27083.6	24.5	5.3	0.28	0.53	357	76	177	14	86	0	176	W	90	4	3	1	2.93
EB123	81140.8	97648.3	84289.3	61486.6	58.8	15.8	0.37	0.36	217	83	346	4	76	1	166	W	89	4	2	1	3.48
EB124	94508.9	99592.3	96221.2	87713.1	13.5	3.5	0.35	0.46	303	29	152	55	49	5	139	W	85	6	6	2	2.31
EB125	62639.8	73224.2	65450.1	49244.9	48.7	11.9	0.32	0.43	187	82	55	4	327	5	57	S	85	4	4	2	3.42
EB126	32800.4	37811.1	32833.4	27756.7	36.2	15.2	0.72	0.09	6	72	189	18	278	0	8	E	90	5	2	2	3.43
EB127	68559.2	78843.1	69567.6	57267.1	37.7	13.3	0.55	0.22	235	4	326	11	108	82	18	W	8	5	3	2	3.34
EB128	27431.4	29992.3	28014.1	24288.1	23.5	7.1	0.43	0.35	6	68	200	21	108	4	18	W	86	5	3	2	3.49
EB129	18184.6	19131.3	18137.0	17285.6	10.7	5.5	1.06	-0.05	195	31	24	59	287	5	17	E	85	6	2	3	1.50
EB130	25325.6	28267.1	26065.5	21644.2	30.6	8.4	0.38	0.39	341	75	187	14	95	6	5	W	84	4	3	1	4.03
EB131	34964.7	39956.9	35322.2	29615.0	34.9	13.1	0.60	0.18	327	31	227	16	113	54	23	W	36	4	2	2	2.63
EB132	21969.0	26972.5	23006.3	15928.0	69.3	17.2	0.33	0.40	36	67	166	16	260	17	170	E	73	5	3	1	3.26
EB133	42297.0	48337.2	43230.5	35323.4	36.8	11.8	0.47	0.29	129	1	218	46	38	43	128	S	47	4	3	2	3.70
EB134	63488.8	70406.8	66369.1	53690.4	31.1	6.1	0.24	0.56	316	50	220	4	124	44	34	W	46	4	4	1	3.96
EB135	35407.9	40408.6	35216.8	30598.3	32.0	14.7	0.85	0.01	295	44	203	2	110	46	20	W	44	4	2	2	2.72
EB136	32949.7	35722.1	34392.3	28734.5	24.3	3.9	0.19	0.65	6	11	260	56	105	28	15	W	62	7	7	1	2.93
EB137	42006.4	49371.6	43851.4	32796.2	50.5	12.6	0.33	0.42	306	25	195	39	58	42	148	W	48	4	3	2	4.33
EB138	20674.2	22332.8	21707.9	17982.0	24.2	2.9	0.14	0.74	323	26	183	59	62	16	152	W	74	4	13	2	4.04
EB139	23392.6	24790.5	24452.3	20934.9	18.4	1.4	0.08	0.84	1	36	180	54	269	0	179	E	90	5	19	1	2.58

site	Km	K1m	K2m	K3m	P%	L%	Pflinn	T	lines	tion	K2D	K2l	K3D	K3l	folia	t	lon	nb	a(K1)	a(K3)	St Er
EB140	980.3	989.2	980.3	971.3	1.8	0.9	0.98	0.01	328	72	188	16	95	10	5	W	80	5	4	5	0.45
EB141	17233.0	17690.8	17446.8	16561.5	6.8	1.4	0.26	0.58	131	11	13	44	221	42	131	N	48	5	10	2	1.05
EB142	15460.9	16466.9	15473.7	14442.0	14.0	6.4	0.84	0.05	65	67	335	0	246	23	156	E	67	5	2	2	1.91
EB143	27327.3	28698.2	27857.2	25426.5	12.9	3.0	0.31	0.51	158	75	326	15	57	2	147	W	88	4	4	1	1.90
EB144	17716.9	18197.1	17907.2	17046.6	6.7	1.6	0.32	0.51	61	64	325	3	233	25	143	E	65	5	5	2	0.87
EB145	14230.5	15079.7	14553.0	13059.0	15.5	3.6	0.31	0.51	312	73	147	17	55	4	145	W	86	5	6	2	1.87
EB146	8667.0	9079.2	8730.5	8191.1	10.8	4.0	0.58	0.24	334	73	163	18	70	1	160	W	89	4	3	2	1.02
EB147	20410.0	21587.9	20859.8	18782.4	14.9	3.5	0.30	0.51	260	72	156	5	63	17	153	W	73	5	6	2	2.50
EB148	22059.6	23844.1	22233.6	20101.2	18.6	7.2	0.64	0.18	154	77	324	7	239	2	149	E	88	5	3	2	1.71
EB149	43733.3	48708.6	44888.9	37602.2	29.5	8.5	0.40	0.37	352	61	169	28	262	0	172	E	90	5	4	2	3.01
EB150	34814.5	36871.1	35103.5	32468.9	13.6	5.0	0.59	0.23	176	41	9	50	272	8	2	E	82	4	12	8	4.97
EB151	23313.9	24904.0	23537.0	21500.9	15.8	5.8	0.58	0.23	185	66	3	21	92	1	2	W	89	4	3	2	1.70
EB152	23300.5	24733.1	23686.9	21481.4	15.1	4.4	0.41	0.39	11	58	187	33	278	3	8	E	87	4	3	1	1.29
EB153	37707.5	39940.5	37956.4	35225.7	13.4	5.2	0.64	0.19	315	61	151	28	57	7	147	W	83	4	3	2	1.12
EB154	34031.2	36634.5	34779.6	30679.6	19.4	5.3	0.38	0.41	158	71	330	15	59	2	149	W	88	4	2	1	2.35
EB155	34402.5	36329.5	35400.6	31477.4	15.4	2.6	0.21	0.64	304	48	163	35	57	19	147	W	71	4	5	1	1.54
EB156	15031.9	15816.0	15058.1	14221.5	11.2	5.0	0.81	0.08	307	28	200	37	62	50	152	W	40	4	2	2	0.92
EB157	28220.9	30364.9	28971.1	25326.4	19.9	4.8	0.32	0.48	303	37	177	38	59	30	149	W	60	4	3	1	2.57
EB158	16861.5	17686.5	17100.5	15797.6	11.9	3.4	0.40	0.40	273	71	163	7	71	18	161	W	72	4	3	1	1.40
EB159	30219.7	32431.2	31003.2	27224.6	19.1	4.6	0.32	0.49	225	76	333	5	64	12	154	W	78	4	3	1	2.21
EB160	25648.0	26507.0	25918.9	24518.2	8.1	2.3	0.39	0.42	136	75	343	14	251	7	161	E	83	4	3	1	0.92
EB161	23155.7	24130.2	23399.6	21937.1	10.0	3.1	0.45	0.35	323	80	149	9	59	1	149	W	89	4	2	1	0.87
EB162	21340.4	22575.7	21423.7	20021.6	12.7	5.4	0.73	0.13	300	37	182	32	63	36	153	W	54	4	3	2	1.63
EB163	27788.7	29174.0	28641.9	25550.2	14.2	1.9	0.15	0.72	294	24	182	41	45	38	135	W	52	4	9	1	2.33
EB164	18697.7	20441.9	19038.7	16612.5	23.0	7.4	0.47	0.31	301	52	165	29	62	21	152	W	69	4	3	2	2.32
EB165	22702.1	24000.9	23263.2	20842.1	15.1	3.2	0.26	0.56	286	39	172	27	57	39	147	W	51	4	3	1	1.93
EB166	27585.5	29732.7	27713.9	25309.8	17.5	7.3	0.71	0.13	325	76	215	5	124	13	34	W	77	4	2	1	2.12
EB167	33171.1	34268.7	33524.6	31719.9	8.0	2.2	0.38	0.43	223	44	349	33	101	31	11	W	59	4	3	1	1.19
EB168	21840.8	22678.1	21679.1	21165.1	7.1	4.6	1.81	-0.30	263	73	8	5	100	15	10	W	75	5	3	5	1.21
EB169	20688.0	21975.1	21340.3	18748.6	17.2	3.0	0.21	0.63	332	62	202	21	104	22	14	W	68	3	5	1	2.01
EB170	25712.6	27563.0	26500.5	23074.3	19.4	4.0	0.26	0.56	17	37	163	47	273	18	3	E	72	4	6	2	3.58
EB171	33774.7	35862.1	34531.9	30930.0	15.9	3.9	0.32	0.49	9	44	188	45	278	1	8	E	89	4	5	2	1.63
EB172	16241.8	17408.6	16819.4	14497.5	20.1	3.5	0.21	0.62	96	67	193	3	283	24	13	E	66	5	7	2	2.60
EB173	20139.6	21034.0	20455.4	18929.3	11.1	2.8	0.34	0.47	88	41	197	20	306	42	36	E	48	4	5	1	1.19
EB174	28940.1	30914.9	29323.5	26581.6	16.3	5.4	0.50	0.30	306	68	209	3	117	22	27	W	68	4	3	2	2.95
EB175	24996.3	26774.4	26052.0	22162.6	20.8	2.8	0.15	0.71	129	46	356	7	255	2	165	E	88	4	10	1	2.87
EB176	12948.0	13977.9	13268.1	11598.0	20.5	5.3	0.35	0.44	249	36	151	10	48	51	138	W	39	4	4	2	1.69
EB177	5717.5	6010.2	5749.4	5392.8	11.4	4.5	0.66	0.18	271	84	189	0	98	5	8	W	85	4	3	2	1.39
EB178	34961.4	38951.7	35615.7	30316.8	28.5	9.4	0.49	0.29	215	44	332	25	81	35	171	W	55	4	4	2	2.43
EB179	10030.4	11023.6	9786.1	9281.6	18.7	12.6	2.07	-0.38	275	9	5	14	147	69	57	N	21	4	2	9	2.16
EB180	26912.1	28813.6	27850.8	24071.7	19.7	3.5	0.21	0.62	339	42	176	47	76	8	166	W	82	4	6	1	2.92
EB181	8608.8	8949.5	8778.3	8098.7	10.5	1.9	0.23	0.61	1	26	245	42	114	37	24	W	53	4	4	1	0.84
EB182	13370.1	13978.0	13676.8	12455.4	12.2	2.2	0.22	0.62	226	71	344	10	77	15	167	W	75	4	9	2	2.04
EB183	46043.2	50818.5	46711.4	40599.6	25.2	8.8	0.54	0.25	282	65	23	5	116	25	26	W	65	4	3	2	2.99
EB184	17251.2	18645.9	17319.1	15788.5	18.1	7.7	0.73	0.11	240	82	29	6	119	4	29	W	86	4	3	2	2.00
EB185	25943.5	28330.7	26517.8	22981.8	23.3	6.8	0.42	0.37	18	79	191	10	282	2	12	E	88	4	3	1	3.00
EB186	36438.0	38624.5	36661.3	34028.2	13.5	5.4	0.66	0.18	212	53	3	32	106	15	16	W	75	4	3	6	1.50
EB187	37365.8	41013.2	37739.4	33344.8	23.0	8.7	0.61	0.20	317	14	216	38	63	48	153	W	42	4	4	3	2.91
EB188	18046.0	18530.4	18259.8	17347.8	6.8	1.5	0.28	0.55	264	28	355	0	85	62	175	W	28	4	5	1	0.77
EB189	579.5	587.8	577.4	573.2	2.5	1.8	2.39	-0.42	168	28	49	39	285	18	15	E	72	4	5	8	0.51
EB190	17603.0	18348.2	18068.1	16392.6	11.9	1.5	0.15	0.73	344	80	233	4	142	9	52	N	81	3	6	1	1.02
EB191	13855.9	14904.8	14286.7	12376.1	20.4	4.3	0.27	0.54	352	34	188	52	92	7	2	W	83	4	7	2	2.85
EB192	25121.7	25749.2	25502.5	24113.4	6.8	1.0	0.17	0.71	332	22	204	56	72	23	162	W	67	4	10	2	1.50
EB193	21066.1	22052.6	21801.5	19344.1	14.0	1.2	0.09	0.83	181	71	356	12	82	0	172	W	90	4	19	2	2.62
EB194	20074.7	20686.8	20482.2	19055.2	8.6	1.0	0.13	0.76	270	39	9	5	98	56	8	W	34	5	11	1	0.94
EB195	16060.1	16313.3	16193.3	15673.5	4.1	0.7	0.22	0.63	192	7	77	73	284	13	14	E	77	5	13	2	0.90
EB196	8534.2	8651.5	8518.5	8432.5	2.6	1.6	1.51	-0.21	212	3	331	79	131	24	41	W	66	8	3	5	0.73
EB197	26585.0	27393.8	26692.8	25668.3	6.7	2.6	0.64	0.20	169	43	289	24	40	34	130	S	56	6	6	4	2.09
EB198	25546.2	26544.6	25522.1	24572.1	8.0	4.0	1.00	-0.02	164	28	272	34	43	46	133	S	44	5	3	4	1.85
EB199	23735.5	24547.3	23768.4	22890.9	7.2	3.3	0.83	0.08	181	48	283	11	22	40	112	S	50	4	3	3	1.41
EB200	20398.9	21097.7	20331.7	19767.3	6.7	3.8	1.27	-0.14	181	51	297	22	42	31	132	S	59	5	8	8	2.53
EB201	16626.8	17944.1	16356.1	15580.2	15.2	9.7	1.78	-0.31	56	0	327	9	157	81	67	N	9	7	2	4	1.92
EB202	11845.6	12634.3	11832.0	11070.6	14.1	6.8	0.92	0.01	250	42	14	30	127	32	37	W	58	7	2	2	1.40
EB203	17487.4	18363.4	17501.0	16597.9	10.6	4.9	0.86	0.05	353	63	86	2	177	27	87	N	63	6	3	2	1.61
EB204	19716.3	20315.3	19732.2	19101.2	6.4	3.0	0.87	0.05	245	76	43	12	134	5	44	W	85	6	4	3	1.08
EB205	17640.7	18103.5	17671.2	17147.3	5.6	2.4	0.78	0.11	205	65	352	21	86	12	176	W	78	7	3	3	1.18
EB206	15493.2	16608.7	15362.2	14508.6	14.5	8.1	1.28	-0.15	190	59	288	5	22	30	112	S	60	8	1	2	2.04
EB207	14029.3	15015.0	13749.3	13323.5	12.7	9.2	2.64	-0.47	96	60	331	20	232	21	142	E	69	7	2	6	1.70
EB208	25384.4	26887.7	25906.3	23359.0	15.1	3.8	0.33	0.47	160	56	329	34	62	5	152	W	85	6	4	1	1.98
EB209	15461.5	16025.4	15774.3	14584.7	9.9	1.6	0.19	0.66	357	2	264	72	83	20	173	W	70	5	9	2	1.65
EB210	15876.5	16456.1	15735.5	15437.9	6.6	4.6	2.27	-0.40	12	7	145	76	281	10	11	E	80	6	2	5	1.78

site	Km	K1m	K2m	K3m	P%	L%	Pflinn	T	linea	tion	K2D	K2I	K3D	K3I	folia	t	ion	nb	a(K1)	a(K3)	St Er
max	94706.3	99592.3	96221.2	90136.1	69.3	29.7	3.61	0.84										8	19	9	4.97
min	86.0	89.1	86.3	82.6	1.8	0.7	0.08	-0.59										2	1	1	0.45
average	33241.2	36043.1	33669.0	30011.4	18.6	6.3	0.68	0.26										5	4	2	2.07
st. dev	18821.8	20692.0	19062.4	16913.8	11.2	4.5	0.60	0.32										1	3	1	0.89
nb site:	210		nb sam/site:	4.5																	

Appendix B AMS directional data plotted on stereograms

KEY

Square = Kmax

Triangle = Kintermediate

Circle = Kmin

Open symbols = sample orientations

Closed symbols = site mean values

NOTE all stereograms are lower hemisphere projections oriented so that north is towards the top of the page

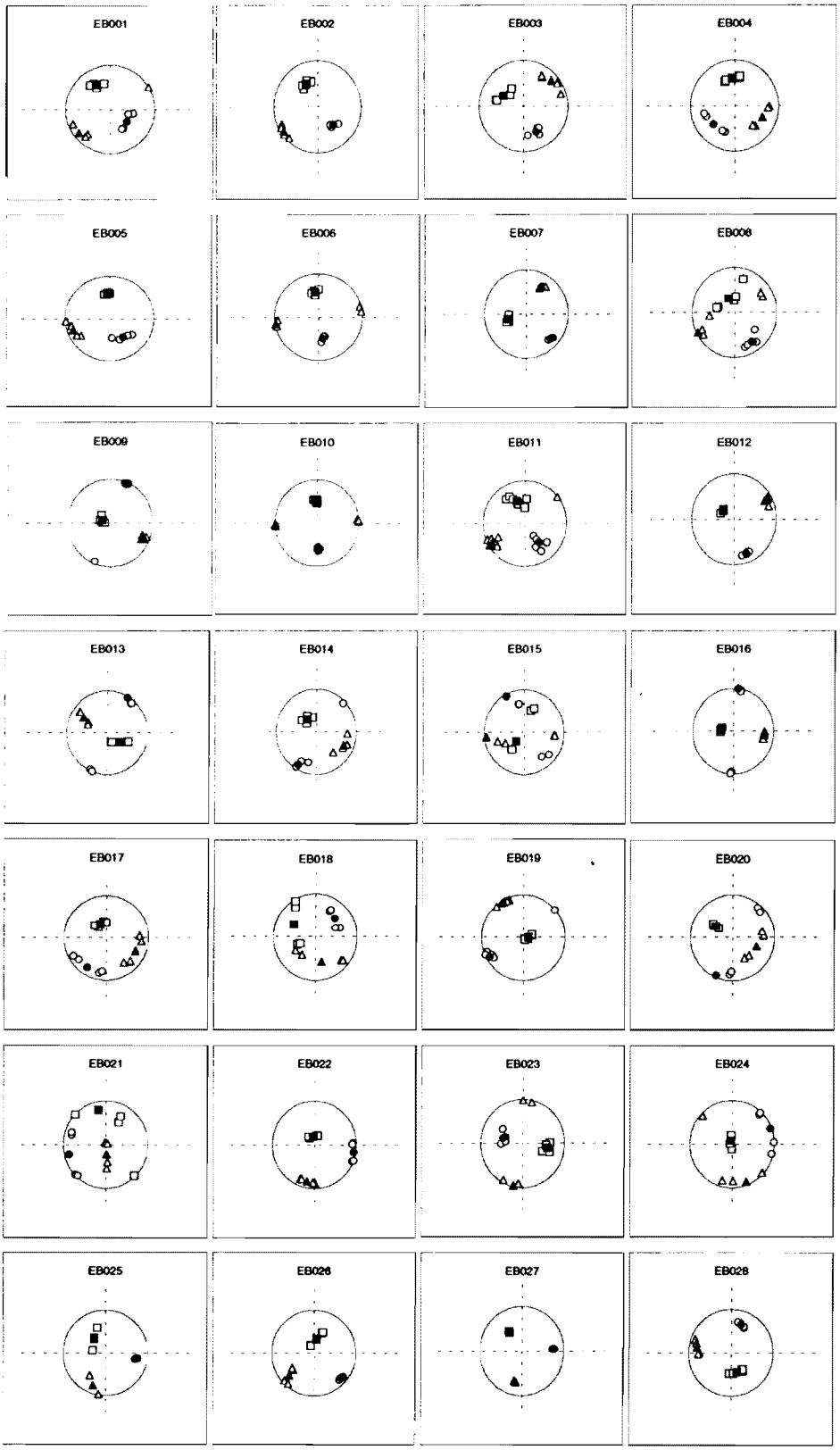
EB001
EB002
EB003
EB004
EB005
EB006
EB007
EB008
EB009
EB010
EB011
EB012
EB013
EB014
EB015
EB016
EB017
EB018
EB019
EB020
EB021
EB022
EB023
EB024
EB025
EB026
EB027
EB028

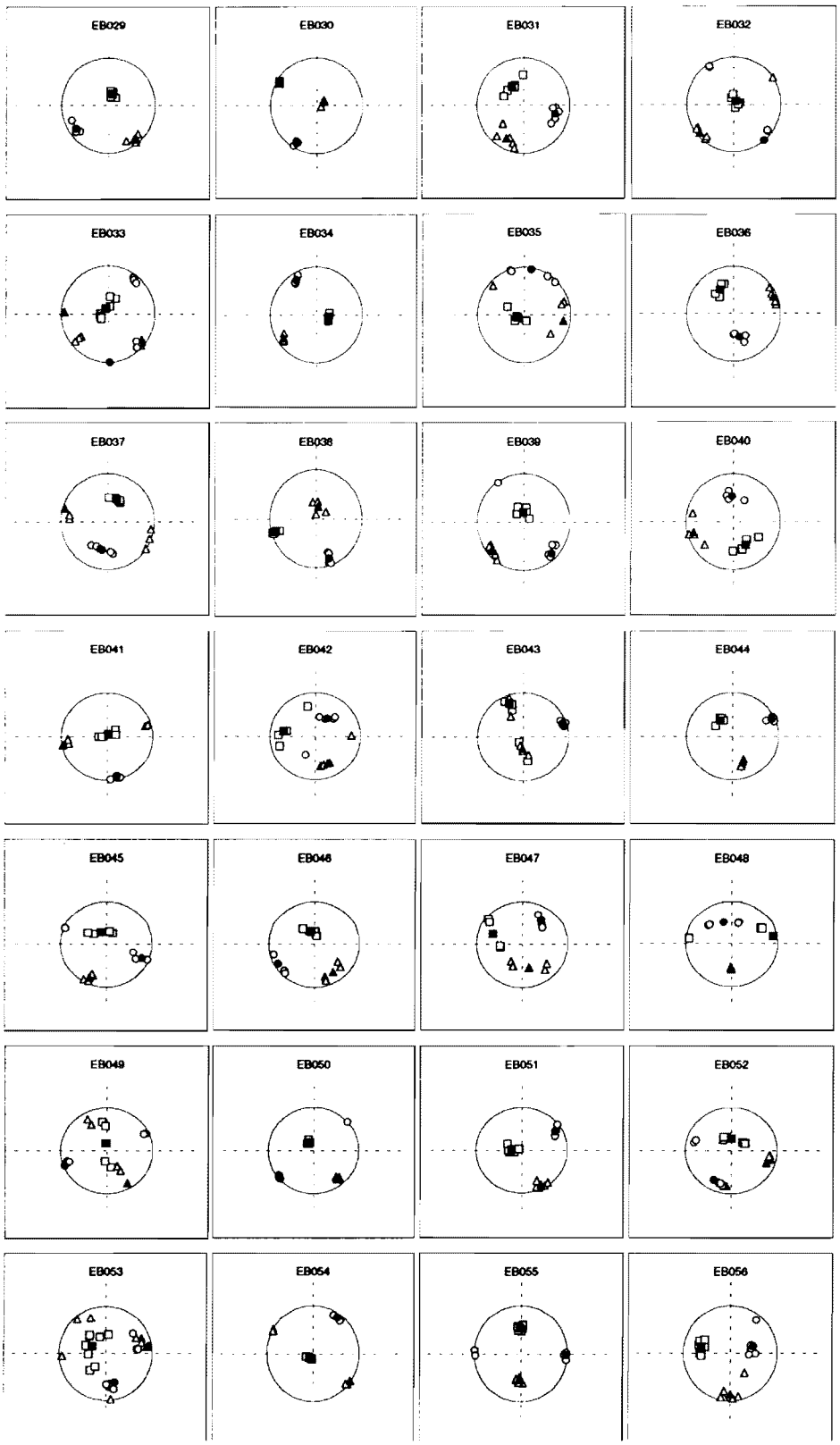
EB029
EB030
EB031
EB032
EB033
EB034
EB035
EB036
EB037
EB038
EB039
EB040
EB041
EB042
EB043
EB044
EB045
EB046
EB047
EB048
EB049
EB050
EB051
EB052
EB053
EB054
EB055
EB056

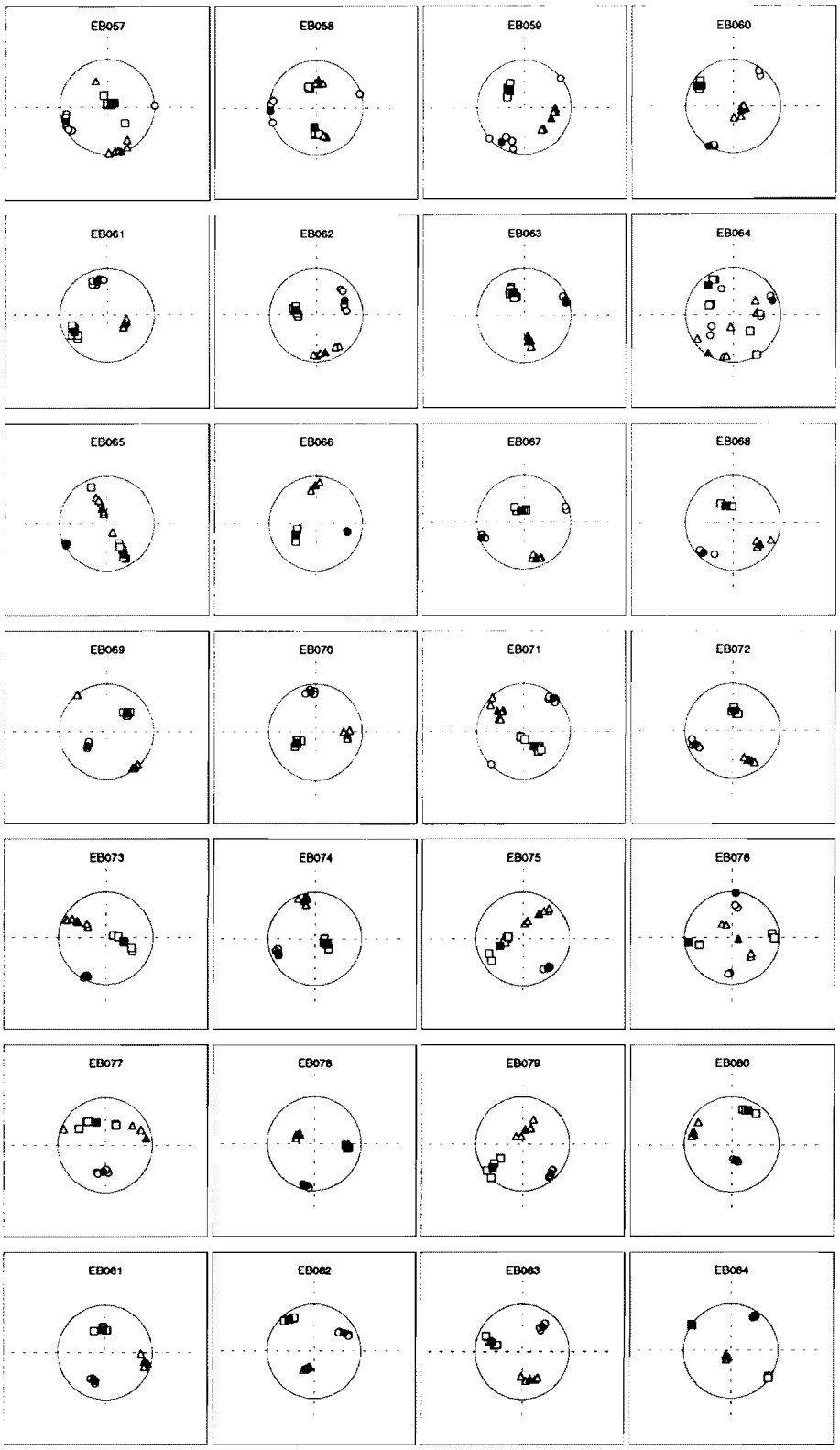
EB057
EB058
EB059
EB060
EB061
EB062
EB063
EB064
EB065
EB066
EB067
EB068
EB069
EB070
EB071
EB072
EB073
EB074
EB075
EB076
EB077
EB078
EB079
EB080
EB081
EB082
EB083
EB084

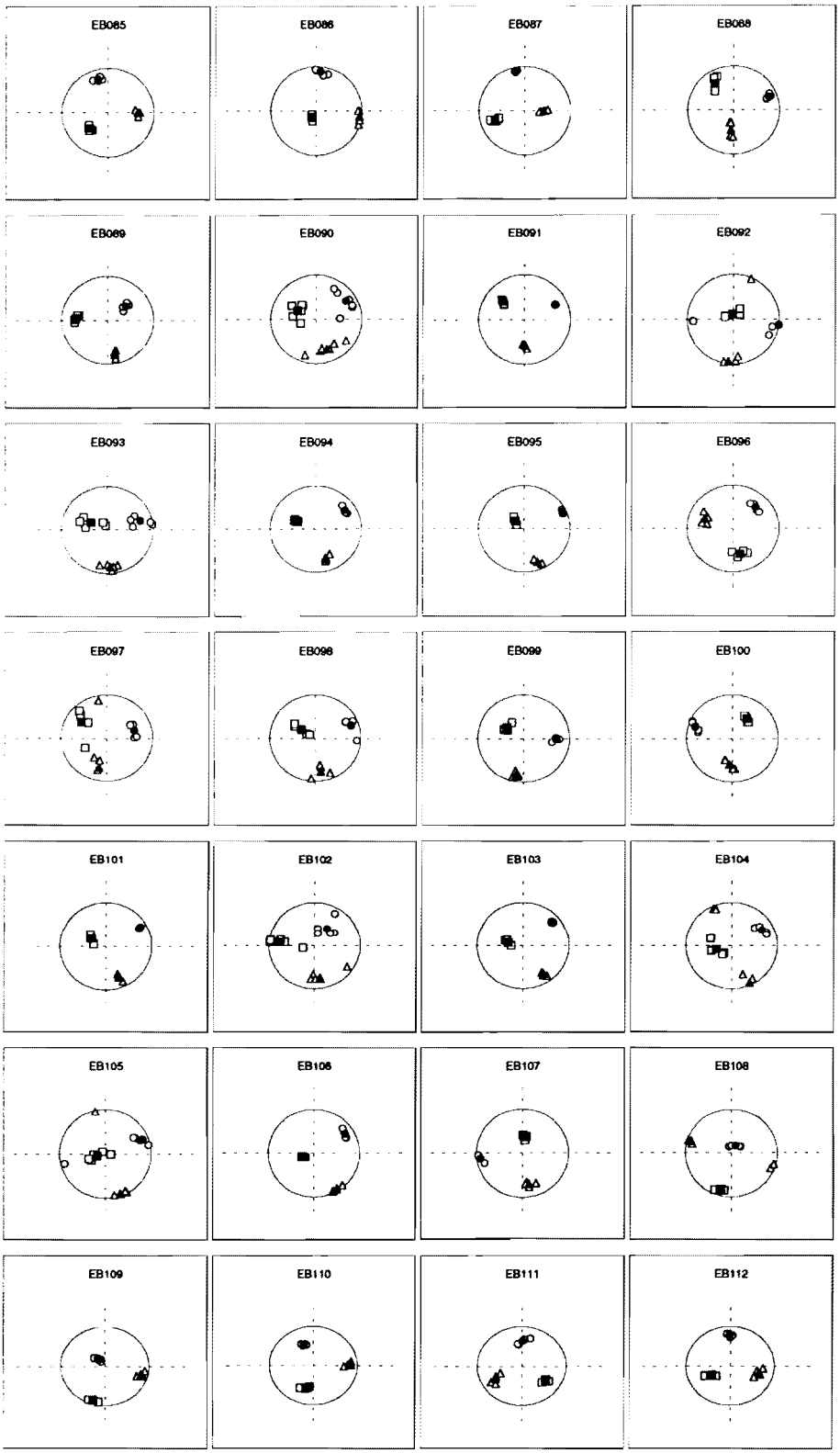
EB085
EB086
EB087
EB088
EB089
EB090
EB091
EB092
EB093
EB094
EB095
EB096
EB097
EB098
EB099
EB100
EB101
EB102
EB103
EB104
EB105
EB106
EB107
EB108
EB109
EB110
EB111
EB112

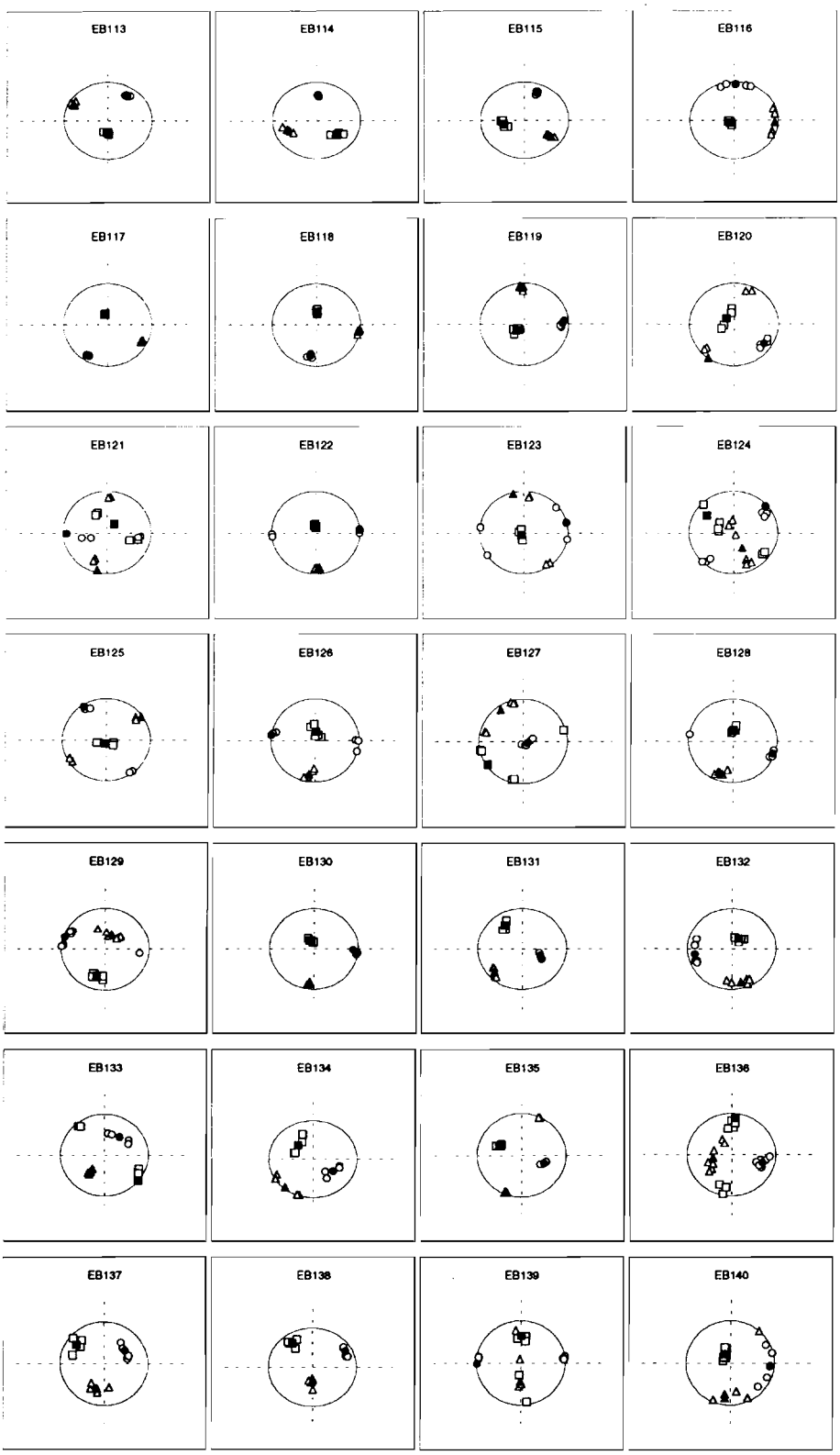
EB113
EB114
EB115
EB116
EB117
EB118
EB119
EB120
EB121
EB122
EB123
EB124
EB125
EB126
EB127
EB128
EB129
EB130
EB131
EB132
EB133
EB134
EB135
EB136
EB137
EB138
EB139
EB140

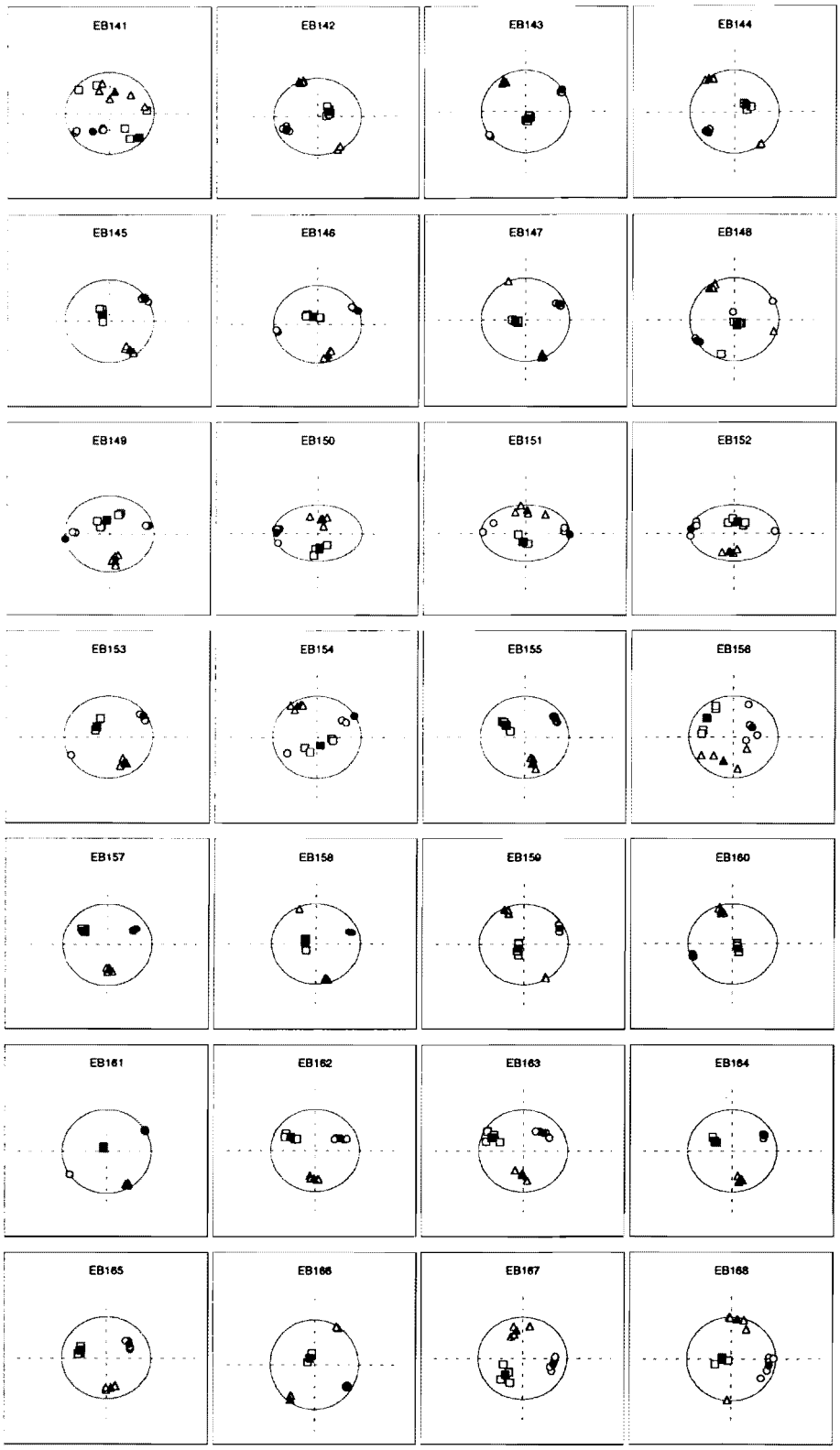
EB141
EB142
EB143
EB144
EB145
EB146
EB147
EB148
EB149
EB150
EB151
EB152
EB153
EB154
EB155
EB156
EB157
EB158
EB159
EB160
EB161
EB162
EB163
EB164
EB165
EB166
EB167
EB168

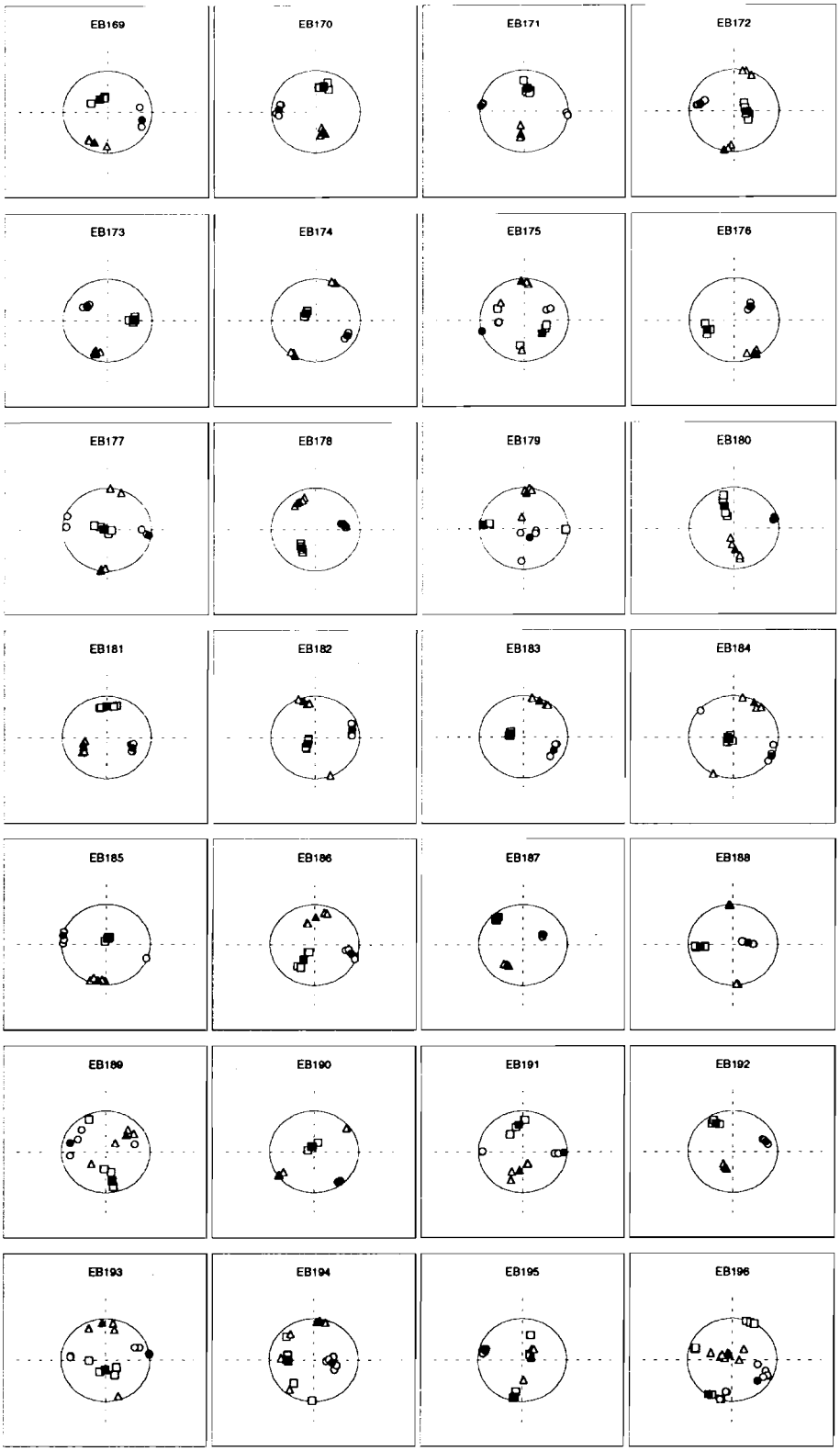
EB169
EB170
EB171
EB172
EB173
EB174
EB175
EB176
EB177
EB178
EB179
EB180
EB181
EB182
EB183
EB184
EB185
EB186
EB187
EB188
EB189
EB190
EB191
EB192
EB193
EB194
EB195
EB196

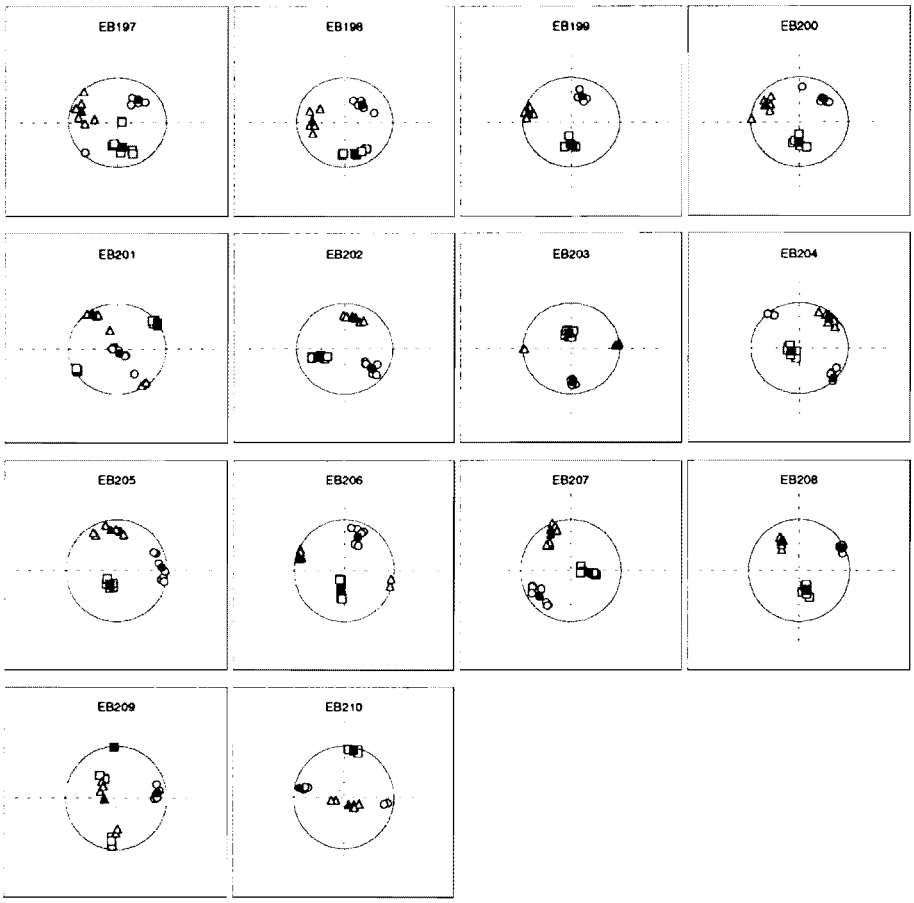
EB197
EB198
EB199
EB200
EB201
EB202
EB203
EB204
EB205
EB206
EB207
EB208
EB209
EB210

Chapter 3. Laccolith-like emplacement model for the Papoose Flat pluton based on porphyroblast-matrix analysis

SVEN S. MORGAN, RICHARD D. LAW

Department of Geological Sciences, Virginia Tech.,
Blacksburg, Virginia 24061-0420.

MATHEW W. NYMAN

Department of Geological Sciences,
University of Michigan, Ann Arbor,
Michigan 48109-1063.

Published in 1998 by the Geological Society of America Bulletin, v. 110, p. 96-110

Abstract

Detailed porphyroblast-matrix analysis within the concordant metasedimentary aureole rocks surrounding the Papoose Flat pluton of eastern California indicates that inclusion trails within porphyroblasts can be used as strain markers to restore the aureole rocks to their pre-pluton emplacement position. Using porphyroblast-matrix relationships, in combination with measurement of stratigraphic sections and whole-rock geochemical analyses, we have determined the kinematics of rotation, the change in thickness and volume, and the amount of translation of the metasedimentary formations within the aureole. These data are consistent with initial emplacement of the magma as an inclined sill and subsequent inflation into a pluton/laccolith. The combination of structural and porphyroblast-matrix analysis leads to a three dimensional kinematic history of the wall rocks where vertical upward translation represents a significant portion of the pluton emplacement-related strain history.

Introduction

In recent years there has been a resurgence of interest among structural geologists and petrologists over the potential mechanisms by which space may be made in the earth's crust to accommodate pluton emplacement. Emplacement mechanisms frequently cited in the literature are either driven by tectonic processes which create space for magma intrusion (shear zones, strike slip bends, p-shears), or depend on the magma to create its own space (diapirism, stoping, ballooning, sheeting, in-situ melting) (see reviews by Pitcher, 1979; Hutton, 1988; Clarke, 1992; Paterson and Fowler, 1993). In spite of new research initiatives, however, the emplacement of granite into the earth's crust remains a controversial and poorly understood process, because the space needed to accommodate the volume of magma can rarely be totally accounted for by the structures surrounding granite plutons. This "space problem" can be particularly acute in cases where the aureole rocks surrounding a pluton lack strain markers. Similarly, the deflection of rock units around plutons, as shown on geologic maps, can also be misleading because the three dimensional aspect of the kinematics involved in producing such deflections are rarely known.

Recent advancements in our understanding of magmatic and solid-state flow fabrics in granites has led to a better understanding of flow during final emplacement (see St. Blanquat and Tikoff 1997 for details), but the question often still remains as to how the wall rocks were displaced in order to make sufficient space for magma emplacement. Detailed structural analyses of aureole rocks are few (e.g. Akaad, 1956; Pitcher and Berger, 1972; Sylvester et al., 1978; Fyson, 1980; Sanderson and Meneilly, 1981; Davis, 1993), partly because of a lack of sufficient strain markers, and partly because it is seemingly difficult to separate the effects of pluton related strains from regionally concentrated deformation within the narrow aureoles of many plutons (Guglielmo, 1994; Vernon et al., 1993a). This is unfortunate, because as observed by H.H. Read (1957, p. 332) "The mechanism of emplacement of these circumscribed bodies is more often to be determined from the structures of their country-rock walls than from their own (structure). Evidence of drag and movement of the wall-rocks, combined with that presented by the metamorphic history of the aureole-rocks, may be decisive."

This paper describes the deformation features within the highly strained aureole rocks surrounding the Papoose Flat pluton of eastern California (Figs. 26 and 27). The Papoose Flat pluton has been considered as a classic example of a ballooning pluton since the work of Nelson et al. (1972) and Sylvester et al. (1978) documented the intense attenuation and

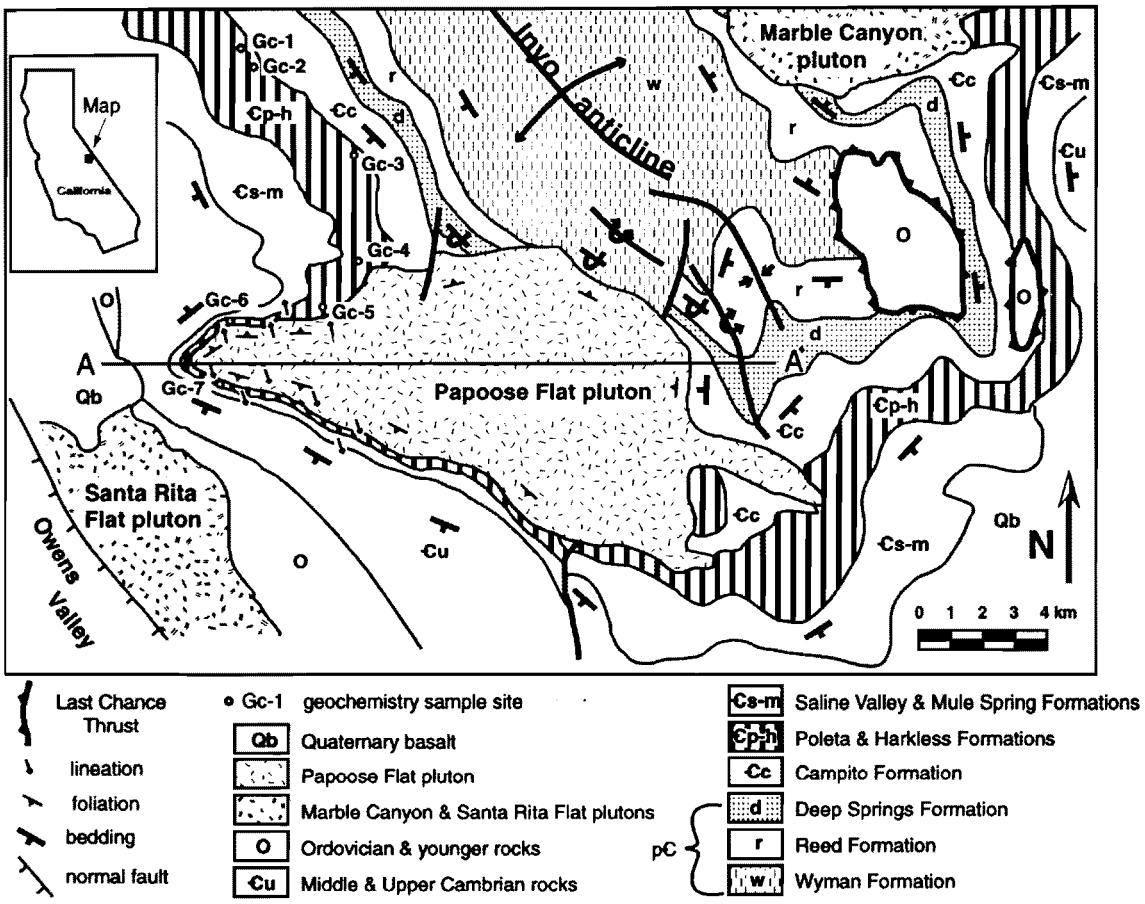

Figure 26. Simplified geologic map of the Papoose Flat pluton and southwestern end of the Inyo anticline (after Nelson et al., 1991). Line of section (A-A') for Figure 27 is indicated.

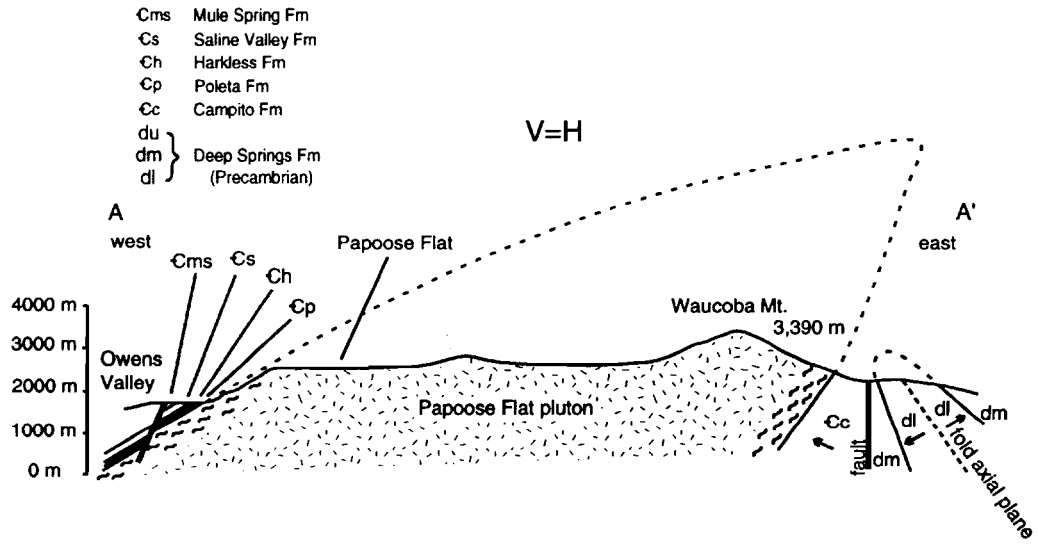

Figure 27. West to east cross section parallel to long axis (see Fig. 26) of the Papoose Flat pluton. Surface geology is based on the geologic map of Nelson et al., (1978, scale 1:62500)(V=H; no vertical exaggeration). Wavy ornament within pluton indicates extent of pluton's gneissic border facies; note that for clarity, the thickness of border facies is highly exaggerated.

concordancy of the aureole rocks surrounding the pluton. More recently, doubt has been cast on the applicability of the ballooning model by both the discovery of simple shear indicators at the margin of the pluton (Law et al., 1990, 1992, 1993; Paterson et al., 1991), and by volume balance calculations in which the calculated pluton 'volume' was compared with the observed wall rock strains (Paterson and Fowler, 1993).

The aim of this paper is to describe a detailed porphyroblast-matrix analysis from samples taken within the metamorphic aureole surrounding the Papoose Flat pluton. The results of this analysis support the use of porphyroblasts as strain markers and also demonstrates how porphyroblast-matrix relationships may aid in determining the sequence of metamorphism versus deformation. Combining the porphyroblast-matrix results with more traditional structural analysis on the aureole and surrounding wall rocks has led to: 1) a full strain analysis of the aureole rocks taking into account shape change, rigid body rotation, volume change and rigid body translation and, 2) a two stage intrusion model of forcible emplacement for the Papoose Flat pluton whereby magma is initially intruded as an inclined sill which then inflates into a laccolith-like pluton.

Geologic Background and Field Relationships

The Papoose Flat pluton is one of several Mesozoic granitic plutons that intrude the central White-Inyo Range of eastern California and which are associated with emplacement of the Sierra Nevada batholith (Bateman et al., 1963; Ross, 1965; Bateman, 1992). The Papoose Flat pluton is amongst the youngest dated plutons in the range with a U-Pb monazite age of 83.1 ± 0.4 Ma (Miller, 1996) and K-Ar ages on biotite of 75-81 Ma (Kistler et al., 1965). The pluton was originally described as a biotite quartz monzonite with K-feldspar megacrysts by Sylvester et al. (1978), although normative compositions of megacryst-poor samples collected from the pluton by Brigham (1984, p. 55) plot within the granite and granodiorite fields as defined by LeMaitre (1989).

The White-Inyo Range is an elongate horst block that trends north-northwest and parallels the trend of the eastern Sierra Nevada Range 15-20 km to the west. The sedimentary rocks in the central White-Inyo Range consist of a late Precambrian through Paleozoic platform margin sequence that exhibits open to tight folds from regional to outcrop scale. The central part of the range is structurally dominated by the Inyo anticline (Fig. 26), which is a north-northwest trending upright fold that can be traced for over 40 km along its

hinge. The Papoose Flat pluton intruded the southwestern limb of the anticline (Nelson et al., 1972; Sylvester et al., 1978), locally overturning and deflecting strata around the pluton. The sedimentary rocks in the range are weakly metamorphosed (sub-greenschist facies - see Ernst et al., 1993; Ernst, 1996; for details), except where they are in contact with the Mesozoic plutons. Within the Inyo anticline north of the Papoose Flat pluton, a well developed regional slaty cleavage strikes north-northwest and dips 5 to 20° more steeply to the southwest than bedding (Fig. 28).

The Papoose Flat pluton is roughly elliptical in shape, the long axis of the pluton trending east-west (Fig. 26). A narrow 'apophysis' of granite protrudes at the eastern end. Around the western half of its perimeter the pluton is surrounded by a concordant aureole of metasedimentary rocks. Within the aureole these plastically deformed lower Cambrian sedimentary units have been attenuated to 10% of their regional stratigraphic thickness and wrap around the western pluton margin and parallel the contact with the pluton for approximately 20 km (Sylvester et al., 1978). The contact with the metasedimentary formations is characteristically very sharp, and within the pluton a solid-state foliation (referred to as the "gneissic border facies" by Sylvester et al., 1978) is strongly developed at distances up to 10-20 m from the margin and decreases in intensity toward the interior of the pluton. The gneissic foliation is best developed around the northwestern, western, and southern margins (Sylvester et al., 1978) as well as along the northeastern margin (St. Blanquat et al., 1994) of the pluton and is parallel to the pluton-wallrock contact. On the northwestern, western, and southern margins both the compositional layering within the aureole and the foliation within the granite dips gently (25-40°) away from the pluton, lending the pluton and surrounding metasedimentary units a domal shape at the present level of exposure which is probably close to the pluton roof (Sylvester et al., 1978). On the eastern margin the pluton-wallrock contact dips steeply toward the pluton, indicating that the current exposure level is much closer to the base of the pluton.

An east to west cross section (Fig. 27) illustrates the sill-like geometry of the pluton. On the western margin, the Poleta Formation lies structurally above the pluton. Stratigraphically, the next lowest formation is the Campito Formation, which is found on the eastern margin structurally below the pluton. If the pluton is removed from the cross section, then there is no missing stratigraphy traced from east to west.

The approximate extent of the contact aureole based on the appearance of porphyroblasts in slate, phyllite and schist has been mapped by Sylvester (1966). An internal, higher temperature component of the aureole was determined by the presence of

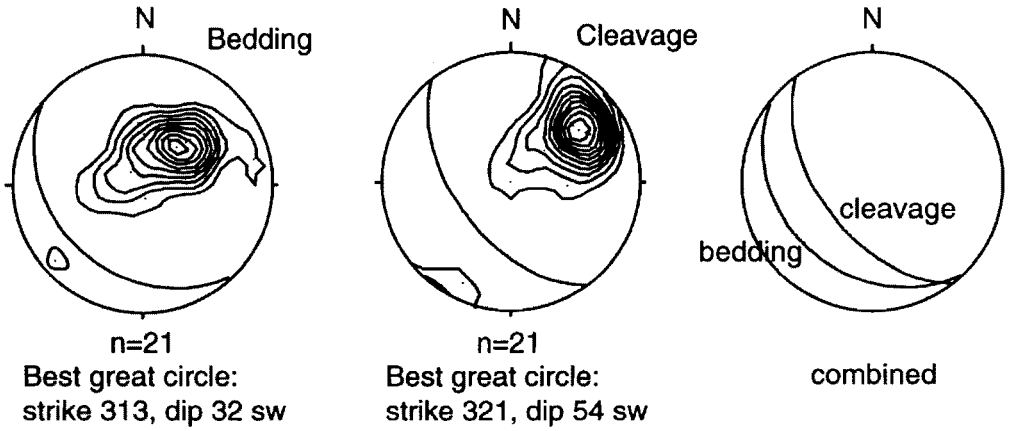

Figure 28. Contoured stereograms of poles to bedding and slaty cleavage within the western limb of the Inyo anticline, north of Papoose Flat pluton.

biotite and andalusite in pelitic schist, with a lower temperature portion defined by the presence of spots of muscovite and biotite in slate. Sylvester et al. (1978) estimated that the aureole is approximately 100-600 m wide along the western margin and up to 1,000 m in width around the eastern part of the pluton. Correcting for contact dip indicates that the actual thickness of the aureole is on the order of 100-200 m measured normal to the contact. Petrologic study of highly strained metacarbonate and metapelitic rocks within the contact aureole surrounding the western part of the pluton indicates that temperature gradients were relatively flat and narrow (<100 m) with only a slight decrease in temperature from 500-550 °C at the pluton/wallrock contact, to 450-500 °C at the aureole's outer margin (Nyman et al., 1995). Based on stratigraphic and structural grounds, Sylvester et al. (1978) estimated that the pluton was intruded at a depth of between 6.4 and 9.2 km.

A well-developed stretching lineation observed in the western part of the aureole and pluton margin lies within the plane of the foliation, plunging to the north-northwest on the north side of the pluton and to the south-southeast on the south side (Fig. 26). Crystallographic fabrics measured in both the plastically deformed aureole quartzite and quartz veins within the pluton's gneissic border facies indicate that this stretching lineation is associated with plane strain (k=1) deformation (Law et al. 1992, 1993). The lineation is oriented perpendicular to the long axes of triaxial (approximate chocolate tablet) boudins in schist and calc-silicate units within the aureole along the south and western margin of the pluton.

Anisotropy of magnetic susceptibility (AMS) data from the Papoose Flat pluton (to be presented in a separate paper), combined with microstructural examination of the same samples from which AMS analyses were obtained, indicate that the solid-state foliation and lineation within both the pluton's aureole and gneissic border facies is parallel to magmatic foliation and lineation within the interior of the pluton (St. Blanquat et al., 1994). The parallelism between the solid-state and magmatic fabrics indicates that the two fabrics developed synchronously and are related to the same event (St. Blanquat et al., 1994).

Porphyroblast-Matrix Relationships

Porphyroblast-matrix relationships within the aureole of the Papoose Flat pluton impose important constraints for modelling rigid body rotation and translation of the aureole rocks associated with pluton emplacement, and also allow determination of the relative

sequence of metamorphism, or porphyroblast growth, versus deformation. The reference frame chosen for presentating our porphyroblast data is the foliation-parallel compositional layering (which we believe represents bedding) within the aureole metasedimentary rocks. In all figures, compositional layering has been rotated into a horizontal orientation in order to view the angular relationships between porphyroblast inclusion trails and compositional layering in the same reference frame - regardless of the dip of the compositional layering at an individual sampling site. Unless otherwise stated, all porphyroblast data are presented on section planes oriented at right angles to the compositional layering and parallel to the stretching lineation; all these diagrams are viewed toward the northeast.

All samples analyzed for porphyroblast-matrix relationships come from the Harkless schist. In the White-Inyo Range the Harkless Formation consists of a series of shale and quartz sandstone units that can be traced into concordancy with the Papoose Flat pluton (Fig. 26) where it has been metamorphosed into a series of quartzite units interlayered with andalusite schist. In the western limb of the Inyo anticline, north of the pluton and its aureole, bedding dips on average at 32° to the southwest, and the shale has a well-defined regionally-developed slaty cleavage that dips approximately 20° more steeply to the southwest (Fig. 28). As the pluton is approached, the slaty cleavage fabric, consisting of fine grained chlorite, muscovite, and quartz is gradually overprinted by a younger foliation associated with contact metamorphism. The younger foliation is oriented parallel to the compositional layering and defined by coarse muscovite porphyroblasts. Within the Harkless schist adjacent to the Papoose Flat pluton, the contact metamorphic assemblage is Qtz+Ms+And+Bt+Pl.

Andalusite porphyroblasts within the Harkless schist exhibit two distinct internal domains based on differences in inclusion trail density and orientation (Morgan, 1992): a) a core region with a high density of planar inclusion trails (S_ic) usually oriented at a low angle to compositional layering (L_C) and, b) a rim region with a low density of inclusions (S_ir) that are coarser grained than in the core and which are continuous in orientation from S_ic and curve sharply into parallelism with the external foliation (S_e) (Fig. 29a, b, and f). S_e is defined by elongate muscovite grains that anastomose around andalusite porphyroblasts; in hand sample S_e generally defines a well-developed foliation that is parallel to compositional layering (L_C).

The orientation of S_ic relative to L_C was measured in thin sections cut both parallel and perpendicular to the lineation and always perpendicular to the compositional layering

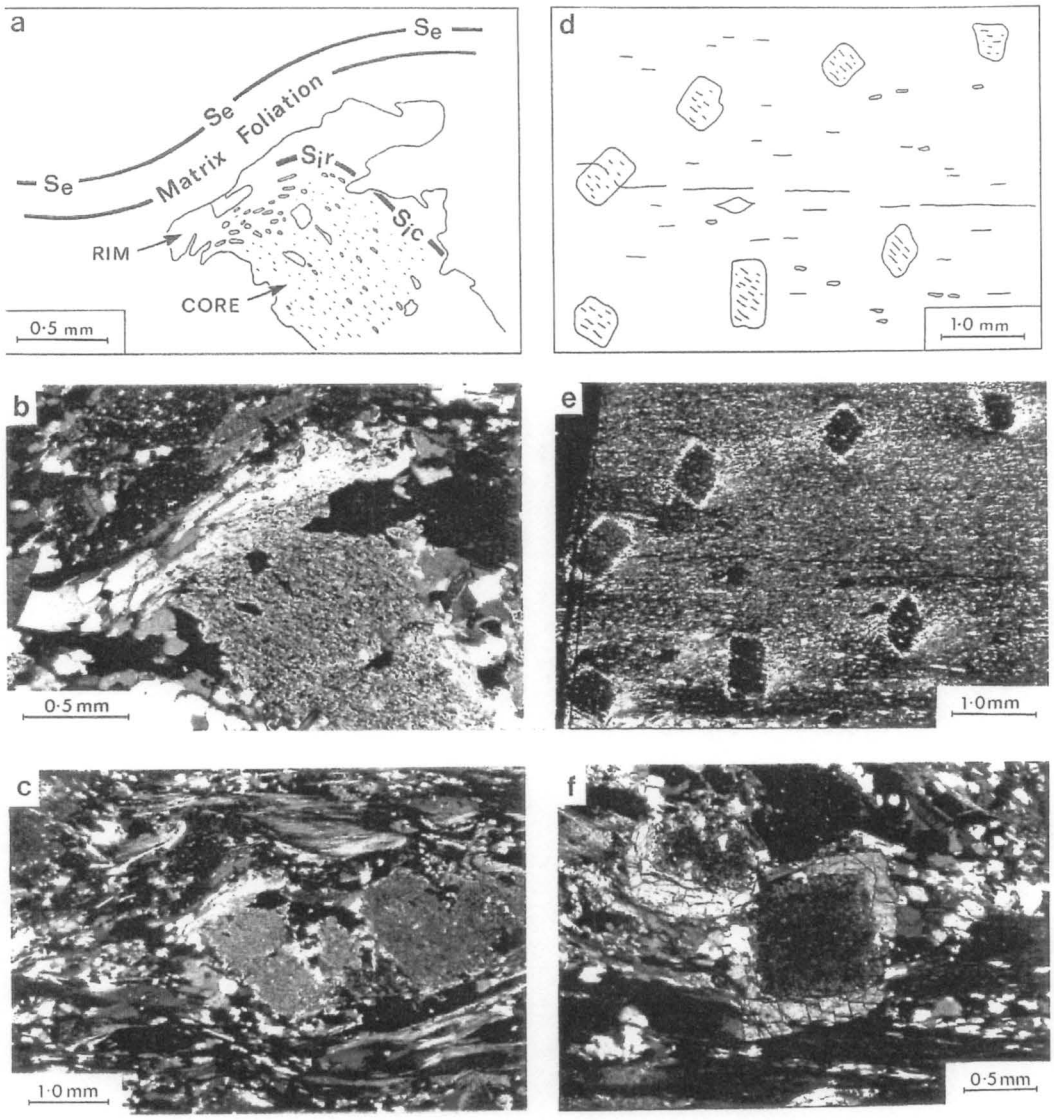

Figure 29. Photomicrographs and tracings of andalusite porphyroblast-matrix relationships. Sketch (a) based on photomicrograph (b) of sample PF 47. S_ic = alignment of inclusion trails observed within the core of porphyroblast. S_ir = alignment of inclusion trails observed within the rim of porphyroblast. S_e = schistosity observed in the (exterior) matrix. L_c = compositional layering. Photomicrograph (c) same as in (a-b) but viewed at smaller scale. (d-e) Andalusite porphyroblast-matrix relationships taken from sample PF 281. (f) Andalusite porphyroblast with core and rim.

(foliation). In most samples andalusite is partially or completely replaced by sericite, thereby limiting the number of samples suitable for porphyroblast-matrix analysis. Porphyroblast inclusion trails from 12 samples taken from around the pluton were measured in thin sections cut parallel to lineation (Fig. 30a). When these data are combined onto one plot and viewed toward the northeast, the two dimensional mean orientation of $S_i c$ is inclined at 8° to L_c measured in a clockwise direction from L_c (i.e. in the thin section plane, the mean angle between compositional layering L_c and the internal inclusion trails within porphyroblasts is 8° measured down to the southeast relative to a horizontal compositional layering - L_c). Note that $S_i c$ has the same angular relationship to L_c regardless whether an individual sample is taken from the northern part of the aureole, where L_c dips to the north, or from the southern part of the aureole, where L_c dips to the south.

Porphyroblast inclusion trails from six samples taken from around the pluton were measured in thin sections cut perpendicular to lineation (Fig. 30b). When these data are combined onto one plot and viewed toward the north-northwest, the two dimensional mean orientation of $S_i c$ is inclined at 8° to L_c measured in a counter-clockwise direction from L_c. In order to obtain the average three dimensional orientation of $S_i c$ (relative to a horizontal L_c), the data from thin sections cut parallel and perpendicular to lineation were combined on a single stereogram (Fig. 30c). Figure 30c portrays the three dimensional orientation of $S_i c$ in sample coordinates when the aureole metasedimentary formations are horizontal, or as if they were "undomed" from concordancy with the pluton and rotated into a horizontal orientation.

Porphyroblast-Matrix Interpretations

There is a spread of porphyroblast inclusion trail ($S_i c$) orientations within each thin section. Regardless of geographic position around the pluton, however, and regardless of the direction and angle of dip of compositional layering (L_c), the majority of inclusion trails within individual thin sections are inclined at a very similar average angle to compositional layering (Figs. 29d and 30). Four inter-related interpretations based on this consistant angular relationship between $S_i c$ and L_c are proposed and help to clarify structural relationships:

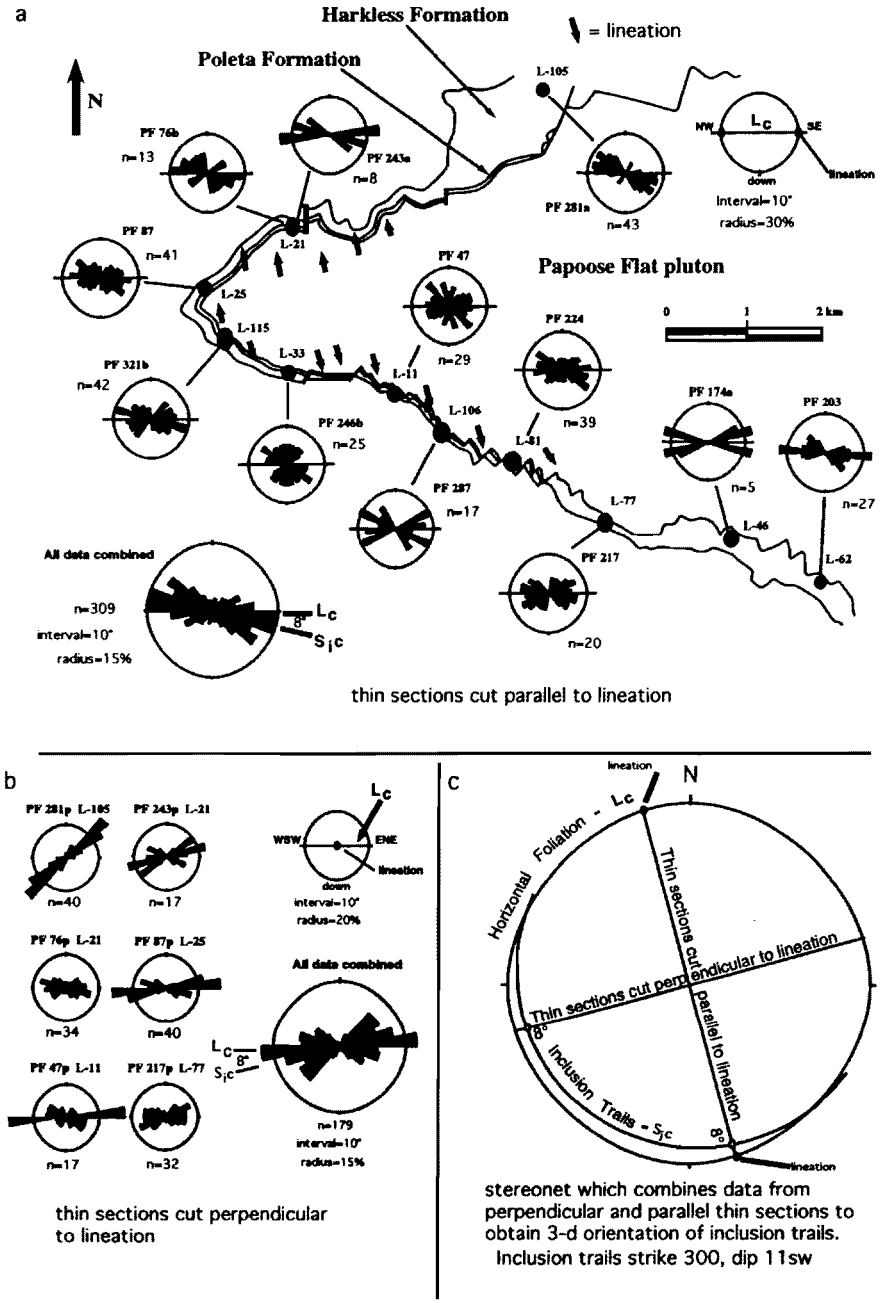

Figure 30. Location map of samples and rose-like diagrams of two-dimensional angular relationship between inclusion trails within cores of andalusiteporphyroblasts (Sic) and compositional layering (Lc). All samples are rotated so that compositional layering, Lc, is horizontal. (a) Bars that reach the circle indicate that 30% of the porphyroblasts measured in that thin section contain orientations of Sic which vary within the 10° interval that the black bar covers. (b) Circle represents 20% of porphyroblasts. (c) Stereogram which combines the data from (a) and (b).

1) Deformation and metamorphism subsequent to andalusite core growth have not caused porphyroblasts to rotate enough (relative to compositional layering) to destroy the orientation of an earlier fabric now preserved as $S_{i}c$ within the porphyroblasts. The spread in orientation of inclusion trails indicates that most porphyroblasts have rotated by a maximum angle of between 10 and 30° with respect to compositional layering, even though these layers have been attenuated to as little as 10% of their original thickness (Sylvester 1966, Sylvester et al. 1978). Very few porphyroblasts have rotated more than 60°. In general, the most convincing argument for non-rotation, or little rotation, of porphyroblasts is the observation of planar to sigmoidal shaped inclusion trails that are found in the same orientation over large areas of individual thin sections (Fig. 29d), even though significant deformation has occurred post-dating porphyroblast growth (Ramsay, 1962; Fyson, 1980; Vernon, 1988a & b, 1989; Jamieson and Vernon, 1987; Johnson, 1990; Morgan et al., 1992).

2) Porphyroblast growth has preserved a penetrative and planar fabric ($S_{i}c$) in the aureole rocks that was at a low angle to compositional layering (i.e. bedding) and which predated andalusite porphyroblast core growth. This older penetrative fabric ($S_{i}c$) represents a slaty cleavage in the original shale that cut bedding at a low angle, as discussed below.

Thin sections from all samples, regardless of location, exhibit a strong alignment of andalusite porphyroblast inclusion trails that are inclined at a small average angle (5-25°) to compositional layering. The slaty cleavage fabric, which is found throughout the western limb of the Inyo anticline to the north and outside of the Papoose Flat pluton's aureole, also consistently dips between 5 and 25° more steeply than bedding (Fig. 28).

The progressive overprinting of this regional slaty cleavage has been studied in a transect located several hundred meters south of the central section of the pluton's southern margin; here attenuation and recrystallization associated with contact metamorphism decreases with distance from the pluton margin. At 200 m from the pluton margin, bedding is concordant to the pluton margin, but the regional slaty cleavage has not been transposed into the aureole fabric. Both bedding and cleavage dip toward the southwest, with cleavage dipping slightly more steeply than bedding. As the pluton is approached and metamorphism and deformation increase, the cleavage is progressively overprinted by a new metamorphic foliation. At 50 m from the contact, andalusite porphyroblasts contain inclusion trails that dip to the southwest slightly more steeply than compositional layering, similar to the bedding-cleavage relationship in the outer aureole a few hundred meters to the south.

3) Andalusite porphyroblast cores grew when the compositional layering (i.e. bedding) within the aureole metasedimentary rocks was originally planar, prior to being domed into its current structural position during pluton emplacement. When the aureole rocks are "undomed" (i.e. the dipping compositional layering surrounding the pluton is unfolded back into a planar, although not necessarily horizontal, configuration) the core inclusion trails (S_{ic}) in andalusite porphyroblasts from the northwestern part of the pluton's aureole become aligned parallel to S_{ic} in porphyroblasts from the southwestern part of the aureole (Fig. 31). This suggests that the andalusite porphyroblasts grew and incorporated the planar fabric as inclusion trails before the aureole rocks were "domed", or deformed around the evolving pluton (Fig. 31). This, in turn, suggests that most porphyroblasts have not rotated significantly (less than 10-30°) with respect to compositional layering, but have rotated with respect to the geographic horizontal as the compositional layering was deformed. In addition, the observation that S_{ic} remains planar and is not folded or sigmoidal in cross section indicates that the andalusite cores grew during a period of "static" contact metamorphism and that core growth was not associated with penetrative deformation.

4) The intense attenuation of the aureole rocks around the margins of the evolving pluton caused the original regional slaty cleavage in the aureole rocks to be rotated with respect to compositional layering (L_C) and become aligned parallel to L_C. The orientation of the original slaty cleavage within the aureole is only preserved as inclusion trails (S_{ic}) within cores of andalusite porphyroblasts and is oriented at a low angle to L_C. S_{ic} curves from the porphyroblast cores into the rims to become aligned parallel to the present matrix foliation, Se. This curvature tracks the rotation of the slaty cleavage, from its original orientation at a low angle to L_C, to its present orientation parallel to L_C (Fig. 32).

Two additional interpretations based on porphyroblast-matrix relationships help determine the timing of andalusite porphyroblast growth in relation to the intense attenuation of the metasedimentary formations:

5) Andalusite core growth predates the development of the present exterior foliation, S_e. Vernon et al. (1993a and b) suggested that one line of evidence for growth of porphyroblasts prior to "ductile foliation development" (i.e. development of a contact metamorphic foliation parallel to pluton margins) is the fine grain size of inclusions within porphyroblasts when compared with the coarser grained matrix outside the porphyroblasts. The fine grained size of inclusions indicates that when porphyroblasts initially started growing and incorporating their matrix, the matrix assemblage had not yet begun reacting to

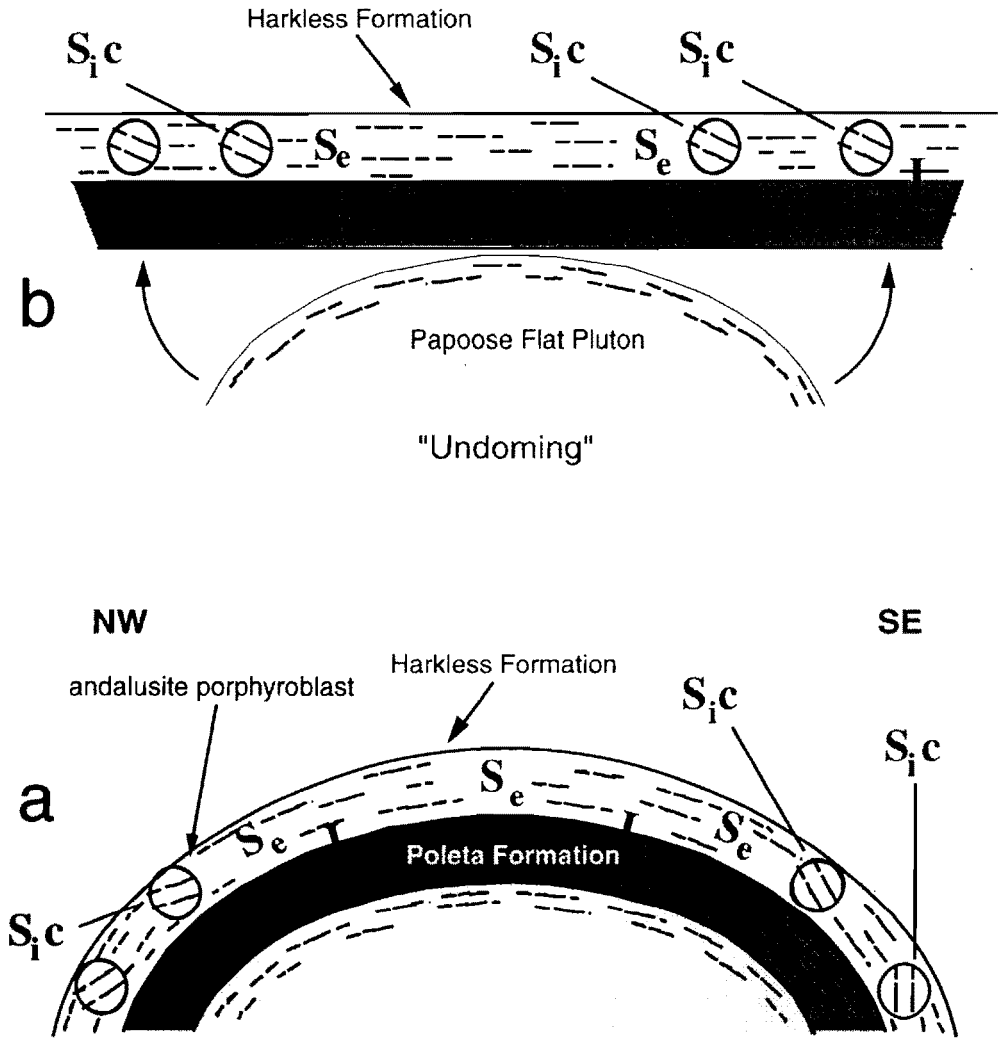

Figure 31. Undoming the aureole rocks (b) from concordancy with the pluton (a) rotates andalusite porphyroblasts so that inclusion trails are parallel in all porphyroblasts regardless of position around the pluton. This relationship indicates that porphyroblasts initially grew when aureole rocks were originally planar, prior to doming into concordancy with the pluton. After Morgan (1992).

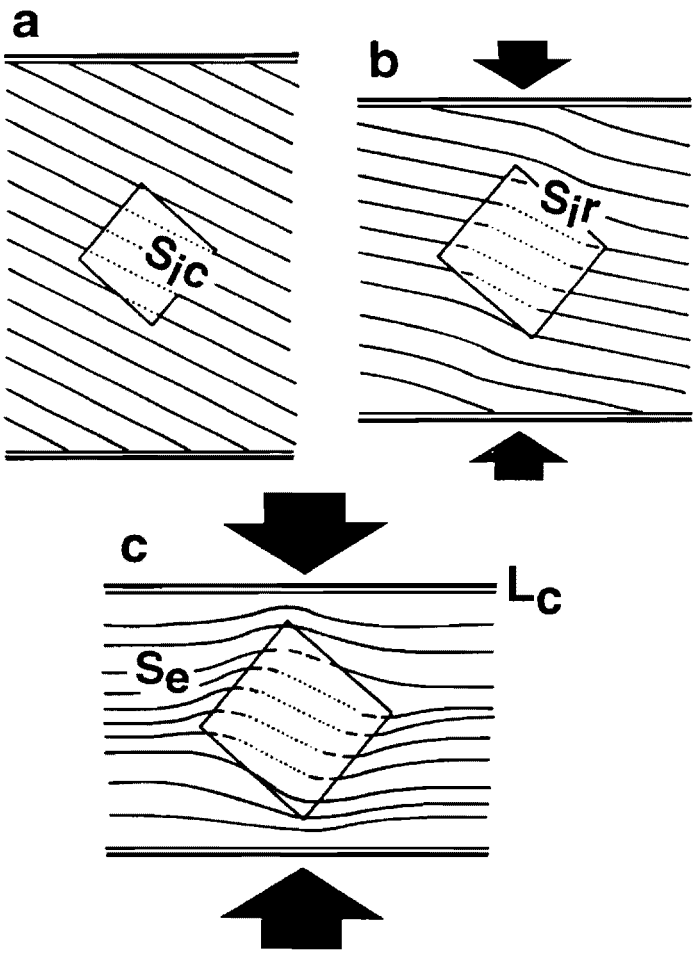

Figure 32. Sequential growth of andalusite porphyroblast and incorporation of matrix as inclusion trails. Note that rotation of exterior matrix foliation into parallelism with compositional layering (Lc) begins late in growth history of porphyroblasts.

the changing physical environment in the aureole. Within the Harkless schist adjacent to the Papoose Flat pluton, the older planar fabric, S_ic, is preserved only within the cores of andalusite porphyroblasts, and is much finer grained than the exterior foliation, S_e (Fig. 29c).

6) Andalusite rim growth is synchronous with the contact metamorphism and intense structural attenuation that produced the exterior foliation, S_e. Inclusion trails in the rims of andalusite porphyroblasts (S_ir) curve from the planar core regions (S_ic) into parallelism with the matrix foliation (S_e) tracking the attenuation event. Inclusions in the rims are also coarser grained than in the core region, indicating that the matrix was finally reacting to the changing physical environment as andalusite porphyroblasts continued to grow.

Aureole Strain Analysis

Complete specification of the strain history a rock body has undergone is an inherently difficult and often impossible task. A complete analysis of the strain path requires information on distortion (shape change), rigid body rotation, volume change and rigid-body translation (Ramsay, 1969). Measurement of all these displacement components is typically impossible, and we suggest that one of the prime reasons for the current controversy over how plutons are emplaced may be the general difficulty in completely specifying the displacements associated with pluton emplacement. The concordant metasedimentary aureole rocks surrounding the Papoose Flat pluton present a rare opportunity for a complete determination of the strain history. With the aid of porphyroblast-matrix relationships as strain markers, together with measurement of stratigraphic sections and whole-rock geochemical analyses, we attempt to demonstrate that: i) the kinematics of rotation, ii) the change in thickness, iii) the change in volume and, iv) the amount of translation of the metasedimentary formations within the aureole rocks, may all be quantified.

Rigid Body Rotation

Assuming that the geometric relationship between inclusion trails within andalusite porphyroblasts and compositional layering represents the same relationship between bedding and slaty cleavage observed outside the pluton aureole, then the intersection angle between

these two planes can be used as a passive marker to restore the concordant aureole formations back to their pre-pluton emplacement positions. Our preferred model restores the western aureole rocks back into the Inyo anticline so that the inclusion trails become realigned parallel to the regionally developed slaty cleavage fabric. This model is based on vertical motion of the pluton and associated translation and rotation of the surrounding wall rocks. The motion of the wall rocks is divided into two separate steps that allow modeling of the motion with a stereonet, although it should be noted that the motion was probably one continuous event.

The first restoration step is to "undome" the northwestern and southwestern aureole compositional layering by rotating around horizontal poles orientated east-northeast (Fig. 33a). These poles of rotation are perpendicular to the lineation and parallel to the long axis of the pluton. This rotation brings the northwestern and southwestern "limbs", which dip away from the pluton, down into a horizontal plane (Fig. 33b). The second restoration step involves rotation of the compositional layering around a horizontal pole oriented north-northwest, parallel to the strike of the southwest limb of the Inyo anticline (Fig. 33b). In this motion the southwest side is rotated down, simultaneously bringing: i) the compositional layering into parallelism with bedding in the southwest limb of the anticline (Fig. 33c) and, ii) the inclusion trails into parallelism with the slaty cleavage found throughout the central White-Inyo Range (c.f. Figs. 28 and 33d).

A model based on horizontal motion, in which the aureole rocks were "bulged" horizontaly out of the Inyo anticline as the pluton inflated outwards to the west during emplacement, was also tested by porphyroblast-matrix analysis. This is the original translation and rotation model assumed by Sylvester et al. (1978), and is consistent with the map pattern of the aureole rocks as they are deflected westwards out of the anticline to surround the pluton. This alternative model is tested by independently rotating the northwestern and southwestern sides of the aureole around vertical poles (Fig. 34a) until they strike parallel to the southwest limb of the Inyo anticline (Fig. 34b). The vertical poles of rotation are located where, in map view, the beds in the western limb of the Inyo anticline begin their deflection into concordancy with the pluton. When the aureole rocks are restored back into the western limb of the anticline with this rotation, inclusion trails are not aligned parallel to one another with respect to compositional layering from the northern limb to the southern limb (Fig. 34b), and they are also not parallel to the orientation of the pre-existing regionally developed slaty cleavage. Therefore this emplacement model, which incorporates

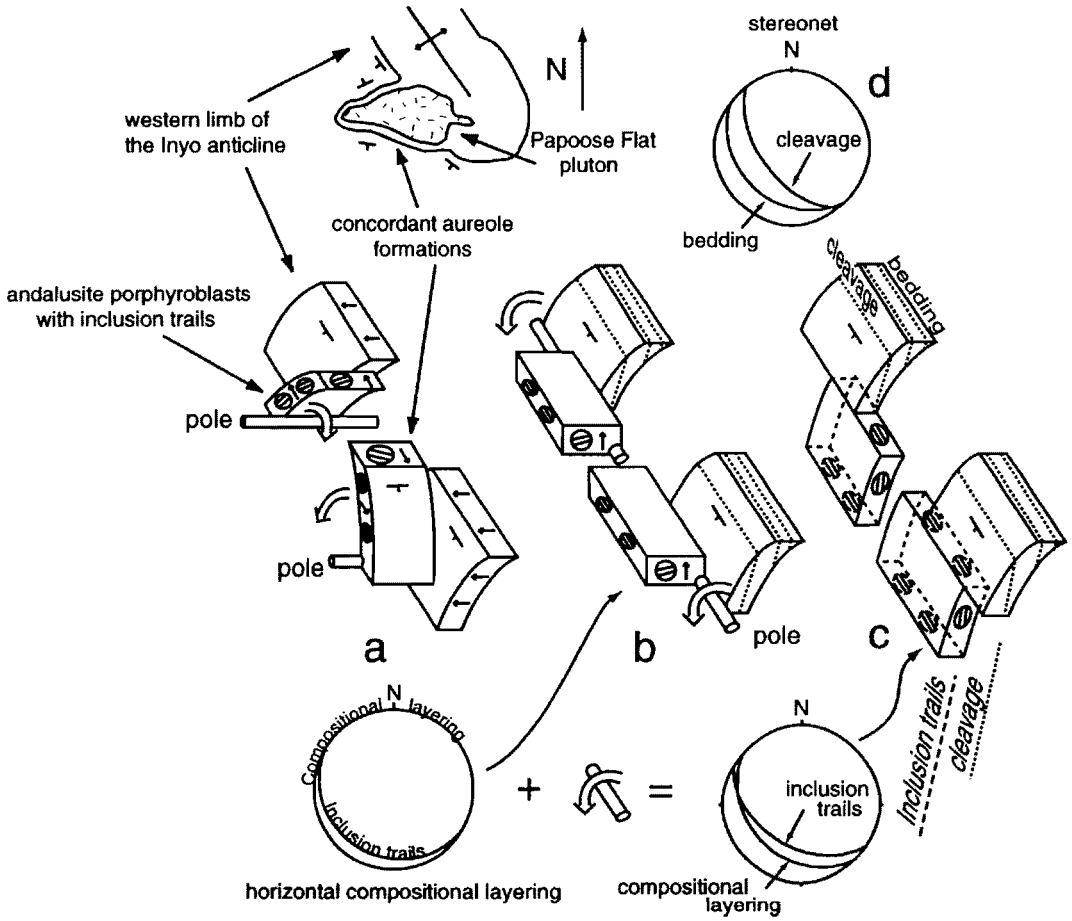

Figure 33. Diagram illustrating the palinspastic restoration of aureole rocks into their pre-pluton position in the western limb of the Inyo anticline using vertical translation and rotation. (a) Present structural position of aureole metasedimentary layering surrounding Papoose Flat pluton. (b) Aureole rocks are undomed. (c) Aureole metasedimentary rocks repositioned into parallelism with bedding in the Inyo anticline. Note how restoration places inclusion trails from andalusite porphyroblasts (stereograms at bottom of diagram) into parallelism with slaty cleavage observed in pelitic rocks from western limb of Inyo anticline indicated by stereogram (d).

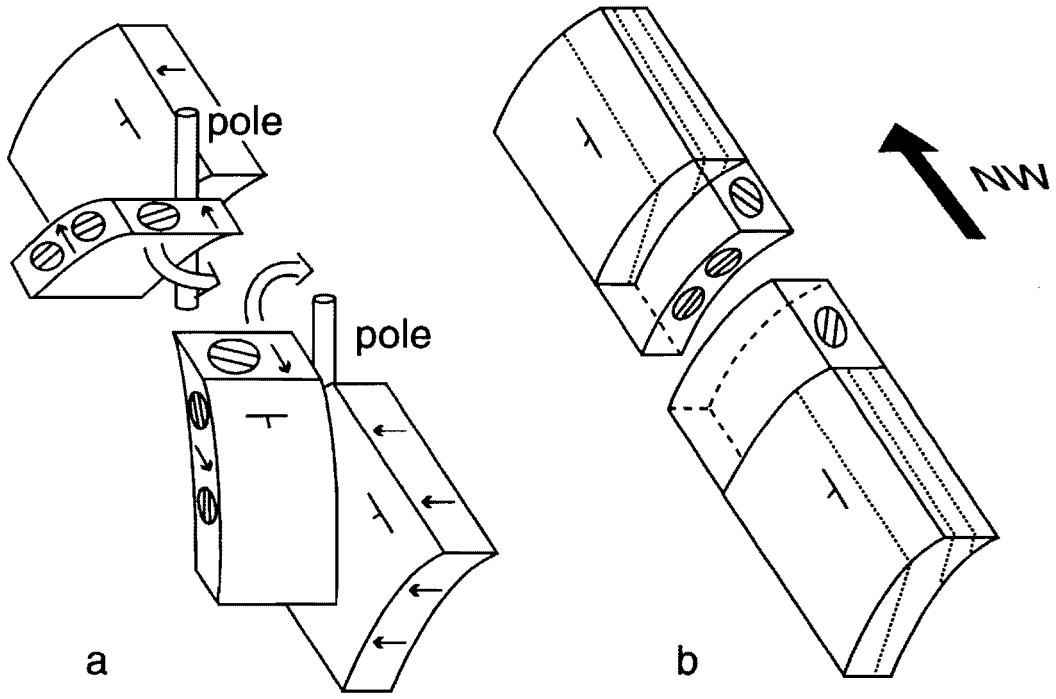

Figure 34. Diagram illustrating incorrect palinspastic restoration of aureole rocks into their pre-pluton position in the western limb of the Inyo anticline using horizontal translation and rotation. (a) Present structural position of aureole metasedimentary layering surrounding pluton. Open arrows indicate rotation necessary to restore compositional layering in aureole rocks into parallelism with bedding in western limb of anticline. (b) Aureole metasedimentary rocks restored. Note how inclusion trails from northern margin do not restore into parallelism with inclusion trails from southern aureole margin, and how inclusion trails are not parallel to the regionally developed slaty cleavage.

horizontal "bulging" and rotation of the western aureole around vertical poles, is rejected. It should be kept in mind, however, that the vertical and horizontal pluton emplacement models investigated here only represent end members of a spectrum of possible solutions.

Distortion (Shape Change)

Sylvester (1966) recorded the pinch and swell of the lower Cambrian metasedimentary formations around the western margin of the pluton by measuring 21 stratigraphic sections through the aureole (see also Sylvester et al., 1978, fig. 11). The regional stratigraphic thickness of 570 to 700 m for the Harkless Formation is reduced to roughly 45 m around the western margin of the pluton. This indicates that the Harkless Formation has been thinned to less than 10% of its original thickness. The greatest degree of attenuation is observed at the westernmost end of the pluton, and decreases in intensity eastward along the northern and southern margins (c.f. Fig. 26). The Saline Valley Formation decreases in thickness from 62 m to 27 m to 16 m traced from east to west in Sylvester's three easternmost traverses along the southern border. Along the same interval, the upper Harkless quartzite and quartz-mica schist decrease in thickness from 66 m to 35 m to 31m traced from east to west.

Volume Change

Seven samples were analyzed for major elements by direct-current plasma spectrometry from the Harkless Formation varying in distance from 5 km north of the pluton to 20 m from the contact in the concordant section around the western margin (Fig. 26). Preliminary whole-rock geochemical analyses indicate there is no significant change in major element concentrations in the Harkless Formation shale as it is metamorphosed and attenuated into aureole schists surrounding the Papoose Flat pluton (Table 3). Therefore, the change in thickness of the Harkless Formation from a regional thickness of 570 to 700 m down to 45 m around the pluton is considered to be due to shape change associated with penetrative strain, and not volume loss.

TABLE 1. HARKLESS FORMATION CHEMICAL ANALYSES

Sample	SiO_2	TiO_2	Al_2O_3	Fe_2O_3	MnO	MgO	CaO	Na_2O	K_2O	Ba	Sr	Total
Gc-1	60.75	0.82	22.01	7.57	0.08	2.17	0.47	0.40	4.02	579.6	99.3	98.3
Gc-2	59.16	0.99	25.75	7.86	0.07	1.87	0.09	1.08	3.62	523.1	146.5	100.49
Gc-3	60.40	0.88	23.27	8.31	0.11	2.42	0.26	0.73	3.70	623.9	141.9	100.06
Gc-4	67.20	0.64	16.64	9.38	0.10	2.60	0.45	0.30	2.00	344.9	88.6	99.31
Gc-5	60.95	0.86	21.86	9.07	0.13	2.68	0.56	0.58	3.32	484.8	119.6	100
Gc-6	61.28	0.91	25.13	6.65	0.07	2.31	0.29	0.11	4.80	613.3	134.3	101.54
Gc-7	58.53	0.88	24.91	8.16	0.12	2.39	0.17	0.36	4.45	763.8	121.4	99.98

Note: Data are in weight percent except for Ba and Sr which are in ppm. Sample locations on Figure 26.

Table 3. Harkless Formation chemical analyses.

Rigid-Body Translation (Vertical)

The amount of rigid-body translation of the aureole rocks is controlled by the kinematics of their rotation, the shape change (thinning) of the metasedimentary formations, and the amount of deflection of the aureole rocks out of the Inyo anticline. By: i) limiting the pluton motion to a vertical upward translation and, ii) assuming that beds in the southwest-dipping limb of the Inyo anticline were constantly oriented across the area prior to intrusion of the Papoose Flat pluton, the amount of vertical translation can be quantified by simple trigonometry (Fig. 35). Area balancing the attenuated stratigraphy also helps to control the amount of translation and helps in understanding the geometry of the pluton at depth (Fig. 36).

The westward deflection of the lower Cambrian section out of the Inyo anticline when in contact with the Papoose Flat pluton is clearly revealed in the geologic map of the region (Fig. 26). At the present topographic level, the Poleta-Harkless contact within the aureole on the northwestern margin of the pluton is deflected approximately 4.2 km west-southwest of its regional position in the Inyo anticline, assuming the regional structures were constantly oriented through the area before intrusion. The Poleta-Harkless contact within the aureole northwest of the pluton is at an elevation of 2680 m, as is the Poleta-Harkless contact at 3 km northeast of the pluton where it is found in the undisturbed southwest limb of the Inyo anticline. Simple trigonometry indicates that the structural depth to the original Poleta-Harkless contact, prior to upward deflection by the pluton, was approximately 2 km below its current outcrop position northwest of the pluton (Fig. 35). These calculations assume the pluton rose vertically out of the southwest-dipping limb of the anticline and also assume a homoclinal structure for the southwestern limb and a dip of 25° for the beds within the homocline. A dip of 25° is a minimum dip for the southwestern limb of the Inyo anticline north of the pluton. Using a dip of 30° for the southwestern limb of the anticline, a vertical translation of 2.4 km is necessary to account for the outcrop position of the Poleta-Harkless contact. Similarly, a dip of 40° would indicate a vertical translation of 3.5 km to bring the Poleta-Harkless contact up to its present outcrop position northwest of the pluton.

The possible sub-surface geometry of the Papoose Flat pluton and its aureole has been investigated by constructing a series of cross sections drawn at right angles to the pluton long axis. These cross sections take into account different possible dip values for the western limb of the Inyo anticline, and therefore different possible amounts of vertical upward translation of the pluton and its aureole. The cross sections are drawn assuming that

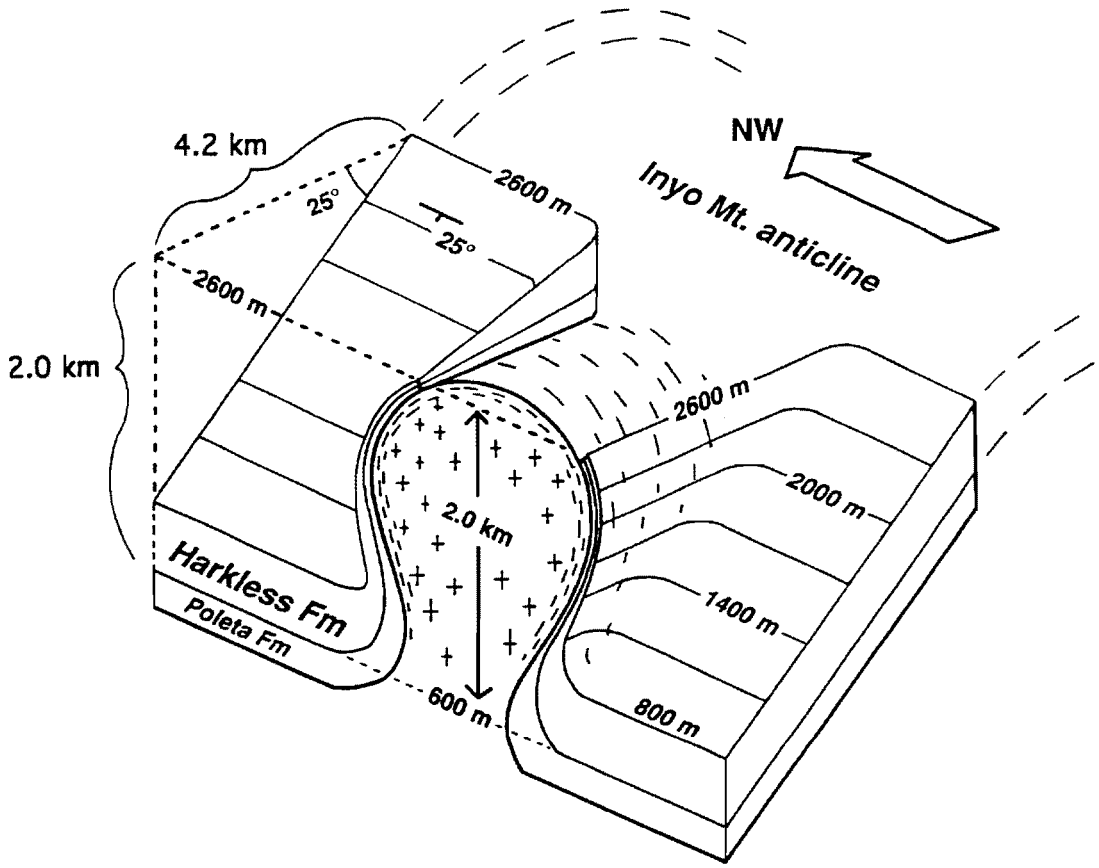

Figure 35. Block diagram illustrating that approximately 2 km of vertical translation is needed to bring the Harkless and Poleta Formations to their present exposure level northeast of the pluton. Dip of beds in the southwest limb of the Inyo anticline is assumed to be a constant 25°, and deflection of the aureole rocks is limited to vertical translation. Dashed lines on sides and top of pluton represent orientation of stretching lineation.

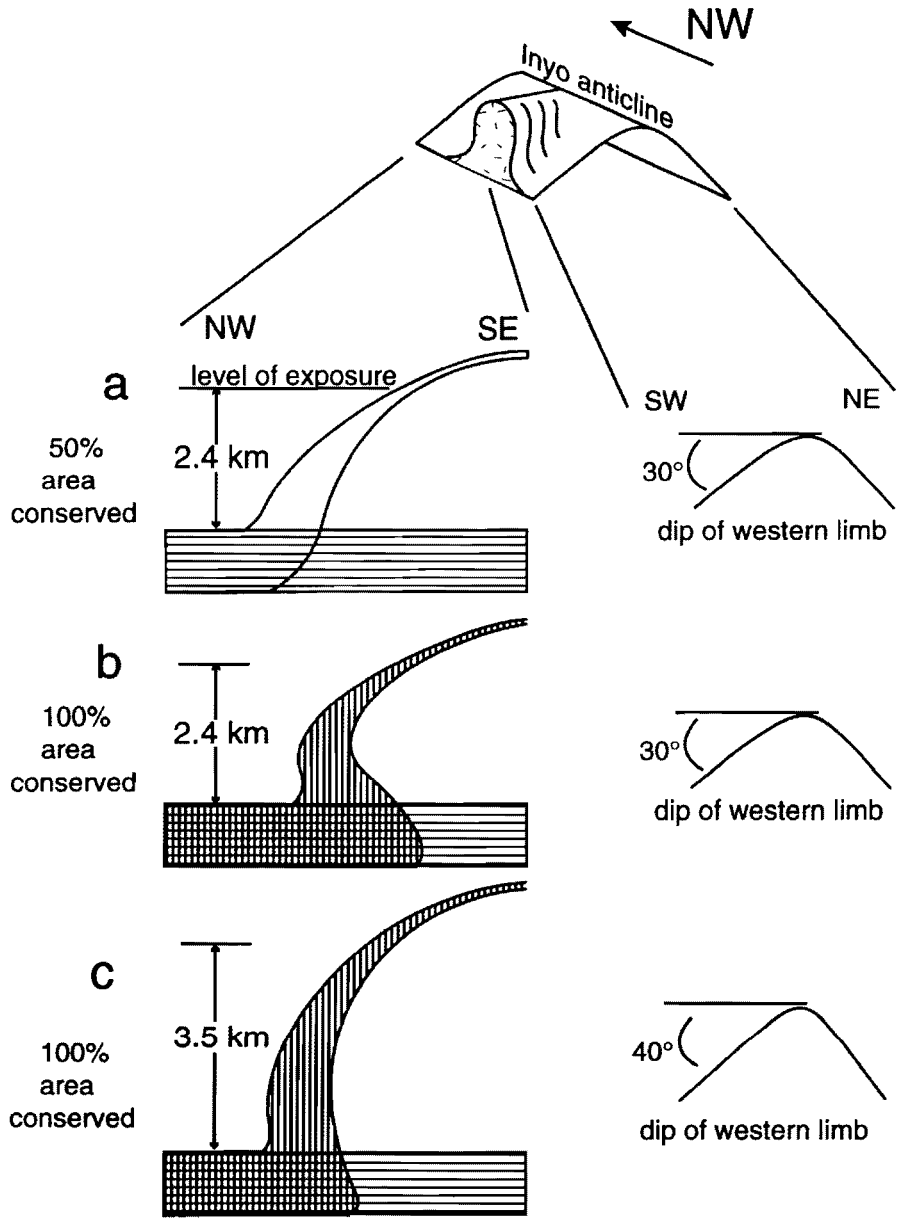

Figure 36. Three cross sections extrapolating the half-pluton shape and geometry of the concordant aureole rocks to depth. Cross sections are drawn parallel to the axis of the Inyo anticline (and parallel to the stretching lineation) and perpendicular to the long axis of the pluton. Vertically lined area (deformed wall rocks) equals horizontally lined area (undeformed wall rocks). (a) Deformed wall rocks (unlined) equal 50% of undeformed wall rocks. (b) Area is conserved due to overturning of wall rocks. Dip of wall rocks in (a) and (b) is 30°, and therefore bedding is transported 2.4km vertically. (c) Dip of bedding in anticline is 40°, and therefore vertical translation is 3.5km.

the thinning of the metasedimentary layers is a result of stretching as the aureole layers were domed over an inflating pluton. In order to test the cross sections, the aureole formations have been area balanced (aureole layers contain the same area before and after deformation) given that they must be 10% of their original thickness by the time they reach the current level of exposure (Fig. 36). Cross sections are drawn parallel to the north-northwest oriented stretching lineation assuming plane strain with no volume loss. The cross sections illustrate how the aureole formations need to be overturned at depth if the western limb of the Inyo anticline is gently dipping (Fig. 36b). This is because in order for the cross section to be area balanced (with shallower dips for the western limb) there is less distance for the aureole layers to be stretched and thinned. More area is created by overturning the layers. If the western limb of the anticline has a dip closer to 40°, then minimal overturning is necessary to area balance the cross section (Fig. 36c).

The assumption of plane strain inherent in the two-dimensional area balancing is locally supported by the fact that both the plastically deformed Harkless quartzite of the aureole and the similarly deformed foliation-parallel quartz veins in the gneissic border facies of the pluton are characterized by a well-developed NNE-SSW trending stretching lineation lying within the mylonitic foliation. Quartz crystallographic fabrics measured by both optical and X-ray texture goniometry methods in over 150 samples of these plastically deformed rocks consistantly indicate that strain symmetry was very close to plane strain ($k=1$) conditions (Law et al. 1992, 1993). Triaxial (approximate chocolate-tablet) boudinage structures, indicating deformation within the flattening ($1>k>0$) strain field, have been recorded however in: i) skarn deposits from the Poleta Formation (Sylvester and Christie 1968) located between the pluton margin and the overlying Harkless quartzite, and ii) limestone of the Mule Springs and Saline Valley formations lying above the Harkless Formation. These plastically deformed rocks also contain a NNW-SSE trending stretching lineation; the greatest separation between the chocolate-tablet boudins is observed in sections cut parallel to lineation and perpendicular to foliation. The local occurence of flattening ($1>k>0$) strains indicates that, with respect to area and volume balancing, less vertical translation and/or less overturning of stratigraphic units at depth (Fig. 36b) is necessary to account for attenuation of the stratigraphy. We reiterate, however, that the minimum possible dip angle for the southwestern limb of the anticline is 25°, indicating a minimum possible vertical translation for the pluton and its aureole rocks of 2.0 km.

Rigid-Body Translation - Horizontal Translation

The Precambrian Wyman Formation, which is the lowest stratigraphic formation exposed in the White-Inyo Range, constitutes the core of the Inyo anticline (Fig. 26). The Inyo anticline is a continuous north-northwest trending upright fold which can be traced for over 40 km along its hinge, and only where the Wyman Formation comes into contact with the eastern margin of the Papoose Flat pluton are the beds overturned, suggesting that emplacement of the pluton is responsible for the overturned section (Sylvester et al., 1978; Nelson 1987). The Reed dolomite, which stratigraphically lies above the Wyman Formation, is also overturned and the whole succession, from the Wyman Formation through the Reed dolomite and overlying Deep Spring Formation and Campito Formation, is more tightly folded on the eastern end of the pluton (Fig. 26) than anywhere else in the Inyo anticline, suggesting that the fold was tightened by lateral translation as the pluton locally expanded outward toward the east.

Emplacement Model

Porphyroblasts and Two Stages of Emplacement

Porphyroblast matrix relationships observed within the Harkless Formation surrounding the western and southern margin of the Papoose Flat pluton can be explained by invoking a model involving two stages of magma injection, the first passive and the second forcible (Fig. 37). The first magma injection produces a sill and introduces a heat source which decreases the viscosity of the overlying sedimentary succession and results in static contact metamorphism and growth of andalusite porphyroblast cores (Fig. 37a). The first injection of magma pre-dates attenuation of the surrounding aureole rocks. A second pulse of magma, under high enough pressure to lift the overlying roof rocks, translates but also plastically attenuates the overlying sedimentary succession (Fig. 37b) now that it is thermally weakened and causes the continued growth of andalusite (rims). The magma may have initially risen along a pre-existing fault (Fig. 37) in a manner similar to that previously proposed for the emplacement history of the Birch Creek pluton (Nelson and Sylvester, 1971), an almost identical age pluton, located 34 km to the north of the Papoose Flat pluton. Our two stage model for evolution of the Papoose Flat pluton is based on the relative timing of porphyroblast growth versus the development of structures within the matrix of the Harkless schist. Within the porphyroblasts evidence exists for a significant period of

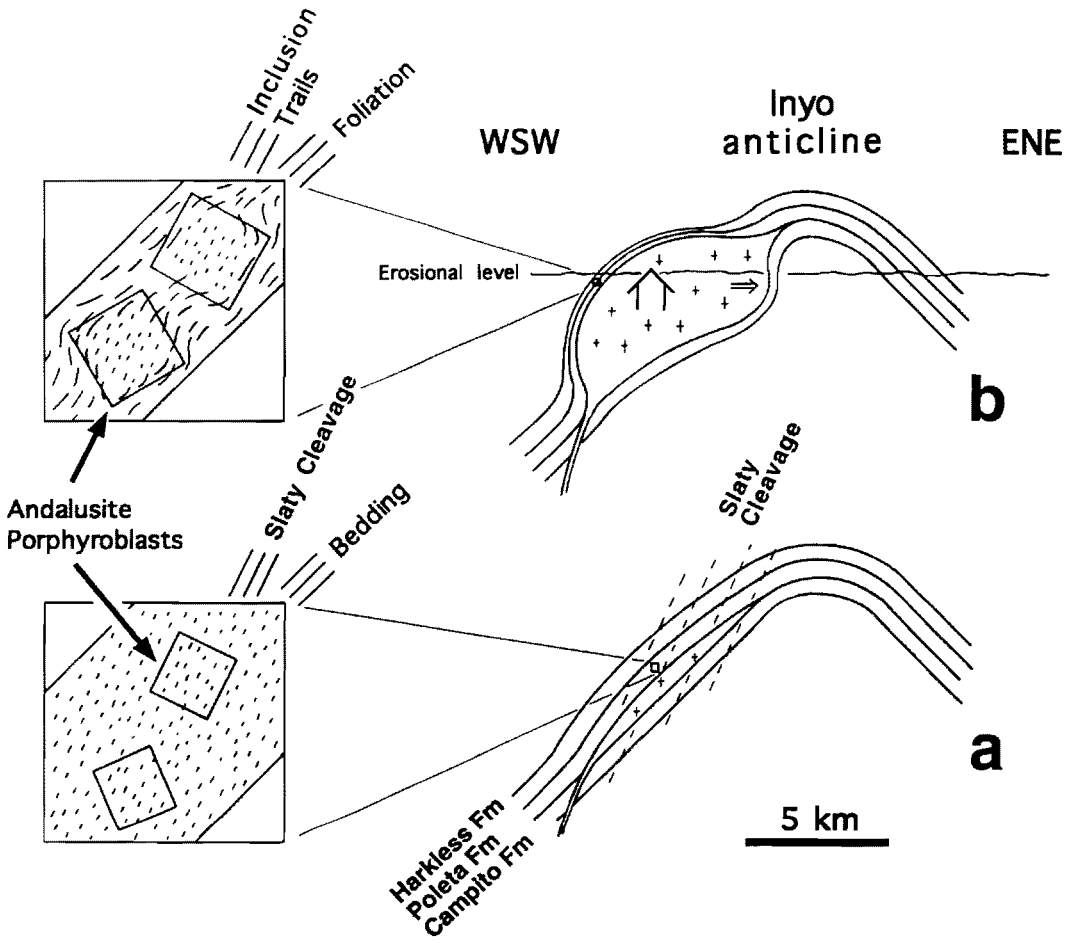

Figure 37. Schematic diagram illustrating two stages of magma emplacement and porphyroblast-matrix development. (a) Magma is emplaced initially as a sill within southwest limb of the Inyo anticline. Andalusite porphyroblasts overgrow regionally developed slaty cleavage fabric in surrounding shale during contact metamorphism. (b) Subsequent pulses of magma into sill cause sill to inflate vertically, but also outward toward the east. Andalusite porphyroblasts continue to grow as the aureole rocks are thinned. Matrix foliation recrystallizes in response to deformation during continued contact metamorphism, and inclusion grains become coarser and curve as matrix foliation wraps around andalusite porphyroblasts during shortening.

andalusite growth before ductile deformation (attenuation and doming) but post-dating the regionally developed slaty cleavage. Porphyroblast core growth is related to initial intrusion of magma as a sill primarily within or below the Poleta Formation. The duration of time taken for andalusite porphyroblasts within the Harkless shales to nucleate and grow to the size of their core region is believed to be the duration of time over which the magma ponded as a sill (Fig. 37a). Porphyroblasts overgrew the slaty cleavage fabric which was oriented at a low angle to bedding and incorporated the fabric as inclusion trails.

The fine grain size of inclusions relative to matrix grains and planar alignment of inclusion trails in the core region of andalusite porphyroblasts (Fig. 29) indicates that the cores grew prior to ductile deformation (Vernon et al., 1993a and b) that was associated with final emplacement of the Papoose Flat pluton. In contrast, inclusions trails within the rim regions of porphyroblasts, S_{ir}, curve into parallelism with the matrix foliation (Fig. 29), a feature commonly used as evidence for syndeformational growth of porphyroblasts (Bell and Rubenach, 1983; Bell et al., 1986; Vernon, 1989). We therefore interpret the porphyroblast core to rim boundary as representing a change in metamorphic and kinematic conditions as inclusions become coarser grained and curved into parallelism with the matrix foliation. This curvature records the onset of ductile deformation within the aureole rocks.

The second pulse of magma is associated with three phenomena: a) the dominantly vertical translation of the overlying sedimentary succession, b) the extreme attenuation of the immediately overlying meta-sedimentary aureole rocks and, c) the growth of andalusite porphyroblast rims (Fig. 37b). It should be noted that, although our model for evolution of the Papoose Flat pluton calls for the emplacement of at least two separate pulses of magma, no documented examples of mineralogical zonation or internal contacts within the pluton have to date been published. However, recently completed work on the anisotropy of magnetic susceptibility, mineralogy and microstructures of the pluton (which will form the subject of a separate paper) indicates that the pluton is indeed zoned mineralogically (M. de Saint Blanquat, personal communication 1997) as well as exhibiting at least rare examples of internal contacts (M. Barton, personal communication 1992; M. de Saint Blanquat, personal communication 1996). The previous difficulty in recognizing distinct intrusions within the pluton which may be associated with these separate magma pulses may, at least in part, be explained by the fact that the western half of the pluton is only exposed close to its roof (Sylvester et al., 1978).

We suggest that upward dilation of the magma chamber produced the doming of the sedimentary units around the pluton now seen at the current exposure level. The sedimentary

succession farther above the pluton, unaffected by the thermal pulse, was passively translated upward in a similar style to the overburden above a laccolith. In this interpretation the NNW-SSE orientation of the stretching lineation observed in the pluton's gneissic border facies and aureole rocks is a result of the east-west orientation of the elongate shape of the inflating magma chamber. The lineation is oriented sub-perpendicular to the elongate shape of the pluton and developed as the solid state carapace (pluton margin and aureole) was stretched around an upward inflating tube-like magma chamber (Fig. 35). Attenuation of the aureole rocks was accompanied by strain-path partitioning, plastic deformation of the quartz-rich units occurring under plane strain (k=1) conditions (Law et al. 1992, 1993), while the limestone and dolomite units appear to have been simultaneously deforming under flattening (1>k>0) conditions (Morgan 1992).

Within the pluton's aureole, extreme attenuation of the metasedimentary layers resulted in rotation of the regional slaty cleavage into parallelism with compositional layering. Porphyroblasts continued to grow during the attenuation event that is recorded in the rims of andalusite porphyroblasts where inclusion trails curve into parallelism with the present foliation. Porphyroblast growth outlasted the deformation, because the outermost rims of andalusite porphyroblasts overgrow the youngest foliation. The metasedimentary units maintained their coherent stratigraphy and were thinned uniformly due to the decreased viscosity of the rocks at elevated temperatures and the relatively homogeneous upward expansion of the pluton.

The sharp curvature of inclusion trails as they turn into parallelism with the matrix foliation attests to the rapid time scale of the deformation relative to the time taken for porphyroblast growth. The sharp curvature occurs over a small volume within the porphyroblasts, and there is no discontinuity or break in inclusion trails from core region through rim region and into the matrix indicating that porphyroblast growth kept up with the imposed strain rate. Based on thermal modelling studies of the Papoose Flat pluton and its aureole rocks, Nyman et al. (1995) estimated that the observed 90% attenuation of the aureole rocks may have taken place in less than 80,000 years at an average strain rate on the order of 10^{-12} sec^{-1} assuming that the pluton was intruded as a single magma pulse. They pointed out, however, that if high aureole temperatures were maintained over a longer time period, by injection of several magma pulses (as inferred from the andalusite prophyroblasts), then strain rates may have been slower (Nyman et al., 1995, p. 640). In our two stage emplacement model, penetrative deformation is only associated with the second pulse of magma injection (during laccolith formation) and therefore the average strain

rate of 10^{-12} sec^{-1} calculated by Nyman et al. (1995) would remain valid. Direct observation of the growth of laccoliths is rare; however examples of the rapid progressive growth of near-surface laccoliths have been documented (see review by Correy 1988, pp. 45-46). One of the most spectacular near-surface examples has been recorded by Minakimi et al. (1951) in Japan where growth of a near-surface laccolith, 1 km long by 0.8 km wide, raised ground level by 170 to 200 m over a 9 month time period, and involved emplacement of approximately 0.1 km^3 of magma.

Sill-Like Geometry

The Papoose Flat pluton is in concordant contact with the lower Cambrian Poleta Formation on its western and southern margins and with the stratigraphically underlying Campito Formation on its eastern margin (Fig. 26). The Poleta Formation dips 30 to 40° away from the pluton on the west and south sides of the pluton and the Campito Formation locally dips steeply toward the pluton on the eastern margin. Only along the central section of the pluton's northern margin, and around the apophysis at the southeast end of the pluton, is the pluton discordant to the surrounding metasedimentary formations (Nelson et al., 1978). The generally concordant shape of the pluton and the observation that there is no missing stratigraphy suggest that the magma initially intruded along bedding between the underlying Campito Formation and the overlying Poleta Formation in the west-dipping limb of the Inyo anticline. An east to west cross section illustrates the concordancy and sill-like geometry of the pluton (Fig. 27).

Further support for an initial sill-like intrusion comes from porphyroblast-matrix relationships which indicate that the first metamorphic event related to intrusion (growth of porphyroblast cores) took place when the overlying Harkless Formation was planar in geometry and situated within the western limb of the Inyo anticline, prior to being domed and intensely strained (attenuated) during vertical inflation of the western part of the magma chamber. Porphyroblast-matrix analysis also indicates that the first metamorphic event was static and occurred prior to ductile attenuation of the aureole rocks.

Speculation on Nature of Pathway for Transport of Magma into a Sill/Laccolith-like Intrusion

In their original model for emplacement of the Papoose Flat pluton, Sylvester et al. (1978, fig. 9) proposed that the pluton was intruded as a steeply dipping dike or wall diapir that truncated the Wyman, Reed, Deep Spring and Campito formations before reaching the level of the Poleta Formation where it then inflated outward to the west deflecting the aureole rocks out of their original position in the Inyo anticline. Sylvester et al. (1978, p. 1217) suggested that the apophysis, which is discordantly intruded into the surrounding country rocks at the eastern end of the pluton (Fig. 26), might "be a vestige of the initial stage of intrusion, judging from the vertical lineations in the granite of the apophysis and the apparently higher temperature metamorphic mineral phases in the adjacent wall rocks." Our palinspastic restoration of the aureole rocks, based on andalusite inclusion trails, has demonstrated that final emplacement of the pluton could not have involved westward-directed horizontal translation of the wall rocks (Fig. 34), but the suggestion that the apophysis might be a feeder dike to the main pluton remains appealing.

The apophysis is situated at a deeper structural level than the main pluton. Inspection of the geologic map by Nelson et al. (1978) reveals that the apophysis-wall rock contacts are currently exposed at an elevation of 1700 - 2070 m above sea level, while the eastern margin of the main pluton is exposed at elevations ranging between 2070 m (mapped junction between apophysis and main pluton) and 2987 m above sea level. Inspection of the geologic map of the pluton (Fig. 26) also indicates that if the WNW-ESE trending apophysis were to continue westward beneath the main pluton its map position would coincide with the crest of the pluton roof which has been domed upwards at the western end of the pluton. The projected extension of the apophysis beneath the main pluton also coincides with the mapped position of several other WNW-ESE trending geologic features in the pluton: i) the hinge line of an elongate magnetic foliation dome recently identified by St. Blanquat et al. (1994) using AMS analysis, ii) a central domain of higher calculated quartz-biotite $\Delta^{18}O$ temperatures (Brigham, 1984, p. 142), iii) an elongate central core domain characterized by magmatic microstructures (St. Blanquat et al., 1994), iv) an elongate myrmekite/microaplite-poor zone located within, and along the axis of, the magmatic domain (St. Blanquat, personal communication 1997). Based on these observed spatial relationships we tentatively suggest that the apophysis may be part of a steeply dipping WNW-ESE striking intrusion

which extends beneath the Papoose Flat pluton and acted as a feeder dike to the pluton during its progressive development from an inclined sill to a laccolith.

Discussion

Three Dimensional Control and the Role of Translation

Structural aspects of pluton emplacement are commonly determined by the kinematics inferred from two dimensional map and outcrop patterns. The map pattern of the deflected wall rocks surrounding the Papoose Flat pluton was used by Sylvester et al. (1978) to infer a model of emplacement for the pluton involving westward (horizontal) translation and expansion. Formation of the gently plunging, NNW-SSE trending, stretching lineation observed across the western part of the pluton and its aureole is not explicitly considered in this model involving westward horizontal expansion. The presence of the stretching lineation has been interpreted by Law et al. (1990, 1992) and Paterson et al. (1991) as indicating that the high strain zone surrounding the western part of the pluton could be associated with regional deformation. In our model, however, lineation developed as the solid-state carapace (pluton margins and aureole) was stretched above an upward-inflating magma chamber (c.f. Fig. 35 and Law et al. 1993, fig. 15).

Many detailed analyses of the structures and strain associated with pluton emplacement have concluded that the space created by aureole strains is insufficient to accommodate the volume of magma intruded (Holder, 1979; John and Blundy, 1993; Paterson and Fowler, 1993; McNulty et al., 1996). Paterson and Fowler (1993) calculated that a maximum of 23% of the volume of the Papoose Flat pluton could be accommodated by ductile flow within the aureole and therefore argued that other mechanisms besides forcible expansion must be operating to create space for the Papoose Flat pluton. Many possible deformation paths can explain the strain surrounding plutons, and inferring the deformation path based on the deflection of two dimensional map patterns is at best an approximation (see Schwerdtner, 1995) and may be why the "space" problem still exists. Furthermore, forcible emplacement has typically been associated with structures indicative of flattening ($1>k>0$) strains, and models of forcible emplacement have been based on radially expanding plutons (Holder, 1979; Ramsay, 1989; Paterson and Fowler, 1993; Guglielmo, 1994). Structures indicative of simple shear surrounding plutons are often attributed to synchronous pluton emplacement and regional deformation. If translation is a large component of forceful pluton

emplacement, which has often been overlooked (Guglielmo, 1994), then simple shear strains should be expected and the radially expanding pluton model for forceful emplacement can only be expected to account for part of the volume of such plutons.

In this paper, wall rock flow is separated into shortening (thinning), and rigid body translation, because all the sedimentary rocks within the concordant aureole surrounding the Papoose Flat pluton have been translated upward, but not all of the same sedimentary rocks have undergone penetrative shortening (attenuation). Calculating the volume produced in the aureole by measuring shortening strains alone will therefore never give a value equal to the volume of the pluton if translation is ignored. The "space" problem is not as acute when the wall and roof rocks move upward, because there is an unlimited amount of "space" that can be created by vertical translation.

Stoping versus Diapirism versus Laccolith Formation

Stoping is not a viable mechanism for creating space for the Papoose Flat pluton because all or most of the wall rocks are accounted for. When the pluton is removed from the surrounding rocks and the void closed up, the section is conformable from the western contact to the eastern contact, i.e., the sedimentary section is mostly complete and there is little missing stratigraphy (Figs. 26 and 27).

If the Papoose Flat pluton rose as a diapir, then it is difficult to explain the overturned Precambrian formations along the eastern margin. Instead of a rim syncline, there is a rim anticline. Away from the pluton to the northwest, the Precambrian formations dip to the southwest as do all the formations in the southwest limb of the Inyo anticline, but their dips increase and overturn abruptly near the pluton contact, rotating counterclockwise when viewed to the northwest. This geometry suggests that bedding initially rotated downward in an overall tightening of the anticline around the eastern end of the pluton. A rising diapir should rotate all bedding upward, in a clockwise motion when viewed to the northwest, as the beds are uplifted and pushed aside by a rising magma body, even during return flow. This action would produce a diapir-associated rim syncline. The interpretation that the dipping beds of the Precambrian formations rotated downward to become overturned indicates that in-situ outward horizontal expansion was at least locally important as an emplacement mechanism along the pluton's northeastern margin, and suggests that the Precambrian formations were initially below the magma chamber (as the floor beneath an inclined sill) (Fig. 37).

The observation that regionally developed slaty cleavage is preserved within the outer aureole south of the pluton, even though bedding was deflected out of its regional position and oriented parallel to the pluton margin, indicates that some wall rocks were translated and at the same time not affected by significant penetrative deformation. This observation has general implications in terms of a mechanism for providing space for emplacement and helps to alleviate the space problem above the Papoose Flat pluton. If the rocks above plutons can be translated upward by folding and faulting, similar to the roof rocks above a laccolith, then the space problem is significantly alleviated, if not removed.

Jackson and Pollard (1988) demonstrated that one of the diorite laccoliths in the Henry Mountains of Utah, USA, uplifted its sedimentary overburden a minimum of 2.5 km and was originally intruded at a depth of 3-4 km. The laccolith is concordant to the overlying sedimentary section and probably initially intruded as a sill; there are numerous sills in the region surrounding the main intrusion. The sedimentary section does not exhibit significant penetrative deformation. Paleomagetic data on the surrounding sills, which dip away from the pluton parallel to the contact, indicate that they initially crystallized in a horizontal position, parallel to bedding, and have since been rotated 75 to 80° from horizontal as the laccolith inflated and domed the overlying sedimentary layers (Jackson and Pollard, 1988). The sills and laccoliths in the Henry Mountains, which were intruded at a shallow level, clearly illustrate that wall rocks can be translated vertically without significant penetrative deformation, and that translation can provide room for intrusions. In this paper we have attempted to demonstrate that intrusion of the deeper level Papoose Flat pluton, which is calculated on structural and stratigraphic grounds to have been intruded at a depth of between 6.4 and 9.2 km (Sylvester et al. 1978, p. 1213), may also have involved kilometer-scale translation of its wall and roof rocks. Mineral paragenesis of the Papoose Flat pluton aureole rocks indicate a pressure of contact metamorphism of beween 3 and 4 kbar (Nyman et al. 1995, p. 635).

If magma flow is responsible for the kilometer scale translation of wall rocks in the upper crust, which seems to be well documented for laccoliths, then how do magmas/plutons express this extreme pressure at deeper levels in the crust? Buoyancy seems to be a controlling factor on where magma originally ponds in the crust (Corry, 1988; Ryan, 1993), but the driving force that produces the characteristic shapes of intrusions such as laccoliths and plutons is not simply buoyancy, and locally magmas seem to be able to exert extreme pressures, in a dominantly vertical direction, on their surrounding wall rocks.

Conclusions

The deformation features surrounding the Papoose Flat pluton have been interpreted by modelling the intrusion as a mid- to upper-crustal laccolith. The concordant metasedimentary aureole surrounding the Papoose Flat pluton is unusual in that a complete strain analysis is possible. With the aid of porphyroblast-matrix relationships, the kinematics of rotation, the change in volume, the change in thickness, and the amount of translation of the metasedimentary formations within the aureole have been quantified and are consistent with initial magma emplacement as an inclined sill and subsequent inflation into a laccolith/pluton.

Detailed porphyroblast-matrix analysis indicates that inclusion trails within the andalusite porphyroblasts record the orientation of a regionally developed slaty cleavage within the original shale and that these inclusion trails may be used as strain markers to restore the aureole metasedimentary layers back to their pre-pluton emplacement position. Inclusion trail analysis indicates that wall rock translation is compatible with a vertical motion for final pluton emplacement.

The combination of structural and porphyroblast-matrix analyses leads to a three dimensional kinematic history of the wall rocks whereby space is produced by a combination of penetrative strain (shortening), vertical and horizontal translation, and rotation. (c.f. Figs. 10 and 11). Space problems encountered with pluton emplacement models which cannot account for all of the volume of a particular pluton by penetrative strain in the surrounding wall rocks may be an indication that translation plays a significant role in the emplacement history.

Acknowledgements

Field and laboratory work was funded through grants from the Geological Society of America, Sigma Xi and University of California White Mountain Research Station to S.S. Morgan, and National Science Foundation grants EAR-9018929 and EAR-9506525 to R.D. Law. The authors particularly wish to thank Allen Glazner for carrying out the chemical analyses which are included in Table 1, Basil Tickoff for suggesting important organizational changes to the manuscript, and Clem Nelson for support and encouragement of our work in the White-Inyo Range. Critical reviews of various drafts of this manuscript by Barbara John, Cees Passchier, Stefan Schmid, Carol Simpson, Art Sylvester, Basil Tickoff and Associate Editor Mike Cosca are gratefully acknowledged.

References

Akaad, M.K., 1956, The northern aureole of the Ardara pluton of County Donegal: Geological Magazine, v. 93, p. 377-392.

Bateman, P.C., Clark, L.C., Huber, N.K., Moore, J.G. and Rinehart, C.D., 1963, The Sierra Nevada batholith: a synthesis of recent work across the central part: U.S. Geological Survey Professional Paper 414-D, 46pp.

Bateman, P.C., 1992, Plutonism in the Central Part of the Sierra Nevada Batholith, California: U.S. Geological Survey Professional Paper 1483, 186pp.

Bell, T.H., and Rubenach, M.J., 1983, Sequential porphyroblast growth and crenulation cleavage development during progressive deformation: Tectonophysics, v. 92, p. 171-194.

Bell, T.H., Fleming, P.D., and Rubenach, M.J., 1986, Porphyroblast nucleation, growth and dissolution in regional metamorphic rocks as a function of deformation partitioning during foliation development: Journal of Metamorphic Geology, v. 4, p. 37-67.

Brigham, R.H., 1984, K-feldspar genesis and stable isotope relations of the Papoose Flat pluton, Inyo Mountains, California: Unpublished PhD thesis, Stanford University.

Clarke, D. B., 1992, Granitoid Rocks: London, Chapman and Hall, 283 p.

Corry, C.E., 1988, Laccoliths; Mechanics of emplacement and growth: Geological Society of America Special Paper, No. 220. 110 p.

Davis, B.K., 1993, Mechanism of emplacement of the Cannibal Creek granite with special reference to timing and deformation history of the aureole: Tectonophysics, v. 224. p. 337-362.

Ernst, W.G., 1996, Petrochemical study of regional/contact metamorphism in metaclastic strata of the central White-Inyo Range, eastern California: Geological Society of America Bulletin, v. 108, p. 1528 - 1548.

Ernst, W.G., Nelson, C.A., and Hall, C.A., 1993, Geology and metamorphic mineral assemblages of Precambrian and Cambrian rocks of the central White-Inyo Range, eastern California: California Department of Conservation, Division of Mines and Geology, Map Sheet 46.

Fyson, W.K., 1980, Field fabrics and emplacement of an Archean granitoid pluton, Cleft Lake, Northwest Territories: Canadian Journal of Earth Sciences, v. 17, p. 325-332

Guglielmo, G., Jr., 1994, Interference between pluton expansion and coaxial tectonic deformation: three-dimensional computer model and field implications: Journal of Structural Geology, v. 16, p. 237-252.

Holder, M.T., 1979, An emplacement mechanism for post-tectonic granites and its implications for their geochemical features, *in* Atherton, M.P., and Tarney, J., eds., Origin of granite batholiths: Geochemical evidence: Nantwich, England, Shiva Press, p. 116-128.

Hutton, D. H. W., 1988, Granite emplacement mechanisms and tectonic controls: Inferences from deformation studies: Royal Society of Edinburgh Transactions, Earth Sciences, v. 79, p. 245-255.

Jackson, M.D., and Pollard, D.P., 1988, The laccolith-stock controversy: New results from the southern Henry Mountains, Utah: Geological Society of America Bulletin, v. 100, p. 117-139.

Jamieson, R.A., and Vernon, R.H., 1987, Timing of porphyroblast growth in the Fleur de Lys Supergroup, Newfoundland: Journal of Metamorphic Geology, v. 5, p. 273-288.

John, B.E., and Blundy, J.D., 1993, Emplacement-related deformation of granitoid magmas, southern Adamello massif, Italy: Geological Society of America Bulletin, v. 105, p. 1517-1541.

Johnson, S.E., 1990, Lack of porphyroblast rotation in the Otago schists, New Zealand: implications for crenulation development, folding and deformation partitioning: Journal of Metamorphic Geology, v. 8, p. 13-30.

Kistler, R.W., Bateman, P.C. and Brannock, W.W., 1965, Isotopic ages of minerals from granitic rocks of the central Sierra Nevada and Inyo Mountains: Geological Society of America Bulletin, v. 76, p. 155 - 64.

Law, R.D., Morgan, S.S. and Sylvester, A.G., 1990, Evidence for large scale shearing during emplacement of the Papoose Flat pluton, California: a re-examination of the microstructures and crystallographic fabrics: Geological Society of America Abstracts with Programs, v. 22, no. 7, p. A183.

Law, R.D., Morgan, S..M., Casey, M., Sylvester, A.G. and Nyman, M., 1992 The Papoose Flat pluton of eastern California: a reassessment of its emplacement history in the light of new microstructural and crystallographic fabric observations: Transactions Royal Society of Edinburgh: Earth Sciences, v. 83, p. 361 - 375.

Law, R.D., Sylvester, A.G., Nelson, C.A., Morgan, S.S., and Nyman, M.W., 1993, Deformation associated with emplacement of the Papoose Flat pluton, Inyo Mountains, eastern California: Geologic Overview and Field Guide, *in* Lahren, M.M., Trexler, J.H., Jr. and Spinosa, C., eds., Crustal evolution of the Great Basin and Sierra Nevada: Cordilleran/Rocky Mountain Section, Geological Society of America Guidebook, Department of Geological Sciences, University of Nevada, Reno, p. 231-261.

LeMaitre, R.W., editor, 1989, A classification of igneous rocks and glossary of terms: Recommendations of the International Union of Geological Sciences Subcommision on the Systematics of Igneous Rocks: Oxford, Blackwell, 193p.

McNulty, B. A., Tong, W., and Tobisch, O. T., 1996, Assembly of a dike-fed magma chamber: The Jackass Lakes pluton, central Sierra Nevada, California: Geological Society of America, v. 108, p. 926-940.

Miller, J., 1996, U/Pb crystallization age of the Papoose Flat pluton, White-Inyo Mountains, California. Geological Society of America Abstracts with Programs, v. 28, no. 5, p. A91.

Minakami, T., Ishikawa, T., and Yagi, K., 1951, The 1944 eruption of Volcano Usu in Hokkaido, Japan; Volcanological Bulletin, series 2, v. 11, p. 5-157.

Morgan, S.S., 1992, Strain path partitioning during forceful emplacement of the Papoose Flat pluton, Inyo Mountains, CA.: Unpublished M.S. thesis, Virginia Polytechnic Institute and State University, Blacksburg, VA.

Morgan, S.S., Law, R.D., and Nyman, M., 1992, Coaxial spinning deformation and non-rotation of porphyroblasts surrounding the Papose Flat pluton, Inyo Mountains, California: Geological Society of America Abstracts with Programs, v. 24, p. A-146.

Nelson, C.A., 1987, Papoose Flat pluton, Inyo Mountains, California, *in* Hill, M.L., ed., Geological Society of America Centennial Field Guide - Volume One - Cordilleran Section, p. 157-160.

Nelson, C.A., and Sylvester, A.G., 1971, Wall rock decarbonation and forcible emplacement of Birch Creek pluton, southern White Mountains, California: Geological Society of America Bulletin, v. 82, p. 2891-2904.

Nelson, C.A., Oertel, G., Christie, J.M., and Sylvester, A.G., 1972, Structure and emplacement history of Papoose Flat pluton, Inyo Mountains, California: Geological Society of America Abstracts with Programs, v. 4, p. 208 - 209.

Nelson, C.A., Oertel, G., Christie, J.M. and Sylvester, A.G., 1977, Geologic map, structure sections and palinspastic map of the Papoose Flat pluton, Inyo Mountains, California.: Geological Society of America Map and Chart Series MC-20.

Nelson, C.A., Hall, C. A., and Ernst, W.G., 1991, Geologic History of the White-Inyo Range, *in* Hall, C.A. ed., Natural History of the White-Inyo Range eastern California: Berkeley and Los Angeles, California, University of California Press, p. 42-74.

Nyman, M.W., Law, R.D. and Morgan, S.S., 1995 Conditions of contact metamorphism, Papoose Flat pluton, eastern California, USA: implications for cooling and strain histories: Journal of Metamorphic Geology v. 13, p. 627-643.

Paterson, S.R., Brudos, T., Fowler, K., Carlson, C., Bishop, K and Vernon, R.H., 1991, Papoose Flat pluton: forceful expansion or postemplacement deformation: Geology, v. 19, p. 324 - 327.

Paterson, S. R., and Fowler, T. K., 1993, Re-examining pluton emplacement processes; Journal of Structural Geology, v. 15, p. 191-206.

Pitcher, W.S., and Berger, A.R., 1972, The geology of Donegal: A study of granite emplacement and unroofing: New York, Wiley, 435 p.

Pitcher, W. S., 1979, The nature, ascent and emplacement of granitic magmas: Geological Society of London Journal, v. 136, p. 627-662.

Ramsay, J.G., 1962, The geometry and mechanics of formation of 'similar' type folds: Geology, v. 70, p. 309-328.

Ramsay, J.G., 1969, The measurement of strain and displacement in orogenic belts, in Kent, P.E., Satterthwaite, G.E., and Spencer, A.M., eds., Time and Place in Orogeny: Geological Society of London Special Publication 3, p. 43-79.

Ramsay, J.G., 1989, Emplacement kinematics of a granite diapir. The Chindamora batholith, Zimbabwe: Journal of Structural Geology, v. 11, p. 191-210.

Read, H.H., 1957, The Granite Controversy: Geological Addresses Illustrating the Evolution of a Disputant: Hertsford, Thomas Murby, 430 p.

Ross, D.C., 1965, Geology of the Independence quadrangle, Inyo County, California: U. S. Geological Survey Bulletin, v. 1181-0, p. 64.

Ryan, M. P., 1993, Neutral buoyancy and the structure of mid-ocean ridge magma reservoirs: Journal of Geophysical Research, v. 98 p. 22321-22338.

Saint Blanquat (de), M., Law, R.D., Bouchez, J.L., and Morgan, S.S., 1994, Emplacement of the Papoose Flat pluton: a reinspection using anisotropy of magnetic susceptibility and microstructures: Geological Society of America Abstracts with Programs, v. 26, p. A-134.

Saint Blanquat (de), M., and Tickoff, B., 1997, Development of magmatic to solid-state fabrics during syntectonic emplacement of the Mono Creek granite, Sierra Nevada Batholith, California, *in* Bouchez, J.-L., Stephens, W.E., and Hutton, D.H., eds., Granite: from melt segregation to emplacement fabrics: Kluwer Academic Publishers, p. 231-252.

Sanderson, D. J., and Meneilly, A. W., 1981, Analysis of three-dimensional strain modified uniform distributions: andalusite fabrics from a granite aureole: Journal of Structural Geology, v. 3, p. 109-116.

Schwerdtner, W. M., 1995, Local displacement of diapir contacts and its importance to pluton emplacement study: Journal of Structural Geology, v. 17, p. 907-910.

Sylvester, A.G., 1966, Structural and metamorphic petrology of the contact aureole of the Papoose Flat pluton, Inyo Mountains, California: Unpublished PhD thesis, University of California at Los Angeles.

Sylvester, A.G., and Christie, J.M., 1968, The origin of crossed-girdle orientations of optic axes in deformed quartzites: Journal of Geology, v. 76, p. 571-580.

Sylvester, A.G., Oertel, G., Nelson, C.A. and Christie, J.M., 1978, Papoose Flat pluton: a granitic blister in the Inyo Mountains, California: Geological Society of America Bulletin, v. 89, p. 1205-1219.

Vernon, R.H., 1988a, Sequential growth of cordierite and andalusite porphyroblasts, Cooma complex, Australia: Microstructural evidence of a pro-grade reaction: v. 6, p. 255-269.

Vernon, R.H., 1988b, Microstructural evidence of rotation and non-rotation of mica porphyroblasts: Journal of Metamorphic Geology, v. 6, p. 595-601.

Vernon, R. H., 1989, Evidence of syndeformational contact metamorphism from porphyroblast-matrix microstructural relationships: Tectonophysics, v. 158, p. 113-126.

Vernon, R. H., Paterson, S. R., and Foster, D., 1993a, Growth and deformation of porphyroblasts in the Foothills terrane, central Sierra Nevada, California: Negotiating a microstructural minefield: Journal of Metamorphic Geology, v. 11, p. 203-222.

Vernon, R.H., Collins, W.J., and Paterson, S.R., 1993b, Pre-foliation metamorphism in low-pressure / high temperature terrains: Tectonophysics, v. 219, p. 241-256.

Chapter 4. Concordant plutons and two periods of porphyroblast growth: Products of multiple magma injection

SVEN S. MORGAN AND RICHARD D. LAW

Department of Geological Sciences, Virginia Tech, Blacksburg, VA 24061

Abstract

The Papoose Flat (U.S.A.), Ardara (Ireland), Cannibal Creek (Australia), and Eureka Valley-Joshua Flat-Beer Creek composite (U.S.A.) plutons are mid-crustal granitoids which we model as being emplaced in a multiple-stage process similar to the intrusive sequence of laccoliths. Each pluton is surrounded by a narrow aureole of concordant metasedimentary rocks which exhibit at least two stages of porphyroblast growth, each stage correlated to a discrete pulse of magma injection. Porphyroblast-matrix relationships in the aureole of each pluton suggest an initial period of static porphyroblast growth and a later period of syn-deformational growth, consistent with initial magma intrusion as a sheet-like body and subsequent inflation-deformation into a pluton/laccolith. Initial emplacement from a feeder dike and into a sheet/sill overcomes the thermo-mechanical problems associated with the ascent of diapirs, and in-situ inflation produces the highly strained concordant aureoles so commonly associated with diapirism.

The zone where metasedimentary layering is concordant to these plutons is narrow relative to the area of the plutons and is confined to the high temperature (andalusite-in isograd) portion of the thermal aureoles. We suggest that such zones of concordancy (termed here as structural aureoles) around plutons are confined to wall rocks that have been thermally softened prior to final, forceful emplacement, and is the reason why structural aureoles are so narrow. Translation and rotation of the thermally softened metasedimentary rocks are the dominant mechanisms in providing space for these plutons; failure to take account of these processes may be the reasons why flattening strains previously measured in these and other aureoles cannot accommodate the volumes of the plutons they surround.

Introduction

The elliptical map view of many plutons, commonly surrounded by an aureole of highly strained metamorphic rocks, has led many earth scientists to propose a diapiric model of ascent and emplacement of magma (e.g., Akaad, 1956; Sylvester, 1964; Pitcher and Berger, 1972; Bateman, 1985; Ramsay, 1989; England, 1992). However, numerical modeling indicates that significant thermal and mechanical problems are associated with magmatic bodies rising under the influence of density contrasts (buoyancy) with their surrounding rocks, thus limiting the applicability of the magmatic diapir model to the lower crust and mantle (Marsh, 1982; Mahon et al., 1988). The mid to upper crust, where many concordant plutons are found, is believed to be too cold, and therefore the density too high, for magmatic diapirs to penetrate. The transfer in thermal energy from the pluton to the overlying rocks necessary to decrease their viscosity would cause crystallization of the pluton and cessation of rise.

In contrast to the 'tear-drop' geometry assumed in simple diapir models, an increasing amount of literature reveals the sheet-like shape of some plutons (Hogan and Gilbert, 1997; Evans et al., 1994) including some of the largest plutons in the western Himalayas (Stern et al., 1989). Gravity modeling also suggests that some elliptical plutons may actually have flat bases with one or several root zones (Vigneresse, 1995). Root zones may actually be dikes, and Clemens and Mawer (1992) and Petford (1996) have calculated that even plutons with batholithic dimensions may be fed by dikes, which would allow magmas to rise into the upper crust before losing their thermal energy and crystallizing.

The remaining problem is how to produce a pluton which is elliptical in map view and surrounded by an aureole of concordant metamorphic rocks by initial intrusion through dikes. Laccoliths constitute the most compelling evidence in the uppermost crust that dikes can act a feeder conduits for elliptical igneous bodies. A laccolith, by definition, is a forcibly intruded igneous body which has uplifted its roof rocks, is concordant to bedding, has a domed cross-section, and is gradational from a sill (Corry, 1988).

Jackson and Pollard (1988) demonstrated that the laccoliths in the Henry Mountains of Utah, U.S.A., were initially intruded as sills at 3-4 km depth, and that subsequent inflation produced the domal shaped igneous bodies. Paleomagnetic vectors on the surrounding sills in the upturned flanks of one of the laccoliths indicate that initial

crystallization occurred when the sills were in a horizontal position, parallel to bedding, and since have been rotated 75 to 80° as the sill below inflated and domed the overlying sedimentary layers, documenting a minimum of two pulses of magma injection. If laccoliths were to be emplaced at 12 km below the surface of the earth, instead of at 3 km, what would be different and how could we distinguish plutons from laccoliths? We suggest the principal difference is that deformation of the wall rocks associated with mid-crustal laccoliths involves shortening strains, rotation, and translation, whereas the deformation associated with upper-crustal laccoliths involves rotation and translation only.

We describe four classic examples of mid-crustal plutons, the Papoose Flat, Ardara, Cannibal Creek, and Eureka Valley-Joshua Flat-Beer Creek (EJB)(Fig. 38), which display structural features that are commonly cited as evidence for diapirism, but can also be associated with laccolith-like emplacement. The geometry of the intrusion relative to the surrounding strata also supports the laccolith emplacement model in the case of the Papoose Flat pluton (Fig. 39). A lack of field data from the other three plutons does not allow detailed geometric modeling of the plutons and their relationships to wall rock strata, but the available field data are compatible with the proposed model.

Microstructural evidence from the metasedimentary rocks surrounding these plutons indicates that the aureole rocks were penetratively deformed at medium grades of contact metamorphism (~500°C) during pluton emplacement, but porphyroblast-matrix relationships indicate that an initial period of static contact metamorphism predated this deformation. In our model, an initial sheet-like intrusion advectively brings a heat source and thermally softens, but does not significantly deform the surrounding sedimentary rocks. Later pulses of magma inflate the sheet-sill into a pluton and result in the high strains so commonly observed around elliptical plutons.

The structural aureole (zone where wall rocks have been deflected out of their regional strike but remain sub-parallel to the pluton margin) surrounding these plutons is confined to the sedimentary rocks which have been metamorphosed under conditions where andalusite is stable (>450°C at 10 km depth), which is also approximately the temperature where feldspar begins to deform plastically. Therefore, based on the mechanical aspects of the metasedimentary rocks, we speculate that the volume of rocks within structural aureoles surrounding mid-crustal plutons is confined to the volume of rocks that has first been thermally softened.

In two of the aureoles, sillimanite and kyanite are also present. Therefore, the depth of emplacement is probably close to but less than the pressure of the Al_2SiO_5 triple point,

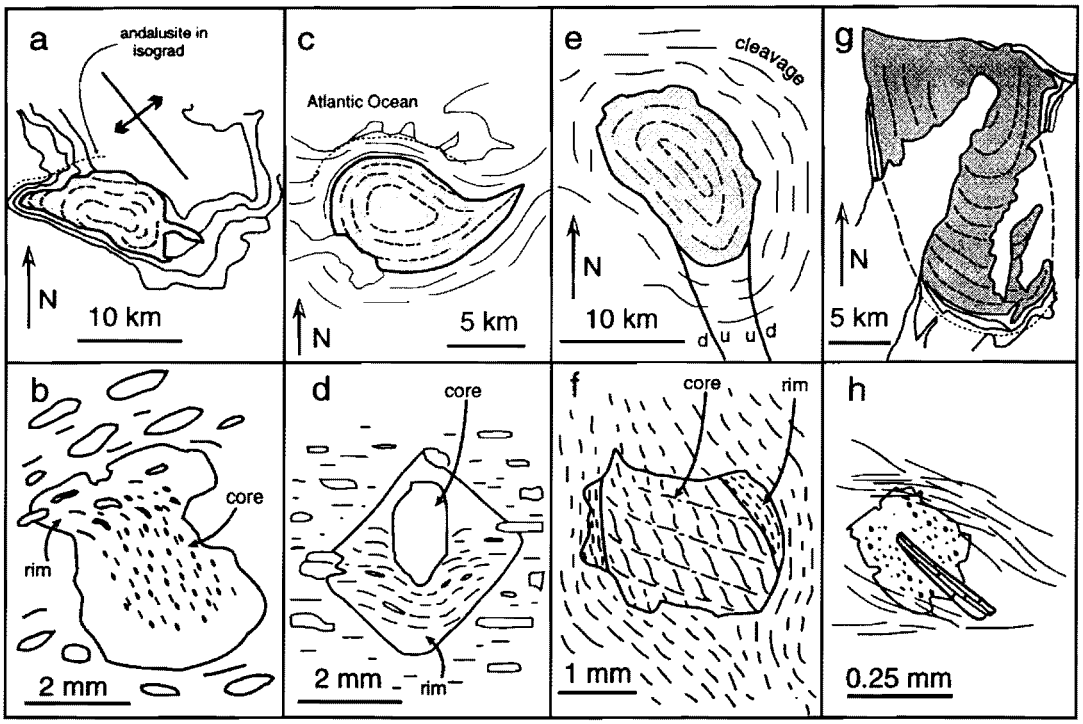

Figure 38. Simplified geologic maps of the four plutons, their internal foliations and structural aureoles, the andalusite-in isograd (dotted line), and sketches of porphyroblast-matrix relationships within their structural aureoles. a) The Papoose Flat pluton, eastern California, USA. After Nelson et al. (1991). b) Andalusite porphyroblast from the aureole of the Papoose Flat pluton. After Morgan et al. (1998a). c) The Ardara pluton, Ireland. After Holder (1979), Pitcher and Berger (1972). d) Andalusite porphyroblast from the aureole of the Ardara pluton. After Akaad (1956). e) The Cannibal Creek granite, north Queensland, Australia. After Bateman (1985) and Davis (1993). f) Andalusite porphyroblast from the aureole of the Cannibal Creek granite. After Davis (1993). g) The Eureka Valley-Joshua Flat-Beer Creek (EJB) composite pluton of eastern California, USA. After Nelson et al. (1991) and Morgan et al. (1998b). h) Porphyroblasts of crystalline silimanite and fibolite after andalusite; from the EJB pluton aureole.

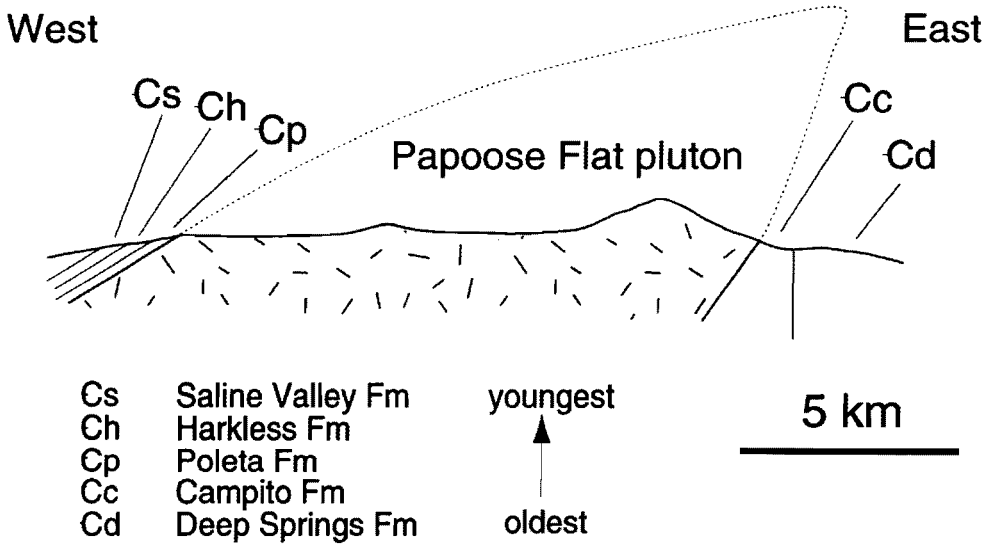

Figure 39. East to west cross section through the Papoose Flat pluton and surrounding lower Cambrian sedimentary rocks. Note the sill-like geometry of the pluton and how there is no mising stratigrphy from east to west (after Morgan et al., 1998a).

which is approximately 4 kbar or 12 km. The surrounding sedimentary rocks have experienced greenschist and lower grades of regional metamorphism, indicating that all the thermal energy required for porphyroblast growth was provided by the plutons themselves. Table 4 provides an overview of the structural and metamorphic characteristics for each pluton.

Geologic Descriptions

Papoose Flat

The Cretaceous Papoose Flat pluton, in the White-Inyo Range of eastern California, is a two-mica quart monzonite and is surrounded by a concordant sequence of lower Cambrian metasedimentary rocks that wrap around the western margin and parallel the contact with the pluton for approximately 20 km. At the western margin, the pluton is in contact with the lower Cambrian Poleta Formation, and the contact dips 20-40° away from the pluton. On the eastern margin, the contact dips steeply into the pluton, indicating that the current exposure level is much closer to the base of the pluton. At the eastern contact, the pluton is in contact with the lower Cambrian Campito Formation (Fig. 39), which is stratigraphically the next formation beneath the Poleta, indicating that the pluton initially intruded as a sill between the two formations (Morgan et al., 1998a). Andalusite porphyroblasts within the schist surrounding the pluton commonly exhibit core-rim morphology with individual growth stages identifiable by differences in inclusion trail density, orientation, and size (Fig. 38)(Morgan et al., 1998a).

The dominant regional-scale penetrative deformational feature in the central White-Inyo Range is a northwest-striking axial planar slaty cleavage (Morgan and Law, 1998b). Regional-scale tectonism has been invoked to explain the high strains developed around and within the western margin of the Papoose Flat pluton (Paterson and Vernon, 1995), but the slaty cleavage is preserved within the aureole rocks as porphyroblast inclusion trails described above, indicating that the penetrative strain in the surrounding country rocks developed prior to pluton emplacement. Using these inclusion trails as passive strain markers, Morgan et al. (1998a) demonstrated that the pluton was initially intruded as an inclined sill which subsequently inflated vertically, stretching and translating the aureole metasedimentary rocks while rotating them away from their regional strike.

	PF	A	CC	EJB
Concordant metasedimentary aureole	x	x	x*	x
Two phases of porphyroblast growth	x	x	x	x
Core inclusion trails reflect pre-pluton foliation	x	x	x	?
Matrix foliation deflected around porphyroblast	x	x	x	x
Deflection of wall rocks at andalusite-in isograd	x	x	?	x
Magmatic foliation parallel to pluton contact	x	x	x	x
Pluton concentrically compositionally zoned	x#	x	No	No
Evidence for initial sill-like geometry	x	?	?	?

*The Cannibal Creek aureole is defined by contact-parallel fold axes and cleavage which wrap around the pluton.
#Unpublished data

Table 4. Summary of pluton aureole characteristics.

Ardara

The Ardara granitic pluton of northwestern Ireland has been interpreted as a diapir (Akaad, 1956; Pitcher and Berger, 1972), as a forcefully expanding pluton with several pulses of magma-induced inflation (Holder, 1979), and as being emplaced during regional deformation (Vernon and Paterson, 1993). The Ardara is a composite pluton with an outer rim of tonalite, an inner rim of granodiorite and quartz diorite, and a core of granodiorite (Fig. 38c). The pluton has intruded Dalradian age metasedimentary rocks and is strongly concordant, deflecting regional structures.

Within the aureole surrounding the Ardara pluton, an inner zone contains sillimanite, followed by a central zone containing andalusite and an outer zone containing both andalusite and kyanite (Pitcher and Berger, 1972). Andalusite, garnet, and staurolite porphyroblasts commonly exhibit a core-rim morphology (Akaad, 1956; Holder, 1979). Some andalusite porphyroblast cores contain fine-grained inclusions oriented at an angle to the exterior foliation that are surrounded by a rim containing inclusion trails that are deflected around the core (Fig. 39d). The rim inclusion trails are continuous into the matrix where the foliation is coarser grained than in the porphyroblast.

Cannibal Creek

The Cannibal Creek granite in North Queensland, Australia (Fig. 38e), intruded turbidites of early-Middle Paleozoic age (Bateman, 1985) and has been interpreted as a ballooning diapir (Bateman, 1985), a piercement diapir (Paterson, 1988; Godin, 1994), and as being emplaced into a developing antiform with associated uplift (Davis, 1993). An inner structural aureole is defined by a well-developed schistosity and an outer structural aureole is defined by a crenulation cleavage (Bateman, 1985). Within the country rocks external to the structural aureole, an earlier crenulation cleavage is developed which is only preserved in the structural aureole as inclusion trails within cores of andalusite porphyroblasts (Davis, 1993; Godin, 1994) and in low strain zones (Davis, 1993). The cores of these andalusite porphyroblasts are surrounded by rims which overgrew the margin parallel foliation (Fig. 38f).

The schistosity surrounding the Cannibal Creek pluton defines an antiform that Davis (1993) associated with regional deformation synchronous with emplacement of the pluton.

However, this fold cannot be traced along its axis on either side of the pluton outside of the structural aureole. Shear sense within the aureole consistently indicates pluton side up motion on both the western and eastern margins. We suggest that the folded, or "domed" schistosity is not the result of synchronous regional deformation, but the result of an inflating mid-crustal magma chamber. The inflation-related wall rock strain was not completely ductile, because faults surrounding the pluton may also have assisted in raising the roof of the pluton. On the SE and SW margins of the pluton, N-S striking faults have been mapped for over 10 km southward from the pluton (Fig. 38e). The sense of displacement on both faults is pluton side up, indicating that the crustal block containing the pluton (and the cover rocks above the pluton) underwent vertical translation.

EJB composite pluton

Stein and Paterson (1996) suggested that the EJB composite pluton of eastern California (Fig 38g) was emplaced through multiple processes. Glazner and Miller (1997) proposed sinking to explain the position of the pluton relative to the wall rocks, because the wall rocks consistently rotate down toward the contact on three sides, and Morgan et al. (1998b) proposed that the EJB pluton was forcefully emplaced into a structural basin. The western, southern, and eastern margins are concordant to the same Neoproterozoic-early Cambrian sedimentary sequence that surrounds the Papoose Flat pluton (Fig. 38a), located 20 km to the south. The northern margin is sharply discordant against a younger pluton. The EJB pluton ranges in composition from granodiorite to quartz monzonite and gabbro, and a magmatic foliation within the pluton is parallel to the wall rock-contact.

Andalusite, kyanite, and sillimanite (crystalline and fibrolitic) are present within the structural aureole surrounding the EJB pluton. Texturally, crystalline sillimanite is found replacing andalusite (Fig. 38h). Late fibrolite is in shear bands replacing biotite. Sillimanite is only observed within 300 m from the pluton, and kyanite is not observed with either sillimanite or andalusite.

Discussion

One way to emplace magma into the upper crust and at the same time avoid many of the thermo-mechanical problems associated with diapirism, is to intrude magma through

dikes (Clemens and Mawer, 1992). Transport of magma to the upper crust through dikes is orders of magnitude faster than in diapirs (Petford, 1996). Dikes are the likely conduit by which sills are emplaced, and abundant evidence exists that dikes are the feeders to laccoliths (Corry, 1998, p. 18). One of the appealing aspects of emplacing magma into the upper crust through dikes is that the magma does not have to spend as much of its thermal budget in transporting itself. This allows a sill or sheet-like magma body to pond in the middle crusts, decreasing the viscosity of the overlying wall rocks, softening them, while not deforming them.

Inclusion trails from porphyroblast cores surrounding the Papoose Flat and Cannibal Creek plutons, and possibly the Ardara pluton, preserve a preexisting regional fabric that has been mostly destroyed in the matrix of the aureole. This indicates that the first pulse of contact metamorphism was not associated with penetrative deformation, but with a nearby magmatic heat source. Therefore, the thermal softening allowed the high plastic strains to develop during the subsequent period of deformation. For example, the concordant, high strain zones surrounding the Papoose Flat, Ardara, and EJB plutons do not extend beyond the andalusite-in isograd (Fig. 38), which is the zone of contact metamorphism associated with the first pulse of magma. Apparently, the andalusite-in isograd can be used, at least for these three plutons, as a marker where the viscosities of the sedimentary wall rocks were lowered enough by the thermal energy from these ponded magmas so that the rocks could deform plastically.

Second stage porphyroblast growth records the flattening of the foliation around the initial porphyroblast cores (Papoose Flat, Ardara, Cannibal Creek) and documents the syn-deformational nature of the porphyroblast rims. During deformation, attenuation of the wall rocks causes the preexisting regionally developed cleavage, which at this stage is rapidly undergoing chemical recombination into a new metamorphic foliation, to wrap around the rigid porphyroblast cores. Porphyroblasts continue to grow producing rims with curved inclusion trails. Inclusions within rims are coarser grained and decrease in number as they curve from core to rim, which suggests an increase in metamorphic grade (Passchier and Trouw, 1996, p. 157), and is consistent with a larger volume of magma being emplaced as the second pulse in the intrusive sequence. Rim inclusion trails are continuous from the core of the porphyroblasts to the matrix foliation (Papoose Flat, Ardara, Cannibal Creek), suggesting that the deformation of the wall rocks is synchronous with the metamorphism that produced the rim growth. We interpret second stage porphyroblast growth as being

associated with outward expansion/upward doming of the wall and roof rocks as the second pulse of magma inflates the original sheet-like intrusion into the final pluton shape.

Translation, rotation, and strain accommodation

The few strain analyses which have been conducted on aureoles have consistently determined that the amount of strain, better defined as shape change, in the aureoles is never enough to accommodate the volume of the pluton (Pitcher and Berger, 1972; John and Blundy, 1993; Paterson and Fowler, 1993), as is the case with the Ardara pluton (Sanderson and Meneilly, 1982; Paterson and Fowler, 1993), the Papoose Flat pluton (Paterson and Fowler, 1993), and with the Cannibal Creek pluton (Bateman, 1985). This lack of sufficiently strained rocks has led to the conclusion that stoping may be creating space (Paterson et al., 1995), for which there is little evidence. Strain analyses have also been conducted on enclaves within the Ardara pluton, where the strains are much higher than in the aureole (Holder, 1979; Sanderson and Meneilly, 1981), which is consistent with our suggestion that much of the strain in aureoles is taken up by translation and rotation. Shape change alone (typically measured as the strain in wall rocks) will not produce the curved map patterns of strata around concordant plutons. Translation and rotation will also not be recorded as strain (shape change), and, therefore, calculations of volume made by penetrative strain will never equal the total volume of the plutons. The upturned flanks of the laccoliths in the Henry Mountains have been rotated and translated and exhibit little internal strain (Jackson and Pollard, 1988). We suggest that in considering concordant plutons, "space" problems exist because translation and rotation of the aureole rocks are not being taken into account in the strain analyses.

Conclusions

Through examination of porphyroblasts grown during contact metamorphism, we propose that four upper crustal plutons with concordant metasedimentary aureoles, the Papoose Flat, Ardara, Cannibal Creek, and EJB, have been emplaced into the upper crust in a manner similar to the intrusive style of laccoliths. Porphyroblasts exhibit two periods of growth, coincident with initial emplacement of the magmas as sills or sheet-like bodies, and

subsequent pulses which inflate the sheets into their final pluton shapes. Three of the four aureoles (Papoose Flat, Ardara, and Cannibal Creek) contain porphyroblasts with inclusion trails that suggest an initially static overgrowth of a preexisting regional cleavage fabric, consistent with passive emplacement of a sill. Inclusion trails in the rims of these porphyroblasts are flattened against the cores, suggesting deformation synchronous with a later pulse of magma during inflation. Within the fourth aureole (EJB), textural evidence indicates second stage porphyroblast growth was synchronous with deformation.

We suggest that concordant plutons, around which stratigraphic units are deflected from their regional positions and orientations, result from a sequence of multiple pulses of magma injection in which the first pulse is initially intruded as a sill or sheet-like shape. The early injection of magma produces a thermal softening of the surrounding rocks allowing for later pulses to attenuate and translate these overlying rocks. The andalusite-in isograd (for mid-crustal plutons) seems to be a marker that delineates the zone of rocks within the thermal aureole which have been sufficiently weakened to facilitate plastic deformation and translation of the overlying and surrounding wall rocks. Incorporating translation and rotation of wall rocks into the emplacement-related deformation may overcome the space problem previously encountered in the study of concordant plutons.

Acknowledgements

The authors wish to thank Brett Davis, Allen Glazner, Michel de Saint Blanquat, and Art Sylvester for reviewing an earlier version of this manuscript. Field and laboratory work on the Californian plutons was funded through grants from the Geological Society of America, Sigma Xi, Virginia Tech, and the University of California White Mountain Research Station to S. S. Morgan, and National Science Foundation grants EAR-9018929 and EAR-9506525 to R. D. Law.

References Cited

Akaad, M.K., 1956, The northern aureole of the Ardara pluton of County Donegal: Geological Magazine, v. 93, p. 377-392.

Bateman, R., 1985, Aureole deformation by flattening around a diapir during in situ ballooning: the Cannibal Creek granite: Journal of Geology, v. 93, p. 293-310

Clemens, J.D., and Mawer, C.K., 1992, Granitic magma transport by fracture propagation: Tectonophysics, v. 204, p. 339-360.

Corry, C.E., 1988, Laccoliths; Mechanics of emplacement and growth: Geological Society of America Special Paper, No. 220. 110 p.

Davis, B.K., 1993, Mechanism of emplacement of the Cannibal Creek Granite with special reference to timing and deformation history of the aureole: Tectonophysics, v. 224. p. 337-362.

England, R.E., 1992, The genesis, ascent, and emplacement of the Northern Arran Granite, Scotland: Implications for granitic diapirism: Geological Society of America Bulletin, v. 104, p. 606-614.

Evans, D.J., Rowley, W.J., Chadwick, R.A., Kimbell, G.S., and Millward, D., 1994. Seismic reflection data and the internal structure of the Lake District batholith, Cumbria, northern England. Proceedings Yorkshire Geological Society, v. 50, p. 11-24

Glazner, A.F., and Miller, D.M., 1997, Late-stage sinking of plutons: Geology, v. 25, p. 1099-1102

Godin, P., 1994, Deformation within the Cannibal Creek pluton and its aureole, Queensland, Australia: a re-evaluation of ballooning as an emplacement mechanisms: Journal of Structural Geology, v. 16, p. 693-708.

Hogan, J.P, and Gilbert, M.C., 1997, Intrusive style of A-type sheet granites in a rift environment: The southern Oklahoma Aulacogen, *in* Ojakangas, R.W., Kickas, A. B., and Green, J.C., eds., Middle Proterozoic to Cambrian Rifting, Central North America: Boulder, Colorado, Geological Society of America Special Paper 312, p. 299-311.

Holder, M.T., 1979, An emplacement mechanism for post-tectonic granites and its implications for their geochemical features, *in* Atherton, M.P., and Tarney, J., eds., Origin of granite batholiths: Geochemical evidence: Nantwich, England, Shiva Press, p. 116-128.

Jackson, M.D., and Pollard, D.P., 1988, The laccolith-stock controversy: New results from the southern Henry Mountains, Utah: Geological Society of America Bulletin, v. 100, p. 117-139.

John, B.E., and Blundy, J.D., 1993, Emplacement-related deformation of granitoid magmas, southern Adamello Massif, Italy: Geological Society of America Bulletin, v. 105, p. 1517-1541.

Mahon, K. I., Harrison, T. M., and Drew, D. A., 1988, Ascent of a granitoid diapir in a temperature varying medium. Journal of Geophysical Research., v. 93, p. 1174-1188.

Marsh, B.D., 1982, On the mechanics of igneous diapirism, stoping, and zone melting. American Journal of Science, v. 282, p. 808-855.

Morgan, S.S., and Law, R.D., 1998 An overview of Paleozoic - Mesozoic age structures developed in the central White-Inyo Range, eastern California: International Geology Review, v. 40, p. 245-256.

Morgan, S.S., Law, R.D. and Nyman, M.W., 1998a, laccolith-like emplacement model for the Papoose Flat pluton based on porphyroblast-matrix analysis: Geological Society of America Bulletin, v. 110, p. 96-110.

Morgan, S.S., Law, R.D. and St Blanquat, M., 1998b, Aureole deformation associated with inflation of the concordant Eureka Valley-Joshua Flat-Beer Creek composite pluton, central White-Inyo Range, eastern California, *in* Behl, R., ed., Geological Society of America, Cordilleran Section 1998 Field Guidebook 5, 30 pp.

Nelson, C.A., Hall, C. A., and Ernst, W.G., 1991, Geologic history of the White-Inyo Range, *in* Hall, C.A., ed., Natural History of the White-Inyo Range eastern California: Berkeley and Los Angeles, California, Univ. California Press, p. 42-74.

Passchier, C.W., and Trouw, R.A.J., 1996, Microtectonics: Germany, Springer-Verlag, 289 p.

Paterson, S.R., 1988, Cannibal Creek Granite: post-tectonic'ballooning' pluton or pre-tectonic piercement diapir?: Journal of Geology, v. 96, 730-736

Paterson, S. R., and Fowler, T. K., 1993, Re-examining pluton emplacement processes: Journal of Structural Geology, v. 15, p. 191-206.

Paterson, S.R., and Vernon, R.H., 1995, Bursting the bubble of ballooning plutons: A return to nested diapirs emplaced by multiple processes: Geological Society of America, v. 107, p. 1356-1380.

Petford, N., 1996, Dykes or diapirs?: Transactions of the Royal Society of Edinburgh: Earth Sciences, v. 87, p. 105-114.

Pitcher, W.S., and Berger, A.R., 1972, The geology of Donegal: A study of granite emplacement and unroofing: New York, Wiley, 435 p.

Ramsay, J.G., 1989, Emplacement kinematics of a granite diapir. The Chindamora batholith, Zimbabwe: Journal of Structural Geology, v. 11, p. 191-210.

Sanderson, D. J., and Meneilly, A. W., 1981, Analysis of three-dimensional strain modified uniform distributions: andalusite fabrics from a granite aureole: Journal of Structural Geology, v. 3, p. 109-116.

Schwerdtner, W. M., 1995, Local displacement of diapir contacts and its importance to pluton emplacement study: Journal of Structural Geology, v. 17, p. 907-910.

Stein, E., and Paterson, S.R., 1996, Country rock displacement during emplacement of the Joshua Flat pluton, White-Inyo Mountains, California, in Oncken, O., and Janssen, C., eds., Basement Tectonics, v. 11, Boston, Kluwer Academic Publishers, p. 35-49

Stern, C.R.,Kligfield, R., Schelling, D., Virdi, N.S., Futa, K., Peterman, Z.E., Amini, H., 1989, The Bhagirathi leucogranite of the high Himalaya (Garhwal, India); Age, petrogenesis, and tectonic implications, in Malinconico, Jr, L.L., and Lillie, R.J., eds., Tectonics of the Western Himalayas, Geological Society of America Special Paper 232, p. 33-46

Sylvester, A.G., 1964, The Precambrian rocks of the Telemark area in south central Norway. III. Geology of the Vrådal granite: Norsk Geologisk Tidsskrift, v. 44, p. 445-482.

Sylvester, A.G., Oertel, G., Nelson, C.A. and Christie, J.M., 1978, Papoose Flat pluton: a granitic blister in the Inyo Mountains, California: Geological Society of America Bulletin, v. 89, p. 1205-1219.

Vernon, R.H., and Paterson, S.R., 1993, The Ardara Granite, Ireland: Deflating an expanded intrusion: Lithos, v. 31, p. 17-31.

Vigneresse, J.L., 1995, Control of granite emplacement by regional deformation: Tectonophysics, v. 249, p. 173-186.

Vita

Sven Morgan was born in New York City in 1963 and grew up in Wilton, Connecticut. I graduated from Allegheny College, in Meadville, Pennsylvania, in 1985. Allegheny is where I first became fascinated with rocks, but I also had a desire to see the world. After working odd jobs and travelling around the world, I joined the Peace Corps in 1987 and became a volunteer in Mauritania, West Africa, for two years, where I taught bedouins how to grow vegetables. My fascination with rocks had not diminished, and I was admitted to Virginia Polytechnic Institute & State Unversity in 1989. I completed my masters degree on the deformation around a pluton in 1992. I began my Ph.D. in geology at VPI & SU in 1994, investigating the questions that my master's degree had left behind. I finished my Ph.D. in 1998 and am currently an instructor at Berea College, in Berea, Kentucky, where I live with my wife and daughter.